MOLECULAR ASPECTS OF NICKEL GENOTOXICITY

BY

FRANCO EGIDIO ROSSETTO, B.Sc.

A Thesis Submitted to the School of Graduate Studies
in Partial Fulfilment of the Requirements
for the Degree
Doctor of Philosophy

McMaster University

© Copyright by Franco Egidio Rossetto, October, 1993

MOLECULAR ASPECTS OF NICKEL GENOTOXICITY

DOCTOR OF PHILOSOPHY (1993)
(Biochemistry)

McMASTER UNIVERSITY
Hamilton, Ontario

TITLE: Molecular Aspects of Nickel Genotoxicity

AUTHOR: Franco Egidio Rossetto, B.Sc.
(McMaster University)

SUPERVISOR: Dr. Evert Nieboer, Professor of Toxicology

NUMBER OF PAGES: xix, 290

ABSTRACT

The main component of the "Nickel Ion Hypothesis" of nickel genotoxicity and carcinogenicity is that the Ni(II) ion is the putative agent - the ultimate carcinogen, irrespective of the identity of the nickel compound to which exposure occurs. In relation to this, the specific hypothesis to be tested was that Ni(II) ions can interact with DNA by both genotoxic and nongenotoxic pathways. The experimental approach adopted had three components. The first involved an examination of the effects of the Ni(II) ion on simple DNA and synthetic polydeoxynucleotides of defined sequence and base composition. In the second part, the interaction of the Ni(II) ion with chromosomes in intact nuclei was investigated. A final component assessed the genotoxic effects of a variety of nickel compounds in a mammalian cell line (AS52) by the characterization of damage at a specific gene locus.

The interaction of Ni(II) with DNA and polydeoxynucleotides was investigated utilizing a variety of spectroscopic (UV, circular dichroism), enzymatic (DNase I digestion susceptibility) and biophysical (sedimentation analysis, ethidium bromide intercalation) techniques. No alteration in structure or conformation was observed for calf thymus DNA, polydA·polydT, or polyd(AT)·polyd(AT) following

incubation with Ni(II) ion. By contrast polyd(GT)·polyd(AC), polydG·polydC and polyd(GC)·polyd (GC) clearly exhibited alterations in structure or conformation. In addition, equilibrium constants were generated for the binding of Ni(II) to these molecules. A comparison of the effects of Ni(II) to those of other metal ions suggested that the interaction of the Ni(II) ion with DNA or polydeoxynucleotides is to some extent base (or basepair) and sequence-context specific. A clear affinity for G/C bases was evident, which was also reflected in the magnitude of the binding constants. All DNAs and polydeoxynucleotides examined featured two binding sites, differing in affinity by approximately two orders of magnitude.

The interaction of the Ni(II) ion with chromosomes in intact nuclei was assessed utilizing UV/visible spectroscopy, resistance to nuclease digestion and electron microscopy. As monitored by spectroscopic techniques, the Ni(II) ion induced a chromosomal condensation which was nickel specific and observable even when Mg(II) ions were present in the buffer. Susceptibility to nuclease digestion decreased in a concentration-dependent manner following an incubation for 96 h with Ni(II). By contrast, no decrease was observed following incubations of 2 or 24 h duration. Ultrastructural changes in chromosome structure were also observed in electron micrographs for the longer exposures. Assessment of binding constants revealed the presence of two Ni(II) sites comparable

in affinity to those observed for simple DNA or polydeoxynucleotides. Only the binding to the weaker site was affected by the Mg(II) ion concentration in the buffer.

Molecular analysis of the AS52 cell line identified and characterized two independent sites of integration of a bacterial *gpt* gene insert. Sequence analysis revealed that the locus designated as the pseudogene (*gpt*$^-$) shared homology with the 5$^-$ and 3$^-$ ends of the *gpt* gene but also involved a unique insert, part of which derived from the β-lactamase gene of the parent transformation plasmid (pSV_2gpt). The pseudogene was not transcribed as deduced from reverse transcriptase (RT) PCR and Northern hybridization analysis. Analysis of nickel-generated mutants yielded three empirically distinct PCR profiles: 1) amplification of both the *gpt* and *gpt*$^-$ loci; 2) absence of the *gpt* band (no amplification); and 3) absence of both the *gpt* and *gpt*$^-$ bands. The overall mutation data demonstrated that nickel compounds are weak mutagens. Furthermore, when compared to spontaneous or EMS (ethyl methanesulphonate) induced mutants, those generated by exposing AS52 cells to nickel compounds exhibited an increase in apparent loci deletions relative to point mutations; the extent of which was compound specific: $NiSO_4$ (water soluble) > $Ni(OH)_2$ (relatively insoluble) > Ni_3S_2 (water-insoluble) = spontaneous > EMS. The latter (i.e., EMS) produced mainly point mutations as reported by other researchers. Preliminary

examination of mutants by Southern hybridization analysis corroborated these findings.

The illustrated ability of the Ni(II) ion to induce conformational changes in DNA and chromosomal condensations in nuclei, and its recognized capability of generating oxygen-derived chemicals clearly point to its potential involvement in epigenetic pathways of carcinogenesis. The confirmation by PCR analysis that nickel compounds are mutagenic and can induce point mutations and apparent loci deletions indicates that genotoxic mechanisms are also plausible.

ACKNOWLEDGEMENTS

I would like to thank the members of my committee, Drs. Calvin Harley, Richard Epand and Darrell Tomkins for their support and guidance throughout the course of this thesis. Appreciation is also expressed for the helpful discussions with Drs. Douglas Bryant and Del Harnish of McMaster University and Dr. Luigi Marzilli of Emory University. HUT cells were kindly supplied by Dr. Ken Rosenthal (McMaster University); AS52 cells and plasmid pSV_2gpt were supplied by Dr. Ken Tindall (US National Institute Environmental Health Sciences).

Thanks are extended to Mrs. Dawn Stetsko for help in the RNA extractions, Mr. Glenn Fletcher for advice and help in the culturing of AS52 cells, and Mrs. Wang Ping Li for technical assistance in the molecular biology portions of my work. Gratitude is also accorded to Dr. John Turnbull for lively discussions and the support and patience shown me as a colleague and employer. In appreciation of her unmatched organizational and word-processing skills, I extend a special thanks to Mrs. Lisa Stevens. Financial support from the Natural Sciences and Engineering Research Council of Canada, the International Lead Zinc Research Organization (ILZRO), the Nickel Producers Environmental Research Association (NiPERA), and in the form of an Ontario Graduate Scholarship is also gratefully acknowledged.

I am deeply indebted to Dr. Evert Nieboer for the initial opportunity to pursue my research goals under his tutelage with much freedom and independence. His continuing support, friendship and encouragement was crucial to the successful completion of my research and thesis.

Throughout the course of my graduate studies, numerous people were steadfast in their support of my efforts. To Robert and Dorrett James, Raji Menon, Alan Stafford and Len Rasile I would like to extend my heartfelt appreciation and thanks. Finally, I would like to express my extreme gratitude to Brigitte for her continuous and unwavering confidence in my abilities to complete this thesis. Without her support and partnership in this endeavour, I do not think this work would have been completed. For this and many other things, I am eternally grateful.

TABLE OF CONTENTS

	PAGE
TITLE PAGE	i
DESCRIPTIVE NOTE	ii
ABSTRACT	iii
ACKNOWLEDGEMENTS	vii
TABLE OF CONTENTS	ix
LIST OF FIGURES	xiii
LIST OF TABLES	xvii
LIST OF ABBREVIATIONS	xviii
I. INTRODUCTION	1
1. GENERAL OVERVIEW OF THESIS	1
2. SUMMARY OF NICKEL TOXICOLOGY	1
2.1 Exposure and Uptake	1
2.2 Carcinogenesis in Man and Animals	5
2.3 Genetic Toxicology	7
2.3.1 Objectives	7
2.3.2 Mutagenesis in Prokaryotic and Eukaryotic Cell Systems	8
2.3.3 Transformation of Cultured Mammalian Cells	10
2.3.4 DNA and Chromosomal Damage and Related Effects	11
2.4 Nickel Carcinogenesis: Mechanistic Implications	13
3. OTHER HEALTH EFFECTS ASSOCIATED WITH EXPOSURE TO NICKEL COMPOUNDS	15
4. CURRENT CONCEPTS IN THE MOLECULAR BIOLOGY OF CANCER	17
5. RESEARCH OBJECTIVES	19

II. Ni(II) INTERACTION WITH SYNTHETIC POLYDEOXY-NUCLEOTIDES AND DNA 21

1. INTRODUCTION 21

1.1 Overview 21
1.2 Specific Research Objectives 24

2. MATERIALS AND METHODS 24

2.1 Chemicals 24
2.2 Polydeoxynucleotide/DNA Solution Preparations 26
2.3 Metal-DNA Interaction 26
2.4 Generation of Metal-DNA UV Spectra and/or Absorbance Ratio Data 28
2.5 Optimization of the Ethidium Bromide Intercalation With Polydeoxynucleotides 29
2.6 Analysis of the Interaction of Ni(II) With Polydeoxynucleotides Utilizing Ethidium Bromide, Deoxyribonuclease I Susceptibiligy and Sedimentation Analysis 30
2.7 Circular Dichroism Investigation of Ni(II)-Polydeoxynucleotide 31
2.8 The Generation of Binding Dissociation for Ni(II)-Polydeoxynucleotide Interactions 32

3. RESULTS 33

3.1 UV Spectra and Absorbance Ratio Data 33
3.2 Optimization of the Interaction of Ethidium Bromide With Polydeoxynucleotides and DNA 54
3.3 Reproducibility of Absorbance Ratio and Ethidium Bromide Fluorescence Data 55
3.4 Analysis of the Interaction of Ni(II)-Ion With DNA and Polydeoxynucleotides 60
3.4.1 Calf Thymus DNA 60
3.4.2 Polyd(GC) -Polyd(GC) 67
3.4.3 PolydG -PolydC 77
3.4.4 Polyd(GT) -Polyd(AC) 85
3.4.5 Polyd(AT) -Polyd(AT) 99
3.4.6 PolydA -PolydT 100
3.5 Generation of Dissociation Constants for the Interaction of Ni(II) With DNA/Polydeoxy-nucleotides 113

4. DISCUSSION 118

III. Ni(II) INTERACTION WITH CHROMOSOMES IN INTACT NUCLEI 134

1. INTRODUCTION 134

1.1 Overview 134
1.2 Specific Research Objectives 137

2. MATERIALS AND METHODS 137

2.1 Chemicals and Reagents 137
2.2 Growth of Transformed Human T-Lymphocytes (HUT Cells) 140
2.3 Isolation of Nuclei 140
2.4 Quantitation of Nuclear DNA 141
2.5 Analysis of the Condensational State of Chromosomes in Intact Nuclei 142
2.6 Digestion of Nuclei With Nuclease 143
2.7 Analysis of Digested Chromosomes Utilizing Diaminobenzoic Acid (DABA) 144
2.8 Generation of Ni(II) Binding Constants for Chromosomes in Isolated Nuclei 145
2.9 Scanning Electron Microscopy of Ni(II) Exposed Nuclei 146

3. RESULTS 147

3.1 Condensation Analysis of Nuclear Chromosomes 147
3.2 Analysis of Nuclease Digested Chromosomes/DNA 152
3.2.1 Assay Characteristics 152
3.2.2 Digestion of Nuclear Chromosomes 152
3.3 Scanning Electron Micrographs of Nuclei Exposed to Ni(II)-Ion 162
3.4 Generation of Ni(II)-Binding Constants for Chromosomes in Nuclei 179

4. DISCUSSION 179

IV. INDUCTION AND ANALYSIS OF Ni(II)-MUTATIONS IN A CHO CELL LINE (AS52) 189

1. INTRODUCTION 189

1.1 Overview 189
1.2 Specific Research Objectives 192

2. MATERIALS AND METHODS 192

2.1 Chemicals and Reagents 192
2.2 AS52 Cells: Culturing and Mutagenicity Testing 196
2.2.1 Normal Cell Culture and Maintenance 196
2.2.2 Mutagenicity Testing 197
2.3 Isolation and Quantitation of Nucleic Acids (DNA, total RNA, mRNA) From Cultured AS52 Cells 198
2.3.1 Isolation of DNA for Molecular Analysis 198
2.3.2 Isolation of DNA for Polymerase Chain Reaction (PCR) Analysis 199
2.3.3 Isolation of Total RNA from Cultured AS52 Cells 199

2.3.4 Isolation of mRNA from Cultured AS52 Cells 201
2.3.5 Quantitation of RNA and DNA 203
2.4 Electrophoretic Analysis of DNA and RNA 204
2.4.1 DNA Agarose Gels 204
2.4.2 DNA Sequencing Gels 205
2.4.3 RNA Formaldehyde-Agarose Gels 206
2.5 Polymerase Chain Reaction (PCR) Methodology 207
2.5.1 PCR of DNA 207
2.5.2 Reverse Transcriptase (RT) PCR of RNA 207
2.5.3 DNA Sequencing Utilizing PCR Technology 210
2.6 Molecular Analysis of RNA and DNA 211
2.6.1 Southern Hybridization Analysis of DNA 211
2.6.2 Northern Hybridization Analysis of RNA 213

3. RESULTS 216

3.1 PCR Analysis of AS52 DNA 216
3.1.1 Genomic DNA 216
3.1.2 Sequencing of PCR Products 223
3.1.3 Analysis of RNA 228
3.2 AS52 Mutant Analysis 235

4. DISCUSSION 245

V. CONCLUDING REMARKS 256

VI. BIBLIOGRAPHY 261

VII. APPENDIX 287

1. LIST OF PUBLICATIONS 287
2. REPRINTS 290

LIST OF FIGURES

FIGURE		PAGE
1	UV Absorbance spectral scans of calf thymus DNA in the presence of Ni(II) ions	35
2	UV Absorbance spectral scans of polydG·polydC in the presence of Ni(II) ions	37
3	UV Absorbance spectral scans of polyd(GT)·polyd(AC) in the presence of Ni(II) ions	39
4	UV Absorbance spectral scans of polyd(GC)·polyd(GC) in the presence of Ni(II) ions	41
5	UV Absorbance spectral scans of polyd(AT)·polyd(AT) in the presence of Ni(II) ions	43
6	UV Absorbance spectral scans of polydA·polydT in the presence of Ni(II) ions	45
7	Absorbance ratio ($A_{295/260}$) data of calf thymus DNA and various polydeoxynucleotides in the presence of increasing Ni(II) ion	49
8	Absorbance ratio ($A_{290/260}$) data of various polydeoxynucleotides in the presence of increasing Ni(II) ion	51
9	Ethidium bromide fluorescence following intercalation into DNA and polydeoxynucleotides as a function of solution pH and EDTA	53
10	Reproducibility of absorbance ratio ($A_{295/260}$) data of polyd(GC)·polyd(GC) in the presence of increasing amounts of Ni(II) ion	57
11	Reproducibility of ethidium bromide fluorescence following intercalation into polyd(GC)·polyd(GC) in the presence of EDTA and increasing amounts of Ni(II) ion	59
12	Absorbance ratio ($A_{295/260}$), EtBr fluorescence and DNase I digestion susceptibility profiles of calf thymus DNA in the presence of increasing amounts of Ni(II) ion	62
13	Sedimentation analysis of calf thymus DNA in the presence of increasing amounts of Ni(II) ion	64

FIGURE		PAGE
14	Circular dichroism (CD) scans of calf thymus DNA in the presence of Ni(II)	66
15	Absorbance ratio ($A_{295/260}$), EtBr fluorescence and DNase I digestion susceptibility profiles of polyd(GC)·polyd(GC) in the presence of increasing amounts of Ni(II) ion	70
16	Absorbance ratio ($A_{295/260}$) and sedimentation analysis of polyd(GC)·polyd(GC) in the presence of increasing amounts of Ni(II) ion	72
17	Circular dichroism (CD) scans of polyd(GC)·polyd(GC) in the presence of Ni(II)	74
18	Circular dichroism (CD) scans of poled(GC)·polyd(GC) in the presence of Ni(II) ion following incubation at different temperatures for 24 h	76
19	Absorbance ratio ($A_{295/260}$), EtBr fluorescence and DNase I digestion susceptibility profiles of polydG·polydC in the presence of increasing amounts of Ni(II) ion	80
20	Sedimentation analysis of polydG·polydC in the presence of increasing amounts of Ni(II) ion	82
21	Circular dichroism (CD) scans of polydG·polydC in the presence of Ni(II) ion	84
22	Absorbance ratio ($A_{295/260}$), EtBr fluorescence and DNase I digestion susceptibility profiles of polyd(GT)·polyd(AC) in the presence of increasing amounts of Ni(II) ion	88
23	Sedimentation analysis of polyd(GT)·polyd(AC) in the presence of increasing amounts of Ni(II) ion	90
24	Circular dichroism (CD) scans of polyd(GT)·polyd(AC) in the presence of Ni(II)	92
25	Absorbance ratio ($A_{295/260}$), EtBr fluorescence and DNase I digestion susceptibility profiles of polyd(GT)·polyd(AC) in the presence of increasing amounts of Ni(II) ion following incubation at 64°C	94
26	Absorbance ratio ($A_{295/260}$) and sedimentation analysis of polyd(GT)·polyd(AC) in the presence of increasing amounts of Ni(II) ion following incubation at 64°C	96
27	Circular dichroism (CD) scans of polyd(GT)·polyd(AC) in the presence of Ni(II) ion following incubation at 64°C	98

FIGURE		PAGE
28	Absorbance ratio ($A_{290/260}$), EtBr fluorescence and DNase I digestion susceptibility profiles of polyd(AT)·polyd(AT) in the presence of increasing amounts of Ni(II) ion	102
29	Sedimentation analysis of polyd(AT)·polyd(AT) in the presence of increasing amounts of Ni(II) ion	104
30	Circular dichroism (CD) scans of polyd(AT)·polyd(AT) in the presence of Ni(II)	106
31	Absorbance ratio ($A_{290/260}$), EtBr fluorescence and DNase I digestion susceptibility profiles of polydA·polydT in the presence of increasing amounts of Ni(II) ion	108
32	Sedimentation analysis of polydA·polydT in the presence of increasing amounts of Ni(II) ion	110
33	Circular dichroism (CD) scans of polydA·polydT in the presence of Ni(II)	112
34	Scatchard plot analysis of the binding of Ni(II) ion with *M. lysodeikticus* DNA	116
35	Illustration of Ni(II)-induced condensation of chromosomes in intact nuclei	149
36	Condensation analysis of chromosomes in the presence of varying amounts of Mg(II)	151
37	Representative standard curve of the DABA assay	154
38	Nuclease digestion of chromosomes in the presence of varying amounts of Ni(II)	157
39	Nuclease digestion of chromosomes following a 24 h incubation in the presence of varying amounts of Ni(II)	159
40	Nuclease digestion of chromosomes following a 96 h incubation in the presence of varying amounts of Ni(II)	161
41	Scanning electron micrographs (x8000) of nuclei exposed to Ni(II) for 2 h	164-8
42	Scanning electron micrographs (x25000) of nuclei exposed to Ni(II) for 24 h	170-4
43	Scanning electron micrographs (x18600) of nuclei exposed to Ni(II) for 96 h	176-8

FIGURE		PAGE
44	Scatchard analysis of Ni(II)-binding to nuclear chromosomes	181
45	Diagram of bacterial inserts of the AS52 cell line	218
46	PCR analysis of AS52 DNA utilizing primers #1 and #2	219
47	PCR analysis of AS52 DNA utilizing primers #3 and #4	220
48	Nested primer PCR analysis of fragments generated by primers #1 and #2	221
49	Sequence of the *gpt* locus of the AS52 cell line	224
50	Sequence of the *gpt* pseudogene (*gpt'*) locus of the AS52 cell line	225
51	Sequence comparison of the *gpt* pseudogene (*gpt'*) to that of β-lactamase, the ampicillum resistance gene of bacteria	227
52	Analysis of RNA (total and messenger) from the AS52 cell line using reverse transcriptase (RT)-PCR	231
53	Generation of biotinylated PCR products to be used as probes for Northern hybridization analysis	232
54	Autoradiograms of mRNA analyzed via Northern hybridization analysis	234
55	PCR analysis of AS52 mutant DNA using primers #1 and #2	237
56	PCR analysis of AS52 mutant DNA using primers #3 and #4	239
57	PCR analysis of AS52 mutant DNA using primers P_1 and P_2	241
58	Representative autoradiogram of Southern hybridization analysis of AS52 mutants	244

LIST OF TABLES

TABLE		PAGE
1	Chemicals and Reagents (Chapter II)	25
2	Polydeoxynucleotides and DNAs	27
3	Separation and Recovery of DNA and Free Nickel Ion By Ultrafiltration (Control Sample)	114
4	Nickel Dissociation Constants for DNAs or Polydeoxynucleotides	117
5	Chemicals and Reagents (Chapter III)	138-9
6	Control Responses of Deoxynucleotides With DABA	155
7	Nickel Dissociation Constants for Chromosomes of Intact Nuclei in the Presence of Mg(II)	182
8	Chemicals, Reagents and Kits (Chapter IV)	193-5
9	Primers	208
10	Summary of Mutants Analyzed	242

LIST OF ABBREVIATIONS

$A_{290/260}$: quotient of absorbances at 290 nm and 260 nm

$A_{295/260}$: quotient of absorbances at 295 nm and 260 nm

bp: base pair

CD: circular dichroism

cDNA: complementary single stranded DNA

CHO: Chinese hamster ovary

DDI: doubly deionized distilled water

ddNTP: dideoxynucleotides

dFBS: dialyzed fetal bovine serum

DNaseI: deoxyribonuclease I

dNTP: deoxynucleotides

EMS: ethylmethylsulfonic acid

EtBr: ethidium bromide

gpt: guanine phosphoribosyl transferase

HPRT: hypoxanthine-guanine phosphoribosyl transferase

KD: binding dissociation constant

$p(dN)_6$: oligodeoxynucleotide of 6 random deoxynucleotides

PCR: polymerase chain reaction

polydA·polydT: duplex polydeoxynucleotide of adenine and thymidine

polyd(AC)·polyd(GT): duplex polydeoxynucleotide of alternating guanine/thymidine and adenine/cytosine

polyd(AT)·polyd(AT): duplex polydeoxynucleotide of alternating adenine and thymidine

polydG·polydC: duplex polydeoxynucleotides of guanine and cytosine

polyd(GC)·polyd(GC): duplex polydeoxynucleotides of alternating guanine and cytosine

RNase: ribonuclease

RT: reverse transcriptase

SD: standard deviation

SEM: scanning electron microscopy

TK: thymidine kinase

UV: ultraviolet

XPRT: xanthine phosphoribosyl transferase

I. INTRODUCTION

I.1 GENERAL OVERVIEW OF THESIS

This thesis is divided into five chapters (I-IV). Chapter I consists of a concise overview of nickel toxicology with an emphasis on genetic toxicology. Chapters II to IV encompass original experimental details and results. Each experimental chapter opens with a brief introductory section addressing the topics specific to that chapter. This is followed by sections describing in detail the methodology, results, and conclusions. Chapter II describes an investigation of the interaction of the Ni(II) ion with polydeoxynucleotides and DNA; Chapter III, the interaction of Ni(II) ions with chromosomes in nuclei; and Chapter IV, the generation and molecular analysis of mutants generated in cultured AS52 Chinese hamster ovary (CHO) cells. In Chapter V, the results obtained and conclusions reached are discussed within the context of recent developments in nickel genotoxicology.

I.2 SUMMARY OF NICKEL TOXICOLOGY

I.2.1 Exposure and Uptake

The systematic study of the toxicity of nickel compounds began in the early 1960s. The catalysts for this development

were the discovery in 1939 of excess lung and nasal cancers among workers of the Mond Nickel Company, Clydach, Wales, U.K. (Morgan, 1958), and the frequent reports of human poisoning and death after inhalation of nickel tetracarbonyl (Sunderman, Jr., *et al.*, 1975).

Non-occupational ambient nickel concentrations are low (e.g. 0.008 $\mu g/m^3$ was the 1982 US average; EPA, 1986). The major contribution to atmospheric nickel originates from the combustion of fossil fuels, with nickel sulfate (water-soluble), nickel oxide, and complex metal oxides containing nickel the predominant forms (EPA, 1986). Occupational exposure to nickel compounds is strongly dependent on the industrial processes considered (Morgan, 1979; Warner, 1984; Mastromatteo, 1986; Nieboer, 1992). In electroplating shops and electrorefining plants, exposure is to aerosols of dissolved nickel salts; ambient nickel concentrations of up to 0.2 mg/m^3 have been reported. Exposures associated with pyrometallurgical refining processes are to nickel oxides and sulfides, as well as to nickel powder as the final product of secondary refining; ambient nickel concentrations are known to exceed 1 mg/m^3 although values of 0.2 mg/m^3 are typical (Warner, 1984; Nieboer *et al.*, 1984; Sunderman, Jr., 1986; Mastromatteo, 1986; Doll, 1990).

Inhalation and ingestion constitute the major routes of nickel uptake in humans (Nieboer *et al.*, 1992; Nieboer and Fletcher, 1993a). Although dermal uptake is insignificant by

comparison, dermal penetration of the Ni(II) ion is paramount in nickel contact dermatitis. Other parenteral routes are of importance to humans only in isolated situations (e.g., hemodialysis, intravenous fluids, prosthetics) although they are common in animal experimental work (e.g., intravenous, intraperitoneal, intramuscular, and intrarenal injections; subcutaneous implants, etc.). Within the occupational setting, inhalation is the primary route; within the general population ingestion is the typical route of exposure.

The primary determinant of the site of nickel particle deposition in the respiratory tract is particle size (Higgins, 1979). In general, but dependent on the ventilatory rate, particles smaller than 10 μm in aerodynamic diameter penetrate the alveolar region of the lung and constitute the respirable fraction (maximum deposition is estimated as 50%, which occurs for particulates with aerodynamic diameters in the 3-5 μm range); particles larger than 0.1 μm deposit in the nasal passages (deposition is estimated to approach 100% for diameters > 10 μm); and particles larger and smaller than 0.5 μm deposit in the tracheobronchial airways (deposition estimates range from 25 to 5%, respectively). Nickel-containing particulates in ambient air and occupational environments typically have diameters below 50 μm, with a significant fraction possessing diameters smaller than 10 to 15 μm (EPA, 1986). Water solubility is an important determinant for the retention of nickel compounds in the

respiratory tract (WHO, 1991). In the respiratory tract, mucociliary clearance competes with direct absorption (after dissolution in case of particulate compounds). By comparison, a range of 14 days to >11 years has been determined for the *in vitro* solubility of particulate nickel compounds in rat renal cytosol, rat serum, and water respectively (Kuehn and Sunderman, Jr., 1982). In humans, typical half-times for elimination from plasma into urine for occupational exposure to water-soluble nickel compounds (exposure mainly by inhalation) are 15 to 40 hours (Tossavainen *et al.*, 1980; Nieboer *et al.*, 1988). A removal half-time of nickel from nasal mucosal tissue of retired nickel refinery workers of 3-4 years has been reported (Torjussen and Andersen, 1979). This is comparable to the removal half-time of nickel from plasma and urine determined in this same study group (Boysen *et al.*, 1982). By comparison, a determination of nickel in nasal biopsies or autopsy lung specimens of nickel workers has clearly indicated an elevated level of nickel (Torjussen and Andersen, 1979; Andersen and Svenes, 1989).

Daily dietary nickel intake from normal diets averages approximately 150 µg; the precise value is dependent on age and country of residence (Nielsen and Flyvhom, 1984; Veien and Andersen, 1986; Pennington and Jones, 1987; Smart and Sherlock, 1987; Nieboer and Fletcher, 1993a). Higher daily intakes are readily achieved with diets containing sources of food naturally rich in nickel such as cocoa, soya products,

nuts (walnut, peanut, hazelnut, almond), oats, buckwheat, oatmeal, bitter chocolate, and dried legumes (Nielsen, 1992). Furthermore, nickel may also be leached from ordinary kitchen utensils during food preparation (Grandjean *et al.*, 1989).

I.2.2 Carcinogenesis In Man and Animals

Nickel-related human cancer constitutes an industrial disease. It is virtually restricted to the nickel-producing industry and is largely historical (Doll, 1984). Recently, an *International Committee on Nickel Carcinogenesis in Man* chaired by Sir Richard Doll has reviewed all the available epidemiological data on human nickel exposures in an attempt at defining forms of nickel associated with increases in cancer of the lung and nasal sinuses (Doll, 1990). This study concluded that increases in respiratory cancer incidence were primarily related to exposures to soluble nickel at concentrations exceeding 1 mg Ni/m^3; whereas less soluble forms of nickel (e.g. oxides and sulfides) induced cancers following exposure to considerably higher nickel levels, namely >10 mg/m^3. Nickel metal itself was not associated with an increased cancer risk. Furthermore, the latency period (i.e. time between first exposure and the clinical manifestation of the tumour) was long, typically greater than 15 years. The evidence on which these conclusions are based derives from the experience of workers in numerous industrial settings worldwide. These locals include: Kristiansand,

Norway (roasting, smelting, calcining departments); Clydach, U.K. (matte roasting, leaching, drying operations); Copper Cliff and Coniston, Canada (sinter operation); and Port Colborne, Canada (leaching, calcining, sintering departments). Although isolated exposures to nickel sulfides were not reported, some of the highest risks of lung and nasal cancers were observed in departments where exposure to nickel sulfides was very high. Concurrently, exposure to nickel oxides were also high in these workplaces. The implication of water-soluble nickel salts (i.e. chlorides or sulfates) as carcinogens (or cocarcinogens) received support from the data derived from electrolysis workers at Kristiansand and from the hydrometallurgical plant at Clydach. The indications were that these latter soluble salts accentuated the risks associated with exposure to the relative insoluble, particulate forms of nickel.

The carcinogenicity of nickel salts and compounds in animals has been extensively studied and reviewed (e.g., IARC, 1990; WHO, 1991; Kasprzak, 1992). One must qualify any conclusions from these reviewed studies by acknowledging that exposures to nickel compounds involved some form of injection as the administration route. The relationship of injection-site-only tumors to human carcinogenic hazards resulting from inhalation exposure is uncertain. Nevertheless, significant numbers of lung carcinomas were induced in rats following intratracheal instillation of metallic nickel in rats.

Subcutaneous administration of nickel pellets or nickel-gallium alloy also produced sarcomas. Intratracheal instillation of nickel oxides and hydroxides in rats produced lung carcinomas; injection experiments were also generally positive for both the monoxide and hydroxide of nickel. Repeated injection studies with nickel chloride, sulfate or acetate may be termed equivocal, with positive results (abdominal cancers) limited to intraperitoneal injection in mice and/or rats. The most compelling evidence for nickel compound carcinogenesis exists for the family of relatively insoluble, particulate nickel sulfides. Both inhalation and multiple intratracheal exposures to nickel subsulfide (Ni_3S_2) were positive in both rats and mice. Administration by a variety of injection routes have also been overwhelmingly positive for the induction of local tumors. Studies with nickel disulfide (NiS_2), crystalline monosulfide (NiS) and nickel ferrosulfide matte also produced injection-site tumors.

I.2.3 Genetic Toxicology

I.2.3.1 Objectives

The following subsections address and attempt to summarize the known genotoxic effects of nickel. While this area of scientific investigation is characterized by many documented reports of genotoxicity, there does exist a certain amount of overlap and redundancy. An attempt has been made to summarize the most salient and innovative aspects of this

research, and the coverage is therefore not intended to be exhaustive. Additional details are presented in the individual Chapters.

I.2.3.2 Mutagenesis in Prokaryotic and Eukaryotic Cell Systems

The induction of mutations by water-soluble Ni(II) salts in prokaryotic systems has been mostly, but not entirely, negative (e.g. for the bacteria *Salmonella typhimurium* (Arlauskas *et al.*, 1985; Biggart and Costa, 1986), *Bacillus subtilis* (Kanematsu *et al.*, 1980), and *Escherichia coli* (Green *et al.*, 1976)). A dose-dependent response has been reported for *Corynebacterium* (Pikálek and Nečásek, 1983). It has been suggested that the negative responses in short-term tests result from an absence of bacterial uptake of Ni(II) due to complex formation with components of the culture medium (Heck and Costa, 1982; Arlauskas *et al.*, 1985). The association and internalization of Ni(II) by both *Pseudomonas tabaci* and *Salmonella* has been confirmed, thus arguing against this hypothesis (Al-Rabee and Sigee, 1984; Biggart and Costa, 1986). DNA damaging agents in *E. coli* and *Salmonella* induce a pleiotropic response known as the "SOS" system (Radman, 1974; Witkin, 1976). One of the experimental "SOS" responses, the induction of lysogenic phages (e.g. λ prophage), has been adopted as a bioassay for genetic damage. In a limited investigation of Ni(II) ion (i.e. $Ni(OOCCH_3)_2$ salt), this metal

ion induced an 8-fold increase in response by comparison to background levels in the induction of λ prophage (Rossman *et al.*, 1984).

Positive mutagenic responses for soluble and/or particulate nickel compounds have been observed in a limited number of eukaryotic cell systems, for example the yeast *Saccharomyces cerevisiae* D7 (Singh, 1983; Singh, 1984), mouse lymphoma L5178Y cells (Amacher and Paillet, 1980), Chinese hamster V79 cells (Miyaki *et al.*, 1979), and mouse FM3A cells (Morita *et al.*, 1991). Conflicting information has been obtained using *Drosophilia melanogaster* although different genetic endpoints were examined in the respective assays (Rasmusan, 1985; Rodriguez-Arnaiz and Ramos, 1986). More recently, genetically engineered Chinese hamster cell lines utilizing incorporated bacterial genes as mutagenesis targets have been described and proven useful in recovering nickel-induced mutations (see Chapter IV; Kargacin *et al.*, 1983; Lee *et al.*, 1993; Fletcher *et al.*, 1993). Murphy and coworkers have described a murine sarcoma virus (MuSV)-based mutagenicity assay in which mutations targeted to v-mos expression can be selected in which nickel chloride was positive (De Mars *et al.*, 1990; Chiocca *et al.*, 1991). Oncogene (specifically K-ras) involvement in nickel mutagenesis and transformation (see Section I.5) has been suggested by mutations observed in rat renal sarcomas (Higinbotham *et al.*, 1992). Similarly, an analogous

involvement of a role for suppressor genes (e.g., p53) has been suggested for mutations induced in transformed primary human kidney epithelial cells (Maehle *et al.*, 1992). Several studies have shown that the co-genotoxicity of some metals may be important in metal carcinogenesis. Nickel ions have been shown to enhance the UV-induced cytotoxicity, mutagenicity, and sister-chromatid exchanges in Chinese hamster V79 cells (Hartwig and Beyersmann, 1987,1989). Moreover, it has also been demonstrated that nickel inhibits the DNA repair of UV-treated Chinese hamster ovary cells (i.e. CHO-K1; Snyder *et al.*, 1989; Lee-Chen *et al.*, 1993).

I.2.3.3 Transformation of Cultured Mammalian Cells

The transforming potential of nickel compounds in a variety of mammalian cells has been clearly established. Both crystalline (e.g., Ni_3S_2) and soluble nickel (e.g. $NiSO_4$) compounds have been utilized in the transformation of Syrian hamster embryo (SHE), baby hamster kidney (BHK), and mouse embryo fibroblasts (C3H/10T½; reviewed in Nieboer *et al.*, 1988). Work with primary cell lines has provided some interesting observations on the transformation potential of nickel compounds. It is noteworthy that both soluble and insoluble particulate nickel compounds do not fully transform primary cells' such as human diploid foreskin fibroblasts, human bronchial and/or kidney epithelial cells but elicit progenitors which display some characteristics of the

transformed state such as increased population doubling potentials, reduced requirement for growth hormones, etc. (Lechner *et al.*, 1984; Biedermann and Landolph, 1987; Tveito *et al.*, 1989). In fact, Haugen and coworkers have transformed such "immortalized" kidney epithelial cells to tumorigenicity in nude mice by the introduction of a viral Ha-ras oncogene into the kidney cells (Haugen *et al.*, 1989). Interestingly, an examination of a clonally-derived line arising from these transformed kidney cells demonstrated that a suppressor gene (specifically p53) was mutated possibly as a result of nickel "immortalization" (Maehle *et al.*, 1992). This gene has been implicated in normal cell proliferation and neoplastic transformation (Cooper, 1990).

I.2.3.4 DNA and Chromosomal Damage and Related Effects

Studies with cultured cells and biochemical studies have demonstrated that nickel compounds detrimentally affect chromosomes, DNA, DNA synthesis, and transcription. One of the effects observed is the induction in CHO cells of DNA strand breaks by $NiCl_2$ and crystalline NiS or Ni_3S_2 (Robison and Costa, 1982; Robison *et al.*, 1982; Patierno and Costa, 1987). Both soluble and particulate nickel compounds induced sister chromatid exchanges (SCEs) in CHO cells (Sen and Costa, 1986), and in cultured human lymphocytes (Saxholm *et al.*, 1981; Larramendy *et al.*, 1981; Newman *et al.*, 1982; Arrouijal *et al.*, 1990; Arrouijal *et al.*, 1992), as well as chromosomal

aberrations in FM3A murine carcinoma cells (Nishimura and Umeda, 1979). In addition, a blockage of CHO cell growth in S phase following exposure to nickel compounds has also been demonstrated (Costa *et al.*, 1982; Conway *et al.*, 1986). Other effects at the genetic level include an induction of DNA repair synthesis in CHO cells by $NiCl_2$ and crystalline NiS (Robison *et al.*, 1983); reduction by Ni(II) in the fidelity of DNA synthesis (Sirover and Loeb, 1976; Loeb and Mildvan, 1981); and weak inhibition by Ni(II) and a slight loss of fidelity in RNA transcription (Niyogi *et al.*, 1981; Niyogi and Feldman, 1981). An apparent chromosome-length shortening following exposure to $NiSO_4$ has been demonstrated in cultured human peripheral lymphocytes (Andersen, 1985). One of the most striking characteristics of the interaction of nickel with chromosomal DNA is the preferential induction of damage to heterochromatic regions (Sen and Costa, 1985; Sen *et al.*, 1987; Patierno *et al.*, 1987).

A number of comments about, or relevant to, the reviewed genotoxic effects are warranted. (1) The water-soluble salts are surprisingly genotoxic when compared with crystalline particulate compounds (see next section for an examination of the implications of this observation). (2) Both histones and nonhistone protein have been implicated in the binding of nickel to chromatin *in vitro* (Patierno *et al.*, 1985; Ciccarelli and Wetterhahn, 1985) or *in vivo* (Ciccarelli and Wetterhahn, 1984). (3) As previously mentioned, nickel prefers

to associate with heterochromatin rather than euchromatin. (4) Single-strand breaks, DNA-protein crosslinks, and DNA interstrand crosslinks have also been induced in rat tissues following intraperitoneal injection of nickel compounds (Ciccarelli and Wetterhahn, 1982). (5) Nickel is a weak mutagen in comparison to other genotoxins. (6) Lastly, an increased level of chromosomal gaps, breaks, or sister chromatid exchanges (SCEs) have been observed for workers employed or retired from a nickel refinery (Waksvik and Boysen, 1982; Waksvik *et al.*, 1984; Gennart *et al.*, 1993). Obviously, the genotoxic potential of nickel compounds is self-evident. Not as clear is the relevance of any (or all) of these effects on the distinct pathways or processes of nickel toxicity, mutagenicity or carcinogenicity.

I.2.4 Nickel Carcinogenesis: Mechanistic Implications

The collective evidence derived from *in vitro* genotoxicity, animal and human carcinogenicity data can be interpreted to indicate that the Ni(II) ion is the putative agent - the ultimate carcinogen. This statement is central to the "Nickel Ion Hypothesis" of nickel genotoxicity and carcinogenicity. This hypothesis maintains that the Ni(II) ion is the active agent in nickel toxicity, mutagenesis and carcinogenesis and that its intracellular concentration and compartmentalization are major determinants, irrespective of the nickel compound to which the organism is exposed. It is

of interest therefore to review this hypothesis and its ramifications and limitations.

Both animal carcinogenicity and human epidemiological data clearly indicate that solid nickel compounds differ in carcinogenic potential. Certain properties of nickel compounds such as particle size, crystallinity, surface charge, and solubilization kinetics are believed to determine respiratory deposition and clearance *in vivo*, as well as cellular uptake *in vitro*; they are said to determine the bioavailability of Ni(II) (reviewed in: Nieboer *et al.*, 1986; Nieboer *et al.*, 1988; Costa, 1991). Endogenous ligands at physiologic concentrations bind Ni(II) tightly and facilitate its mobilization, transport and subsequent renal excretion. Presumably, extracellular and intracellular pools of particulate nickel compounds in the lung and nasal tissues overwhelm clearance processes and thus provide a continuous inward cellular flux of Ni(II). A half-life of 3-4 years has been assigned to such particulate pools in retired workers; by contrast, the clearance of water soluble salts is more rapid (half-lives of 1-2 days in humans). Consequently, the probability of intracellular accumulation of Ni(II) in individuals exposed to water-soluble salts is lowered, as is presumably the opportunity to express fully its carcinogenic potential. Potency differences are also implied by the epidemiologic data. As previously discussed, the highest cancer risk is associated with exposure to refinery dust

composed of solid nickel oxides and sulfides of relatively low solubility.

From this overview it may be concluded that the "nickel ion hypothesis" predicts a range of carcinogenic potencies for nickel compounds. Thus, the observed effects will depend on a number of physicochemical properties of nickel compounds, their biological residence time, the magnitude of pools built up in exposed organs, and the effective intracellular load of Ni(II) in affected tissue. It is obvious that the "Nickel Ion Hypothesis" as stated leaves a number of unresolved issues in nickel carcinogenesis which severely limit the understanding of this process. Namely, (1) there is a lack of understanding concerning the dynamics of nickel compounds in the body; and (2), the precise events at the molecular level involving Ni(II) that induce mutation and/or affect gene expression relevant to the carcinogenic process are poorly understood.

I.3 OTHER HEALTH EFFECTS ASSOCIATED WITH EXPOSURE TO NICKEL COMPOUNDS

A rather uniform prevalence of nickel dermatitis (7-10% in females, 1-2% in males) has been noted in worldwide population studies (Grandjean *et al.*, 1989). In dermatological clinics 10-20% of females react to nickel, compared to 2-10% of males. The majority of these patients are exposed to non-occupational sources of nickel, primarily resulting from the leaching of nickel from inexpensive

earrings, other jewellery or wrist watches. Ear piercing is also a recognized determinant. Nevertheless, occupation-related nickel dermatitis is a common diagnosis in reports of permanent disability involving skin diseases (Grandjean *et al.*, 1989).

Nickel-related asthma is a rare phenomenon, although periodic case reports and case series studies arising from occupational settings have been reported since 1973 (reviewed in Nieboer and Fletcher, 1993b). In all cases exposures were to aerosols of nickel(II) salt solutions. As for other respiratory allergens, three types of responses are observed. The first is an immediate response with the development of bronchoconstriction in minutes which is reversible with bronchodilators and appears to be antibody mediated. The second corresponds to a late response typically occurring 2-12 hours after exposure which may not be completely reversed with bronchodilators and appears to involve inflammatory processes. The third type is dual, characterized by both the immediate and late responses occurring in the same individual.

Reproductive and developmental effects in humans have not been reported in conjunction with exposure to nickel compounds until very recently (Clarkson *et al.*, 1985; WHO, 1991). In a preliminary and qualitative report, Chashchin *et al.* (1993) have expressed concern about apparent increases in spontaneous abortions and structural malformations (especially cardiovascular and musculoskeletal defects) in new-born babies

whose mothers were employed in Russian nickel refineries. Analogous effects in animals are much better documented (Sunderman *et al.*, 1983; Clarkson *et al.*, 1985; Nieboer *et al.*, 1988). Toxicity to both spermatozoa and embryos has been noted. Nickel is known to cross the placenta in rodents, with malformations at birth including ocular, skeletal and neuronal defects. Experiments with nickel tetracarbonyl provide the clearest indication of teratogenicity (Sunderman *et al.*, 1979, 1980). Chloride salts of Ni^{2+} (like those of Co^{2+}, Zn^{2+}, and Cd^{2+}) have been shown to be embryotoxic and teratogenic in the FETAX Assay (Frog Embryo Teratogenesis Assay: *Xenopus*) (Luo *et al.*, 1993).

Nickel compounds possess low nephrotoxicity in humans. In a survey of electrolytic refinery workers, Sanford and Nieboer (1992) found no evidence of renal toxicity based on clinical chemistry indices including the measurement of total protein and β_2-microglobulin in urine, creatinine clearances, and dipstick tests of urines for ketones, bilirubin, glucose, nitrite, blood, urobilinogen and protein. By contrast, evidence of nickel-induced nephropathy is stronger in animals (see Sanford and Nieboer, 1992).

I.4 CURRENT CONCEPTS IN THE MOLECULAR BIOLOGY OF CANCER

As already implied by the discussion in Section I.2.3.2, molecular mechanisms of nickel carcinogenesis overlap the current and mainstream concepts in the molecular biology of

cancer. A brief summary of the latter is presented in this section. Most tumours, whether benign or malignant, are clonal in origin. The process of tumourigenesis is considered to consist of a number of stages (Weinberg, 1989; Harris, 1991). Each stage involves a genetic alteration at the gene or chromosomal level (Cooper, 1990). Traditionally, the main steps in chemical carcinogenesis have been postulated to be initiation, promotion, and progression. The current model of colorectal cancer consists of six steps including metastasis (Fearon and Vogelstein, 1990). Indeed, a multistage model is consistent with epidemiological studies of respiratory cancers arising from exposure to nickel compounds (Kaldor *et al.*, 1986). At the molecular level, oncogenes are capable of inducing one or more aspects of the neoplastic phenotype, while suppressor genes are normal cellular genes whose loss of function leads to the same outcome. Oncogenes are dominant, while suppressor genes are functionally recessive since both homologous copies must be inactivated (Cooper, 1990; Fearon and Vogelstein, 1990). Oncogenes represent abnormally expressed (e.g., through amplification or transposition) or mutated forms (e.g., point mutations or deletions) of proto-oncogenes (i.e., the normal cellular homologue). Two general categories of chemical carcinogens have been identified, namely genotoxic and nongenotoxic (epigenetic) agents (Perera, 1991). Tumour promoters are assigned to the latter category and appear to increase expression of genes related to cell

proliferation. Interestingly, it has recently been pointed out that such enhanced expression may indirectly be responsible for increased chromosomal aberrations and point mutations (Rahmsdorf and Herrlich, 1990).

I.5 RESEARCH OBJECTIVES

The mechanisms of nickel carcinogenesis are not well understood. Earlier it was pointed out (Section I.2.3, I.2.4) that both water soluble and particulate nickel compounds are considered to be carcinogenic to humans, but they are virtually nonmutagenic in bacterial systems and only weakly so in mammalian cell cultures. It is our hypothesis that nickel compounds can interact with DNA by both genotoxic and nongenotoxic pathways. Within the multistep genetic model of cancer, the nongenotoxic processes would correspond to epigenetic or promotional effects regulating gene expression, while the genotoxic responses involve gene or chromosomal mutations (Weinberg, 1989; Harris, 1991; Perera, 1991; Cooper, 1990; Ashby and Purchase, 1992). The experimental approach adopted to seek corroborating evidence involved an initial examination of the effects of Ni(II) ion on simple DNA or polydeoxynucleotides of defined sequence and base composition. The second component investigated the interaction of Ni(II) ion with chromosomes in intact nuclei. A final component assessed the genotoxic effects of soluble (i.e. $NiSO_4$) and insoluble nickel compounds (i.e. Ni_3S_2, $Ni(OH)_2$) in a mammalian

cell line (AS52) by the characterization of damage induced at a specific gene locus. Through the utilization of increasingly more complex states of DNA, basic and fundamental principles of Ni-DNA interaction were to be identified and assessed.

II. Ni(II) INTERACTION WITH SYNTHETIC POLYDEOXYNUCLEOTIDES AND DNA

II.1 INTRODUCTION

II.1.1 Overview

DNA is able to adopt a number of double helical conformations, the most common being the right-handed A, B, C types, and the left-handed Z type (Tunis-Schneider and Maestre, 1970; Leslie *et al.*, 1980; Dickerson *et al.*, 1982a,b; Dickerson, 1983; Rich *et al.*, 1984; Jovin *et al.*, 1987; Paleček, 1991; Cheng and Pettitt, 1992). Variations of helical parameters such as helical twist, rise per base pair, base inclination, propeller twist and base roll indicate that within these helical families resides a degree of structural flexibility and heterogeneity (Leslie *et al.*, 1980; Dickerson *et al.*, 1982a,b; Dickerson, 1983; Paleček, 1991; Cheng and Pettitt, 1992). Transitions between helical conformations are facilitated by a variety of environmental factors, such as mono- and divalent ions, changes in helix hydration, base modification or binding, and stabilization into regions of supercoiling (reviewed in: Rich *et al.*, 1984; Jovin *et al.*, 1987; Paleček, 1991; Cheng and Pettitt, 1992).

In addition to simple helices, DNA can adopt a variety of ternary or quaternary higher order structures in the presence of multivalent cations (e.g. di/trivalent metals, spermidine^{3+}), neutral or anionic polymers and/or organic solvents. These structures consist of inter- or intra-molecularly collapsed, condensed or aggregated DNA molecules (toroids, rods, spheres; e.g. ψ form) and other types which may be devoid of helical content (e.g. P form) (Jordan *et al.*, 1972; Lerman, 1974; Shin and Eichhorn, 1977; Walter and Luck, 1977; Gosule and Schellman, 1978 Widom and Baldwin, 1980; Zehfus and Johnson, 1981; Castleman and Erlanger, 1982; Eichhorn *et al.*, 1982; Zacharias *et al.*, 1983; Zehfus and Johnson, 1984; Shin *et al.*, 1986; Shin *et al.*, 1988). More recently, triplet strands of DNA (H form) have posed a certain intellectual and experimental challenge (Lyamichev *et al.*, 1987; Kohwi and Kohwi-Shigematsu, 1988; Sen and Gilbert, 1988; Htun and Dahlbert, 1989; Kohwi, 1989; Lyamichev *et al.*, 1989; Panyutin *et al.*, 1989; Bernues *et al.*, 1990; Campos and Subirana, 1991; Kohwi-Shigematsu and Kohwi, 1991; Paleček, 1991; Yagil, 1991: Cheng and Pettitt, 1992).

A common feature of both helical and tertiary or quaternary structural transition is the ability of metal ions to participate in such processes. As an index of interaction, structural and/or conformational transitions may be assessed utilizing spectrometric, biophysical and enzymatic techniques. Spectrometric analysis involves both circular dichroism (CD)

and UV absorption spectrometry. The former is a sensitive indicator of DNA structure and has been utilized extensively (for theoretical considerations, see Walton and Blackwell, 1973; Tinoco *et al.*, 1980). Nucleic acids absorb light in the far UV region with an ϵ_{max} at approximately 260 nm. This is due to electronic transitions in the purine and pyrimidine rings; namely $\pi \rightarrow \pi^*$ transitions and a smaller component resulting from $n \rightarrow \pi^*$ transitions in the high-wavelength tail of the absorption spectrum. Alterations in DNA or polydeoxynucleotide conformation tend to be reflected by changes in the UV spectrum as observed for Z DNA (reviewed in: Rich *et al.*, 1984; Jovin *et al.*, 1987) or metal induced ψ-DNA (Yamane and Davidson, 1962; Jensen and Davidson, 1966; Walter and Luck, 1977). Biophysical techniques have utilized sedimentation on centrifugation and the ability of conformers of polydeoxynucleotides/DNA to bind ethidium bromide (EtBr). The generation of higher order tertiary or quaternary structures have previously been demonstrated to elicit structures which are readily sedimented by centrifugation (Wolf *et al.*, 1977; van de Sande and Jovin, 1982; van de Sande *et al.*, 1982; Votavová *et al.*, 1986; Knoll *et al.*, 1988; Chaires and Norcum, 1988; Rossetto and Nieboer, 1993). Ethidium bromide is an organic molecule that interacts strongly with nucleic acids via intercalation. This interaction produces a large increase in the fluorescence quantum yield of ethidium bromide (reviewed in: Berman and Young, 1981; Neidle and Abraham, 1984).

II.1.2 Specific Research Objectives

The focus of the work presented in this chapter is the characterization of the interaction of Ni(II) ion with DNA. To facilitate this investigation, polydeoxynucleotides of defined sequence have been used in addition to DNA of various sources. As noted in the preceding overview, a variety of techniques are available for the monitoring of the interaction of metal with DNA/polydeoxynucleotide. More specifically, the present study utilized UV absorbance spectroscopy and a derivative absorption ratio (i.e. $A_{295/260}$, $A_{290/260}$), CD spectroscopy, ethidium bromide intercalation, sedimentation on centrifugation, and resistance to enzymatic (i.e. DNaseI) digestion as a measure of the Ni(II)-DNA/ polydeoxynucleotide interaction. Binding constants for Ni(II) ion were also generated for all polydeoxynucleotides and DNAs examined. Components of this study have been previously reported (Nieboer *et al.*, 1989; Rossetto and Nieboer, 1993).

II.2 MATERIALS AND METHODS

II.2.1 Chemicals

Table 1 is a compendium of the various chemicals, reagents, sources and any additional information pertaining to the experiments described in this chapter. Doubly distilled deionized water (DDI) was used in all solution preparation. Ni(II) ion stock solutions (not including those used in generating binding constants, Section I.1.8) were made by

Table 1: Chemicals and Reagents

Identity	Formula	Source	Grade	Lot #
Nickel Nitrate Hexahydrate	$Ni(NO_3)_2 \cdot 6H_2O$	BDH Chem. Co.	AnalaR	6822790
Nickel Chloride Hexahydrate	$NiCl_2 \cdot 6H_2O$	BDH Chem. Co.	AnalaR	6872030J
Magnesium Sulfate Septahydrate	$MgSO_4 \cdot 7H_2O$	BDH Chem. Co.	AnalaR	42545
Boric Acid	H_3BO_3	BDH Chem. Co.	Assured	87645
Potassium Dihydrogen Orthophosphate	KH_2PO_4	BDH Chem. Co.	Assured	87380
Ethylene-diaminetetraacetic Acid	EDTA	BDH Chem. Co.	Assured	96257/5589
Nitric Acid	HNO_3	Baker Chem. Co.	Ultrex	B02116
4-(2-hydroxyethyl)-1-piperazine-ethanesulfonic acid (Hepes)	NA**	Sigma Chem. Co.	Cell Culture	110H-5613
Ethidium Bromide	NA	Sigma Chem. Co.	Reagent	92F-0353
Tris(hydroxymethyl)-aminomethane	NA	Boehringer Mannheim	Electrophoretic	DCA121/3-93
Deoxyribonuclease (DNase I)	NA	Pharmacia	Ultrapure	BK0512101
63-Nickel Chloride	$^{63}NiCl_2$	Amersham*	NA	NA

* Templeton, Univ. of Toronto, Toronto, Canada; 11.32 mCi/mg, 1.49 mCi/ml, 1.66×10^{-6} M.
** Not available/not applicable

dissolving $Ni(NO_3)_2 \cdot 6H_2O$ in DDI at room temperature with constant stirring. After dissolution, the pH of the solution was adjusted to approximately 1.7 with nitric acid in order to prevent hydrolysis of the metal ion (Baes and Mesner, 1976). Two concentrated stock solutions of 50.93 mM and 410.97 mM were stored at room temperature until diluted with DDI prior to use.

II.2.2 Polydeoxynucleotide/DNA Solution Preparation

All polydeoxynucleotides/DNA were dissolved in a 10 mM Hepes buffer (pH 7.6) at room temperature. Estimation of concentrations were performed at appropriate wavelengths (see Table 2) on a Perkin Elmer Lambda 3B UV/VIS Spectrophotometer utilizing the molar absorptivities presented in Table 2. Solutions were used immediately or stored at 4°C for a maximum of 3 weeks prior to use. Calculated concentrations correspond to base pairs of DNA per litre of solution. Working concentrations of polydeoxynucleotides/DNA in most experiments were in the 15-40 μM range. Concentrations of stock DNA solutions used in binding constant determinations were in the range of 40-115 μM.

II.2.3 Metal-DNA Interaction

The interaction of Ni(II) with DNA was studied with different quantities of DNA depending on the nature and type of subsequent investigative procedure. For the analysis of

Table 2: Polydeoxynucleotides and DNAs

Identity	Source	Absorbance[1,2] Maxima (nm)	Molar Absorptivity (ϵ) (M^{-1} cm^{-1})
polyd(GC)·polyd(GC)	Pharmacia	254	8400
polydG·polydC	Pharmacia	253	7400
polyd(GT)·polyd(AC)	Pharmacia	258	6500
polyd(AT)·polyd(AT)	Pharmacia	262	6600
polydA·polydT	Pharmacia	260	6000
Calf Thymus DNA	Sigma	260	6600
M. Lysodeikticus	Sigma	260	6600

[1] R.D. Wells *et al.*, 1970.
[2] J.B. Lee *et al.*, 1982.

absorbance ratios and recording of UV spectra (Section II.2.4), DNase I susceptibility assessments (Section II.2.6), and sedimentation analysis (Section II.2.6), 500 µl or 700 µl of DNA was incubated with 0-50 µl of diluted Ni(II) stock solution at 37°C (or 64°C) for 2.5 h. Sample matched background incubations contained 500 µl or 700 µl of 10 mM Hepes (pH 7.6) in lieu of DNA. All solutions were made to a final constant volume of 550 µl or 750 µl with DDI.

When CD analysis was performed (Section II.2.7), 2.0 ml of DNA, 0-200 µl of diluted Ni(II) stock solution, and DDI to a total volume of 2.5 ml were normally incubated at 37°C for 2.5 h prior to analysis. For certain experiments, this treatment protocol was altered to consist of incubations at 24°C, 37°C, 65°C for 24 h. Sample matched background incubations contained 2.0 ml of 10 mM Hepes (pH 7.6) in lieu of DNA.

II.2.4 Generation of Metal-DNA UV Spectra and/or Absorbance Ratio Data

All analyses were performed on a Perkin-Elmer Lambda 3B UV/Vis Spectrophotometer at ambient room temperature and utilizing quartz cuvettes. Prior to the generation of any data, the spectrometer was adjusted for any absorbance dissimilarities in either the sample or reference cuvette by running a background scan with 10 mM Hepes (pH 7.6) in both cuvettes and storing this in memory (i.e. "zeroing" the

instrument). Solutions of Ni(II)-DNA were typically scanned from 330-230 nm and recorded on a Perkin Elmer R100A recorder. All scans were generated against a solution of 10 mM Hepes (pH 7.6) as a reference.

For the measurement of absorbance ratios, individual measurements were performed at 260 nm, 290 nm and 295 nm utilizing a solution of 10 mM Hepes (pH 7.6) as a reference. Absorbance contributions arising from Ni(II) ion alone were corrected for by the subtraction of absorbances at these wavelengths of Ni(II)-ion matched solutions containing no DNA. The absorbance ratio at 295 nm and 260 nm ($A_{295/260}$) was utilized for calf thymus DNA, polyd(GT)·polyd(AC), polydG·polydC, polyd(GC)·polyd(GC); that at 290 nm and 260 nm ($A_{290/260}$) was used for polydA·polydT and polyd(AT)·polyd(AT).

II.2.5 Optimization of the Ethidium Bromide Interaction with Polydeoxynucleotides

A variety of buffers containing ethidium bromide (EtBr; 0.5 µg/ml) were prepared with pH values ranging from 8-12. These were: 20.35 mM Tris, 0.5 mM EDTA, pH 8.00; 22.02 mM Tris, pH 8.00; 23.44 mM Tris, 0.5 mM EDTA, pH 9.01; 21.66 mM Tris, pH 9.05; 21.80 mM boric acid, 0.5 mM EDTA, pH 10.03; 22.73 mM boric acid, pH 10.03; 22.03 mM KH_2PO_4, 0.5 mM EDTA, pH 11.02, 25.15 mM KH_2PO_4, 11.02; 22.57 mM KH_2PO_4, 0.5 mM EDTA, pH 12.00; 22.68 mM KH_2PO_4, pH 11.99. Three aliquots of DNA (100 µl) were added to 2.0 ml of EtBr-buffer in 10 x 75 mm

borosilicate tubes, mixed thoroughly by finger flicking and read immediately for fluorescence on a Gilson Spectra/glo Fluorometer. Pursuant to DNA intercalation, fluorescence of EtBr is monitored at 600 nm following excitation at 525 nm (Paoletti *et al.*, 1971). Filters utilized in the fluorometer were from Mandel Corp. (Canada):#520-3X, 520 nm; #2-63M, 600-680 nm. Three replicates of each DNA aliquot/EtBr-buffer combination were assayed.

II.2.6 Analysis of the Interaction of Ni(II) with Polydeoxynucleotides Utilizing Ethidium Bromide, Deoxyribonuclease I Susceptibility, and Sedimentation Analysis

Aliquots of Ni(II)-DNA (750 µl) were prepared as outlined in Section II.2.2. Following a 3 h incubation at 37°C, absorbance ratio data were obtained as outlined in Section II.2.4. The samples were then split into a 500 µl aliquot (EtBr and sedimentation analysis) and a 250 µl aliquot (DNase I digestion susceptibility).

For the initial EtBr analysis, 3 aliquots of Ni(II)-DNA (25 µl) were taken and added to 2.0 ml of EtBr reagent (22.02 mM Tris, pH 8.02) as described in Section II.2.5. An additional 3 aliquots of Ni(II)-DNA (25 µl) were combined with 1 µl of 0.5 M EDTA and 2.0 ml of EtBr reagent as noted. The remaining 350 µl was centrifuged at 16,000 x g for 12 min at room temperature in an Eppendorf microcentrifuge (Model 5415).

Three aliquots (25 µl) of the supernatant were removed and analyzed with 2.0 ml of EtBr reagent in the presence of EDTA as previously described.

A stock solution of DNase I (1.24 mg/ml, 2976 U/ml; in 0.15 M NaCl, 50% glycerol) was diluted 100-fold in dilution buffer (5 mM $MgSO_4 \cdot 7H_2O$, 5.1 mM Hepes, pH 7.9) to a final working solution of 10.24 µg/ml (29.76 U/ml) immediately prior to use. To the second portion of Ni(II)-DNA (250 µl), a 25 µl aliquot of diluted DNase I was added and the mixture incubated at 37°C for 4 h. The reaction was terminated by the addition of 20 µl of 0.5 M EDTA. Three aliquots (25 µl) of digested sample were removed and analyzed following the addition of 2.0 ml of EtBr reagent as noted above.

For EtBr, sedimentation and DNase I digestion analysis, blank tubes containing 10 mM Hepes pH 7.6 in lieu of DNA were examined as negative background controls.

II.2.7 Circular Dichroism Investigation of Ni(II)-Polydeoxynucleotide

All CD studies were performed on an $AVIV_R$ Circular Dichroism Spectrophotometer at ambient room temperature utilizing quartz cuvettes. Ni(II)-DNA (2.5 ml) was prepared as described in Section II.2.3. Scans were typically from 350-230 nm. All data collected were stored and manipulated on IBM AT or similar computer hardware.

II.2.8 The Generation of Binding Dissociation for Ni(II)-Polydeoxynucleotide Interactions

The separation of bound and unbound Ni^{63} fractions was based on a procedure used in the separation of bound and unbound label during radioiodination utilizing ultra filtration (Lipford *et al.*, 1990). Prior to generation of binding constants, all DNAs were extensively dialyzed against excess amounts (>100 x) of 10 mM Hepes, 2 mM NaCl pH 7.4 for 96 h at room temperature with one change of dialysis buffer. Dialysis membrane ("Metal Free" Prepared Dialysis Tubing; BRL/Life Technologies Inc.) was certified metal free and possessed a MW cutoff of 12,000-14,000 Daltons.

Samples consisted of 100 µl of DNA (or buffer), 10 µl of Ni^{63} (Table 1), 0-100 µl of a freshly prepared $NiCl_2 \cdot 6H_2O$ solution (501.38 µM) and DDI to a final volume of 200 µl. Final concentrations of DNA ranged 20-55 µM; Ni(II) concentrations ranged 0.1-250 µM. All samples were incubated for 18 h at room temperature. Ultrafiltration units (Millipore, Ultrafree-MC filter units, 10,000 mw) were prewashed with 100 µl of 5 mM Hepes, 1 mM NaCl pH 7.4. Following centrifugation at 2000 x g, 15 min at room temperature, both filtrate and filter retentate were removed. Samples were introduced into the units and spun for 2000 x g, 30 min at room temperature. The filter retentate (i.e. bound Ni-DNA) was washed with 50 µl of buffer (5 mM Hepes, 1 mM NaCl pH 7.4) and respun for an additional 15 min. To the washed

retentate, 75 µl DDI was added and the sample was totally removed and counted three times in a scintillation counter with 10 ml ACS liquid scintillant (Amersham Canada Ltd.). Stock radioactive $^{63}NiCl_2$ was quantified for total nickel by atomic absorption spectrometry (AAS) and served as a radiolabel tracer in subsequent stock nickel solutions (see Table 1). A known quantity of the latter stock solution was counted and used to quantify DNA-bound Ni^{2+}. All samples counted (i.e. bound Ni^{2+}-DNA) were corrected for background binding of Ni^{2+} to filter units prior to data manipulation. Analysis of data employing Scatchard plots (Scatchard, 1949) was performed utilizing BDATA-Ligand Binding Analysis Software (EMF Software, USA).

II.3 RESULTS

II.3.1 UV Spectra and Absorbance Ratio Data

The interaction of various polydeoxynucleotides and calf thymus DNA with Ni(II) ion has been investigated by UV spectroscopy. Spectral scans are presented in Figures 1-6.

It is clear from Figure 1 that the interaction of Ni(II) ion with calf thymus DNA did not affect its UV spectrum substantially. There exists an absorbance maximum at 260 nm which decreases slightly in intensity (hypochromism) following increasing Ni(II)-ion interaction. Absorbance changes at lower wavelengths (<240 nm) correlate with increasing amounts of free Ni(II) ion in solution, perhaps

Figure 1: UV absorbance spectral scans of calf thymus DNA in the presence of Ni(II) ion. Numbers correspond to spectra with the following mole ratios (Ni/bp) and absorbance ratios ($A_{295}/_{260}$) respectively: 1) 0.00 and 0.119; 2) 1.74 and 0.130; 3) 2.62 and 0.127; 4) 4.37 and 0.124; 5) 7.65 and 0.114. DNA concentration was 31.06 μM.

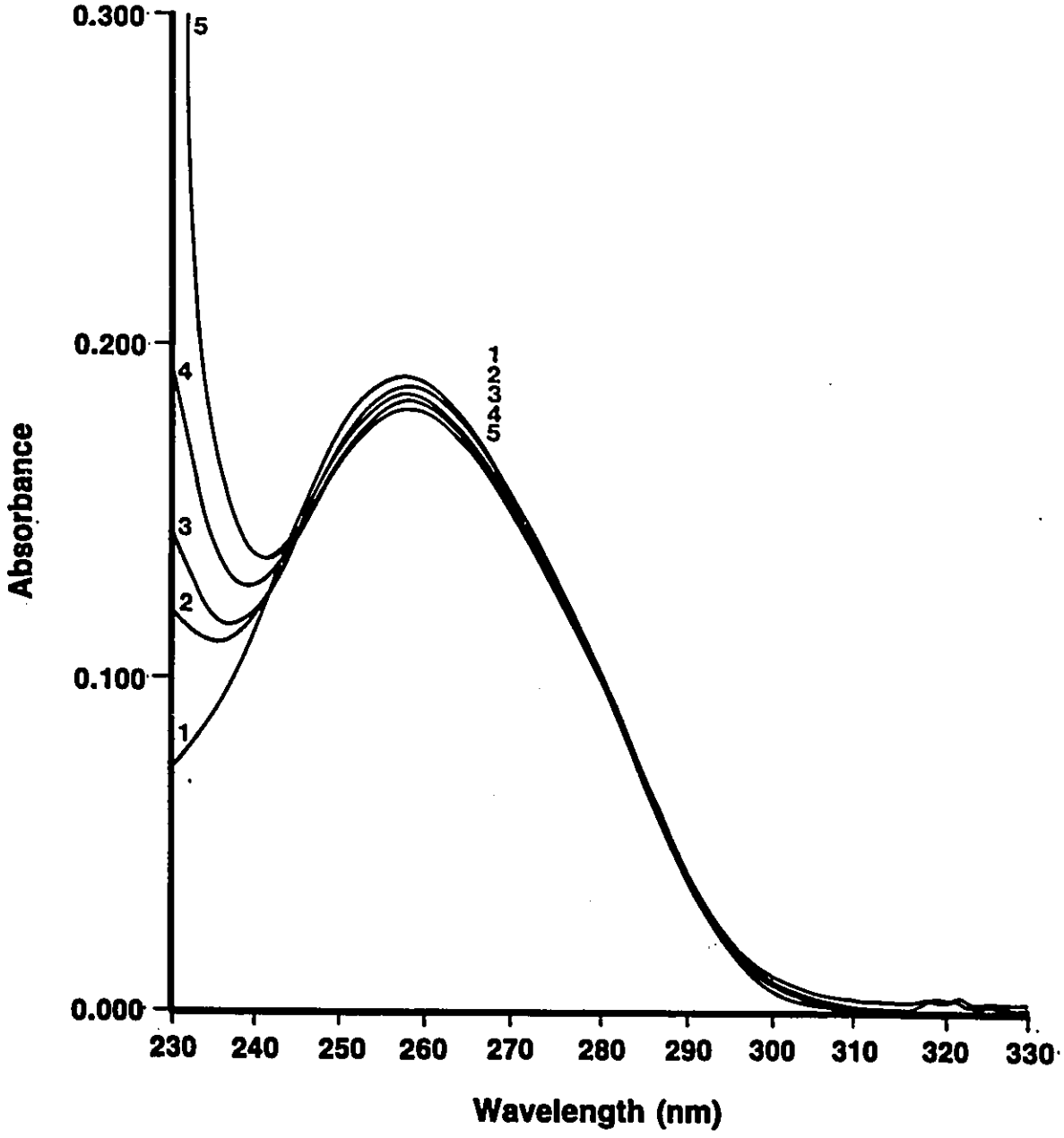
0.300
0.200
0.100
0.000
Absorbance
5
4
3
2
1
1
2
3
4
5
230
240
250
260
270
280
290
300
310
320
330
Wavelength (nm)

Figure 2: UV absorbance spectral scans of polydG·polydC in the presence of Ni(II) ion. Numbers correspond to spectra with the following mole ratios (Ni/bp) and absorbance ratios ($A_{295}/_{260}$) respectively: 1) 0.00 and 0.119; 2) 1.04 and 0.125; 3) 1.69 and 0.132; 4) 2.60 and 0.139; 5) 4.15 and 0.130; 6) 7.27 and 0.128. Polydeoxynucleotide concentration was 24.56 μM.

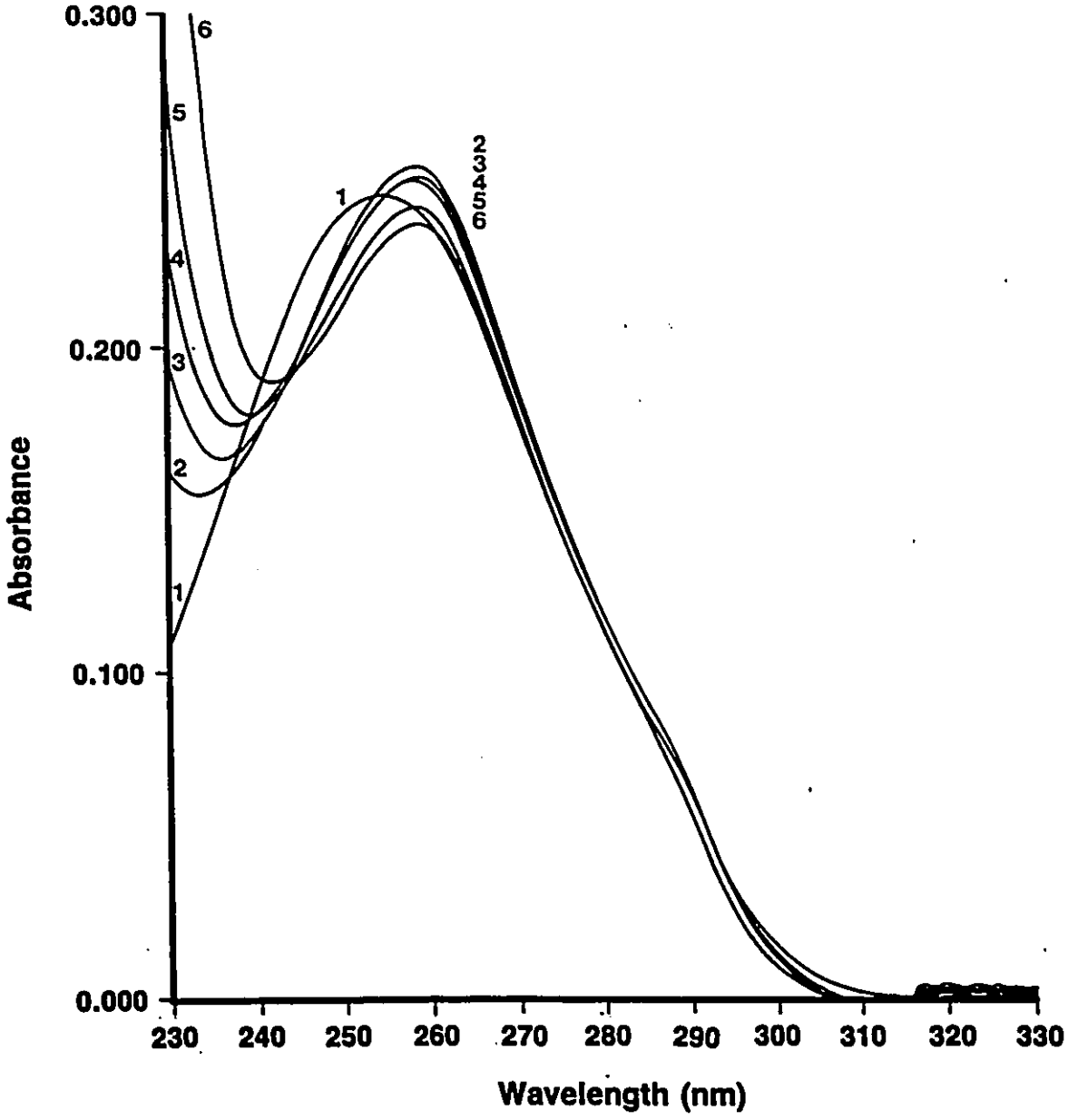
0.300
0.200
0.100
0.000
Absorbance
230
240
250
260
270
280
290
300
310
320
330
Wavelength (nm)
1
2
3
4
5
6

Figure 3: UV absorbance spectral scans of polyd(GT)·polyd(AC) in the presence of Ni(II) ion. Numbers correspond to spectra with the following mole ratios (Ni/bp) and absorbance ratios ($A_{295}/_{260}$) respectively: 1) 0.00 and 0.102; 2) 1.11 and 0.096; 3) 6.66 and 0.091; 4) 13.31 and 0.093. Polydeoxynucleotide concentration was 29.85 μM.

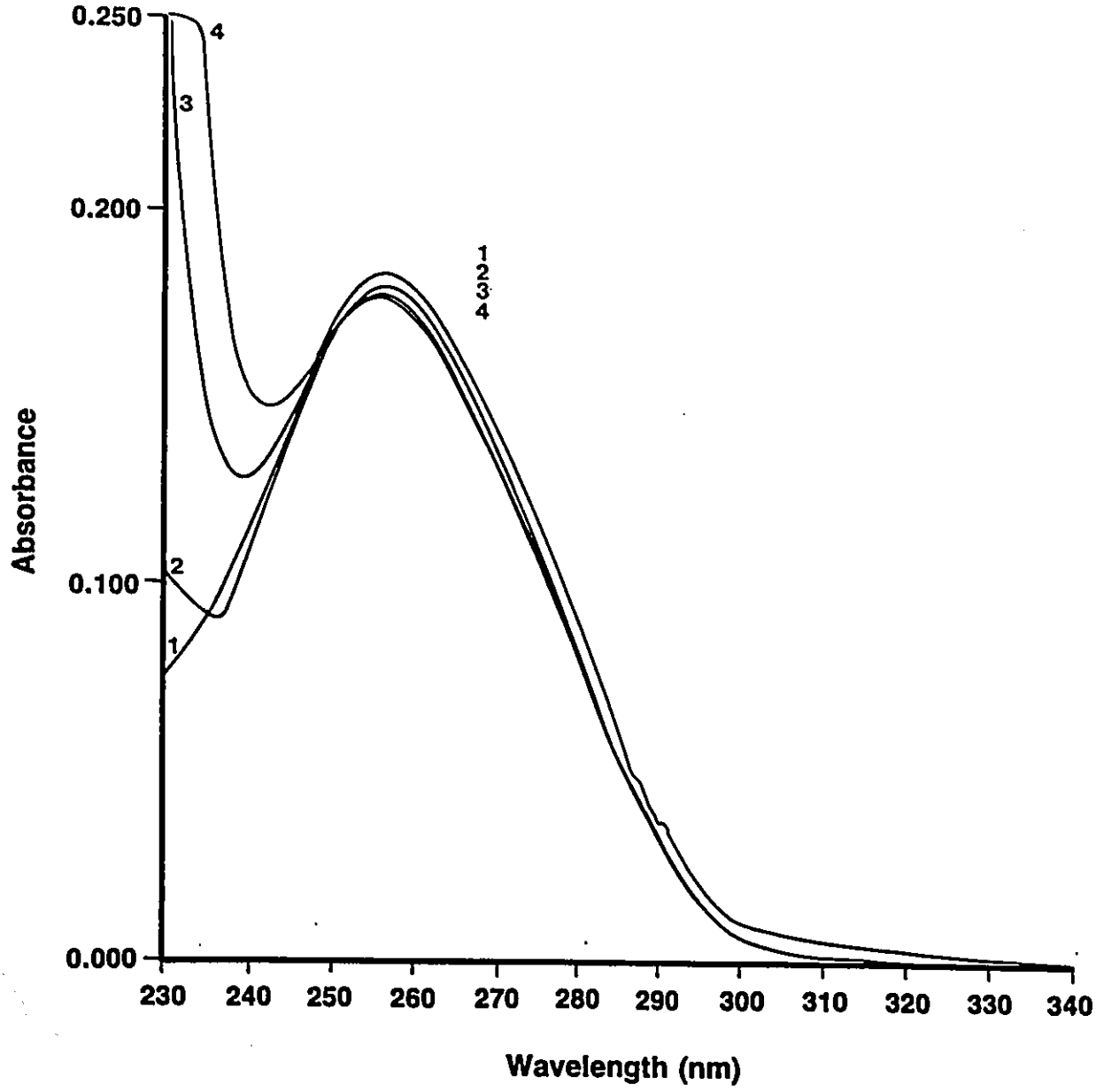
0.250
0.200
0.100
0.000
Absorbance
1
2
3
4
230
240
250
260
270
280
290
300
310
320
330
340
Wavelength (nm)

Figure 4: UV absorbance spectral scans of polyd(GC)·polyd(GC) in the presence of Ni(II) ion. Numbers correspond to spectra with the following mole ratios (Ni/bp) and absorbance ratios ($A_{295}/_{260}$) respectively: 1) 0.00 and 0.133; 2) 1.25 and 0.163; 3) 1.99 and 0.202; 4) 2.99 and 0.211; 5) 3.99 and 0.280; 6) 4.98 and 0.347; 7) 6.23 and 0.350; 8) 7.7 and 0.351; 9) 8.96 and 0.345. Spectrum number 10 corresponds to Ni ion at a concentration of 271.63 μm in the absence of polydeoxynucleotide. Polydeoxynucleotide concentration was 27.26 μM. Arrows denote isobestic points.

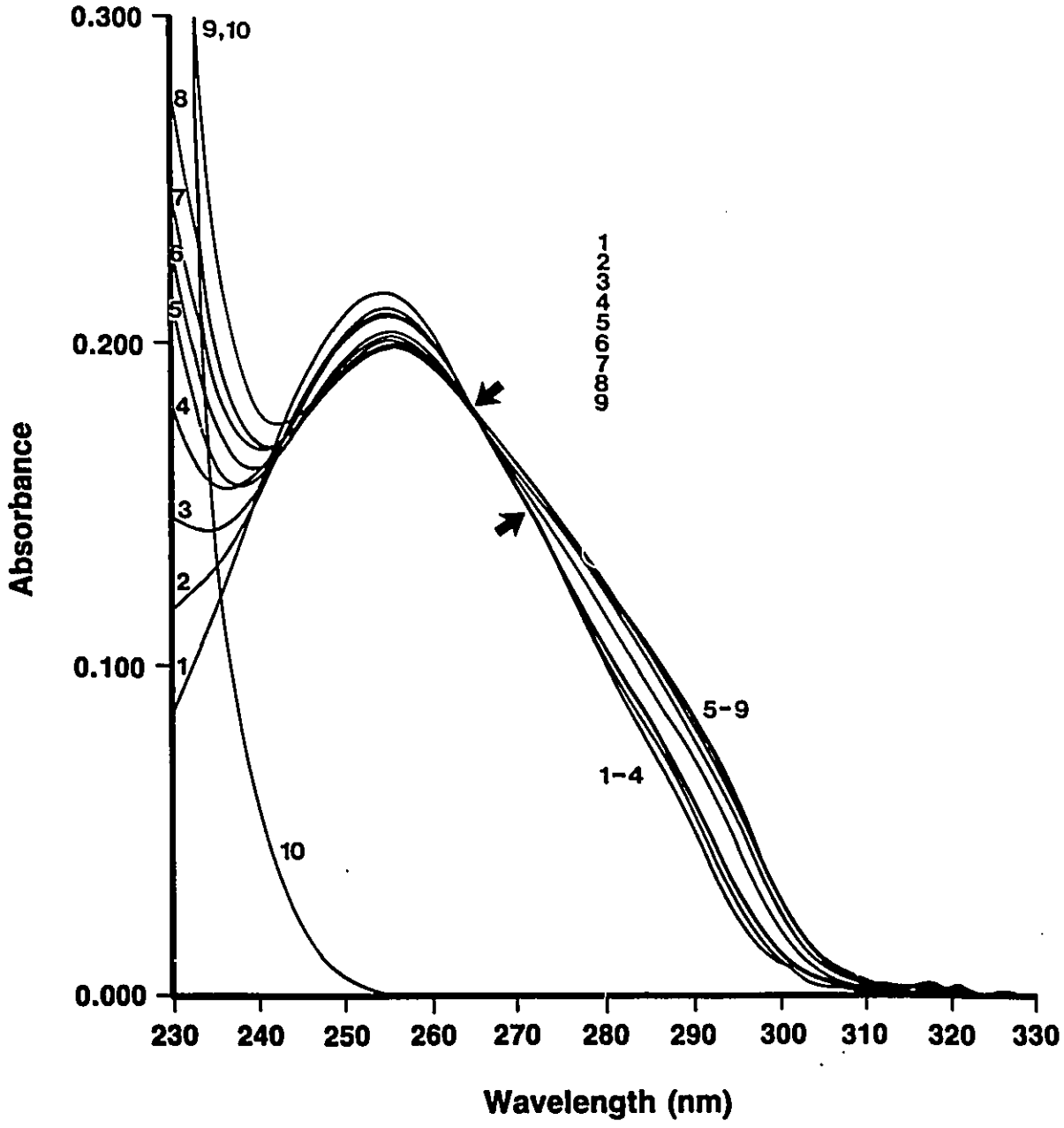
0.300
0.200
0.100
0.000
Absorbance
9,10
8
7
6
5
4
3
2
1
10
1
2
3
4
5
6
7
8
9
5-9
1-4
230
240
250
260
270
280
290
300
310
320
330
Wavelength (nm)

Figure 5: UV absorbance spectral scans of polyd(AT)·polyd(AT) in the presence of Ni(II) ion. Numbers correspond to spectra with the following mole ratios (Ni/bp) and absorbance ratios ($A_{290}/_{260}$) respectively: 1) 0.00 and 0.163; 2) 2.43 and 0.150; 3) 4.04 and 0.155; 4) 8.08 and 0.161. Polydeoxynucleotide concentration was 33.65 μM.

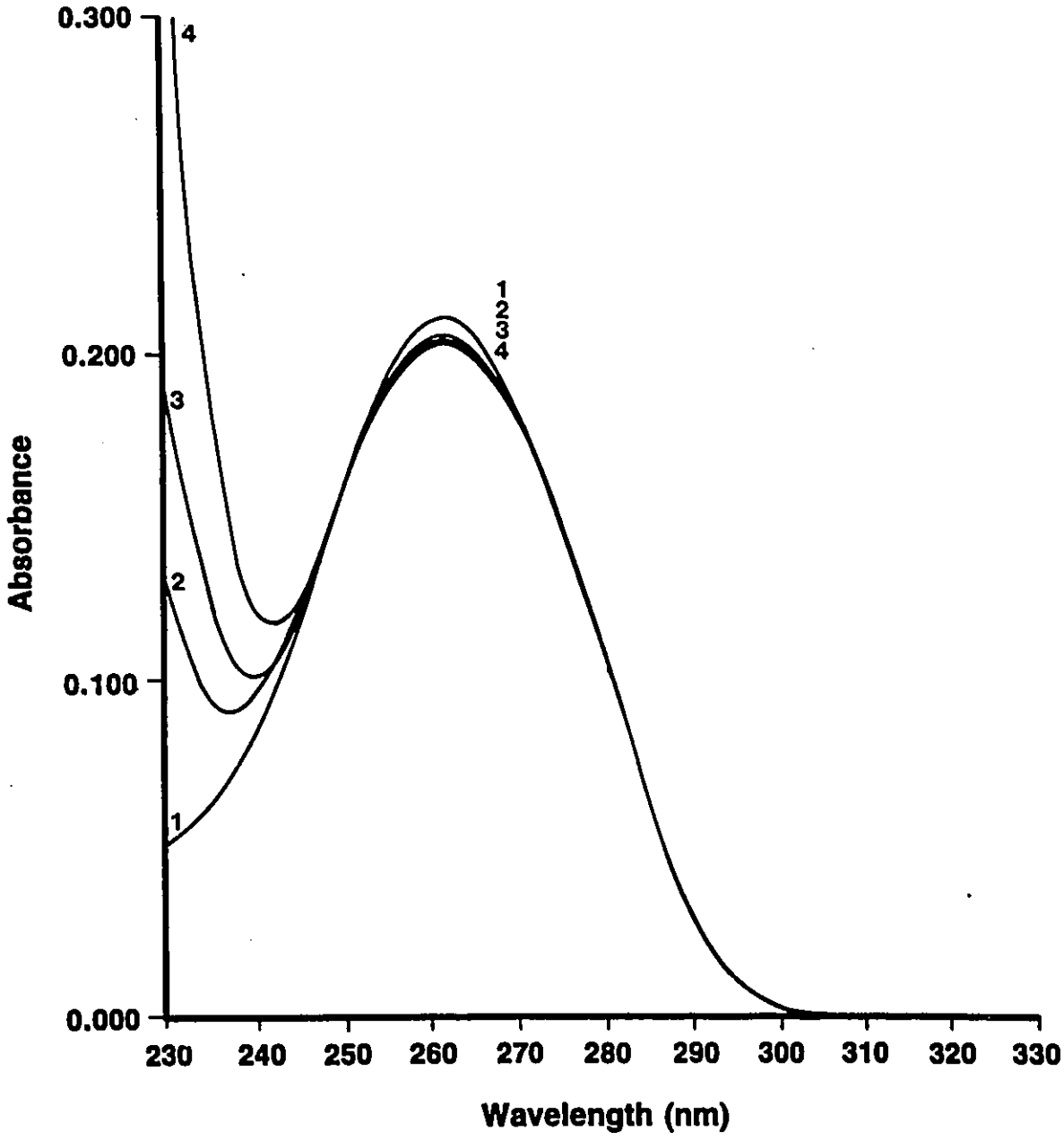
0.300
0.200
0.100
0.000
Absorbance
4
3
2
1
1
2
3
4
230
240
250
260
270
280
290
300
310
320
330
Wavelength (nm)

Figure 6: UV absorbance spectral scans of polydA·polydT in the presence of Ni(II) ion. Numbers correspond to spectra with the following mole ratios (Ni/bp) and absorbance ratios ($A_{290}/_{260}$) respectively: 1) 0.00 and 0.169; 2) 1.92 and 0.168; 3) 3.98 and 0.180; 4) 8.61 and 0.173. Polydeoxynucleotide concentration was 41.00 μM.

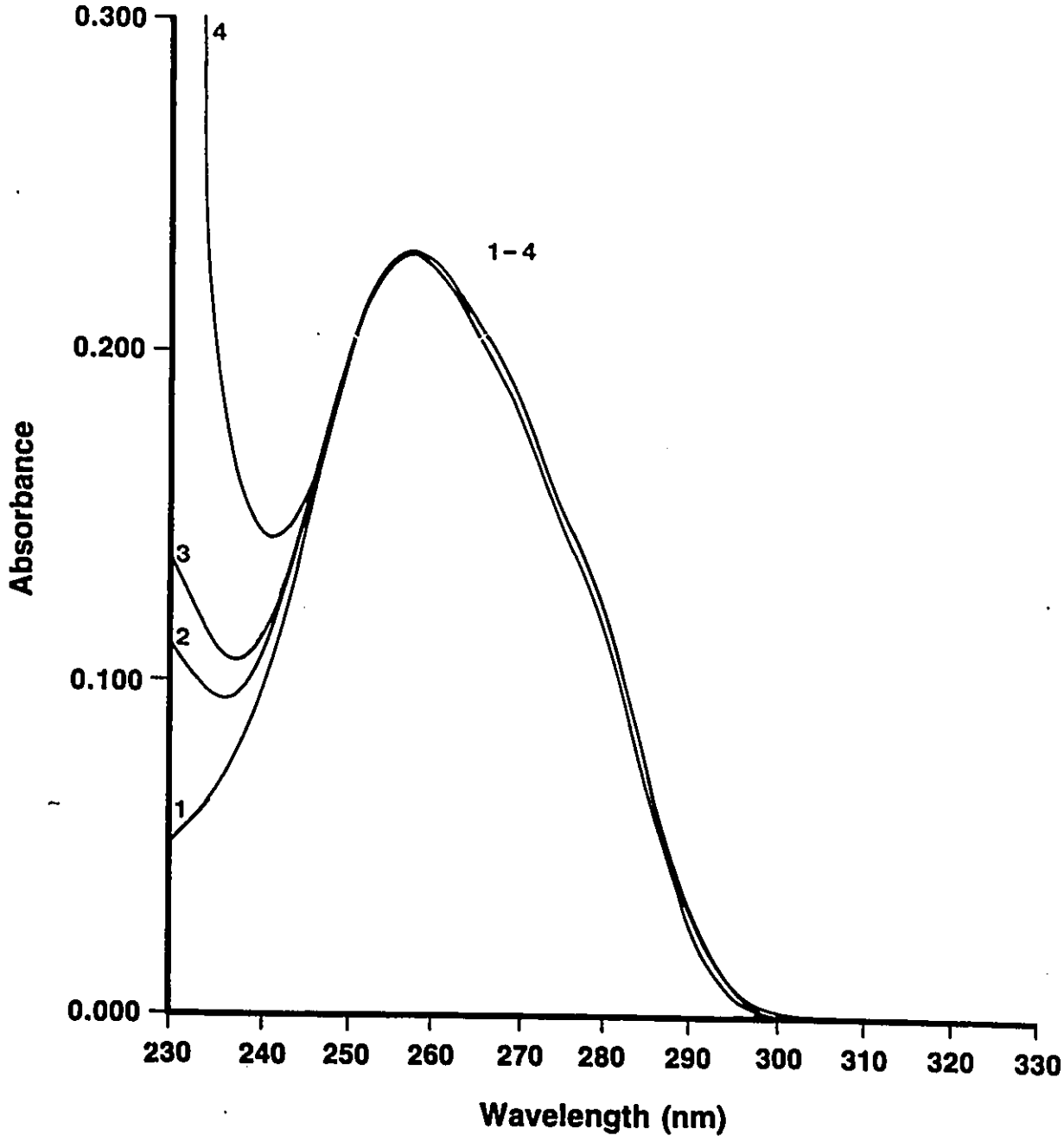
0.300
0.200
0.100
0.000
Absorbance
4
1-4
3
2
1
230
240
250
260
270
280
290
300
310
320
330
Wavelength (nm)

reflecting some interaction with a buffer component (see scan #10, Figure 4 for Ni(II) ion control). These latter changes at lower wavelengths are consistently observed in all spectra recorded (Figures 1-6). Also note that no interference due to Ni(II) ion absorption at wavelengths greater than 254 nm are observed (Figure 4, data not shown).

PolydG·polydC in the absence of Ni(II) ion possesses a simple spectrum with an absorbance maximum at 253 nm (Figure 2). Addition of Ni(II) ion results in subtle but distinct alterations in this spectrum. First, there is a shift in the spectral maximum to a higher wavelength (approximately 258 nm) which is stable for all Ni(II) polydG·polydC mixtures. As levels of Ni(II) ion increase, the intensity of this spectral maximum decreases moderately.

Figure 3 depicts the interaction of poly d(GT)· polyd(AC) with Ni(II) ion. It is evident that the interaction with this polydeoxynucleotide results in subtle changes to the absorbance spectrum. Although no wavelength shift of the maximum is observed, a slight decrease in the absorbance value is seen following increasing interaction with Ni(II) ion.

The most pronounced effects on polydeoxynucleotide spectra are observed following the interaction of Ni(II) ion with polyd(GC)·polyd(GC) (Figure 4). As levels of Ni(II) ion increase, there is a clear intensity decrease at the absorbance maximum (254 nm). In addition, increasing interaction with Ni(II) ions results in the development of a

distinctive spectral "shoulder" in the region of 270-300 nm. This "shoulder" becomes more pronounced as increasing levels of Ni(II) ion are added to the polydeoxynucleotide. Two isobestic points are also observed. At low concentrations of Ni(II) ion (Ni/bp mole ratio <3), a distinct isobestic point occurs at 272 nm. The second isobestic point observed at 265 nm may be viewed as arising from all spectra recorded, or perhaps only from spectra generated at higher levels of Ni(II) ion (i.e. Ni/bp mole ratios > 3).

No substantial spectral changes are observed following the interaction of Ni(II) ion with polyd(AT)·polyd(AT) (Figure 5). A slight decrease in absorbance at 260 nm is observed for this polydeoxynucleotide in the presence of Ni(II) ion; increasing nickel ion concentrations do not augment this slight decrease.

PolydA·polydT does not exhibit any spectral alterations following the interaction with Ni(II) ion (Figure 6). The absorbance maximum at 260 nm is unaltered at all concentrations of Ni(II) ion; no spectral shifts are observed to higher or lower wavelengths.

To simplify the analysis of spectral data, ratios incorporating absorbance values at 295 nm and 260 nm (calf thymus DNA, polydG·polydC, polyd(GC)·polyd(GC), polyd(GT)·polyd(AC)) or 290 nm and 260 nm (polydA·polydT, polyd(AT)·polyd(AT)) are utilized (Figures 7 and 8). (Please note that not all scans represented by points in Figures 7 and

Figure 7: Absorbance ratio ($A_{295}/_{260}$) data of calf thymus DNA and various polydeoxynucleotides in the presence of increasing amounts of Ni(II) ion. The figure legend describes the symbols utilized. Concentrations were as follows: calf thymus DNA, 31.06 µm; polydG·polydC, 24.56 µm; polyd(GT)·polyd(AC), 29.85 µm; poly(GC)·polyd(GC), 27.26 µM.

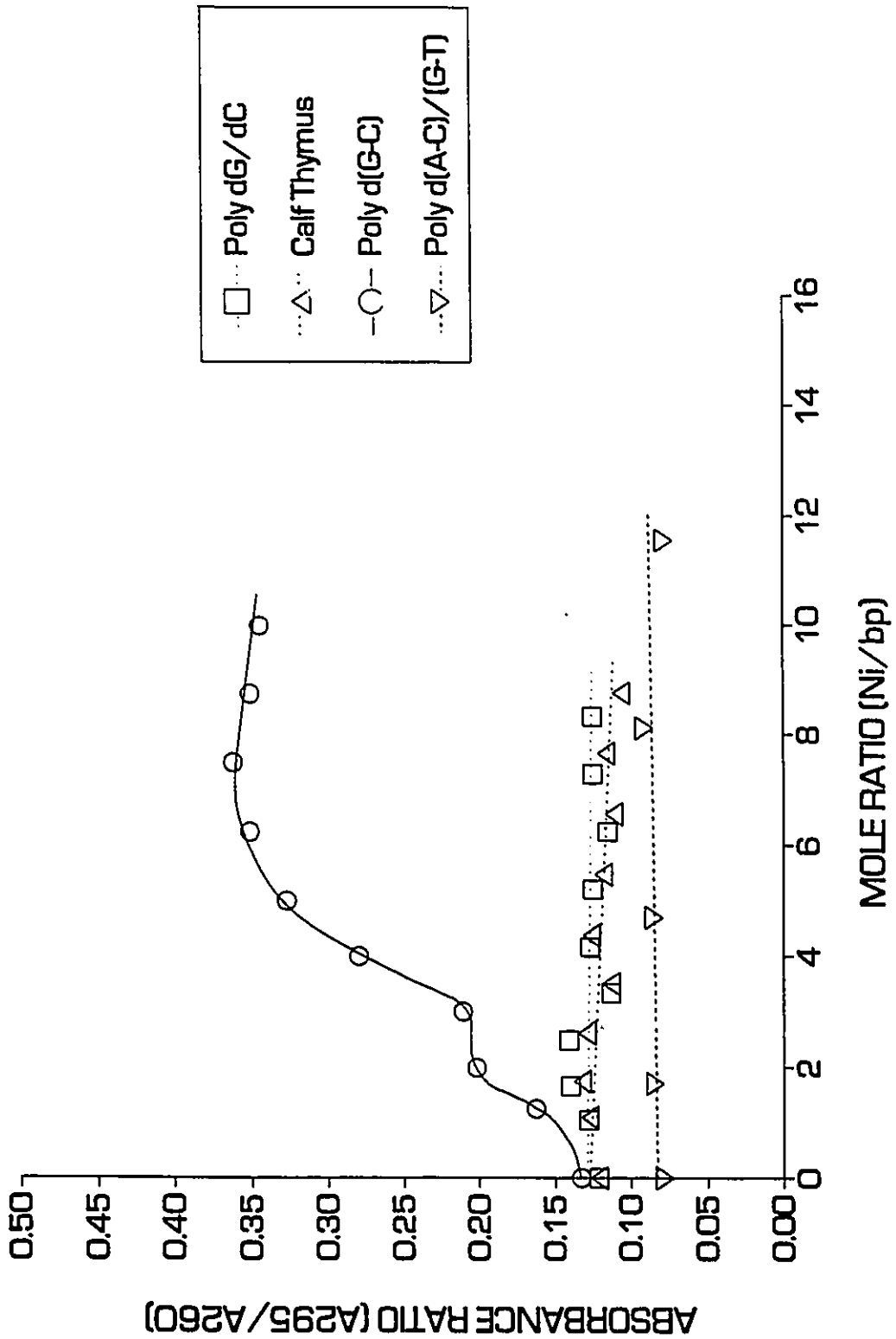
Poly dG/dC
Calf Thymus
Poly d(G-C)
Poly d(A-C)/(G-T)
ABSORBANCE RATIO (A295/A260)
0.50
0.45
0.40
0.35
0.30
0.25
0.20
0.15
0.10
0.05
0.00
0
2
4
6
8
10
12
14
16
MOLE RATIO (Ni/bp)

Figure 8: Absorbance ratio ($A_{290}/_{260}$) data of various polydeoxynucleotides in the presence of increasing amounts of Ni(II) ion. The figure legend describes the symbols utilized. Concentrations were as follows: polyd(AT)·polyd(AT), 33.65 µM; polydA·polydT, 41.00 µM.

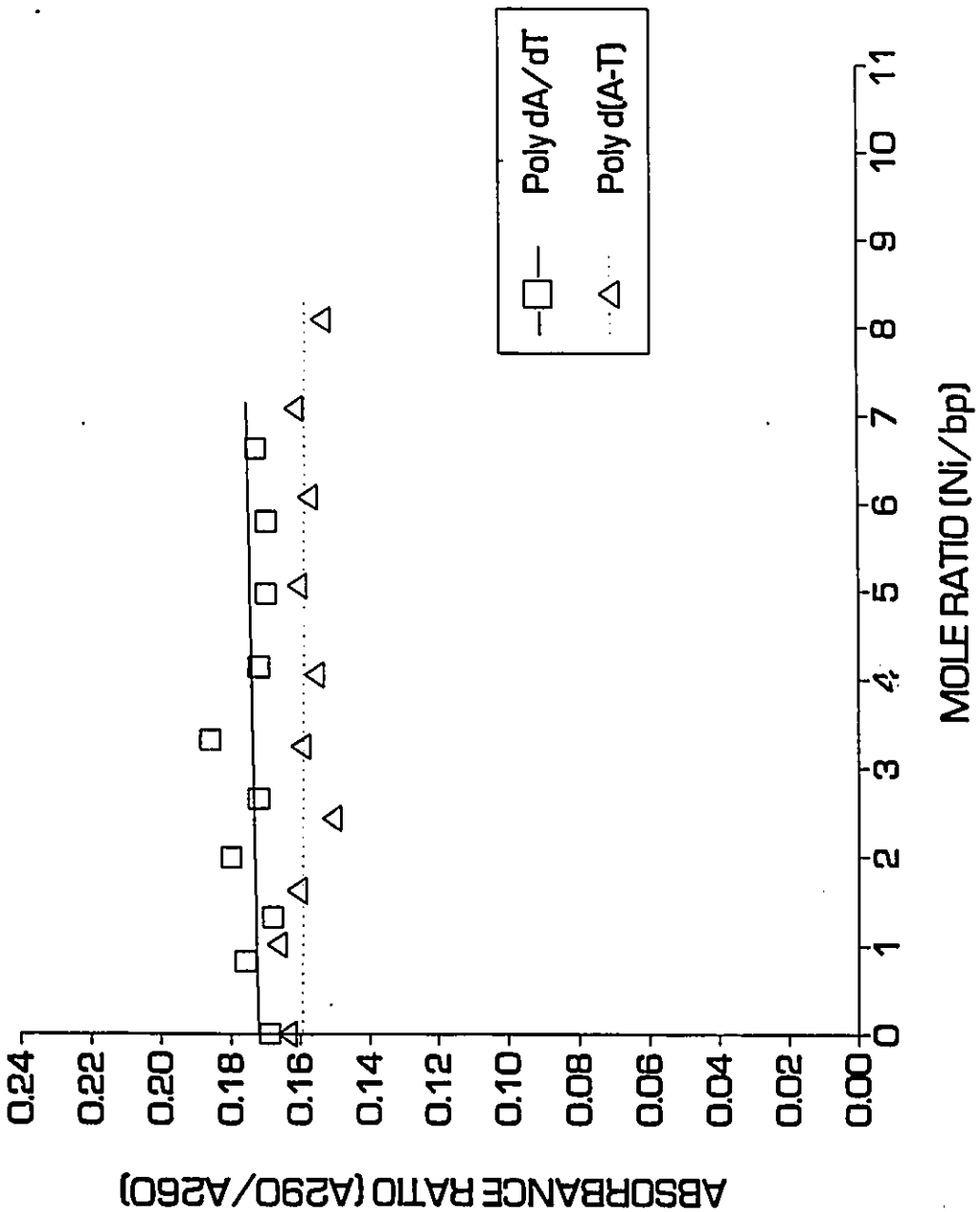
ABSORBANCE RATIO (A290/A260)
0.24
0.22
0.20
0.18
0.16
0.14
0.12
0.10
0.08
0.06
0.04
0.02
0.00
0
1
2
3
4
5
6
7
8
9
10
11
MOLE RATIO (Ni/bp)
Poly dA/dT
Poly d(A-T)

Figure 9: Ethidium bromide fluorescence following intercalation into DNA and polydeoxynucleotides as a function of solution pH and EDTA. Symbols utilized are described in the figure legend. Concentrations were as follows: calf thymus DNA, 31.06 μM; polydG·polydC, 36.08 μM; polyd(GC)·polyd(GC), 27.26 μM; polydA·polydT, 40.50 μM; polyd(AT)·polyd(AT), 33.79 μM.

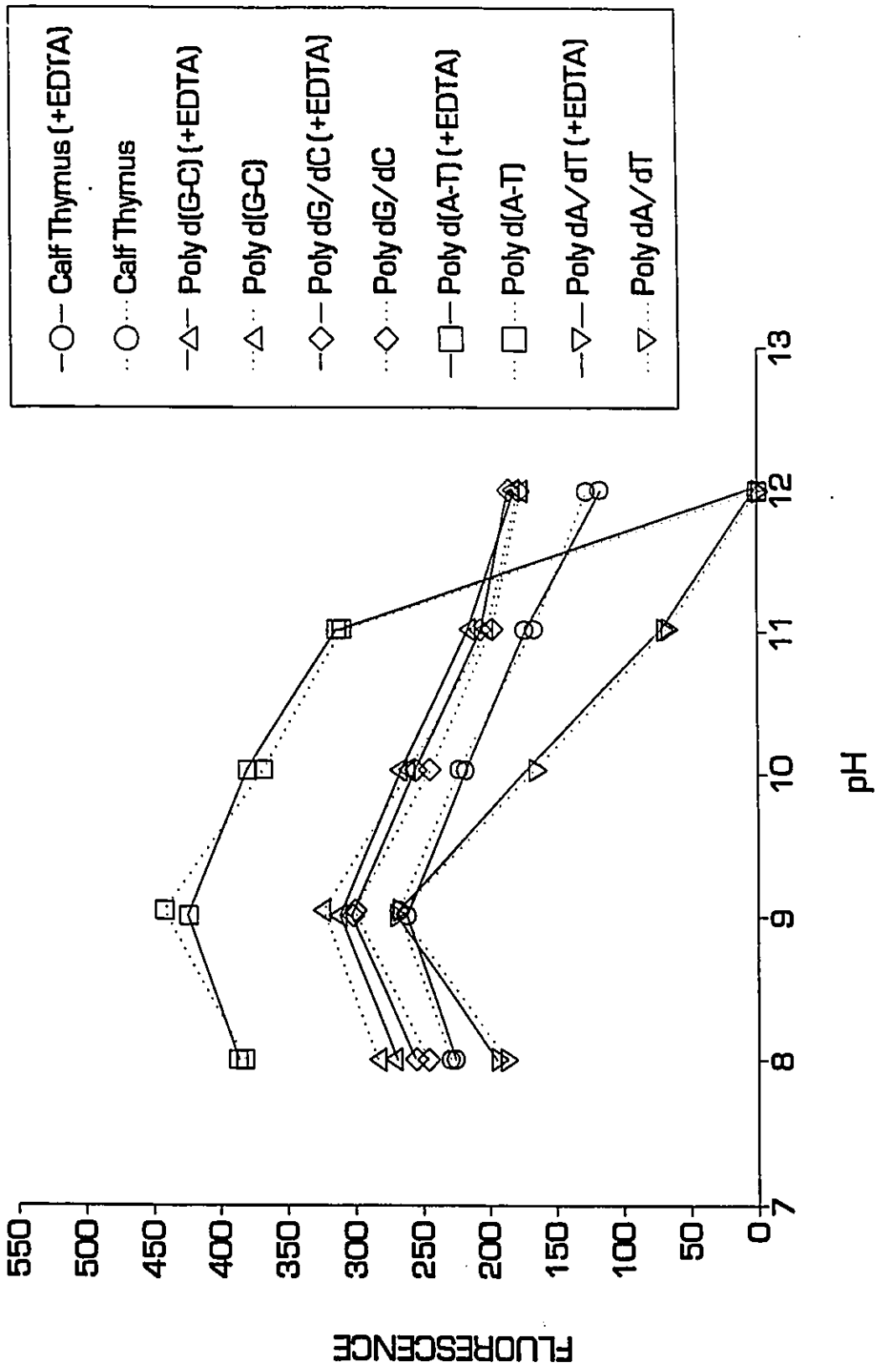
Calf Thymus (+EDTA)
Calf Thymus
Poly d(G-C) (+EDTA)
Poly d(G-C)
Poly dG/dC (+EDTA)
Poly dG/dC
Poly d(A-T) (+EDTA)
Poly d(A-T)
Poly dA/dT (+EDTA)
Poly dA/dT
FLUORESCENCE
0
50
100
150
200
250
300
350
400
450
500
550
7
8
9
10
11
12
13
pH

8 are presented in Figures 1 through 6.) As previously described for Figures 1-6, these wavelengths are sensitive to alterations in absorbance and to the development of spectral "shoulders" (see Figure 4). The presentation of spectral data as absorbance ratios ($A_{295/260}$, $A_{290/260}$) as in Figures 7 and 8, demonstrate that few major perturbations in spectra occur following interaction of Ni(II) ion with polydeoxynucleotides except in the case of polyd(GC)·polyd(GC). For this latter polydeoxynucleotide, the distinct spectral changes (Figure 4) are clearly reflected in the absorbance ratio data (Figure 7).

The absorbance ratio data for polyd(GC)·polyd(GC) suggest a biphasic process for the interaction of Ni(II) ion with polydeoxynucleotide (Figure 7). At low levels of Ni(II) ion (Ni/bp mole ratio <3), an initial plateau is observed ($A_{295/260}$ = 0.23). Addition of Ni(II) ion results in a subsequent sharp transition to a new plateau ($A_{295/260}$ = 0.35). These plateaus are consistent with the grouping or relatedness of spectra (i.e. isobestic points) previously described for this polydeoxynucleotide.

II.3.2 Optimization of the Interaction of Ethidium Bromide With Polydeoxynucleotides and DNA

The interaction and intercalation of EtBr with various polydeoxynucleotides and DNA in a variety of buffers is presented in Figure 9. For all DNAs tested, an increase in buffer pH from 8 to 9 results in a slight increase in

fluorescence of intercalated EtBr. Increasing the buffer pH stepwise to 12, generated incremental decreases in EtBr fluorescence for all DNAs. For both polydA·polydT and polyd(AT)·polyd(AT), EtBr fluorescence in a buffered solution at pH 12 was totally abrogated. The presence of EDTA in the buffered solutions does not affect the EtBr intercalation and subsequent fluorescence.

II.3.3 Reproducibility of Absorbance Ratio and Ethidium Bromide Fluorescence Data

For most experiments, the absorbance data measured and the subsequently derived absorbance ratio resulted from single measurements. Statistical analysis of an experiment monitoring the interaction of Ni(II) ion with polyd(GC)·polyd(GC) is presented in Figure 10. Standard deviations obtained from triplicate measurements confirm that intra-experimental (instrumental) errors are minimal (i.e. standard deviations range from 0.001 to 0.009). Similar results were observed for fluorescence measurements (Figure 11). In this case intra-experimental (instrumental) standard deviations were also minimal (3 to 15 arbitrary units, with 0 - 500 a typical range). The low deviations observed precluded the inclusion of error bars on all subsequent figures, although all fluorescence measurements were routinely assessed in triplicate.

Figure 10: Reproducibility of absorbance ratio ($A_{295}/_{260}$) data of polyd(GC)·polyd(GC) in the presence of increasing amounts of Ni(II) ion. The concentration of polydeoxynucleotide was 18.57 μM. Error bars denote standard deviations derived from triplicate measurements.

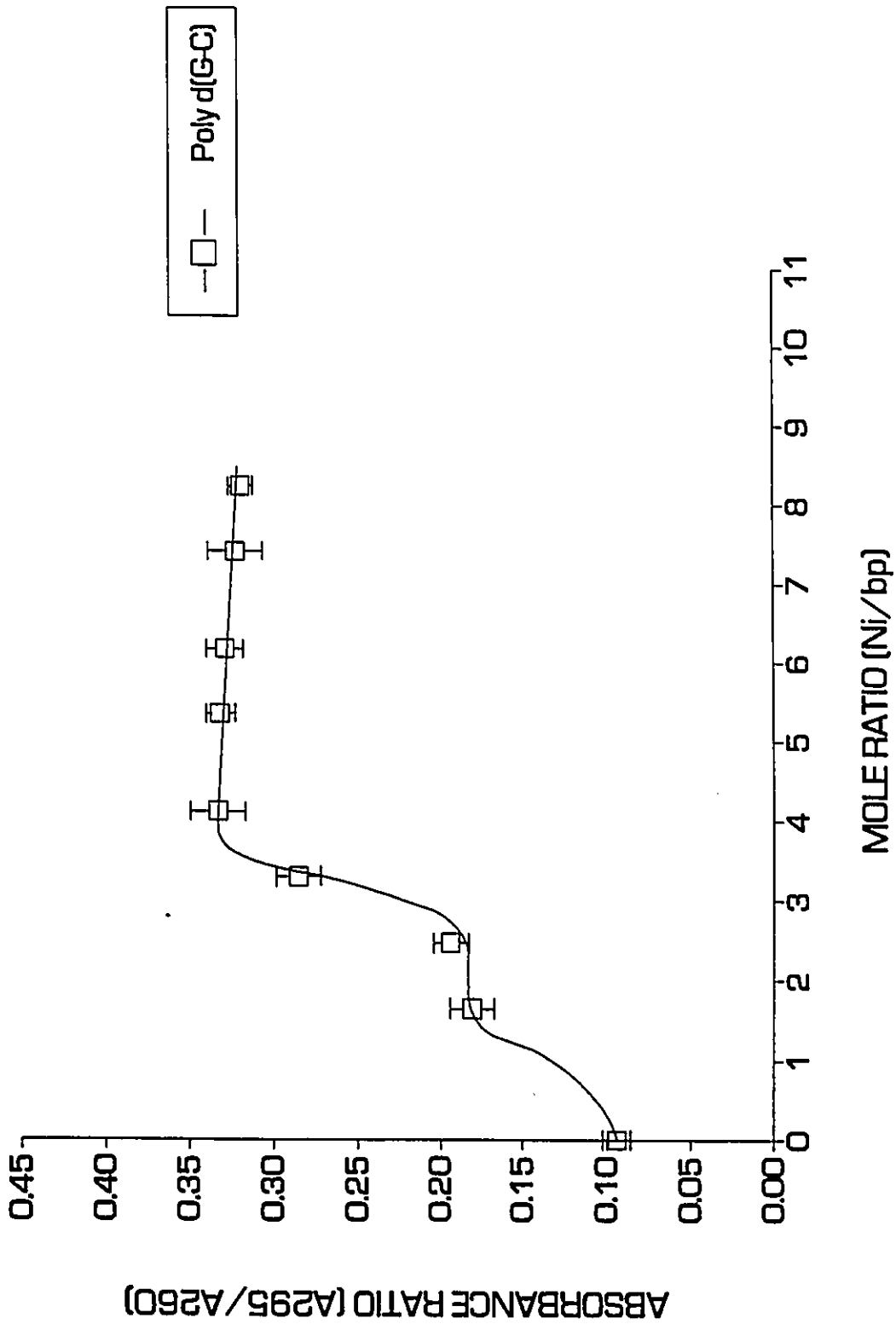
Poly d(G-C)
ABSORBANCE RATIO (A295/A260)
0.45
0.40
0.35
0.30
0.25
0.20
0.15
0.10
0.05
0.00
0
1
2
3
4
5
6
7
8
9
10
11
MOLE RATIO (Ni/bp)

Figure 11: Reproducibility of ethidium bromide fluorescence following intercalation into polyd(GC)·polyd(GC) in the presence of EDTA and increasing amounts of Ni(II) ion. Polydeoxynucleotide concentration was 18.57 μM. Error bars denote standard deviations derived from triplicate measurements.

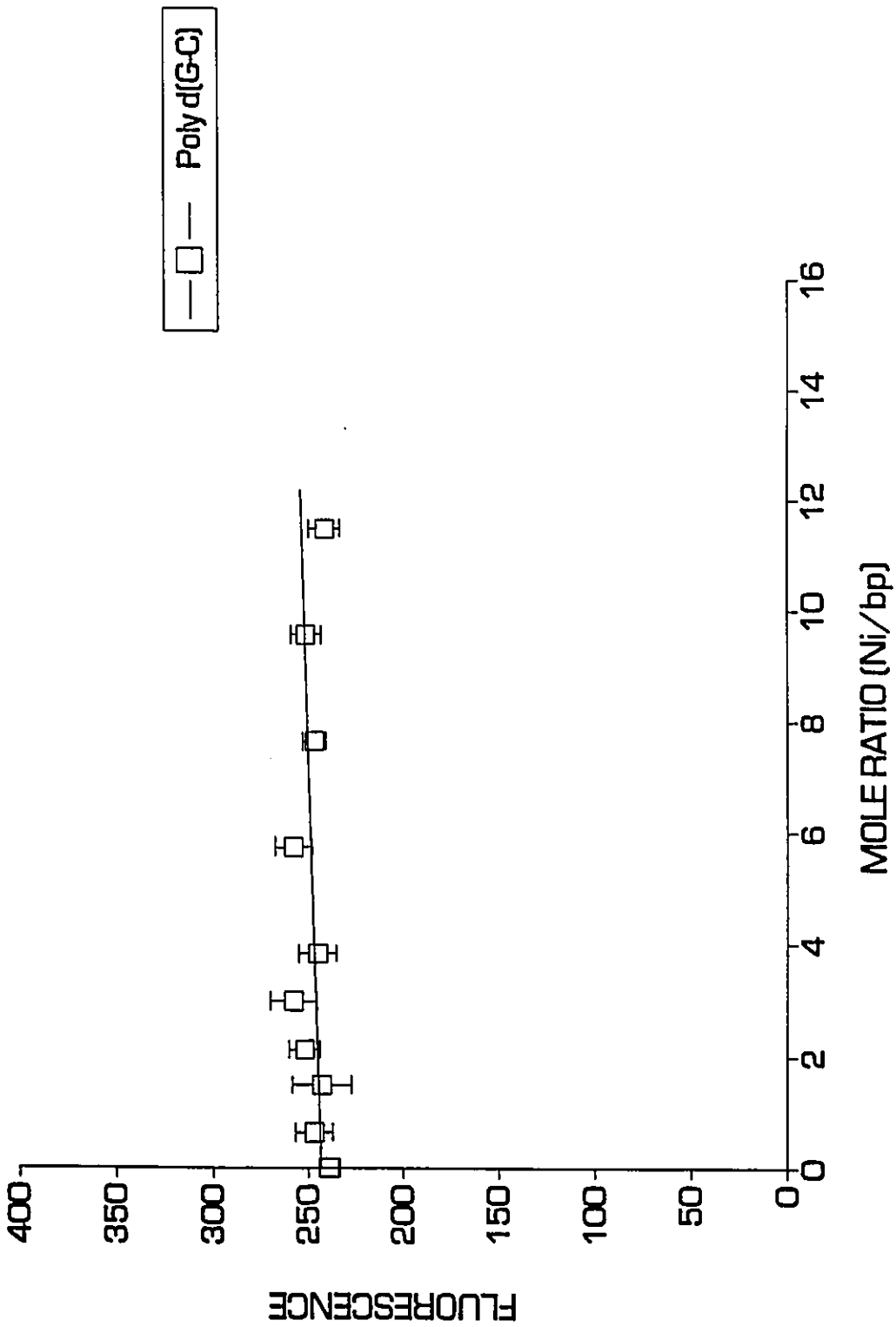
Poly d(G-C)
FLUORESCENCE
MOLE RATIO (Ni/bp)
400
350
300
250
200
150
100
50
0
0
2
4
6
8
10
12
14
16

II.3.4 Analysis of the Interaction of Ni(II)-Ion with DNA and Polydeoxynucleotide

II.3.4.1 Calf Thymus DNA

A complete analysis of the interaction of Ni(II) ion with calf thymus DNA with respect to absorbance ratios and DNase I digestion susceptibility is presented in Figure 12; the sedimentation profile is provided in Figure 13 and a CD analysis in Figure 14.

As previously described for calf thymus DNA (Figure 1 and 7), the interaction with Ni(II) ion does not appreciably alter the absorbance spectrum of the DNA which is reflected in a fairly constant absorbance ratio (Figure 12, see also Figure 7). Furthermore, the ability of EtBr to intercalate into this DNA is not affected by Ni(II) ion (Figure 12). The presence or absence of EDTA has no significant effect on the fluorescence. Ni(II) ion interaction does not render the DNA resistant to DNase I digestion (Figure 12) nor does it induce sedimentation of the DNA (Figure 13).

Analysis of the Ni(II) ion-DNA interaction with circular dichroism (CD) spectroscopy does not provide evidence for any gross structural or conformational alterations (Figure 14). The CD spectrum of native calf thymus DNA is characterized by a negative peak at 245 nm and a positive peak at 275 nm. The addition of increasing amounts of Ni(II) ion does not appreciably affect this latter positive signal, although a reduction in amplitude of the negative signal is induced in a concentration dependent manner (Figure 14).

Figure 12: Absorbance ratio ($A_{295}/_{260}$), EtBr fluorescence and DNase I digestion susceptibility profiles of calf thymus DNA in the presence of increasing amounts of Ni(II) ion. The figure legend describes the symbols utilized. The concentration of DNA was 32.27 μM.

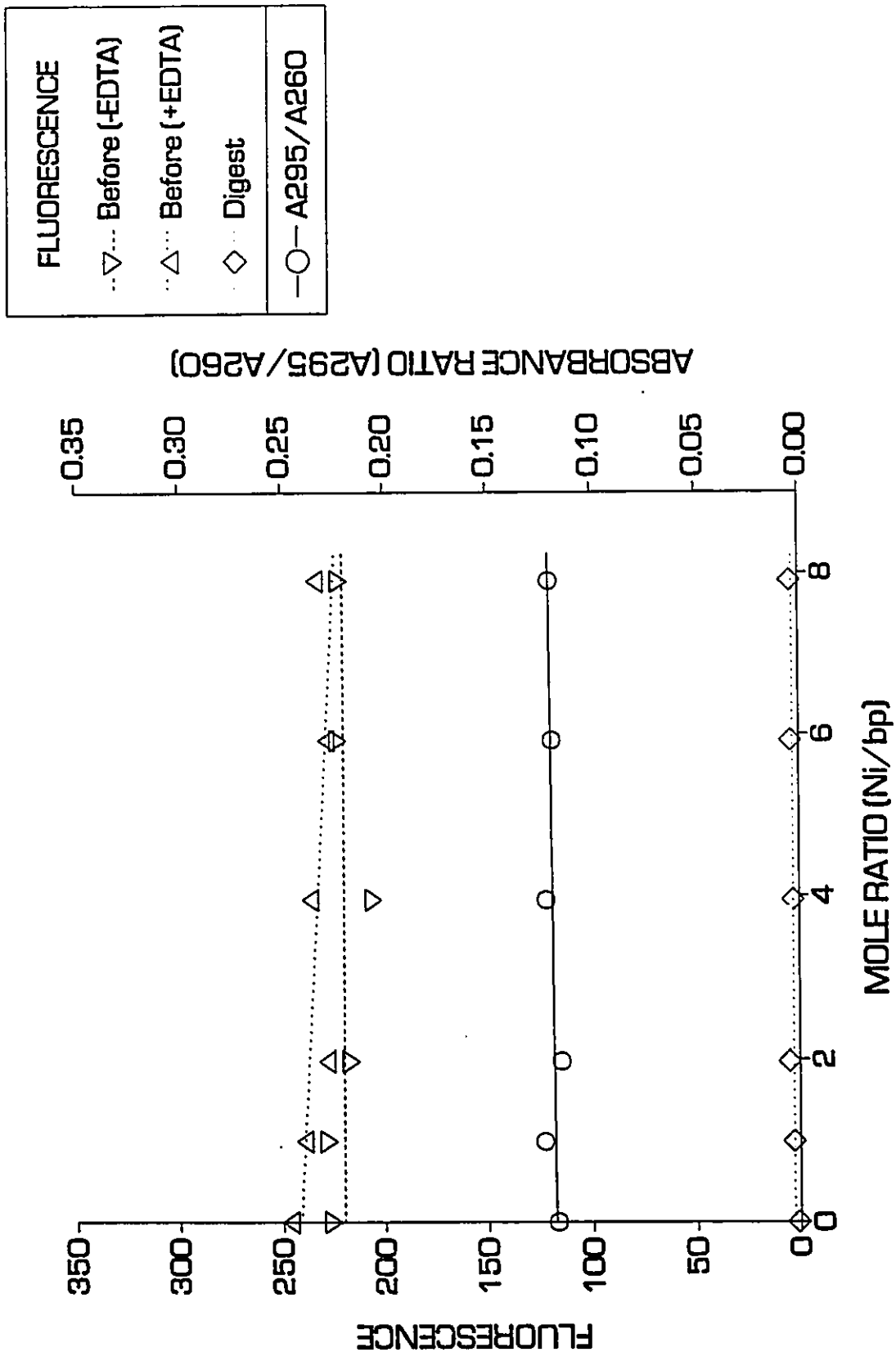
FLUORESCENCE
Before (-EDTA)
Before (+EDTA)
Digest
A295/A260
ABSORBANCE RATIO (A295/A260)
0.35
0.30
0.25
0.20
0.15
0.10
0.05
0.00
350
300
250
200
150
100
50
0
FLUORESCENCE
0
2
4
6
8
MOLE RATIO (Ni/bp)

Figure 13: Sedimentation analysis of calf thymus DNA in the presence of increasing amounts of Ni(II) ion. For comparison, EtBr-fluorescence (+ EDTA) is also presented. The figure legend describes the symbols utilized. The concentration of DNA was 32.27 μM.

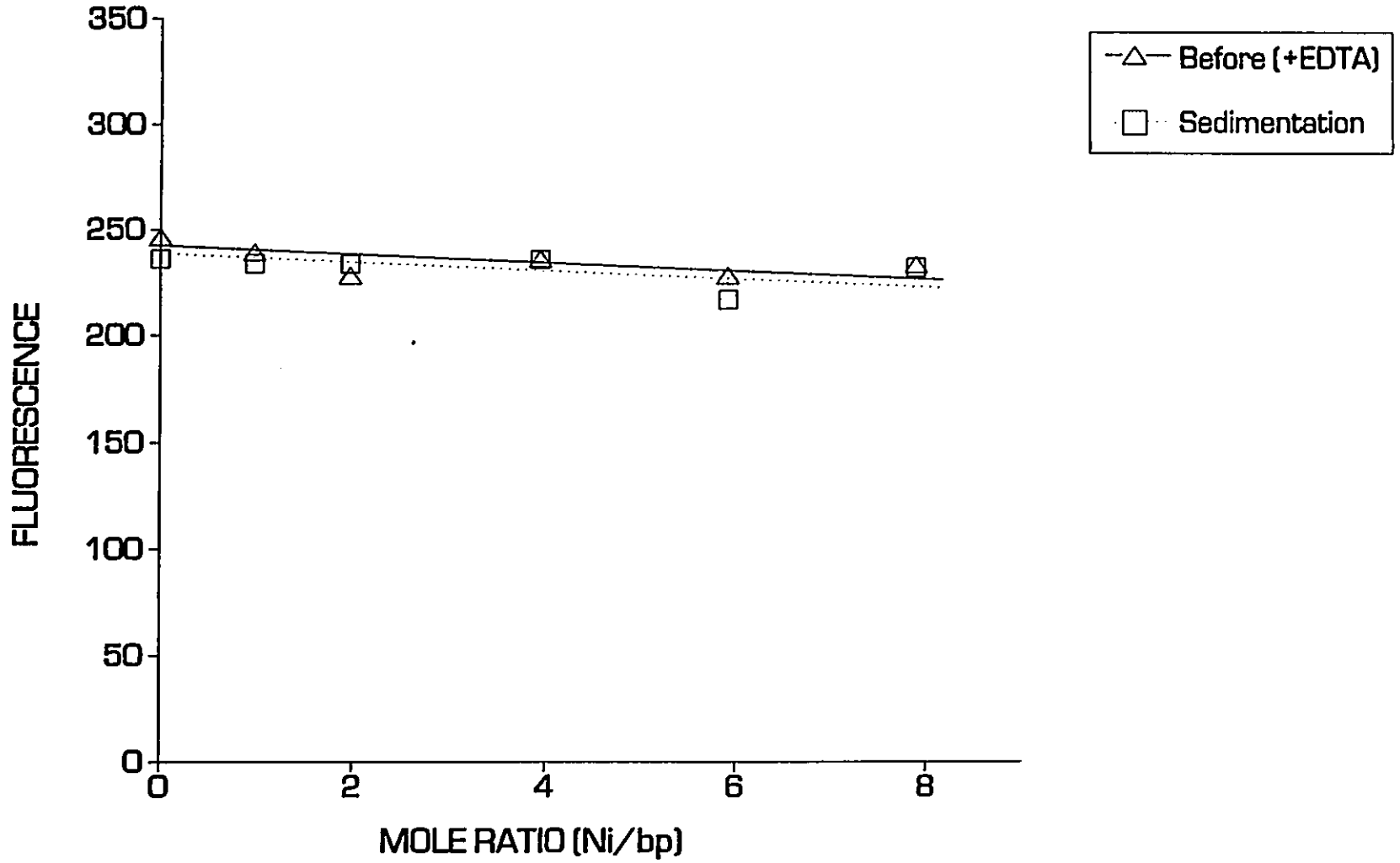
350
300
250
200
150
100
50
0
FLUORESCENCE
0
2
4
6
8
MOLE RATIO (Ni/bp)
Before (+EDTA)
Sedimentation

Figure 14: Circular dichroism (CD) scans of calf thymus DNA in the presence of Ni(II). Numbers correspond to CD scans with the following mole ratios (Ni/bp) and absorbance ratios ($A_{295}/_{260}$) respectively: 1) 0.00 and 0.114; 2) 1.89 and 0.119; 3) 7.89 and 0.115. DNA concentration was 32.27 μM.

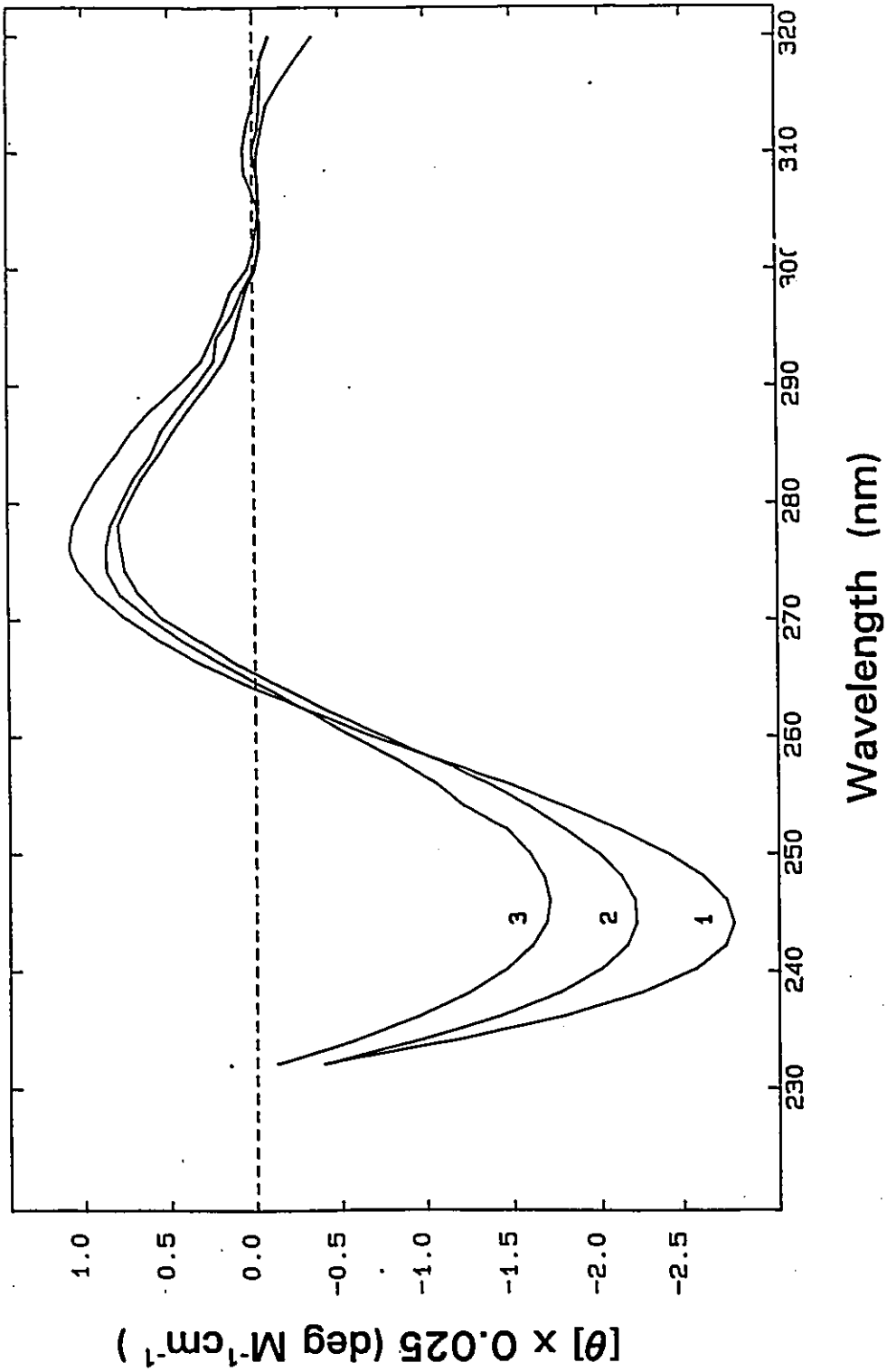
[θ] x 0.025 (deg M-1cm-1)
1.0
0.5
0.0
-0.5
-1.0
-1.5
-2.0
-2.5
230
240
250
260
270
280
290
310
320
1
2
3
Wavelength (nm)

II.3.4.2 Polyd(GC)·Polyd(GC)

A complete analysis of the interaction of polyd(GC)·polyd(GC) with Ni(II) ion is presented in Figures 15-18. As expected from the initial spectral analysis (Figures 4 and 7), distinct alterations in polydeoxynucleotide structure are observed.

Absorbance ratio data ($A_{295/260}$) are consistent with that already reported (cf. Figure 15 with 7). As increasing amounts of Ni(II) ion interact with the polydeoxynucleotide, there is a transition to a well defined plateau ($A_{295/260}$ = 0.2; Ni/bp mole ratio from 1.7 to 3.0). Additional Ni(II) ion induces a sharp increase in absorbance ratio to a final plateau ($A_{295/260}$ = 0.34; Ni/bp mole ratio > 6) (Figure 15). In the absence of EDTA, the decrease in ethidium bromide fluorescence parallels the increase in the absorbance ratio at transition (Figure 15). At Ni/bp mole ratios less than 4, fluorescence is relatively stable; at mole ratios greater than 6 fluorescence is also stable, albeit at reduced levels. The midpoint of the fluorescence transition parallels that of the transition of absorbance ratios between plateaus. The presence of EDTA in the fluorescence buffer abrogates this fluorescence transition (Figure 15).

The interaction of Ni(II) ion with polyd(GC)·polyd(GC) also renders this polydeoxynucleotide resistant to DNase I digestion at higher Ni/bp mole ratios (>6) (Figure 15). At low levels of Ni(II) ion corresponding to the first absorbance

ratio plateau, the polydeoxynucleotide is readily digested. The transition from DNase I sensitivity to insensitivity parallels the absorbance ratio and fluorescence transitions (-EDTA) previously discussed (Figure 15).

The sedimentation profile of this polydeoxynucleotide following interaction with Ni(II) ion is presented in Figure 16. At low concentrations of Ni(II) ion corresponding to the first absorbance ratio plateau (Ni/bp mole ratio > 4), the polydeoxynucleotide is not sedimentable. At progressively higher Ni(II) ion levels, there is a steady increase in sedimentability. This latter phenomenon does not correspond to a clear transition as observed for the absorbance ratio, DNase I digestion or EtBr fluorescence (Figure 16, see also Figure 15).

The CD spectra of Ni(II)-polyd(GC)·polyd(GC) are depicted in Figure 17. The initial polyd(GC)·polyd(GC) ($A_{295/260}$ = 0.108) spectrum is characterized by a negative peak at 250 nm, and a broad positive peak spanning from 270 to 310 nm. The initial addition of Ni(II) ion (Ni/bp mole ratio = 0.316; $A_{295/260}$ = 0.128) results in the shifting of the negative peak to 255 nm with a slight reduction in amplitude and a narrowing of the broad positive peak (280-310 nm). Further additions of metal (Ni/bp mole ratio = 2.534; $A_{295/260}$ = 0.191) results in a slight decrease in the amplitude of the negative peak at 255 nm, loss of the positive peak and the concomitant development of a small negative shoulder at 285 nm. Higher levels of Ni(II)

Figure 15: Absorbance ratio ($A_{295}/_{260}$), EtBr fluorescence and DNase I digestion susceptibility profiles of polyd(GC)·polyd(GC) in the presence of increasing amounts of Ni(II) ion. The figure legend describes the symbols utilized. Polydeoxynucleotide concentration was 20.83 μM.

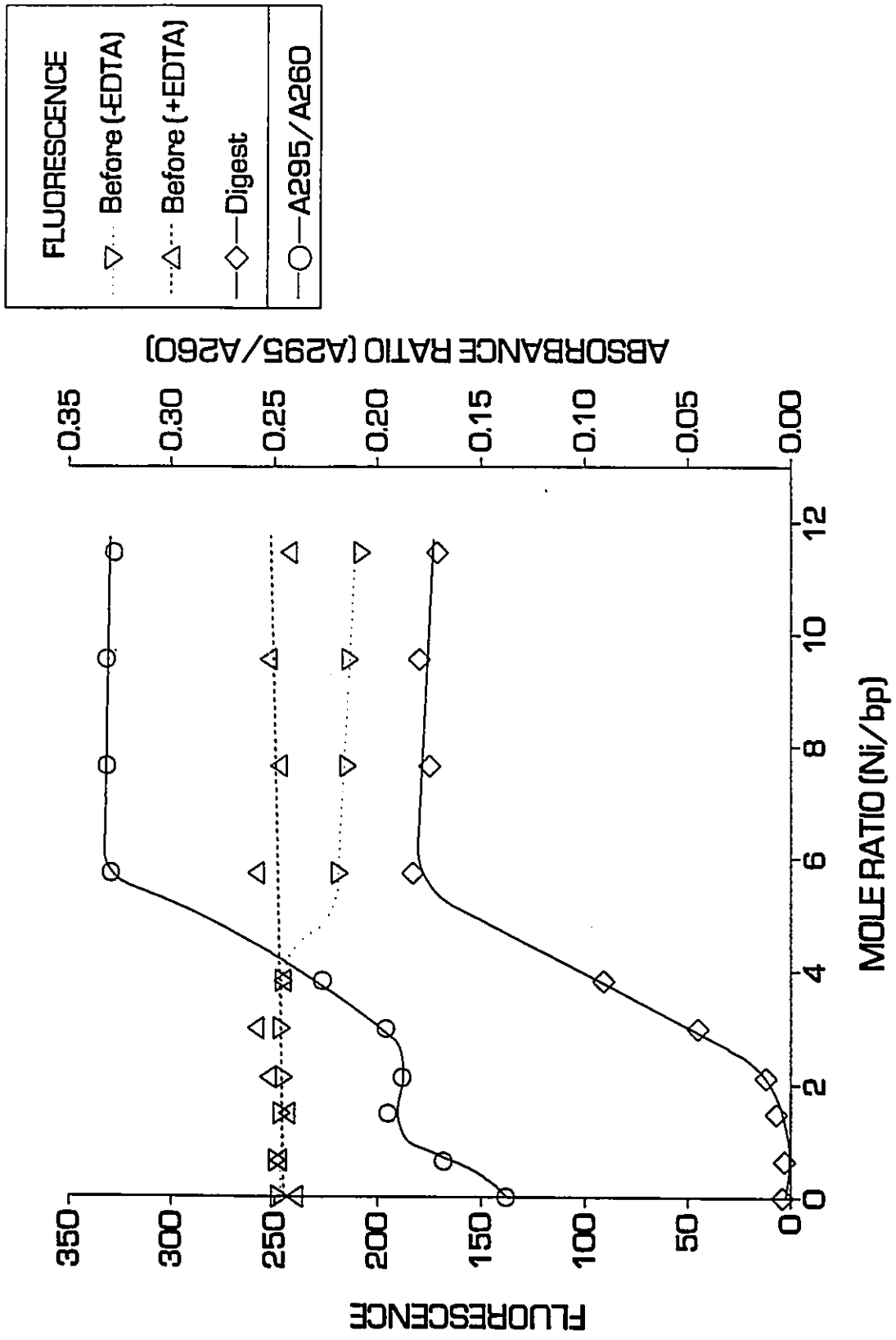
FLUORESCENCE
Before (-EDTA)
Before (+EDTA)
Digest
A295/A260
FLUORESCENCE
ABSORBANCE RATIO (A295/A260)
MOLE RATIO (Ni/bp)
0
50
100
150
200
250
300
350
0.00
0.05
0.10
0.15
0.20
0.25
0.30
0.35
0
2
4
6
8
10
12

Figure 16: Absorbance ratio ($A_{295}/_{260}$) and sedimentation analysis of polyd(GC)·polyd(GC) in the presence of increasing amounts of Ni(II) ion. For comparison, EtBr fluorescence (+ EDTA) is also presented. The figure legend describes the symbols utilized. The concentration of polydeoxynucleotide was 20.83 μM.

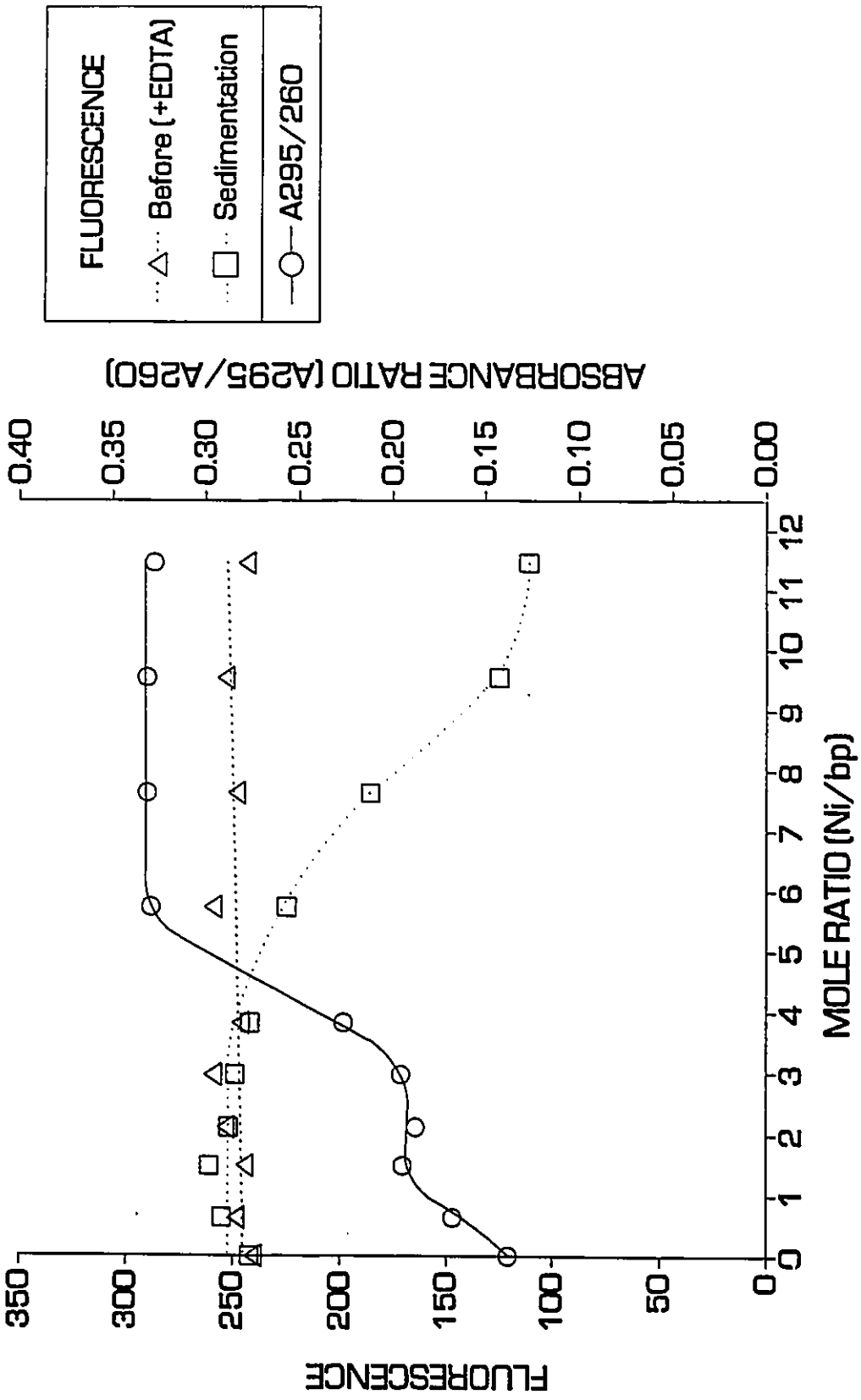
FLUORESCENCE
Before (+EDTA)
Sedimentation
A295/260
ABSORBANCE RATIO (A295/A260)
FLUORESCENCE
MOLE RATIO (Ni/bp)
0.40
0.35
0.30
0.25
0.20
0.15
0.10
0.05
0.00
350
300
250
200
150
100
50
0
0 1 2 3 4 5 6 7 8 9 10 11 12

Figure 17: Circular dichroism (CD) scans of polyd(GC)·polyd(GC) in the presence of Ni(II). Numbers correspond to CD scans with the following mole ratios (Ni/bp) and absorbance ratios ($A_{295}/_{260}$) respectively: 1) 0.00 and 0.108; 2) 0.32 and 0.128; 3) 2.53 and 0.191; 4) 3.51 and 0.241; 5) 9.78 and 0.339. Polydeoxynucleotide concentration was 20.83 μM.

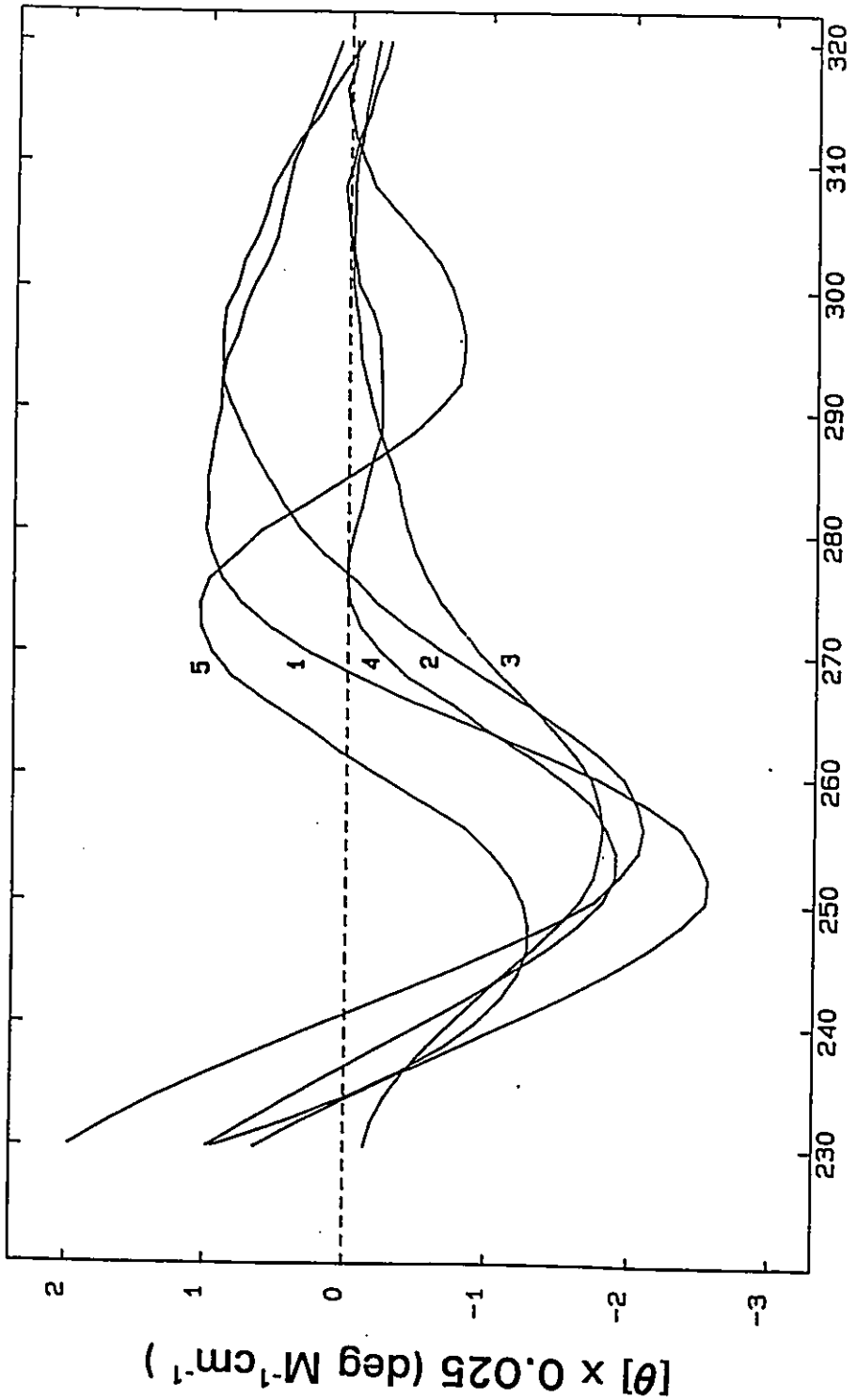
[θ] x 0.025 (deg M-1cm-1)
2
1
0
-1
-2
-3
230
240
250
260
270
280
290
300
310
320
Wavelength (nm)
5
1
4
2
3

Figure 18: Circular dichroism (CD) scans of polyd(GC)·polyd(GC) in the presence of Ni(II) ion following incubation at different temperatures for 24 h. Numbers correspond to CD scans with the following mole ratios (Ni/bp), absorbance ratios ($A_{295}/_{260}$), incubation temperatures and times respectively: 1) 12.65, 0.364, 37°C, 24 h; 2) 12.65, 0.406, 64°C, 24 h; 3) 12.65, 0.357, 37°C, 3h; 4) 12.65, 0.351, 24°C, 24 h; 5) 0.00, 0.150, 37°C, 24 h. Polydeoxynucleotide concentration was 24.17 μM.

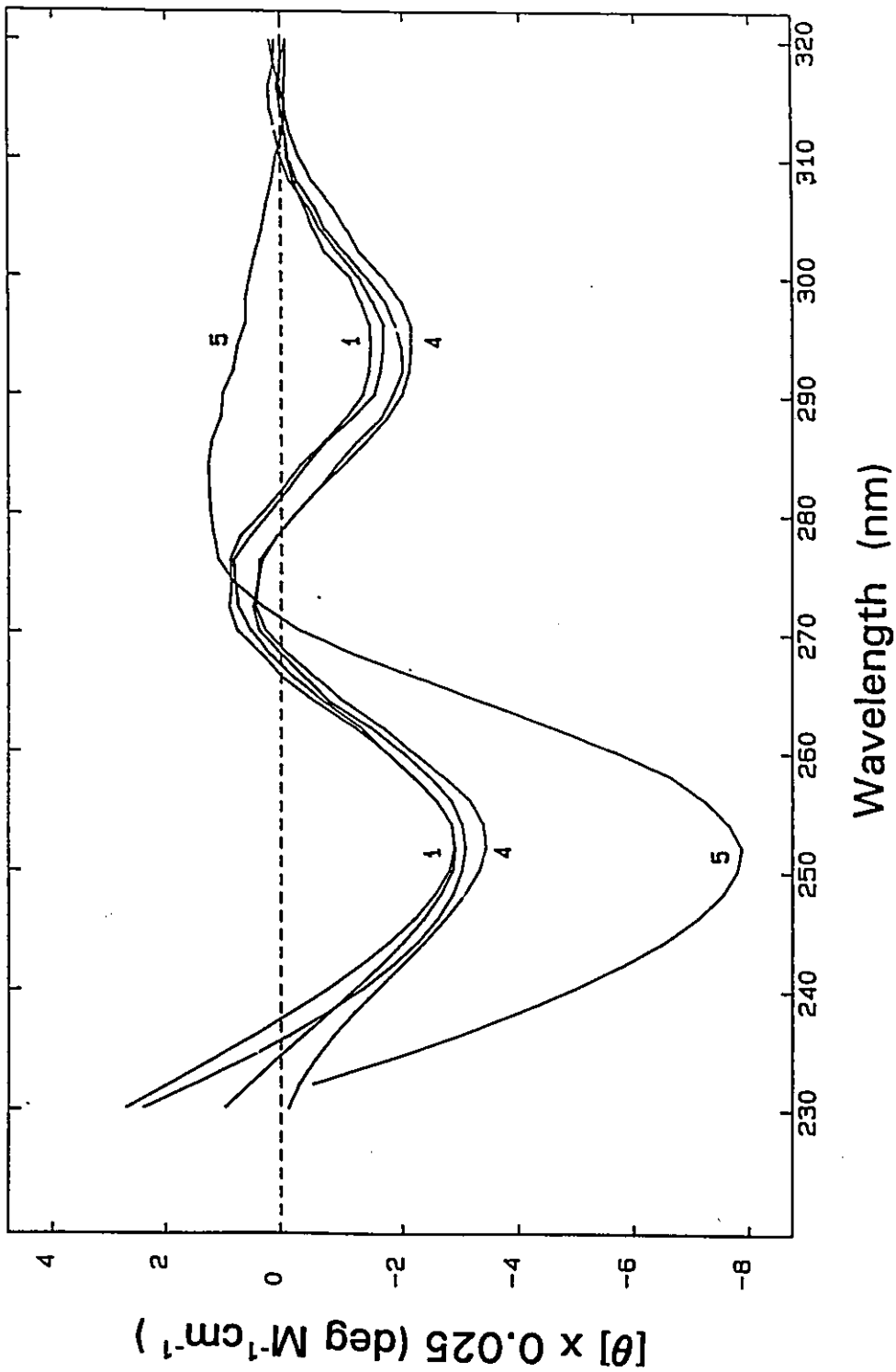
[θ] x 0.025 (deg M-1cm-1)
Wavelength (nm)
4
2
0
-2
-4
-6
-8
230
240
250
260
270
280
290
300
310
320
1
4
5
1
4
5

ion (Ni/bp mole ratio = 2.512; $A_{295/260}$ = 0.241) induce a DNA conformation with CD spectra characterized by a shift to 253 nm of the major negative peak and the development of a small but distinct negative peak at 295 nm. Higher levels of metal (Ni/bp mole ratio = 9.780; $A_{295/260}$ = 0.339) induce an inverted spectrum characterized by a smaller negative peak at 248 nm, a positive peak at 270 nm, and an additional larger negative peak at 295 nm. The interaction of even higher levels of Ni(II) ion with polyd(GC)·poly(GC) (Ni/bp mole ratio = 12.65) for longer periods of time (24 h) at various temperatures (24°C, 37°C, 65°C) do not fundamentally alter this final conformation of the polydeoxynucleotide as reflected by the CD spectra (Figure 18).

II.3.4.3 PolydG·PolydC

The analysis of the interaction of Ni(II) ion with polydG·polydC is presented in Figures 19-21. Absorbance ratio and DNase I digestion susceptibility data are provided in Figure 19; the sedimentation profile is provided in Figure 20 and a CD spectral analysis in Figure 21.

In the presence of Ni(II) ion, the UV spectra of polydG·polydC are slightly altered (Figure 2). In addition to a spectral shift of the maximum from 253 nm to 258 nm, there is a nickel-ion concentration dependent decrease in absorbance value at 258 nm (λmax). Although distinct, these alterations are not sufficiently significant so as to be reflected in the

absorbance ratio data (Figure 19; see also Figure 2 and 7). By contrast, in the presence of metal ion the fluorescence of intercalated EtBr decreases steadily in a metal concentration dependent manner, levelling off at a Ni(II) ion-polydeoxynucleotide mole ratio greater than 8 (Figure 19). The presence of EDTA in the EtBr buffer solution abrogates this effect completely (Figure 19). Under the conditions used for DNase I digestion in these studies, polydG·polydC in the absence of metal demonstrates some intrinsic resistance to digestion (Figure 19). As Ni(II) ion concentrations are increased, a transition to an increased degree of digestion resistance occurs, plateauing at mole ratios greater than 2. Although this increase is slight (approximately 2 fold) it is constant over the higher metal-polynucleotide mole ratios examined (Figure 19). No increase in sedimentation is observed for the polydeoxynucleotide in the presence of Ni(II) ion (Figure 20). However, there does exist an intrinsic level of sedimentation which is constant both in the absence and presence of increasing amounts of Ni(II) ion.

The CD spectra obtained for polydG·polydC are similar to the UV absorbance spectra in that slight but distinct changes are observed in the presence of Ni(II) ion (Figure 21). PolydG·polydC is characterized by a single positive peak at 260 nm. In the presence of Ni(II) ion, there is a slight but noticeable decrease in amplitude of the positive peak in a concentration dependent manner. Furthermore, an isobestic

Figure 19: Absorbance ratio ($A_{295}/_{260}$), EtBr fluorescence and DNase I digestion susceptibility profiles of polydG·polydC in the presence of increasing amounts of Ni(II) ion. The figure legend describes the symbols utilized. Polydeoxynucleotide concentration was 29.19 μM.

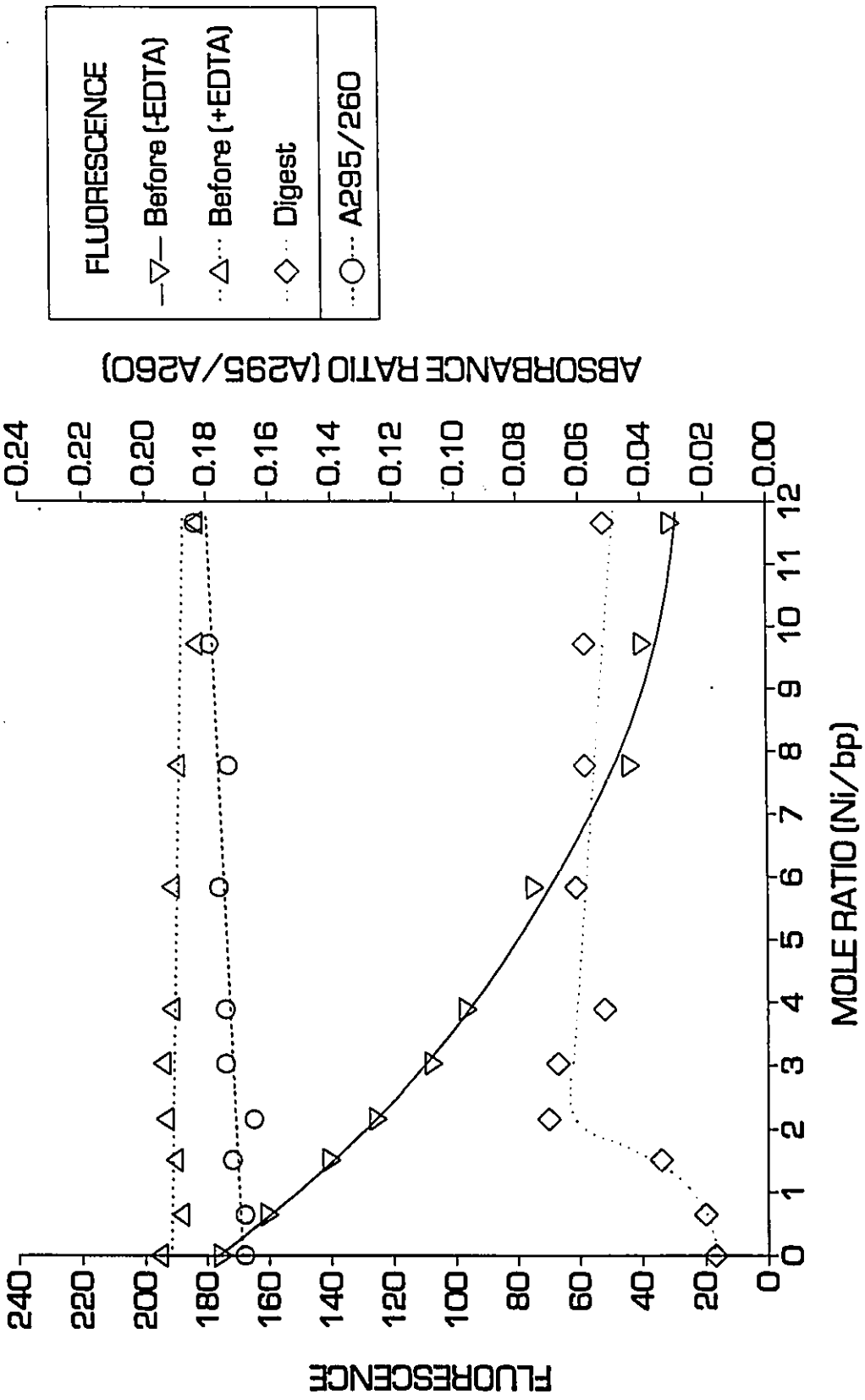
FLUORESCENCE
Before (-EDTA)
Before (+EDTA)
Digest
A295/260
ABSORBANCE RATIO (A295/A260)
FLUORESCENCE
MOLE RATIO (Ni/bp)
0
20
40
60
80
100
120
140
160
180
200
220
240
0.00
0.02
0.04
0.06
0.08
0.10
0.12
0.14
0.16
0.18
0.20
0.22
0.24
0 1 2 3 4 5 6 7 8 9 10 11 12

Figure 20: Sedimentation analysis of polydG·polydC in the presence of increasing amounts of Ni(II) ion. For comparison, EtBr-fluorescence (+ EDTA) is also presented. The figure legend describes the symbols utilized. The concentration of polydeoxynucleotide was 29.19 μM.

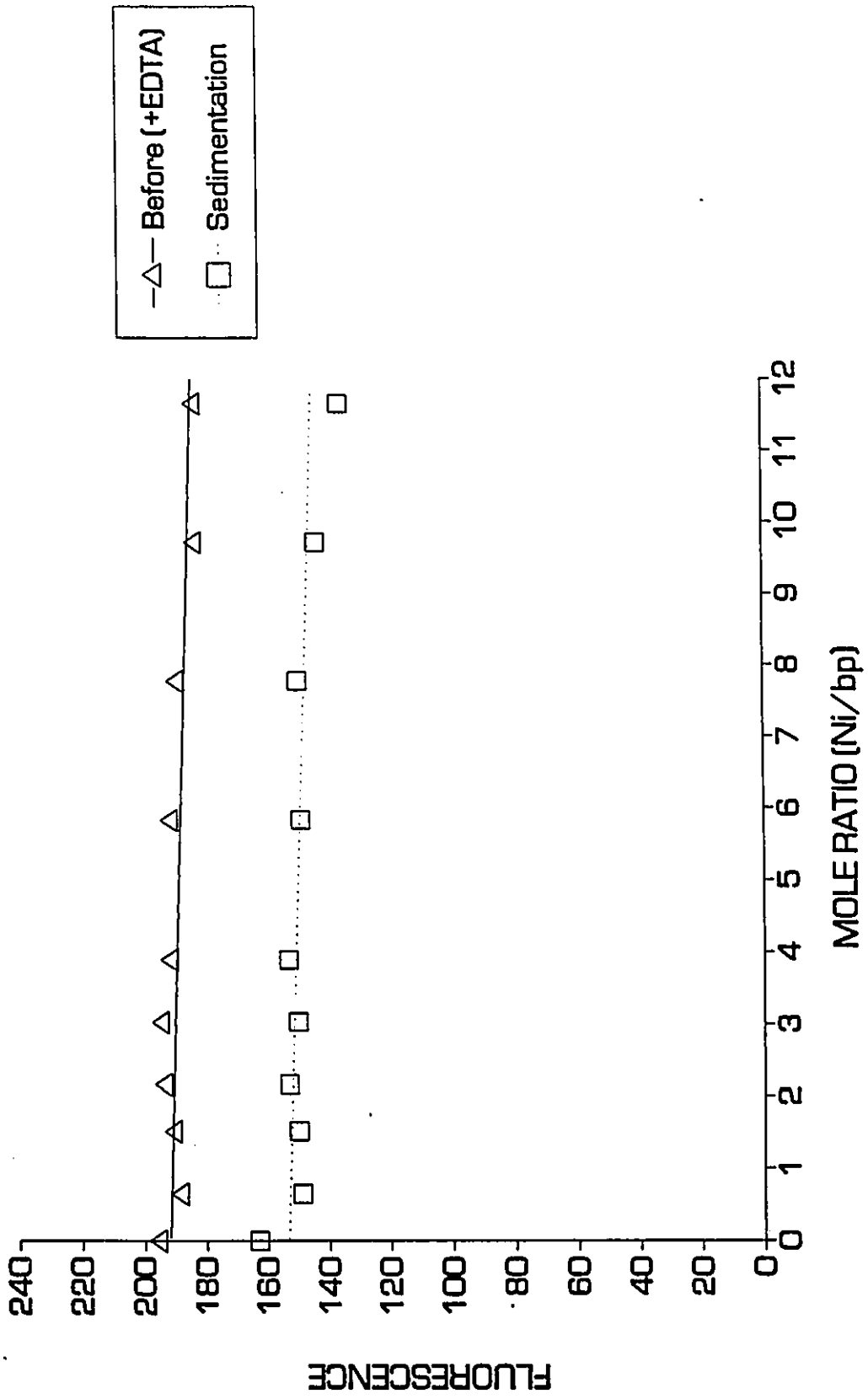
Before (+EDTA)
Sedimentation
FLUORESCENCE
MOLE RATIO (Ni/bp)
0
20
40
60
80
100
120
140
160
180
200
220
240
0
1
2
3
4
5
6
7
8
9
10
11
12

Figure 21: Circular dichroism (CD) scans of polydG·polydC in the presence of Ni(II). Numbers correspond to CD scans with the following mole ratios (Ni/bp) and absorbance ratios ($A_{295}/_{260}$) respectively: 1) 0.00 and 0.123; 2) 0.87 and 0.130; 3) 3.49 and 0.121; 4) 8.72 and 0.125. Polydeoxynucleotide concentration was 29.19 μM.

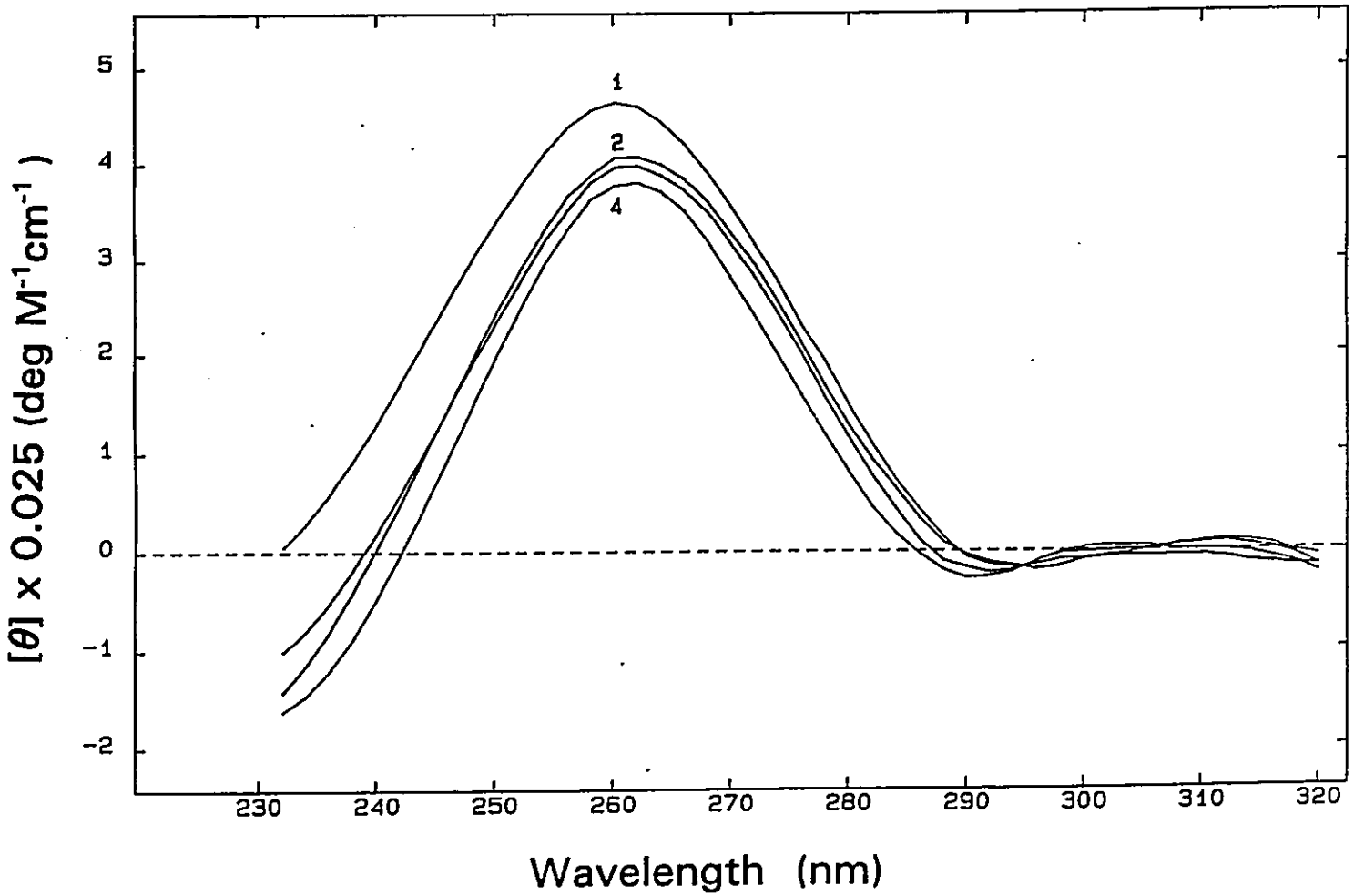
[θ] x 0.025 (deg M-1cm-1)
5
4
3
2
1
0
−1
−2
1
2
4
230
240
250
260
270
280
290
300
310
320
Wavelength (nm)

point at 295 nm is observed for the spectra depicted.

II.3.4.4 Polyd(GT)·Polyd(AC)

By contrast to most of the other polydeoxynucleotides tested, Ni(II) ion-polyd(GT)·polyd(AC) mixtures were incubated at two temperatures (37°C and 64°C) prior to further analysis.

Following the 37°C incubation, the absorbance ratio data did not demonstrate any appreciable transition or change as previously described (Figure 22, compare with Figure 3 and 7). In addition, EtBr fluorescence is not affected at any Ni(II)/bp mole ratio in the presence or absence of EDTA (Figure 22). At all levels of metal, the polydeoxynucleotide is completely susceptible to DNase I digestion (Figure 22). Although polyd(GT)·polyd(AC) displays some intrinsic ability to sediment in the absence of metal ion, this characteristic is independent of ion concentration in the range utilized in these experiments (Figure 23).

The CD spectra do not provide any clear evidence for novel transitions of conformations. The polydeoxynucleotide, in the absence of Ni(II) ion, is characterized by a large negative signal at 245 nm and a broad positive peak centred at 280 nm (Figure 24). The addition of metal results in a slight increase in amplitude of the negative signal and an abrogation of the positive signal at 280 nm (Figure 24).

The results following incubation at 64°C are quite distinct from those described for the 37°C incubation. The

absorbance ratio data depicts a clear biphasic transition somewhat analogous to that observed for polyd(GC)·polyd(GC) (Figure 25, compare with Figure 15). By comparison, the plateaus in this case are reduced in value. At mole ratios between 2-5, a plateau at an absorbance ratio of 0.11 is observed. Between mole ratios of 5 and 7, there is a sharp transition to a plateau in absorbance ratio of approximately 0.15 (Figure 25). The EtBr fluorescence of this polydeoxynucleotide also demonstrates a transition in the mole ratio range of 5 to 7 (Figure 25) from stable pre- to post-transitional plateaus. The presence of EDTA in the absorbance buffer negates this transition completely (Figure 25). Furthermore, DNase I digestion susceptibility follows a similar transition in the mole ratio range of 5 to 7. Below Ni(II)/bp mole ratios of 5, the polydeoxynucleotide is digestible; above mole ratios of 7, substantial resistance is observed and is stable over the concentrations of Ni(II) ion utilized (Figure 25). By contrast, this polydeoxynucleotide is not sedimented at any concentration of Ni(II) ions (Figure 26).

The CD spectra of this polydeoxynucleotide incubated at 64°C differs from that incubated at 37°C. In the absence of Ni(II) ion, the spectrum is characterized by a single negative peak at 255 nm (Figure 27; contrast with Figure 24). As levels of Ni(II) ion are increased, the sole change in the spectrum is a concentration-dependent decrease in amplitude of

Figure 22: Absorbance ratio ($A_{295}/_{260}$), EtBr fluorescence and DNase I digestion susceptibility profiles of polyd(GT)·polyd(AC) in the presence of increasing amounts of Ni(II) ion. The figure legend describes the symbols utilized. Polydeoxynucleotide concentration was 29.85 μM.

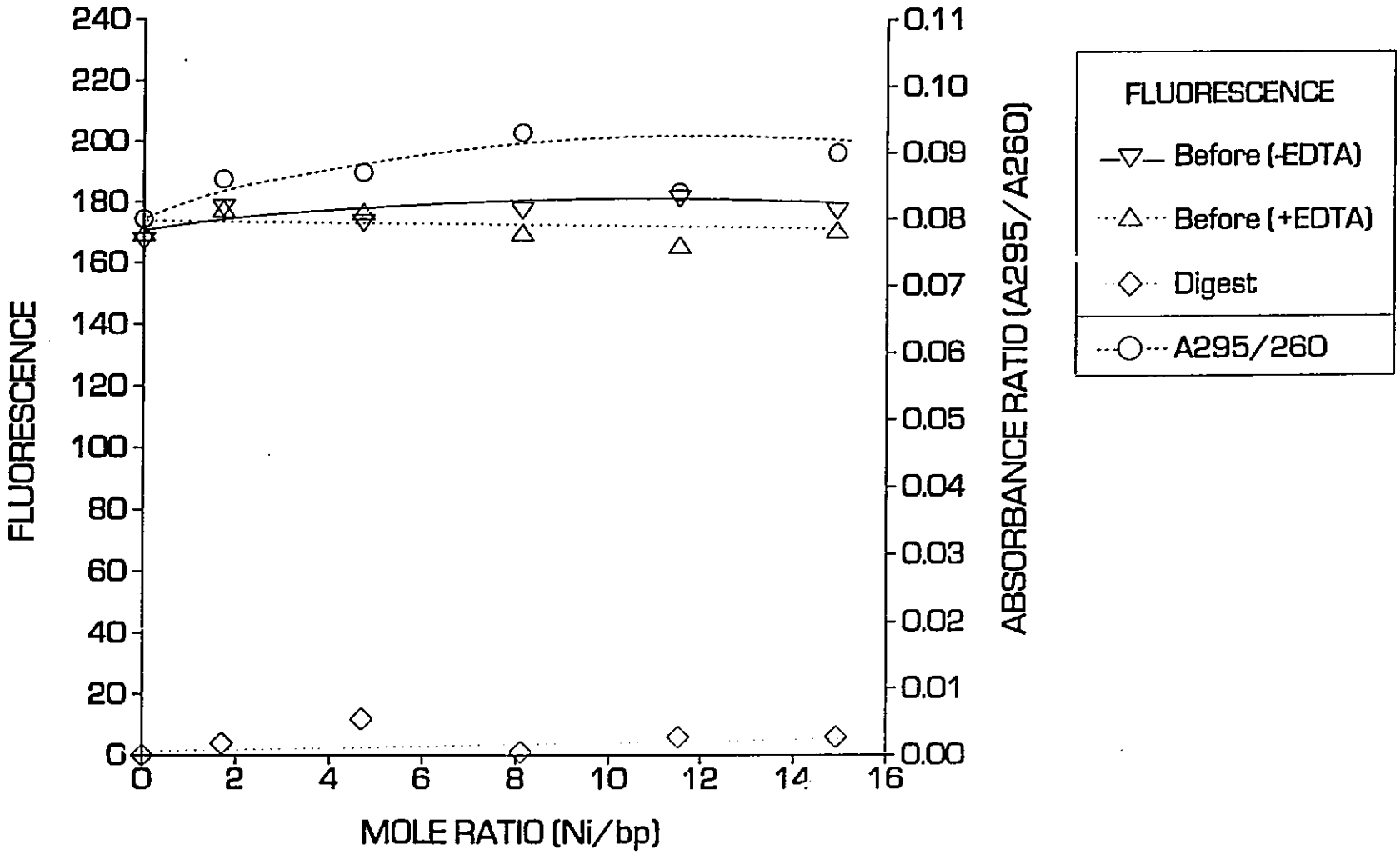
FLUORESCENCE
240
220
200
180
160
140
120
100
80
60
40
20
0
0.11
0.10
0.09
0.08
0.07
0.06
0.05
0.04
0.03
0.02
0.01
0.00
ABSORBANCE RATIO (A295/A260)
0
2
4
6
8
10
12
14
16
MOLE RATIO (Ni/bp)
FLUORESCENCE
Before (-EDTA)
Before (+EDTA)
Digest
A295/260

Figure 23: Sedimentation analysis of polyd(GT)·polyd(AC) in the presence of increasing amounts of Ni(II) ion. For comparison, EtBr-fluorescence (+ EDTA) is also presented. The figure legend describes the symbols utilized. The concentration of polydeoxynucleotide was 29.85 μM.

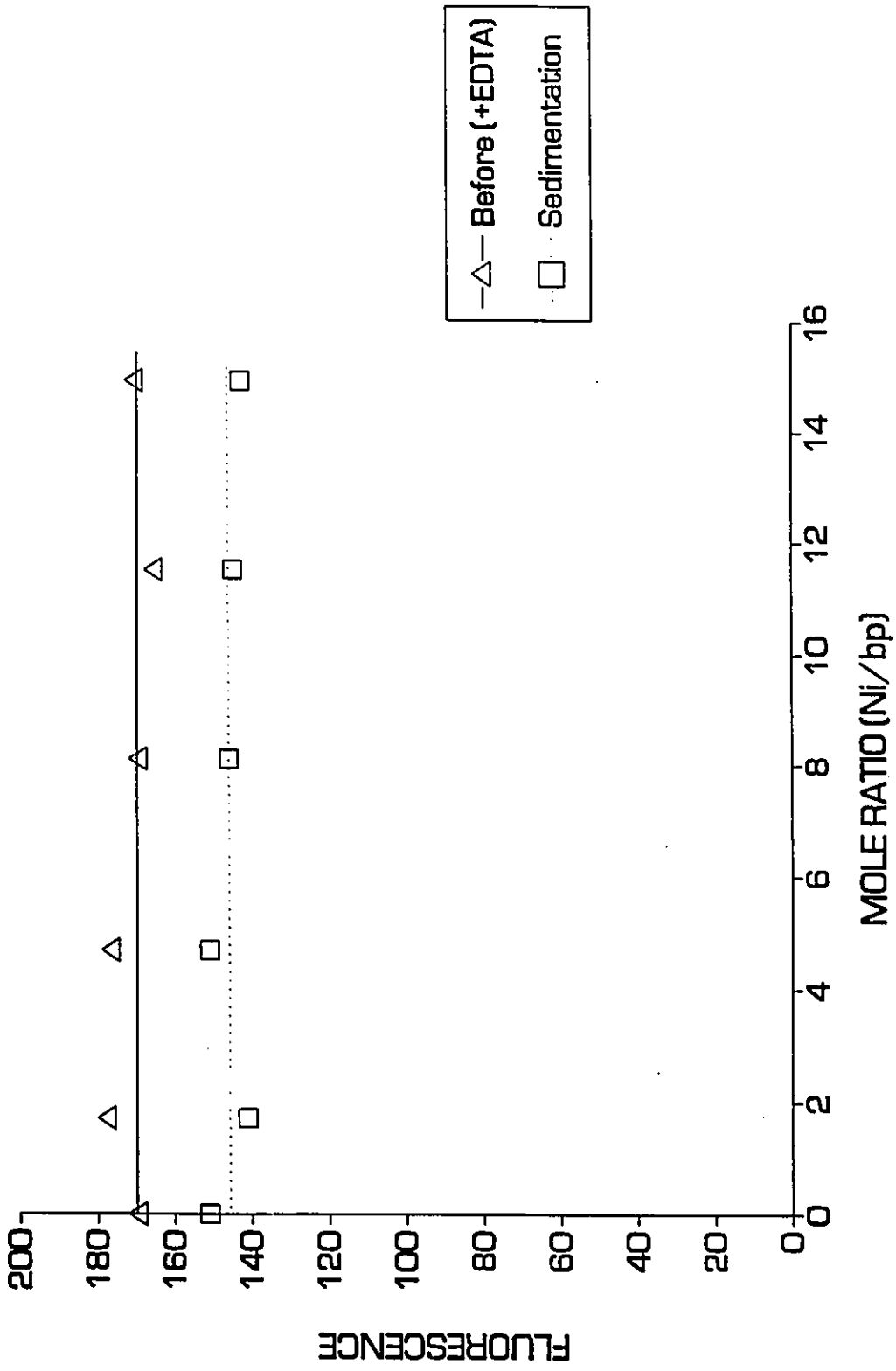
—△— Before (+EDTA)
□ Sedimentation
FLUORESCENCE
MOLE RATIO (Ni/bp)
0
20
40
60
80
100
120
140
160
180
200
0
2
4
6
8
10
12
14
16

Figure 24: Circular dichroism (CD) scans of polyd(GT)·polyd(AC) in the presence of Ni(II). Numbers correspond to CD scans with the following mole ratios (Ni/bp) and absorbance ratios ($A_{295}/_{260}$) respectively: 1) 0.00 and 0.096; 2) 6.66 and 0.091; 3) 13.31 and 0.093. Polydeoxynucleotide concentration was 29.85 μM.

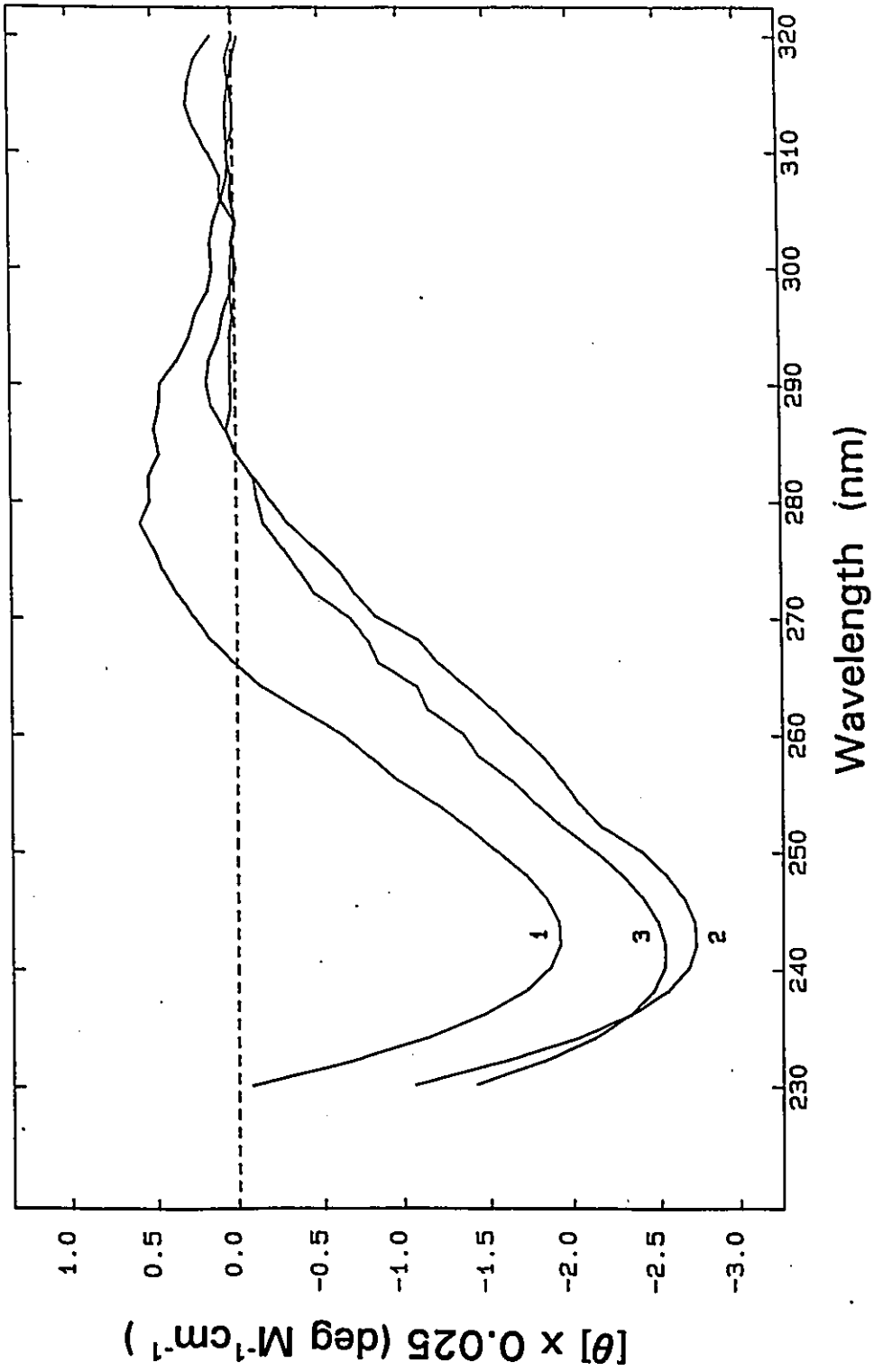
[θ] x 0.025 (deg M⁻¹cm⁻¹)
1.0
0.5
0.0
-0.5
-1.0
-1.5
-2.0
-2.5
-3.0
230
240
250
260
270
280
290
300
310
320
Wavelength (nm)
1
2
3

Figure 25: Absorbance ratio ($A_{295}/_{260}$), EtBr fluorescence and DNase I digestion susceptibility profiles of polyd(GT)·polyd(AC) in the presence of increasing amounts of Ni(II) ion following incubation at 64°C. The figure legend describes the symbols utilized. Polydeoxynucleotide concentration was 29.85 μM.

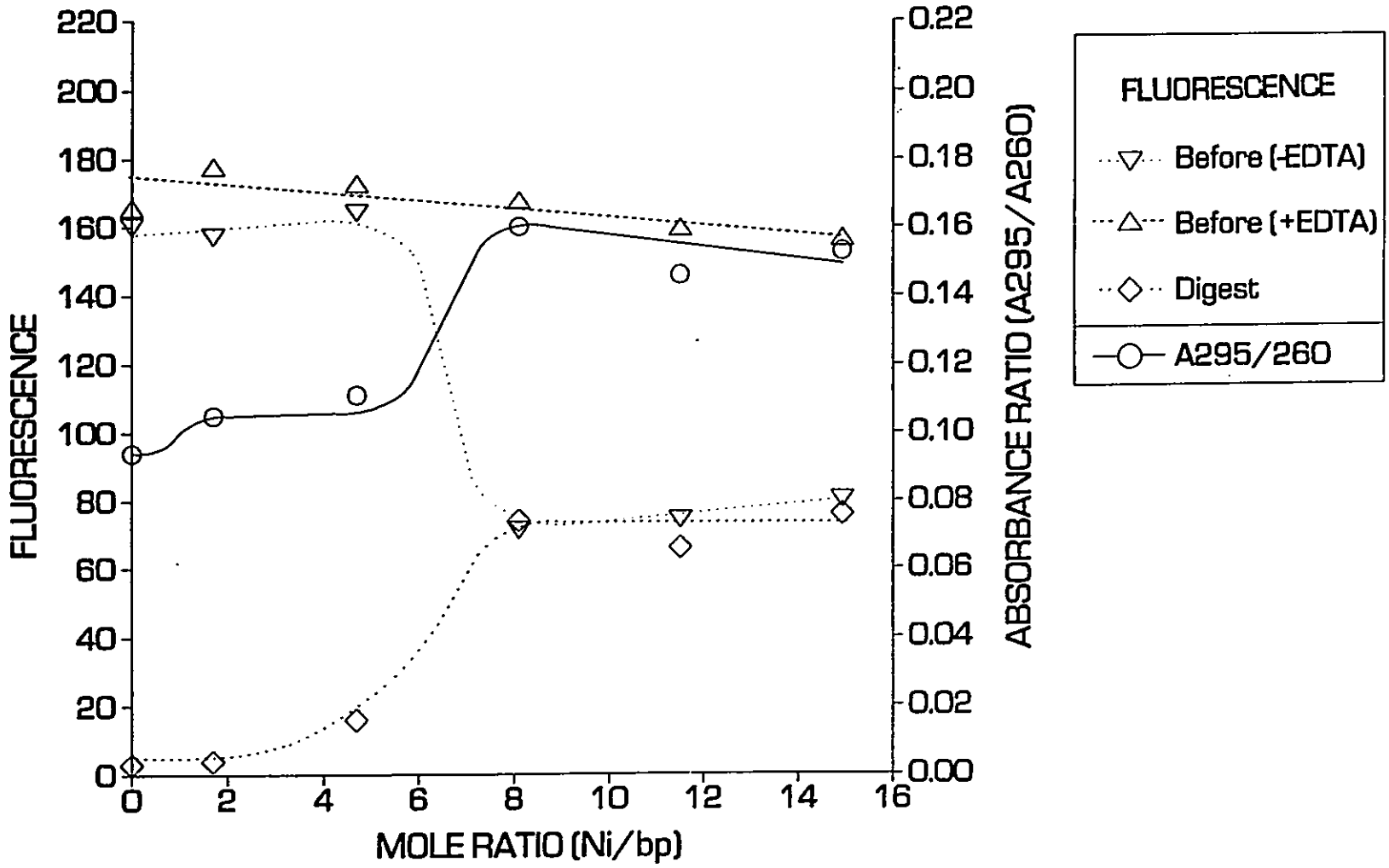
FLUORESCENCE
220
200
180
160
140
120
100
80
60
40
20
0
0.22
0.20
0.18
0.16
0.14
0.12
0.10
0.08
0.06
0.04
0.02
0.00
ABSORBANCE RATIO (A295/A260)
0
2
4
6
8
10
12
14
16
MOLE RATIO (Ni/bp)
FLUORESCENCE
Before (-EDTA)
Before (+EDTA)
Digest
A295/260

Figure 26: Absorbance ratio ($A_{295}/_{260}$) and sedimentation analysis of polyd(GT)·polyd(AC) in the presence of increasing amounts of Ni(II) ion following incubation at 64°C. For comparison, EtBr fluorescence (+ EDTA) is also presented. The figure legend describes the symbols utilized. The concentration of polydeoxynucleotide was 29.85 μM.

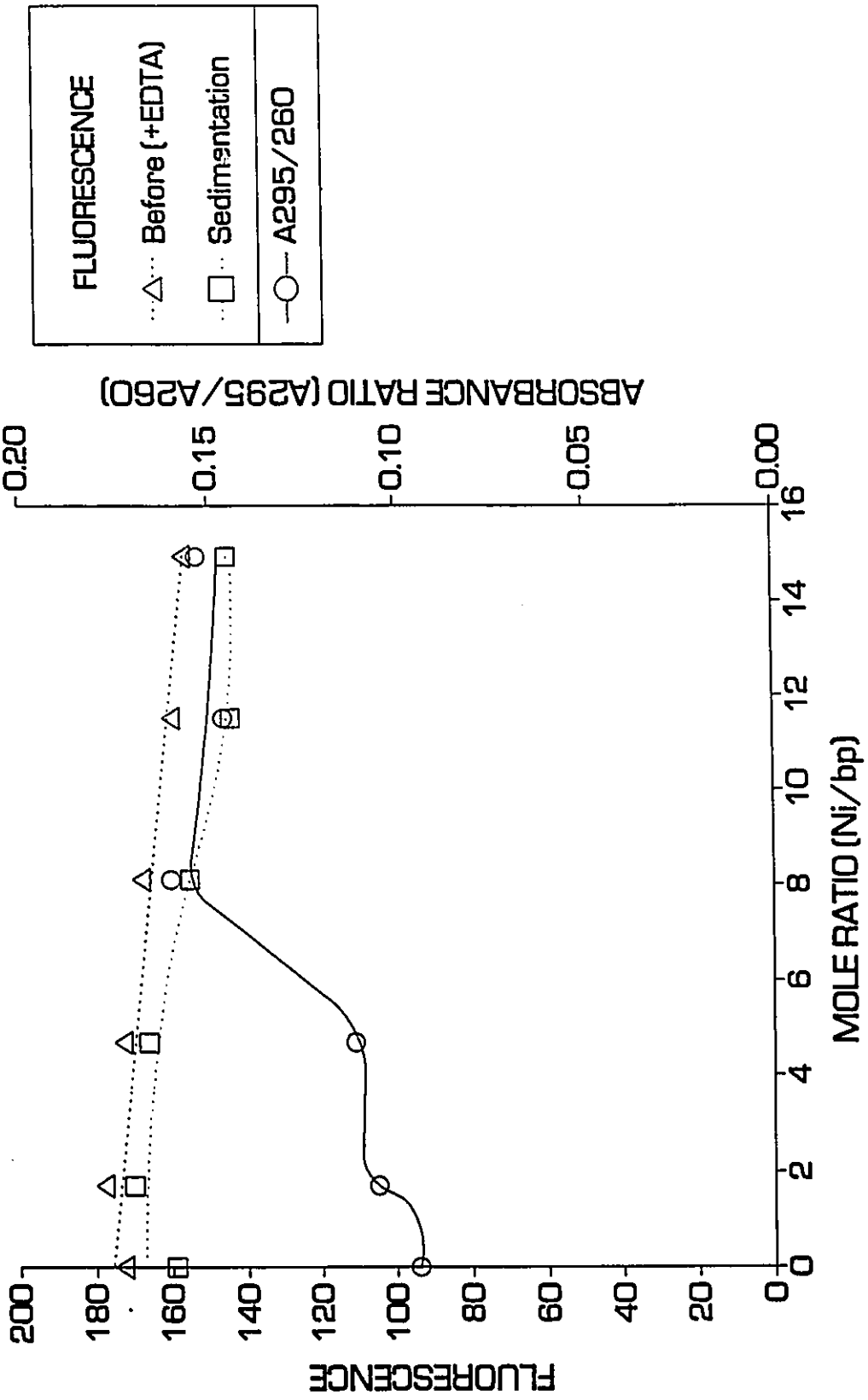
FLUORESCENCE
Before (+EDTA)
Sedimentation
A295/260
ABSORBANCE RATIO (A295/A260)
0.20
0.15
0.10
0.05
0.00
FLUORESCENCE
200
180
160
140
120
100
80
60
40
20
0
0
2
4
6
8
10
12
14
16
MOLE RATIO (Ni/bp)

Figure 27: Circular dichroism (CD) scans of polyd(GT)·polyd(AC) in the presence of Ni(II) ion following incubation at 64°C. Numbers correspond to CD scans with the following mole ratios (Ni/bp) and absorbance ratios ($A_{295}/_{260}$) respectively: 1) 0.00 and 0.090; 2) 1.84 and 0.103; 3) 8.05 and 0.158; 4) 11.50 and 0.176. Polydeoxynucleotide concentration was 29.85 μm.

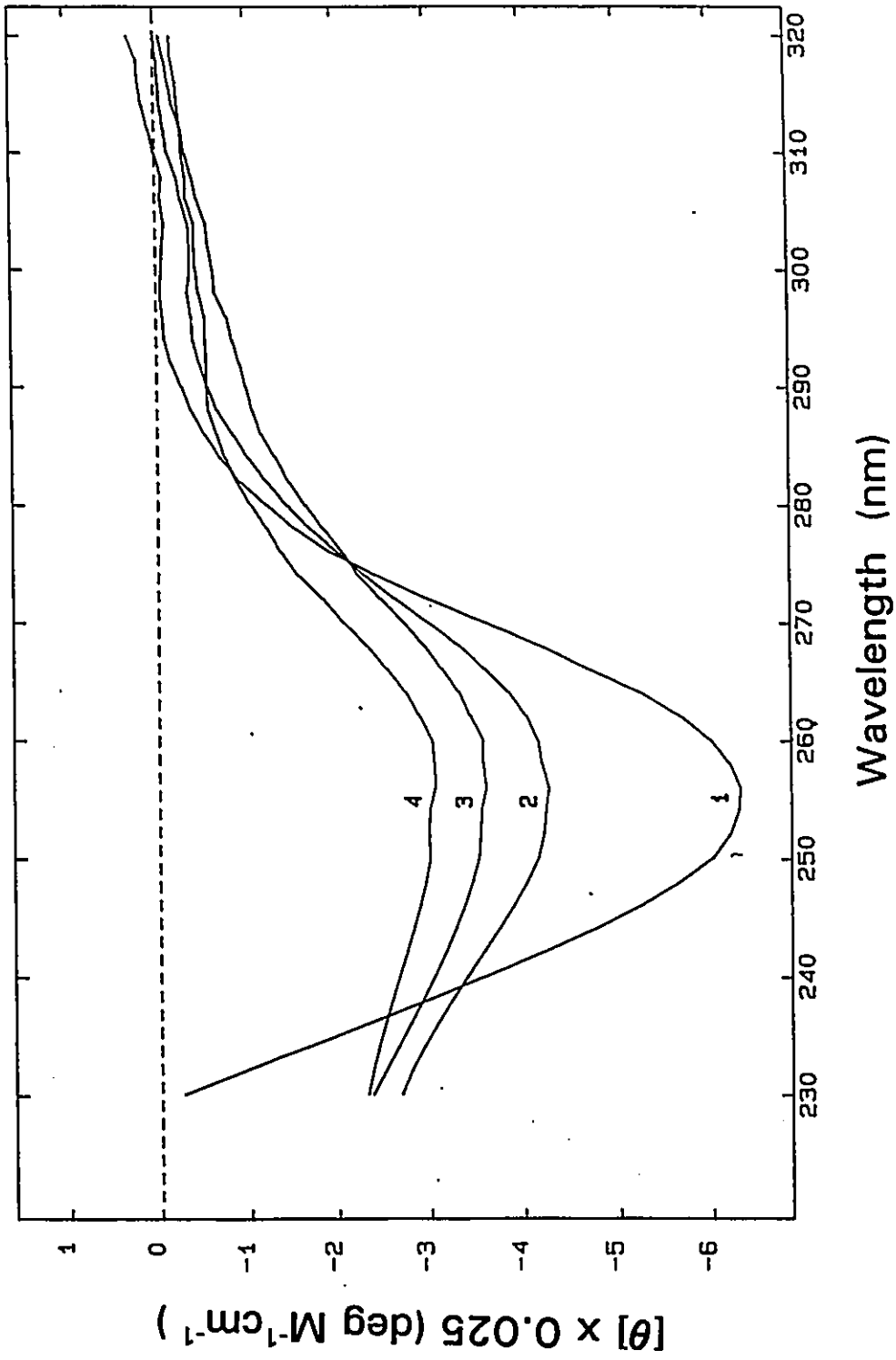
[θ] x 0.025 (deg M-1cm-1)
1
0
-1
-2
-3
-4
-5
-6
230
240
250
260
270
280
290
300
310
320
Wavelength (nm)
1
2
3
4

this negative signal (Figure 27).

II.3.4.5 Polyd(AT)·Polyd(AT)

A complete analysis of the interaction of Ni(II) ion with polyd(AT)·polyd(AT) with respect to absorbance ratios and DNAse I digestion susceptibility is presented in Figure 28 with the sedimentation profile in Figure 29 and the CD analysis in Figure 30.

As previously described for this polydeoxynucleotide (Figures 5 and 8), the interaction with Ni(II) ion does not appreciably alter the absorbance spectrum of the polydeoxynucleotide, thus a constant absorbance ratio is observed (Figure 28, see also Figure 8). Furthermore, EtBr fluorescence is not affected by Ni(II) ion in the presence or absence of EDTA (Figure 28). Metal ion interaction does not render the polydeoxynucleotide resistant to DNase I digestion (Figure 28), nor does it induce sedimentation (Figure 29).

CD spectra do not provide any evidence for significant structural alterations occurring in polyd(AT)·polyd(AT) following Ni(II) interaction. In the absence of metal, the CD trace is characterized by a negative peak at 245 nm and a positive peak at 268 nm. In the presence of Ni(II) ions, the amplitude of both peaks shift slightly in a negative direction in a metal ion concentration dependent manner (Figure 30).

II.3.4.6 PolydA·PolydT

An analysis of the interaction of Ni(II) ion with polydA·polydT with respect to absorbance ratios and DNase I digestion susceptibility is presented in Figure 31; the sedimentation profile is provided in Figure 32 and a CD analysis in Figure 33.

As depicted in Figures 6 and 8, the interaction of Ni(II) ion with polydA·polydT does ıot affect the absorbance spectrum and thus, the absorbance ratio of this polydeoxy-nucleotide in the presence of increasing Ni(II) ion (Figure 31). In addition, EtBr fluorescence is not affected (Figure 31), nor is resistance to DNase I digestion observed (Figure 31). Sedimentation is not induced by interaction with Ni(II) ion (Figure 32).

The CD spectra of the Ni(II)-polydA·polydT confirm that no changes in polydeoxynucleotide structure occur following addition of metal (Figure 33). In the absence of nickel ions, the CD trace is characterized by a negative peak at 245 nm and a second smaller negative peak at 278 nm. Slight differences in peak amplitudes are observed at varying concentrations of Ni(II) ion but no consistent concentration-dependent variations are noted (Figure 33).

Figure 28: Absorbance ratio ($A_{290}/_{260}$), EtBr fluorescence and DNase I digestion susceptibility profiles of polyd(AT)·polyd(AT) in the presence of increasing amounts of Ni(II) ion. The figure legend describes the symbols utilized. Polydeoxynucleotide concentration was 32.27 μM.

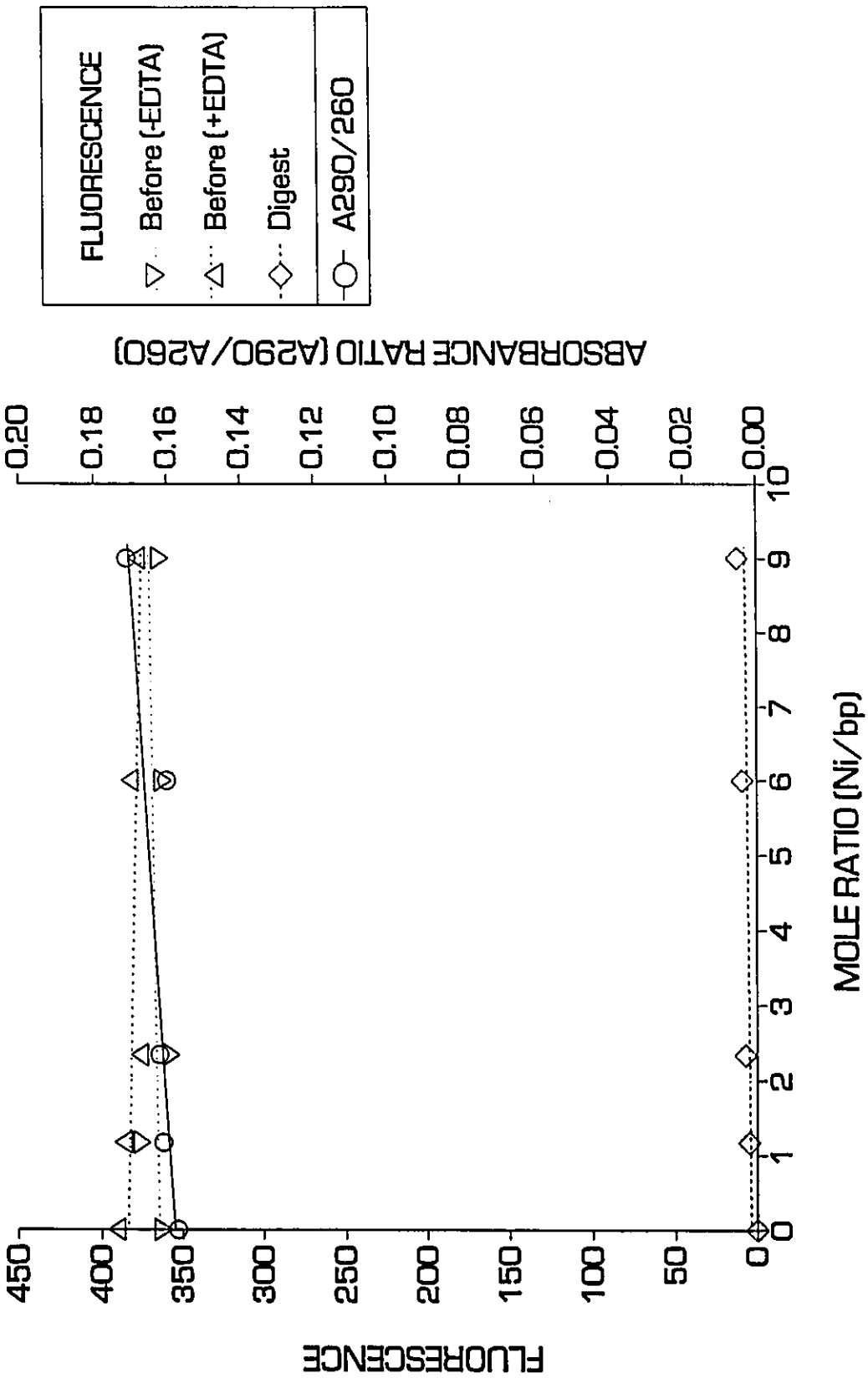
FLUORESCENCE
Before (-EDTA)
Before (+EDTA)
Digest
A290/260
ABSORBANCE RATIO (A290/A260)
FLUORESCENCE
MOLE RATIO (Ni/bp)
0.20
0.18
0.16
0.14
0.12
0.10
0.08
0.06
0.04
0.02
0.00
450
400
350
300
250
200
150
100
50
0
0
1
2
3
4
5
6
7
8
9
10

Figure 29: Sedimentation analysis of polyd(AT)·polyd(AT) in the presence of increasing amounts of Ni(II) ion. For comparison, EtBr-fluorescence (+ EDTA) is also presented. The figure legend describes the symbols utilized. The concentration of polydeoxynucleotide was 32.27 μM.

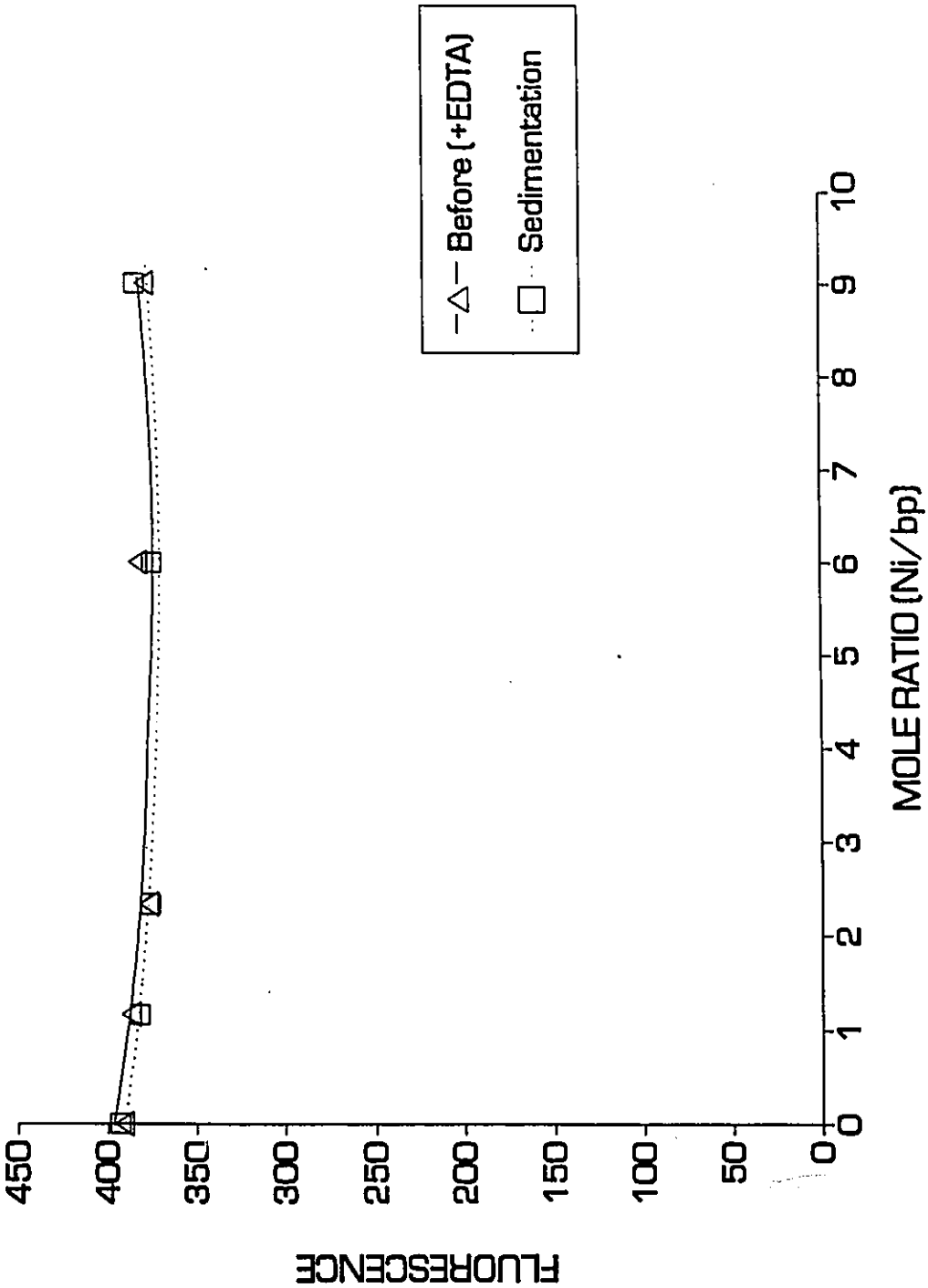
FLUORESCENCE
450
400
350
300
250
200
150
100
50
0
0
1
2
3
4
5
6
7
8
9
10
MOLE RATIO (Ni/bp)
Before (+EDTA)
Sedimentation

Figure 30: Circular dichroism (CD) scans of polyd(AT)·polyd(AT) in the presence of Ni(II). Numbers correspond to CD scans with the following mole ratios (Ni/bp) and absorbance ratios ($A_{290}/_{260}$) respectively: 1) 0.00 and 0.146; 2) 0.79 and 0.146; 3) 3.16 and 0.148; 4) 7.89 and 0.138. Polydeoxynucleotide concentration was 32.27 μM.

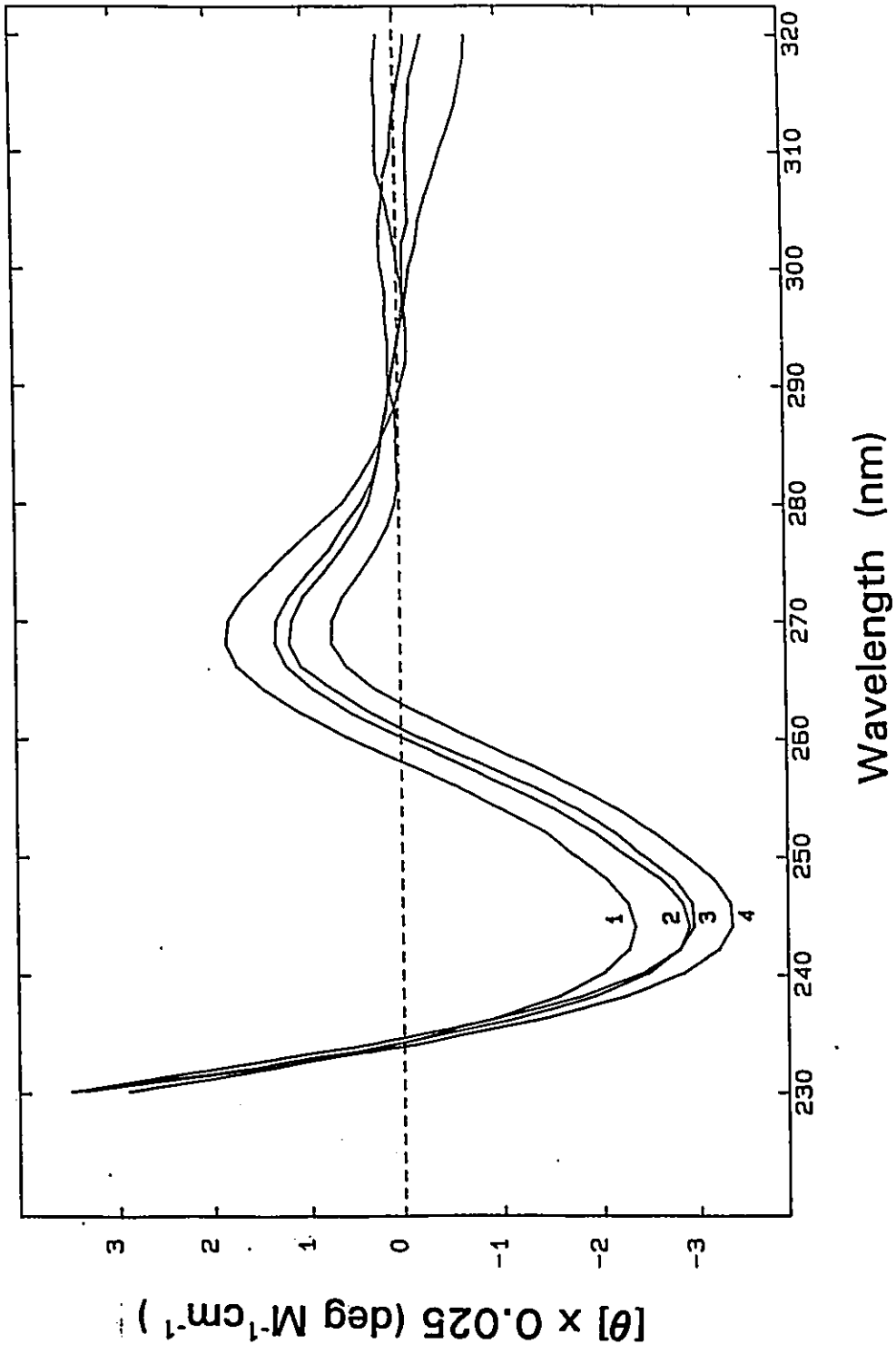
[θ] x 0.025 (deg M-1cm-1)
3
2
1
0
-1
-2
-3
230
240
250
260
270
280
290
300
310
320
Wavelength (nm)
1
2
3
4

Figure 31: Absorbance ratio ($A_{290}/_{260}$), EtBr fluorescence and DNase I digestion susceptibility profiles of polydA·polydT in the presence of increasing amounts of Ni(II) ion. The figure legend describes the symbols utilized. Polydeoxynucleotide concentration was 34.50 μM.

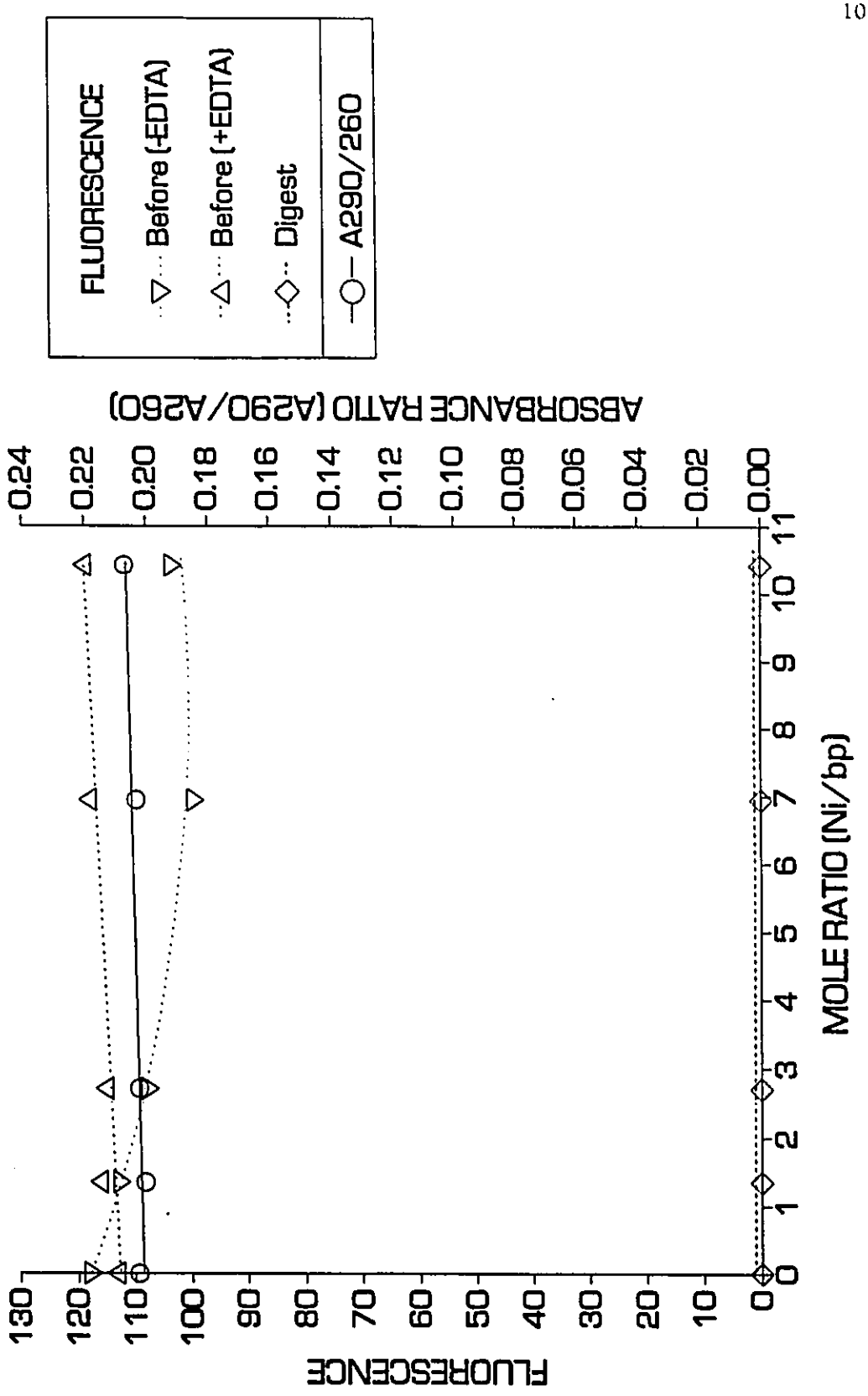
FLUORESCENCE
Before (-EDTA)
Before (+EDTA)
Digest
A290/260
FLUORESCENCE
ABSORBANCE RATIO (A290/A260)
MOLE RATIO (Ni/bp)
0
10
20
30
40
50
60
70
80
90
100
110
120
130
0.00
0.02
0.04
0.06
0.08
0.10
0.12
0.14
0.16
0.18
0.20
0.22
0.24
0
1
2
3
4
5
6
7
8
9
10
11

Figure 32: Sedimentation analysis of polydA·polydT in the presence of increasing amounts of Ni(II) ion. For comparison, EtBr-fluorescence (+ EDTA) is also presented. The figure legend describes the symbols utilized. The concentration of polydeoxynucleotide was 34.50 μM.

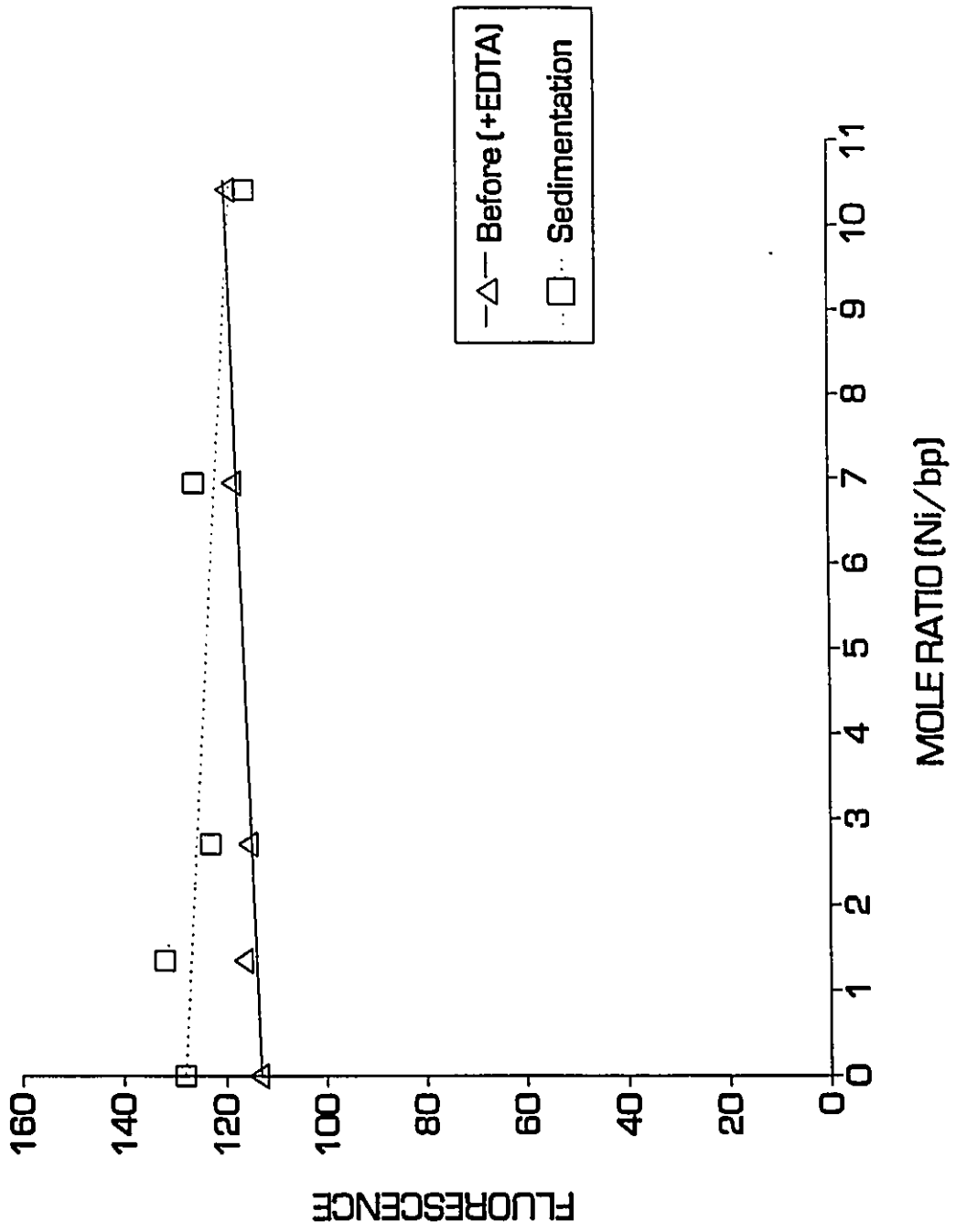
FLUORESCENCE
160
140
120
100
80
60
40
20
0
0
1
2
3
4
5
6
7
8
9
10
11
MOLE RATIO (Ni/bp)
Before (+EDTA)
Sedimentation

Figure 33: Circular dichroism (CD) scans of polydA·polydT in the presence of Ni(II). Numbers correspond to CD scans with the following mole ratios (Ni/bp) and absorbance ratios ($A_{290}/_{260}$) respectively: 1) 0.00 and 0.173; 2) 1.77 and 0.167; 3) 2.95 and 0.171; 4) 7.38 and 0.169. Polydeoxynucleotide concentration was 34.50 μM.

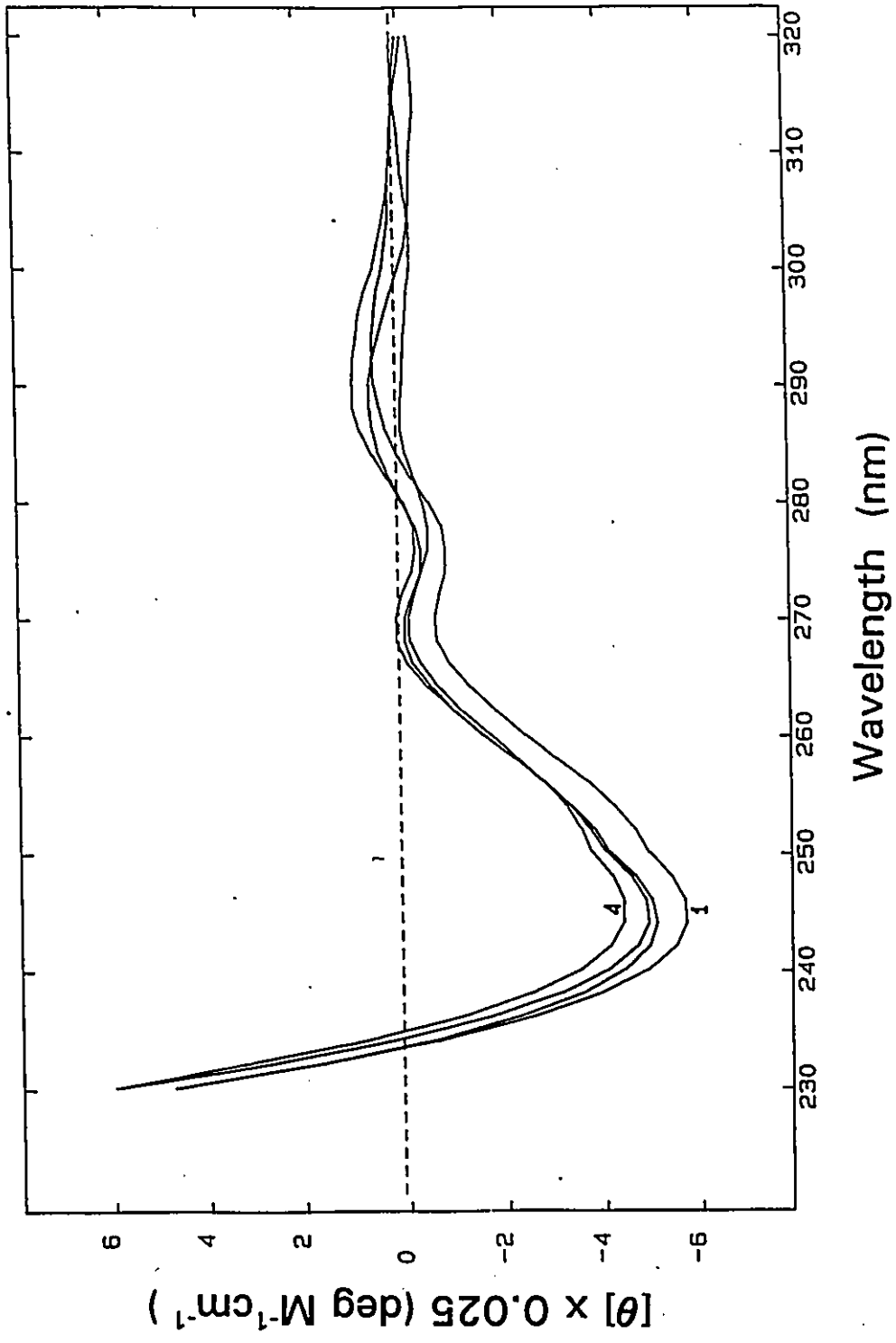
[θ] x 0.025 (deg M-1cm-1)
6
4
2
0
-2
-4
-6
230
240
250
260
270
280
290
300
310
320
Wavelength (nm)
1
4
1

II.3.5 Generation of Dissociation Constants for the Interaction of Ni(II) With DNA/Polydeoxynucleotides

As described in Section II.2.8, ultrafiltration is utilized to separate DNA-bound from free nickel ion. In distinct control experiments, DNA or ^{63}Ni alone were employed to verify the separation and recovery of components. Typical data are presented in Table 3. Recovery of DNA in the filter retentate is typically greater than 99%. By contrast, free Ni(II) ion readily passes through the filter and is recovered in the filtrate (>98%); less than 1% is retained in the filter retentate.

Scatchard analyses of nickel binding to DNA/polydeoxynucleotides present several consistent characteristics for all DNA/polydeoxynucleotides examined. A typical Scatchard plot is presented in Figure 34 (i.e., *M. lysodeikticus*). The plot shows a marked deviation from linearity. At low concentrations of nickel, there is a positive slope in the plot; at higher concentrations two distinct segments of negative slope are observed. Dissociation constants of nickel are derived from the slopes of these negative segments. X-intercepts of these segments denote fractional occupancy, a quantitative measure of moles of Ni bound per mole of DNA base pairs pertaining to that specific set of binding sites. Table 4 provides a compilation of binding constants for all the polydeoxynucleotides or DNAs tested. It must be restated that

Table 3: Separation and Recovery of DNA and Free Nickel Ion By Ultrafiltration (Control Sample)

	Total DNA Fluorescence (arbitrary units)	Ni^{63} CPM (Total)
Test Solution	385	4.38×10^5
Filtrate	1	4.28×10^5
Filter Retentate	382	3.38×10^3

Figure 34: Scatchard plot analysis of the binding of Ni(II) ion with *M. lysodeikticus* DNA. DNA concentration was 27.05 μM.

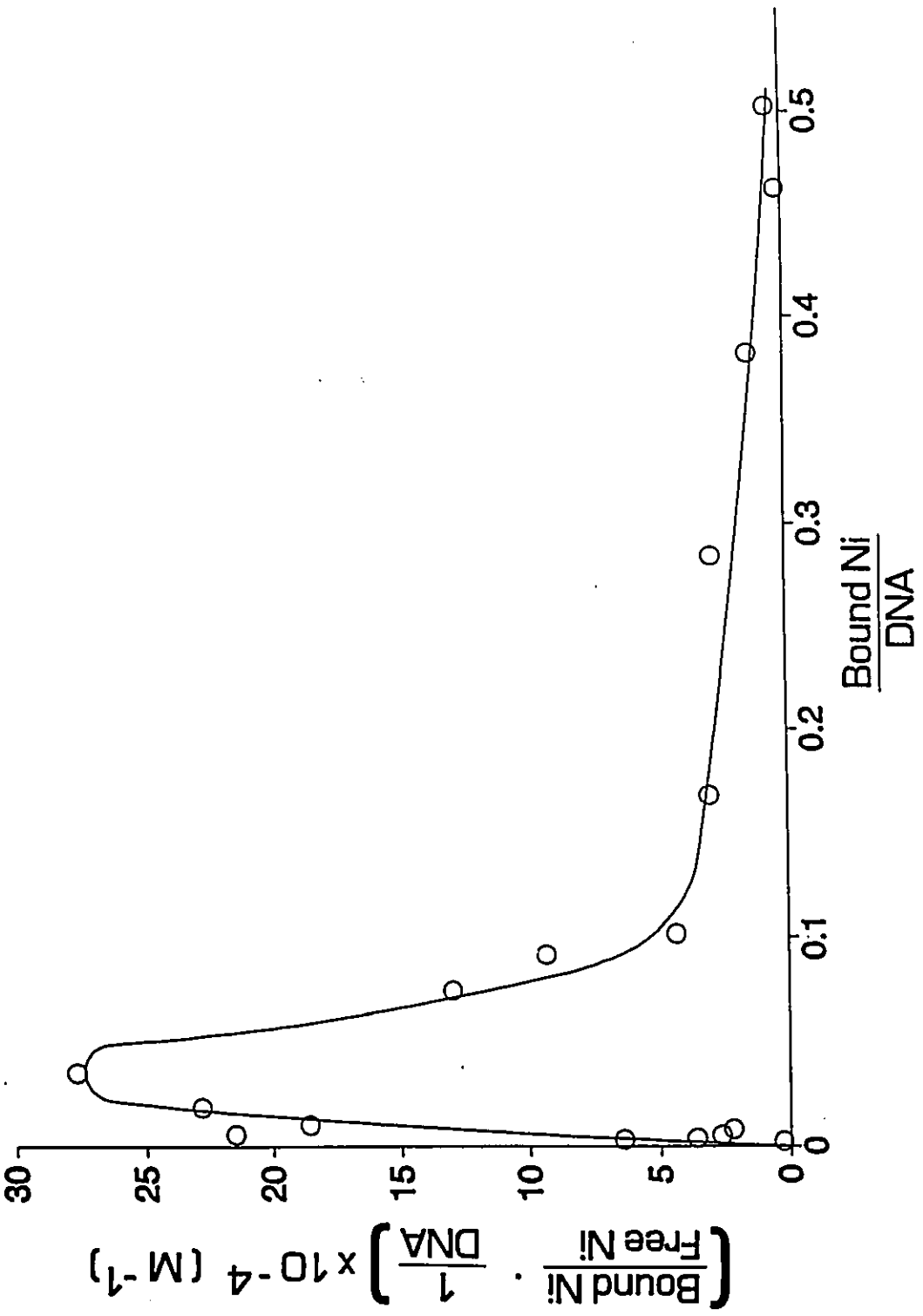
$\left(\frac{\text{Bound Ni}}{\text{Free Ni}} \cdot \frac{1}{\text{DNA}}\right) \times 10^{-4}\ (M^{-1})$
30
25
20
15
10
5
0
0
0.1
0.2
0.3
0.4
0.5
$\frac{\text{Bound Ni}}{\text{DNA}}$

Table 4: Nickel Dissociation Constants For DNAs or Polydeoxynucleotides

Identity	$KD_1 \pm$S.D. (M)*	Fractional Occupancy**	$KD_2 \pm$S.D. (M)	Fractional Occupancy
polydG·polydC	$(4.23 \pm 0.05) \times 10^{-8}$	0.005	$(4.29 \pm 0.02) \times 10^{-6}$	0.455
M. Lysodeikticus	$(1.38 \pm 0.03) \times 10^{-7}$	0.067	$(1.73 \pm 0.01) \times 10^{-5}$	0.569
polyd(GC)·polyd(GC)	$(1.49 \pm 0.01) \times 10^{-6}$	0.089	$(3.46 \pm 0.02) \times 10^{-5}$	0.283
polyd(GT)·polyd(AC)	$(1.55 \pm 0.01) \times 10^{-6}$	0.056	$(1.35 \pm 0.01) \times 10^{-5}$	0.277
Calf Thymus	$(2.04 \pm 0.04) \times 10^{-6}$	0.133	$(1.81 \pm 0.03) \times 10^{-4}$	0.546
polyd(AT)·polyd(AT)	$(4.60 \pm 0.02) \times 10^{-6}$	0.318	$(1.40 \pm 0.03) \times 10^{-4}$	0.643
polydA·polydT	$(7.02 \pm 0.06) \times 10^{-6}$	0.263	$(3.10 \pm 0.01) \times 10^{-4}$	0.287

* S.D. - Standard deviation.
** Defined as atoms of Ni bound per base pair of DNA or polydeoxynucleotide.

all evaluations of dissociation constants and fractional occupancies were performed utilizing BDATA-Ligand Binding Analysis Software (EMF Software, USA) and not performed manually.

II.4 DISCUSSION

Initial investigations of the interaction of Ni(II) ion with DNA or polydeoxynucleotides resulted in the UV spectra depicted in Figures 1-6. It is obvious that the interaction with metal results in negligible alterations to the spectra with the exception of polyd(GC)·polyd(GC) (Figure 4). To simplify and facilitate the presentation of spectral data, an absorbance ratio (i.e. $A_{295/260}$) is utilized for calf thymus DNA, polydG·polydC, polyd(GC)·polyd(GC) and polyd(GT)·polyd (AC). A slightly different ratio ($A_{290/260}$) was employed for polydA·polydT and polyd(AT)·polyd(AT). Both ratios incorporate wavelengths that are close to absorbance maxima and far-UV spectral "tails"; regions in the spectra that are generally affected by conformational or structural transitions. It must also be noted that at the wavelengths used in the absorbance ratios there is negligible interference from the absorbance of Ni(II) ion in solution (Figure 4, scan 10). Thus the ratio data presented in Figures 7 and 8 are a reasonable depiction of spectral alterations due to Ni(II)-polydeoxynucleotide interactions. (More detailed analysis of individual polydeoxynucleotides or DNA will be presented

below.) Good reproducibility is clearly established by the data presented in Figure 10 (standard deviations range from 0.001 to 0.009). The use of such absorbance ratios to monitor the B → Z transition in polyd(GC)·poly(GC) has been reported (van de Sande *et al.*, 1982; van de Sande and Jovin, 1982; Liquier *et al.*, 1984; Nieboer *et al.*, 1989; Rossetto and Nieboer, 1993) and has been found to correlate with the corresponding CD data (van de Sande *et al.*, 1982; van de Sande and Jovin, 1982; Rossetto and Nieboer, 1993).

Preliminary assessments of the ability of ethidium bromide to intercalate into DNA/polydeoxynucleotides as a function of buffer pH provided some interesting data (Figure 9). Two conclusions are readily apparent: 1) there is a consistent decrease in fluorescence as the pH is raised above 9 for all polydeoxynucleotides/DNA tested; 2) the presence of EDTA in the buffer solution has no effect on the fluorescence of ethidium bromide. A similar decrease in ethidium bromide fluorescence at higher pH values has previously been reported for both polydA·polydT and polyd(AT)·polyd(AT) (Morgan *et al.*, 1979). Furthermore, the reproducibility of the assay is excellent as is illustrated by the data presented in Figure 11 (standard deviations range from 3 to 15 arbitrary units).

The interaction of Ni(II) ion with calf thymus DNA presents a clear scenario in which DNA is not affected by metal ion (Figures 1, 12-14). None of the techniques utilized for analysis suggested any alteration in DNA structure or

conformation. Although the CD spectra presented in Figure 14 provide some slight evidence for a Ni(II) ion-specific effect (i.e. decrease in amplitude of negative peak), no deviation from the spectrum associated with the B conformer of DNA is exhibited (Tunis-Schneider and Maestre, 1970; Girod *et al.*, 1973; Ivanov *et al.*, 1973; Wolf *et al.*, 1977; Hanlon *et al.*, 1978; Baase and Johnson, 1979; Votavová *et al.*, 1986; Bokma *et al.*, 1987). Similar conclusions may be derived for polydA·polydT and polyd(AT)·polyd(AT).

In the presence of Ni(II) ion, polydA·polydT does not exhibit any significant alteration in structure or conformation (Figures 6, 31-33). The CD spectra for polydA·polydT presented in Figure 33 is similar to the C-conformation of calf thymus DNA with a subtle but distinct difference (Tunis-Schneider and Maestre, 1970; Ivanov *et al.*, 1973; Girod *et al.*, 1973; Wolf *et al.*, 1977; Baase and Johnson, 1979). For the C-conformation of this DNA, the negative "shoulder" in the region of 270-280 nm is more distinct in appearance than that observed for polydA·polydT in Figure 33. X-ray diffraction analyses of fibers of polydA·polydT have been performed by numerous groups (Arnott and Selsing, 1974; Leslie *et al.*, 1980; Alexeev *et al.*, 1987; Nelson *et al.*, 1987; Aymami *et al.*, 1989). Although there exists some disagreement as to the exact conformation assumed, consensus does occur on several points. Principally, the polydeoxynucleotide exists in solution and fiber as a right-

handed molecule with a conformation related to the B-form but with a distinctly narrow minor groove. By comparison, C-conformations of DNA are also right-handed, but possessing shallower and narrower grooves than the B form (Ivanov *et al.*, 1973; Hanlon *et al.*, 1978). If one views the right-handed helical conformers as a continuum of structures (Kennard and Hunter, 1989), one can postulate that the conformation of polydA·polydT exists at the junction of both structural groups.

For polyd(AT)·polyd(AT), the data presented (Figures 5, 28-30) adequately demonstrate that little alteration in structure or conformation results from Ni(II) ion interaction in the concentration range examined. The CD scans presented in Figure 30 portray a right-handed B-type conformation in the presence of Ni(II) ion (for comparison, refer to calf thymus DNA previously discussed) as expected for this polydeoxynucleotide (Leslie *et al.*, 1980; Shin *et al.*, 1986; Lilley and McClellan, 1987; Bourtayre *et al.*, 1987; Kypr and Vorlicková 1988; Vorlicková *et al.*, 1988). However, polyd(AT)·polyd(AT) is able to undergo a variety of conformational transitions under different conditions. In the presence of high concentrations of cesium fluoride (>5M), this polydeoxynucleotide adopts a novel conformation (X-DNA) possessing a "zig-zag" double helix backbone sharing certain features with that of Z-DNA (Kypr and Vorlicková, 1988; Vorlicková *et al.*, 1988). Furthermore, the generation of ψ-

DNA in the presence of Co(III) ions has also been reported (Shin *et al.*, 1986).

The most interesting characteristic of polyd(AT)·polyd(AT) is its documented ability to adopt left-hand conformations (i.e. Z-DNA) as monitored by IR spectroscopy (Adam *et al.*, 1986), CD and UV spectroscopy (Bourtayre *et al.*, 1987) and Raman spectroscopy (Ridoux *et al.*, 1988; Miskovsky *et al.*, 1989). This polydeoxynucleotide was examined by IR spectroscopy in the presence of different counter ions (Na^+, Cs^+, Ni^{2+}) and a variety of water content conditions (relative humidity between 100 and 47%). Z-DNA was induced in polyd(AT)·polyd(AT) at a relative humidity of 76% and 2 Ni^{2+} per nucleotide (Adam *et al.*, 1986). The other reports of Z-DNA formation utilized conditions of both high salt (5M NaCl) and $NiCl_2$ (90 mM) (Bourtayre *et al.*, 1987; Ridoux *et al.*, 1988; Miskovsky *et al.*, 1989), with nickel exposure corresponding to a Ni/bp ratio greater than 60. Recently, it has been reported that a $(dA\text{-}dT)_{16}$ cloned insert adopted a left-handed structure in a supercoiled plasmid under conditions (2 M NaCl, 0.2 M $NiCl_2$, or 1 M $NiCl_2$ alone) which do not induce Z-DNA in the linear plasmid or polyd(AT)·polyd(AT) alone (Nejedlý *et al.*, 1989). A $(dA\text{-}dT)_5$ block placed in the centre of a 32 bp self-complementary alternating purine-pyrimidine insert also adopted a left-handed structure at substantially lower $NiCl_2$ concentrations (10 mM $NiCl_2$, 0.2 M NaCl) (Klysik *et al.*, 1988). Obviously, the conditions

utilized in the present studies (i.e., low ionic strength, Ni/bp ratios < 12) were insufficient to overcome the transition energy barrier of the B → Z transition for this polydeoxynucleotide (reviewed in: Rich *et al.*, 1984; Jovin *et al.*, 1987).

The scenario presented for the interaction of Ni(II) with polyd(GT)·polyd(AC) is more intriguing. Following an incubation at 37°C, no major alteration in polydeoxynucleotide structure and conformation is observed (Figures 3, 22-24). CD spectra depicted in Figure 24 suggest that the conformation may undergo a transition to a C form in the presence of Ni(II) ion. As for polydA·polydT, this assignment is not definitive since the spectra of Ni(II)-polyd(GT)·polyd(AC) differ in the 270-280 nm region from the canonical C-conformation (Tunis-Schneider and Maestre, 1970; Ivanov *et al.*, 1973; Girod *et al.*, 1973; Wolf *et al.*, 1977; Baase and Johnson, 1979). By contrast, incubation at 64°C results in distinct changes in polyd(GT)·polyd(AC) in the presence of Ni(II) ion. As depicted in Figure 25, the absorbance ratio data ($A_{295}/_{260}$) suggest a biphasic transition to a final conformer. Moreover, DNase I digestion resistance and a decreased ability of EtBr to intercalate parallels the second, major transition of this biphasic process. Sedimentation in this case is not induced by Ni(II) ion (Figure 26). CD spectra reinforce the conclusion that structural alterations result from Ni(II) ion interaction (Figure 27). In the absence of metal-ion

following an incubation at 64°C, the CD spectra is reminiscent to that of polyd(GT)·polyd(AC) incubated at 37°C in the presence of Ni(II) ion (cf. Scan 1, Figure 27 with Scans 2 and 3, Figure 24). With increasing metal ion, the spectra alter in an ion concentration manner (Figure 27). Conditions for the conversion of this polydeoxynucleotide to a left-handed Z conformer have been documented. As described for polyd(AT)·polyd(AT), these include exposure to high concentrations of both monovalent salts (4-5 M) and $NiCl_2$ (40-95 mM) or relatively low humidity coupled with nickel ion at levels of 1 Ni^{2+}/nucleotide (Taillandier *et al.*, 1984; Taboury and Taillandier, 1985; Adam *et al.*, 1986; Bourtayre *et al.*, 1987; Ridoux *et al.*, 1988). Under more moderate conditions (10 mM NaCl, 40 mM $NiCl_2$), Ni^{2+}-polyd(GT)·polyd(AC) undergoes a B → coil transition as the solution temperature is raised to 75°C, leading to an irreversible precipitation of the coil form (Taboury and Taillandier, 1985). This latter observation, coupled with the experimental data presented above are suggestive of an alteration in conformation of this polydeoxynucleotide following Ni(II) ion interaction in this report. Although a final conformation cannot be definitively assigned, it must deviate significantly from traditional right-handed helical forms since the conformation must exclude EtBr and be resistant to DNase I digestion. A coiled or aggregated state (i.e. ψ-form) is excluded as a possibility since the Ni(II)-polydeoxynucleotide is not sedimented; a Z-

conformer is excluded by virtue of the CD spectral data.

For polydG·polydC, the UV spectra obtained in the presence of Ni(II) ion are suggestive of an alteration in polydeoxynucleotide structure resulting from metal interaction (Figure 2). Although slight, these changes are distinctive and Ni(II)-ion specific (i.e. shift in absorbance maximum), and occur in a metal-concentration-dependent manner (i.e. hypochromism at absorbance maximum). These alterations in the UV spectrum are not reflected when the absorbance data are analyzed as absorbance ratios ($A_{295}/_{260}$) (Figures 7 and 19). This clearly demonstrates the limitations in utilizing the absorbance ratio as a sole means of identifying transitions; subtle changes in absorbance data may not appreciably affect the observed quotient. The CD data presented in Figure 21 concurs with the UV spectral data in that Ni(II) ion does have some effect on polydG·polydC. By itself or in the presence of Ni(II) ion, this polydeoxynucleotide presents a CD trace typical of the canonical A-form of DNA (Tunis-Schneider and Maestre, 1970; Girod *et al.*, 1973; Ivanov *et al.*, 1973). The designation of polydG·polydC as an A-type conformer has been verified by X-ray crystallography (McCall *et al.*, 1985) and Raman spectroscopy (Nishimura *et al.*, 1986). The slight changes in CD spectra resulting from Ni(II) ions are clearly concentration dependent. Coupled with the observation of an isobestic point, one can speculate on the existence of a family of A-conformer variants induced through interaction

with the Ni(II) ion. Both the fluorescence and digestion susceptibility data are in agreement with the interpretation that some structural alteration in polydG·polydC does occur (Figure 19).

PolydG·polydC is somewhat unique in that it is a member of a restrictive family of sequences which may adopt stable, triplex structures (i.e., H-form DNA, reviewed in: Paleček, 1991; Yagil, 1991; Cheng and Pettitt, 1992). It must be noted that environmental factors such as supercoiling density, ionic strength, counterion type and pH are critical in determining the exact structure of the triplex formed. At neutral conditions in the presence of Mg^{2+}, Mn^{2+} or Ca^{2+}, polydG·polydC sequences adopt a triplex structure consisting of unprotonated base triads of GGC. Within these structures, a pair of G-C are involved in normal Watson-Crick base pairing, the third strand G is paired with the other G via Hoogsten base pairing and the final C strand remains single stranded (Paleček, 1991; Yagil, 1991; Cheng and Pettitt, 1992). It is highly unlikely that Ni(II)-polydG·polydC adopts a similar triplex structure. Both the UV spectral and CD data are not suggestive of the generation of a structure with a component of single stranded DNA; no significant hyperchromism is noted in the UV spectra nor significant alterations observed in CD spectra. Furthermore, it has been reported that metals which are known to bind to base nitrogens (i.e N_7 of purines; Zn^{2+}, Co^{2+}, Cu^{2+}) are unable to induce H-form DNA in contrast to counterions

which predominantly bind phosphate groups (i.e. Mg^{2+}, Ca^{2+}) (Kohwi, 1989; Campos and Subirana, 1991). This is not surprising since the N_7 of the guanine involved in normal Watson-Crick base pairing is participating in Hoogsten base pairing with the second G within the triplex structure (Paleček, 1991; Yagil, 1991). Since the Ni^{2+} ion has preference for the N_7 of purines within DNA (see below), one may conclude that triplex H-DNA is an unfavourable conformation for Ni(II) polydG·polydC.

Amongst the polydeoxynucleotides and DNA examined, the clearest indication of an effect by Ni(II) ion on structure/conformation is observed for polyd(GC)·poly(GC) (Figures 4,7,15-18). The work presented in this thesis is the most systematic investigation of the effect of Ni(II) ion with this polydeoxynucleotide to date. It is clear from the UV spectra generated that Ni(II) ion interaction elicits distinct changes (Figure 4). Moreover, these changes (i.e., hypochromism at absorbance maximum, spectral "shoulder" development) are consistent with spectral alterations associated with the formation of left-handed Z-DNA by a variety of agents, including Ni(II) ion (Behe and Felsenfled, 1981; van de Sande *et al.*, 1982; van de Sande and Jovin, 1982; Liquier *et al.*, 1984; Rich *et al.*, 1984; Hacques and Marion, 1986; Jovin *et al.*, 1987). Presenting the spectral data as absorbance ratios results in the depiction of a biphasic process as previously noted for this metal (van de Sande *et*

al., 1982; Liquier *et al.*, 1984; Nieboer *et al.*, 1989; Rossetto and Nieboer, 1993). Not surprisingly changes in the Ni(II)-poly(GC)·polyd(GC) UV spectra parallel the two phases of transitions observed in the absorbance ratio plots (compare Figure 4 with 7). The presence of isobestic points in the spectra suggest that the conformations depicted by the first and second transitions respectively are in equilibrium and represent a continuum of Ni(II)-induced conformational change.

The CD traces in Figure 17 both corroborate and verify the fact that Ni(II) ion ultimately induces a Z-conformation. In the absence of ion, polyd(GC)·polyd(GC) displays a CD spectrum of a classical B-conformation; following interaction with significant amounts of Ni(II) ion the CD spectrum is inverted, indicative of the Z-conformation as previously noted for Ni-ZDNA (Liquier *et al.*, 1984; Haques and Marion, 1986; Rossetto and Nieboer, 1993) or ZDNA induced by alternate methods (Behe and Felsenfeld, 1981; Eichhorn *et al.*, 1982; van de Sande and Jovin, 1982; Zacharias *et al.*, 1982; Roy and Miles, 1983; Zacharias *et al.*, 1983; Fazakerley, 1984; Rich *et al.*, 1984; Behe and Felsenfeld, 1985; Grunberger *et al.*, 1985; Thomas and Bloomfield, 1985; Woisard *et al.*, 1985; Jovin *et al.*, 1987; Preisler, 1987; Chaires and Norcum, 1988; Shin *et al.*, 1988; Thomas and Thomas, 1990; Sagi *et al.*, 1991; Votavová *et al.*, 1991). An identity for the conformation of polydeoxynucleotide corresponding to the first transition is also suggested by the CD spectra presented in Figure 17 (i.e.

Scan 3). This transition CD trace is consistent with those previously documented for similar Ni(II)-polyd(GC)·poly(GC) mixtures (Hacques and Marion, 1986; Liquier *et al.*, 1984; Rossetto and Nieboer, 1993) and is reminiscent of the C-conformation of DNA (Tunis-Schneider and Maestre, 1970; Girod *et al.*, 1973; Ivanov *et al.*, 1973; Hanlon *et al.*, 1978).

Additional evidence for the assignment of the left-handed Z conformation to the final Ni(II) ion induced transition product is presented in Figure 15. Both the insensitivity of Z-DNA to DNase I digestion and a reduced ability of ethidium bromide (EtBr) to intercalate into Z-DNA have been reported (van de Sande and Jovin, 1982; van de Sande *et al.*, 1982; Rich *et al.*, 1984; Nieboer *et al.*, 1989; Rossetto and Nieboer, 1993). For both EtBr intercalation and DNase I digestion susceptibility, a clear distinction can be made between phenomena occurring with right-handed DNA conformers (i.e. B/C conformers) and left-handed conformers (i.e. Z-DNA), paralleling the right → left transition depicted by the absorbance ratio data (Figure 15).

Under certain conditions (i.e. prolonged incubation, incubation at elevated temperatures, high cation levels), Z-DNA may undergo a further transition to an alternate Z-conformation (Z*). This latter form possesses an identical CD trace to that of Z-DNA but is characterized primarily by an ability to be readily sedimented out of solution, which is indicative of some state of condensation and/or intermolecular

aggregation (van de Sande and Jovin, 1982; van de Sande and Jovin, 1982; Hacques and Marion, 1986; Chaires and Norcum, 1988). The data presented in Figures 17 and 18 clearly indicate that at high mole ratios of Ni(II) ion (Ni/bp > 10), a similar process is occurring for Ni(II)-polyd(GC)·poly(GC), consistent with previous data for this metal (van de Sande *et al.*, 1982; Hacques and Marion, 1986). The Z* conformation is distinct from other condensed/aggregated forms of polyd(GC)·polyd(GC) such as ψ-DNA (Eichhorn *et al.*, 1982; Zacharias *et al.*, 1983; Shin *et al.*, 1988; Thomas and Thomas, 1990).

An overall examination of the data presented suggests that the interaction of Ni(II) ion with DNA and polydeoxynucleotides is to some extent base (or basepair) specific. A clear affinity for G/C bases is evident when structural or conformational transitions are utilized as a measure of interaction. This latter conclusion is supported by the dissociation constants generated for these polydeoxynucleotides/DNAs presented in Table 4. Several trends and generalizations are readily apparent following examination of these data. All DNAs and polydeoxynucleotides analyzed demonstrated two binding sites, differing in binding affinity by approximately two orders of magnitude. A clear positive correlation is evident between the affinity of both sites and the G/C content of the DNA. While the values for fractional occupancy do not vary significantly for the low

affinity sites (range 0.643 to 0.277; equivalent to 1 Ni/3 bases to 1 Ni/7 bases), the converse is true for the high affinity sites (range 0.005 to 0.318; 1 Ni/400 bases to 1 Ni/6 bases). One apparent anomaly is the observation of a more avid high affinity site in *M. Lysodeikticus* DNA (>60% G/C content) than polyd(GC)·polyd(GC). A possible explanation may stem from the G/C sequence context of these respective species. The *M. Lysodeikticus* DNA sequence is more random, with a higher probability of tandem arrays of Gs and Cs (similar to polydG·polydC) by contrast to the dogmatic dinucleotide GC repeat of polyd(GC)·polyd(GC). It seems clear that high affinity for Ni(II) ion binding is a function of both high G/C content and sequence context. Although dissociation constants for Ni-polydeoxynucleotides have not been previously documented, the value reported for the high affinity site of calf thymus DNA is similar to one reported by Kasprzak and colleagues (5.35×10^{-6} M vs. 2.04×10^{-6} M; Kasprzak *et al.*, 1986).

As reported for calf thymus DNA by Kasprzak and coworkers (1986), the positive slope at low values of Ni_{Bound}/DNA (Figure 34) suggests a cooperative binding event. A similar feature is noted in Scatchard plots for all DNAs and polydeoxynucleotides examined. This can be qualitatively explained in the following manner: at first, binding of Ni ion to DNA is very weak; the DNA with unbound Ni ion (ligand) is presumed to be in a weakly binding state, and the first

ligands bound are mostly going to distinct, high affinity sites on the DNA. The filling of these initial sites on DNA somehow increases the affinity of the remaining high affinity sites, and binding becomes stronger as more sites are filled.

Much data has been reported concerning the interaction of metals (including nickel) with DNA and/or polydeoxynucleotides. The most likely site of the high affinity binding is the N-7 site of purines (Eichhorn, 1981; Lippard, 1982; Jack *et al.*, 1977; Marzilli *et al.*, 1980; Jia and Marzilli, 1991; Jia *et al.*, 1991; Taboury *et al.*, 1984; Taillandier *et al.*, 1984; Taboury and Taillendier, 1985; Adam *et al.*, 1986a; Adam *et al.*, 1986b; Ridoux *et al.*, 1988; Miskovsky *et al.*, 1989; Riazance-Lawrence and Johnson, 1992). In addition, exocyclic base oxygen atoms may also be involved in direct and long range interactions with metal ions via the bridging action of water molecules (Marzilli, 1981; Gessner *et al.*, 1985; Sorokin *et al.*, 1987). Similar long range interactions with phosphate oxygens are also possible (Marzilli, 1981). These latter sites may be responsible for the second, lower affinity binding site of Ni(II) ion within DNA. More recently, we have reported on the ability of 20 metals to induce cooperative conformational or structural transitions in polyd(GC)·polyd(GC) (Appendix I; Rossetto and Nieboer, 1993). This ability was seen to be an intrinsic property of all metal ions examined. A strong correlation was observed ($y = -1.01(\log X) + 3.26$, $r=0.95$, $n=20$) between the

metal ion/poly d(GC)·polyd(GC) mole ratio required for the transition midpoint (X) and a covalent index to complex stability (y) of the metal ions. This relationship was independent of the types of transitions observed (i.e. monophasic or biphasic) or of specific conformations (i.e. B, Z, ψ). The y index utilized measured the ability of metal ions to bind to nitrogen and/or sulphur donor atoms in ligands compared to oxygen centers; equilibrium analysis indicated that the mole ratio (x) corresponding to transition midpoints decreased with increasing affinity of metal ions for polyd(GC)·polyd(GC).

The data presented in this chapter clearly indicate that Ni(II) ions interact with polydeoxynucleotides and DNA. In simple systems utilizing polydeoxynucleotides of well-defined base composition and sequence, this interaction is manifested in structural or conformational changes and transitions. Furthermore, the strength of this interaction is base (or base pair) dependent and demonstrates some sequence context specificity.

III Ni(II) INTERACTION WITH CHROMOSOMES IN INTACT NUCLEI

III.1 INTRODUCTION

III.1.1 Overview

The structure, packaging and functioning of nuclear DNA is an area of intense scientific scrutiny. Numerous review articles have appeared documenting and highlighting various aspects of this research (Igo-Kemenes *et al.*, 1982; Eissenberg *et al.*, 1985; Tsanev and Tsaneva, 1986; Butler 1984; Nicolini, 1988; Gross, 1988; van Holde, 1990). The brief "overview" presented below is not exhaustive but merely provides a familiarization of chromosomes and chromosomal structure. The descriptions of DNA packaging into nucleosomes and chromosomes derive from the above-mentioned reviews and references therein, which are not individually cited.

Within the nucleus, DNA must be packaged into a condensed state. This process must be ordered and controlled, readily accessible to polymerases and numerous effector molecules. The most basic unit of the chromosome is the nucleosome; each nucleosome consisting of 146 bp of DNA wrapped in 1.8 left-handed turns around a core of two each of the histones H2A, H2B, H3 and H4. Histone H1 appears to be positioned outside the core protein regions, in association with DNA as it enters and exits the histone core. The H1 also interacts with

"linker" DNA, typically 20-100 bp per nucleosomal subunit. In addition, there are many non-histone proteins present in much smaller amounts than any histone. Thus, while the quantities of histones suggest an active and fundamental role in DNA packaging, the non-histone proteins are more likely involved in catalytic (e.g. phosphorylation) or control (e.g. transcription) functions. In addition to a role in modulating the folding of chromatin (probably involving structural levels higher than tertiary), some non-histone proteins may also have essential structural functions.

The primary feature of chromosomes is the linear array of nucleosomes along the DNA. This "string of beads" is further folded to form the basic chromatin fiber. This structure is typified by the 20-40 nm (i.e. solenoidal) fibers predominating in whole cells and *in vitro* (i.e. isolated nuclei) under "physiological" salt and buffer conditions. A third chromosomal structural level involves the folding of chromatin fibers into loops or domains. Stretches of chromatin (35-85 kb of DNA) are thought to be anchored onto a supporting structure of the nucleus that has been termed the matrix, lamina, envelope, nuclear membrane or scaffold (in the case of metaphase chromosomes).

Domains of chromatin (spanning kilobases) that are transcriptionally active exhibit a heightened general sensitivity to nuclease digestion, perhaps an order of magnitude greater than bulk chromatin. In addition to these

large domains, there exist smaller nucleosome-free regions which are thought to represent the "open windows" that permit access of cis-acting DNA sequences to trans-acting control factors (known as nuclease hypersensitive sites). These smaller regions are operationally defined by their pronounced susceptibility to digestion or chemical modification, typically being several orders of magnitude more sensitive than bulk chromatin and should be differentiated from the former, larger domains of nuclease sensitivity.

Recent developments have clearly demonstrated that chromatin structure is significantly affected by the ionic environment (i.e. mono/divalent ions) experienced by the chromosomes or nuclei (Aaronson and Woo, 1981; Horvath and Horz, 1981; Weith, 1983; Earnshaw and Laemmli, 1983; Borochov *et al.*, 1984; Ausio *et al.*, 1984; Dixon and Burkholder, 1985a,b; Gralloch *et al.*, 1987; Makarov *et al.*, 1987). An effective, but little used approach to surveying the effects of ionic conditions on chromatin structure involves the use of UV/visible light absorption spectrometry of chromatin. The spectral absorbance of nuclear suspensions is highly correlated with chromatin structure and shows a peak absorbance at 260 nm (A_{260}) and a shoulder at 320 nm (A_{320}) (Olins and Olins, 1972; Dixon and Burkholder, 1985b). Chromatin condensation results in a decrease in absorption at 260 nm with a concomitant increase at 320 nm. Relaxation of chromatin structure produces an opposite result.

III.1.2 Specific Research Objectives

The work presented in this chapter involves the characterization of the interaction of Ni(II) ion with chromosomes in isolated nuclei of a T-lymphocytic (HUT) cell line. More specifically, the condensational state of chromosomes in a variety of buffer conditions was investigated using both UV and visible light absorption spectroscopy and susceptibility to nuclease digestion. In addition, binding constants for the interaction of Ni(II) with chromosomes in nuclei were also assessed in physiological buffers incorporating varying levels of Mg(II).

III.2 MATERIALS AND METHODS

III.2.1 Chemicals and Reagents

Table 5 contains a compendium of the various chemicals, reagents, sources and any additional information pertaining to the experiments described in this chapter. Doubly distilled deionized water was used in all solution preparations. All tissue culture solutions were filter-sterilized (0.22 μm) or autoclaved. Specific formulations of appropriate solutions (i.e. media, buffers, etc.) are stated in the ensuing sections.

Table 5: Chemicals and Reagents

Chemical Name	Formula	Source	Grade	Lot #
General Chemicals:				
4-(2-hydroxyethyl)-1-piperazine ethanesulfonic Acid (HEPES)	NA*	Sigma Chem. Co.	Cell Culture	110H-5613
Ethylene-diaminetetraacetic Acid (EDTA)	NA	BDH Chem. Co.	Assured	96257/5589
Nickel Sulfate	$NiSO_4$	BDH Chem. Co.	Analytical	86226
Sodium Chloride	NaCl	BDH Chem. Co.	Analytical	105850/22120
Potassium Chloride	KCl	BDH Chem. Co.	Analytical	96582/7360
Potassium Dihydrogen Orthophosphate	KH_2PO_4	BDH Chem. Co.	Assured	87380
Tris(hydroxymethyl)-aminomethane	NA	Boehringer Mannheim	Electrophoretic	DCA121/3-93
Magnesium Chloride	$MgCl_2$	BDH Chem. Co.	Analytical	105685/29914
Phenol	NA	BRL	Ultrapure	AA3201
Chloroform	$CHCl_3$	Caledon	Reagent	01374A
Human Placental DNA	NA	Sigma Chem. Co.	Ultrapure	128F-6693-1
Sucrose	NA	BDH Chem. Co.	Analytical	101945/115
Ethidium Bromide	NA	Sigma Chem. Co.	Reagent	92F-0353
Calcium Chloride	$CaCl_2$	BDH Chem. Co.	Analytical	106823/2516
Triton X-100	NA	BioRad	Electrophoretic	M4594
Diaminobenzoic Acid (DABA)	NA	Aldrich Chem. Co.	Analytical	19322CY
Phenyl methyl sulfonyl fluoride (PMSF)	NA	Sigma Chem. Co.	Reagent	570752
Perchloric Acid	$HClO_4$	Baker	Ultrex	552340
Hydrochloric Acid	HCl	Fisher	Reagent	288321
Black Charcoal	NA	Sargent-Welch Sci. Co.	NA	4J01C
Ultrapure dNTP Set dATP, dGTP, dTTP, dCTP		Pharmacia	Ultrapure	NA
^{63}Ni Chloride	$^{63}NiCl_2$	Amersham**	NA	NA

continued ...

Table 5 (continued)

Chemical Name	Formula	Source	Grade	Lot #
Enzymes:				
Ribonuclease A (RNase A)	NA	Sigma Chem. Co.	Molecular	NA
Proteinase K	NA	Boehringer Mannheim	Molecular	13259025-34
Micrococcal Nuclease	NA	Boehringer Mannheim	Molecular	10362935-21
Tissue Culture:				
RPMI Medium	NA	McMaster Stores	Tissue Culture	NA
Sodium Pyruvate	NA	McMaster Stores	Tissue Culture	NA
L-Glutamine	NA	McMaster Stores	Tissue Culture	NA
Fetal Bovine Serum	NA	Gibco/BRL	Tissue Culture	NA
Penicillum G	NA	Sigma Chem. Co.	Tissue Culture	NA
Streptomycin	NA	Sigma Chem. Co.	Tissue Culture	NA

* Not available/not applicable.
** Kindly provided by Dr. D. Templeton, Univ. of Toronto, Toronto, Canada; 11.32 mCi/mg, 1.49 mCi/ml, 1.66×10^{-9} M.

III.2.2 Growth of Transformed Human T-Lymphocytes (HUT Cells)

HUT cells were a gift of Dr. Ken Rosenthal (Dept. of Pathology, McMaster University). Suspension growth of cells was at 37°C, 95-100% humidity and 5% CO_2 (continuous flow). They were routinely split once a week. Two millilitres of cells (4-6 x 10^5 cell/ml) were reseeded in 48 ml of "complete RPMI" growth buffer, lightly stoppered and allowed to grow for one week (RPMI medium with additives: 10 mM sodium pyruvate, 10% (v/v) fetal calf serum, 100 units/ml of both penicillum G and streptomycin, 2 mM of L-glutamine, 10 mM Hepes (pH 7.5)). Cells were collected by low-speed centrifugation (1200 x RPM, 15 min, room temperature) when needed.

III.2.3 Isolation of Nuclei

Cells were pelleted as described in Section 2.2 and the nuclei isolated by a procedure based on a methodology described in Langmore and Paulson (1983) which has been demonstrated to consistently result in the isolation of nuclei (and constituents) possessing intact physiological and structural characteristics. Pelleted cells were resuspended in ice cold "Lysis Buffer" (10.32 mM Tris•HCl (pH 7.26), 10.20 mM KCl, 2.24 mM $MgCl_2$, 2.03 mM $CaCl_2$, 10 μM PMSF)) at a concentration of 2-4 x 10^7 cells/ml. Suspensions were vortexed at room temperature for 20 sec, placed on ice for 10 min, and then revortexed for 20 sec. Cell suspensions were

then made 1% (v/v) in Triton X-100, placed on ice for 5 min and then vortexed for 10 sec. Nuclei were pelleted (1500 x RPM, 15 min, room temperature) and then resuspended in 2 ml of "Isolation Buffer" (10.07 mM Hepes, 0.52 mM $CaCl_2$, 1.99 mM $MgCl_2$, 59.56 mM KCl, 16.26 mM NaCl, 10 μM PMSF, pH 7.61). One-ml aliquots of this nuclei suspension were then thoroughly mixed with 6 ml of 2.2 M sucrose in "Isolation Buffer". Following centrifugation (Sorval RC2B centrifuge; 40,000 x g, 60 min, 4°C), the nuclei pellet was resuspended in 5 ml of "Isolation Buffer" supplemented with 0.5% (v/v) Triton X-100. Nuclei were isolated from suspension following low speed centrifugation (1500 x RPM, 15 min, room temperature). Nuclei pellets were resuspended in 5 ml of "Isolation Buffer" and subsequently reisolated by low speed centrifugation. This wash step was repeated two more times. Final resuspension of the nuclear pellet was in 2.5 to 3.5 ml of "Isolation Buffer". All nuclei preparations were stored on ice and used immediately. Periodically, nuclei preparations were assessed for purity by fluorescence staining utilizing acridine orange (Arndt-Jovin and Jovin, 1989).

III.2.4 Quantitation of Nuclear DNA

DNA from nuclei was first isolated and subsequently quantified by EtBr intercalation and fluorescence. Twenty-five microlitres of resuspended nuclei (or buffer as background control) was added to 200 μl of "Nuclei Lysis

Buffer" ("Lysis Buffer" (Section 2.3) with 0.5% (w/v) SDS), 15 µl of RNase A (10 mg/ml in DDI) was then added and the sample incubated for 30 minutes at room temperature. An aliquot of Proteinase K was added (10 mg/ml in DDI) and the sample incubated for 90 min at 60°C. An aliquot (75 µl) of the digested nuclei sample was then extracted with 75 µl of phenol/chloroform (24:1, v/v); 5 µl of the aqueous layer were removed and assayed with EtBr reagent (12.38 mM KH_2PO_4, 0.5 mM EDTA, pH 11.99; Morgan *et al.*, 1979). The assumption implicit in this assay is that intercalation of EtBr into reference and sample DNA is similar (see Chapter II.1.5). Reference DNA utilized was ultrapure human placental DNA (50 µg/ml). Typical concentration measurements utilized 5 µl (250 ng) of this DNA as a standard per assay. Fluorescence was measured as previously described (Chapter I.1.5) on a Gilson Spectra/glo Fluorometer. The sample's fluorescence was compared to the standard's fluorescence and corrected for procedural dilutions.

III.2.5 Analysis of the Condensational State of Chromosomes in Intact Nuclei

The isolation of nuclei utilized in the analysis of nuclear chromosomal condensation was performed as described in Section 2.3. Stock nickel sulphate solutions were prepared in DDI. Aliquots of nuclei suspensions (20-80 µg of DNA) were combined with aliquots of nickel sulphate stock solutions, DDI

and sufficient 5 x "Buffer A" to make the final solution 1 x in buffer (10.11 mM Hepes, 0.51 mM $CaCl_2$, 60.01 mM KCl, 15.75 mM NaCl, pH 7.52). Supplements of $MgCl_2$ (206.10 mM) were added to the nuclei solutions when appropriate. All solutions of nuclei were paired with negative control solutions containing all components excluding nuclei. Absorbances at 260 nm and 320 nm were measured with a Perkin Elmer 3B UV/VIS Spectrophotometer utilizing 1 x "Buffer A" as the reference solution. All samples were corrected for background absorbance utilizing the sample-matched negative controls. Samples were prepared and analyzed in triplicate.

III.2.6 Digestion of Nuclei With Nuclease

Stock solutions (10x) of nickel sulphate solutions were prepared in DDI immediately prior to use. Aliquots of nuclei suspensions (700-1000 µg total DNA) were added to nickel solutions, DDI and sufficient 5 x "Isolation Buffer" to make the final solution 1x in "Isolation Buffer" and a final DNA concentration of approximately 500 µg/ml. Solutions were incubated for the appropriate times at 4°C prior to nuclease digestion. Micrococcal nuclease (15 units/µl stock) was added to a final amount of 1 unit/20 µg DNA and allowed to incubate at room temperature for varying times (0, 5, 15, 30 min). At suitable times, aliquots (100 µl) were removed; the reaction was stopped with 5 µl of 0.5 M EDTA. Aliquots from terminated reactions were stored at -20°C for further analysis.

III.2.7 Analysis of Digested Chromosomes Utilizing Diaminobenzoic Acid (DABA)

The determination of the extent of chromosome digestion was performed utilizing an assay previously described (Kissane and Robins, 1958; Kapp *et al.*, 1974). The principle behind the assay is the reaction of soluble purine deoxynucleotides with 3,5-diaminobenzoic acid (DABA) resulting in the generation of a product quantitated by fluorescence. Diaminobenzoic acid was dissolved in sufficient DDI (final concentration of 0.4 g/ml), 2 g of black charcoal was added and the resultant mixture stirred for 10 min at room temperature. The mixture was then filtered 2 times through Whatman 540 filter paper prior to use in the assay. For the generation of standard curves, aliquots of a dATP solution (96.74 μm) were employed. Nucleotide specificity was illustrated by examining solutions containing individual dNTPs (i.e. dATP, dTTP, dCTP, dGTP).

Frozen aliquots of digested nuclei (105 μl) were thawed and 13 μl of ice-cold perchloric acid added. Samples were incubated on ice for 30 min, spun at 10,000 x g for 5 min at room temperature (Eppendorf Microcentrifuge), and two aliquots of the supernatant removed for further analysis. These aliquots were added to 400 μl of the prepared DABA reagent and incubated at 60°C for 60 min. Samples were allowed to cool to room temperature (30 min) at which time 1.5 ml of 1 N HCl was added. Sample fluorescence was monitored on a Gilson

Spectra/glo Fluorometer at an excitation wavelength of 420 nm and an emission wavelength of 520 nm (Mandel Filters #5-58X and #520-3X, respectively). Samples without digestion (i.e. t=0 min) were used to obtain background corrections. The extent of digestion is reported as a percentage of the total initial DNA-base pairs digested.

III.2.8 Generation of Ni(II) Binding Constants for Chromosomes in Isolated Nuclei

Samples were prepared essentially as described in Section III.2.5. Approximately 25-40 μg of DNA was present per sample tube in a final volume of 500 μl. All nickel stock solutions contained Ni^{63} in radiotracer amounts. Samples were incubated for 5 min at room temperature, then spun for 18,000 x g at room temperature for 5 min. Three aliquots of 100 μl each was removed from the supernatant (i.e. unbound Ni(II)), counted and the nickel quantified by scintillation spectrometry as described in Chapter II, Section 2.8. A known quantity of stock solution was counted and used for calibration. All samples counted were corrected for background levels of radioactivity (typically 1-2 counts/second). Analysis of data employing Scatchard plots (Scatchard, 1949) was performed utilizing the BDATA-Ligand Binding Analysis Software (EMF Software, USA) package described in Chapter II, Section 2.8.

III.2.9 Scanning Electron Microscopy of Ni(II) Exposed Nuclei

Scanning electron microscopy (SEM) was performed at the Life Sciences Electron Microscopy Unit, Department of Biology (McMaster University) by Derrick Flannigan under the supervision of Dr. Gary Leppard. Isolated nuclei in "Isolation Buffer" were obtained as described in Section 2.3. All electron microscopy work, including fixing, staining and sectioning, was performed by Mr. Flannigan. Briefly, nuclei were incubated for 1 h in 2% glutaraldehyde in cacodylate buffer at 10°C. Preparations were then washed 3 times in the buffer alone followed by an incubation in 1% osmium tetroxide for 30 min, at 10°C. Following a final buffer wash, samples were dehydrated by washing with ethanol solutions of increasing ethanol concentrations (i.e. 50, 70, 90, 95, 100, 100%). Samples were then mixed with an equivolume of ethanol/Spurr resin for 30 min then with pure Spurr resin for 30 min. This was followed by a final change of Spurr resin which was allowed to polymerize for 8 h at 70°C. Ultrathin sections were cut on a RMC MT-7 Ultramicrotome, sections picked up on aluminum grids and post-stained with uranyl acetate and lead citrate. Sections were viewed with a JEOL JEM-1200 EX II electron microscope; EDX analysis performed on a SUN work station running IMIX software from PGT (Princeton Gamma-Tech).

III.3 RESULTS

III.3.1 Condensation Analysis of Nuclear Chromosomes

The fluorescence microscopy examination of the isolated nuclei indicated a high degree of purity (bright orange fluorescing spheres against a dark background) free from cytoplasmic contamination (red fluorescence; Arndt-Jovin and Jovin, 1989). Condensation of chromosomes was monitored by the difference in absorbances at 260 nm and 320 nm ($\Delta A = A_{260}-A_{320}$; see Figure 35). At Ni(II) levels below 1 x 10^{-5} M a plateau is observed with an ΔA value of approximately 0.120. A second plateau at lower ΔA values is observed at Ni(II) concentrations greater than 5 x 10^{-4} M. Both plateaus are joined by a sharp transition with a midpoint at approximately 5 x 10^{-5} M Ni(II). Triplicate sampling of reaction mixtures demonstrate good reproducibility in ΔA (± 0.002 to ± 0.009).

Figure 36 is a representation of the condensational process of nuclear chromosomes in the presence of increasing amounts of Mg(II) ion. Transitions are observed in the presence of all levels of Mg(II) ion. Furthermore, transition midpoints occur at approximately 5 x 10^{-5} M Ni(II) for all curves. As Mg(II) concentrations are increased, pretransition plateau values decrease in a concentration-dependent manner.

Figure 35: Illustration of Ni(II)-induced condensation of chromosomes in intact nuclei. All samples were examined in triplicate. Buffer conditions were: 10.11 mM Hepes, 0.51 mM $CaCl_2$, 60.01 mM KCl, 15.75 mM NaCl, 0.54 mM $MgCl_2$, pH 7.52. The bars denote one standard deviation.

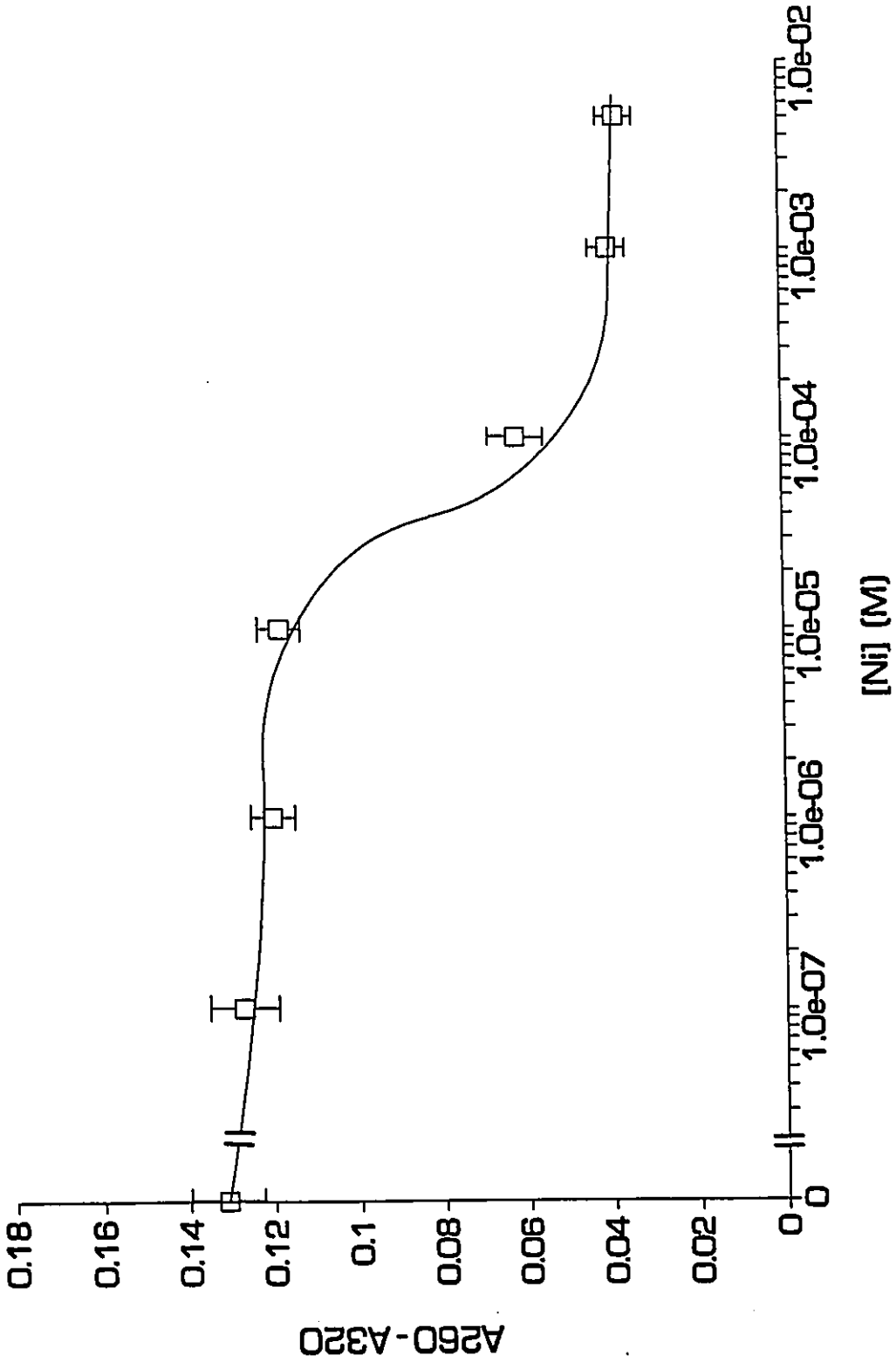
A260 - A320
0.18
0.16
0.14
0.12
0.1
0.08
0.06
0.04
0.02
0
1.0e-07
1.0e-06
1.0e-05
1.0e-04
1.0e-03
1.0e-02
[Ni] (M)

Figure 36: Condensation analysis of chromosomes in the presence of varying amounts of Mg(II). Buffer conditions were: 10.11 mM Hepes, 0.51 mM $CaCl_2$, 60.01 mM KCl, 15.75 mM NaCl, pH 7.52 and the indicated concentrations of Mg(II). Note that A260-A320 has been multiplied by a factor of 100.

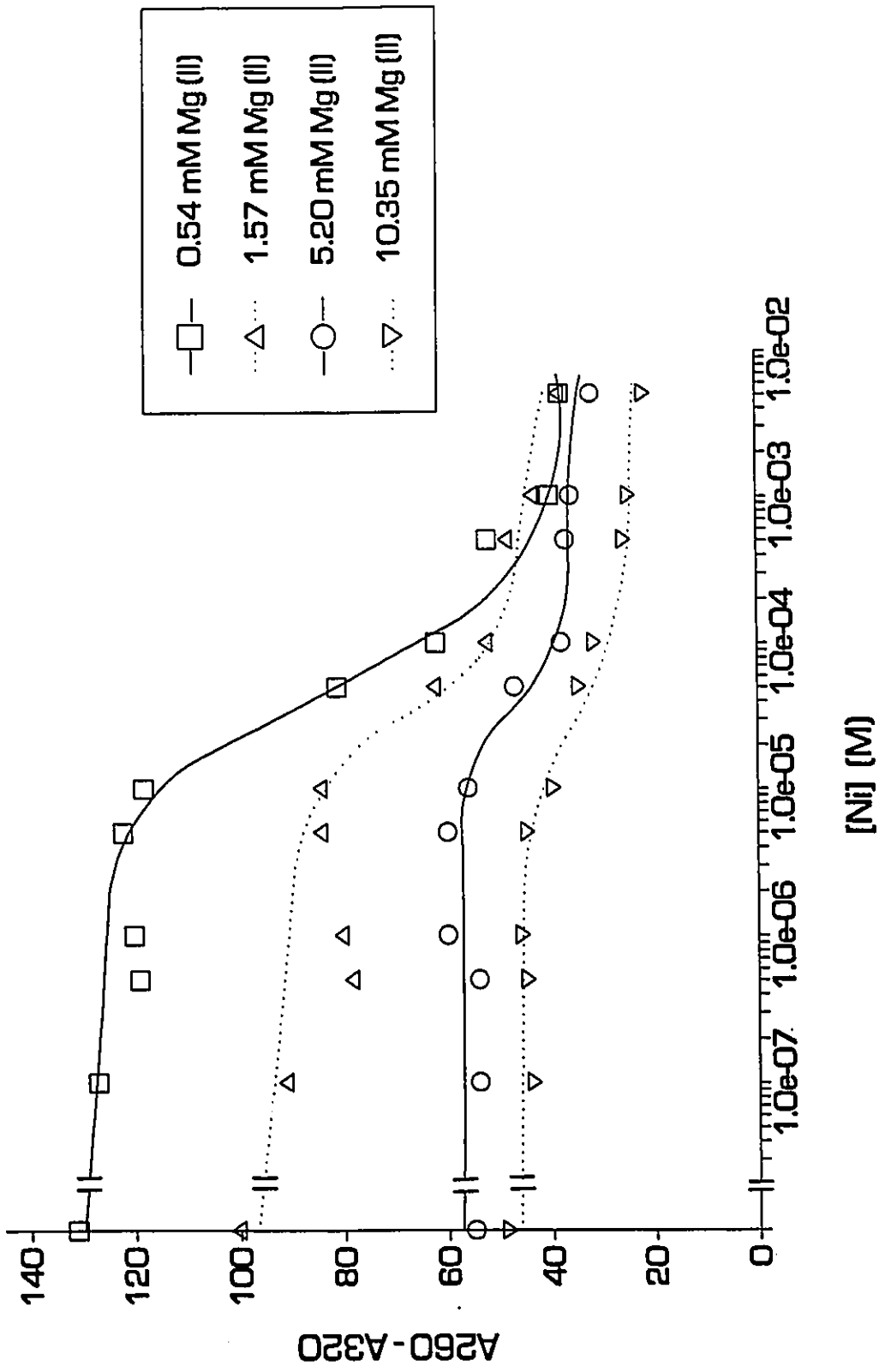
0.54 mM Mg (II)
1.57 mM Mg (II)
5.20 mM Mg (II)
10.35 mM Mg (II)
A260 - A320
140
120
100
80
60
40
20
0
1.0e-07
1.0e-06
1.0e-05
1.0e-04
1.0e-03
1.0e-02
[Ni] (M)

III.3.2 Analysis of Nuclease Digested Chromosomes/DNA

III.3.2.1 Assay Characteristics

The linear, concentration-dependent response of the purine deoxynucleotide (dATP) is presented in Figure 37. All samples were assayed in triplicate with variations sufficiently small (i.e. fluorescence values range from 1 to 4 units) to be excluded from this graphical representation. A definite linear response is observed over the concentration range examined ($y = 60.09 x - 5.589$; $r = 0.9991$). The specificity of the assay for purine over pyrimidine deoxynucleotides is verified by the data compiled in Table 6. Levels of dTTP or dCTP up to 75 nmoles did not produce appreciable product fluorescence. By contrast, both dATP and dGTP elicited strong responses in the assay.

III.3.2.2 Digestion of Nuclear Chromosomes

The digestion of nuclear chromosomes following an incubation of varying times in the presence of Ni(II) ion is presented in Figures 38-40. All samples were analyzed in triplicate. The values obtained for these triplicate measurements ranged minimally (i.e. 0.1 to 0.2 nmoles corresponding to a "% Digested" range of 0.4-0.8%), thus are not represented on the figures.

Following an incubation of 2 h with Ni(II) ion, chromosomes are not rendered more resistant or hypersusceptible to nuclease digestion (Figure 38). A similar

Figure 37: Representative standard curve of the DABA assay. All samples were analyzed in triplicate (with SD values too small to indicate in the figure). Regression parameters are: $y = 60.09 x - 5.589$, $r = 0.9991$.

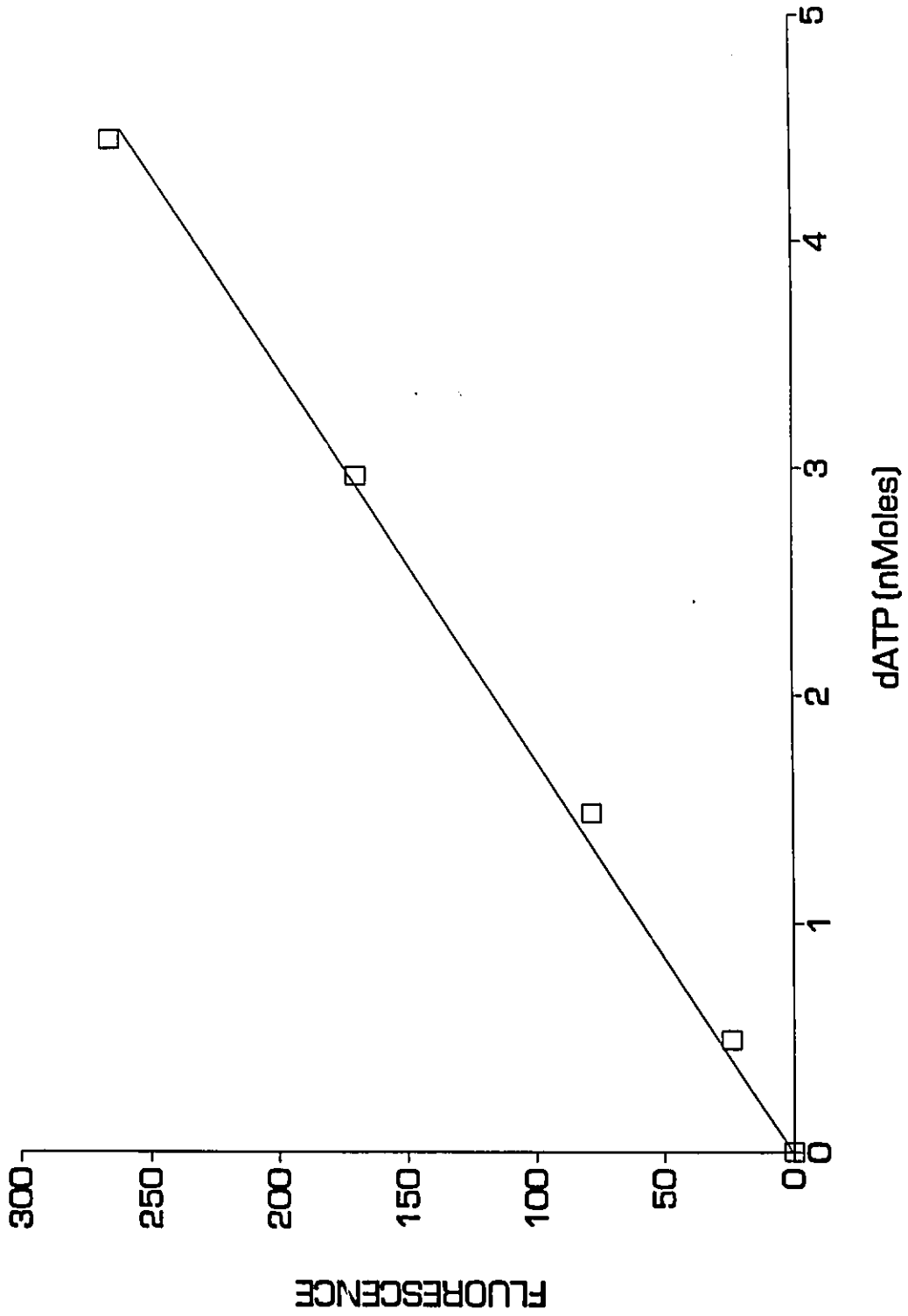
FLUORESCENCE
300
250
200
150
100
50
0
0
1
2
3
4
5
dATP (nMoles)

Table 6: Control Responses of Deoxynucleotides With DABA

Chemical Name	nmoles	Fluorescence (± SD)[1,2]
dTTP	5.9	1 ± 1
dTTP	29.5	1 ± 1
dTTP	73.8	1 ± 1
dCTP	4.0	2 ± 2
dCTP	19.9	2 ± 1
dCTP	49.8	2 ± 1
dATP	4.1	240 ± 5
dATP	20.7	790 ± 4
dATP	51.8	866 ± 1
dGTP	4.0	238 ± 6
dGTP	19.8	798 ± 3
dGTP	49.5	867 ± 1

[1] SD, standard deviation.
[2] Fluorescence units are arbitrary and range from 0 to 1000.

Figure 38: Nuclease digestion of chromosomes in the presence of varying amounts of Ni(II). Incubation of nuclei with Ni(II) was for 2 h at room temperature prior to nuclease digestion. Buffer conditions were: 10.11 mM Hepes, 0.51 mM $CaCl_2$, 60.01 mM KCl, 15.75 mM NaCl, 1.99 mM $MgCl_2$, pH 7.52 and the range of Ni(II) concentrations indicated.

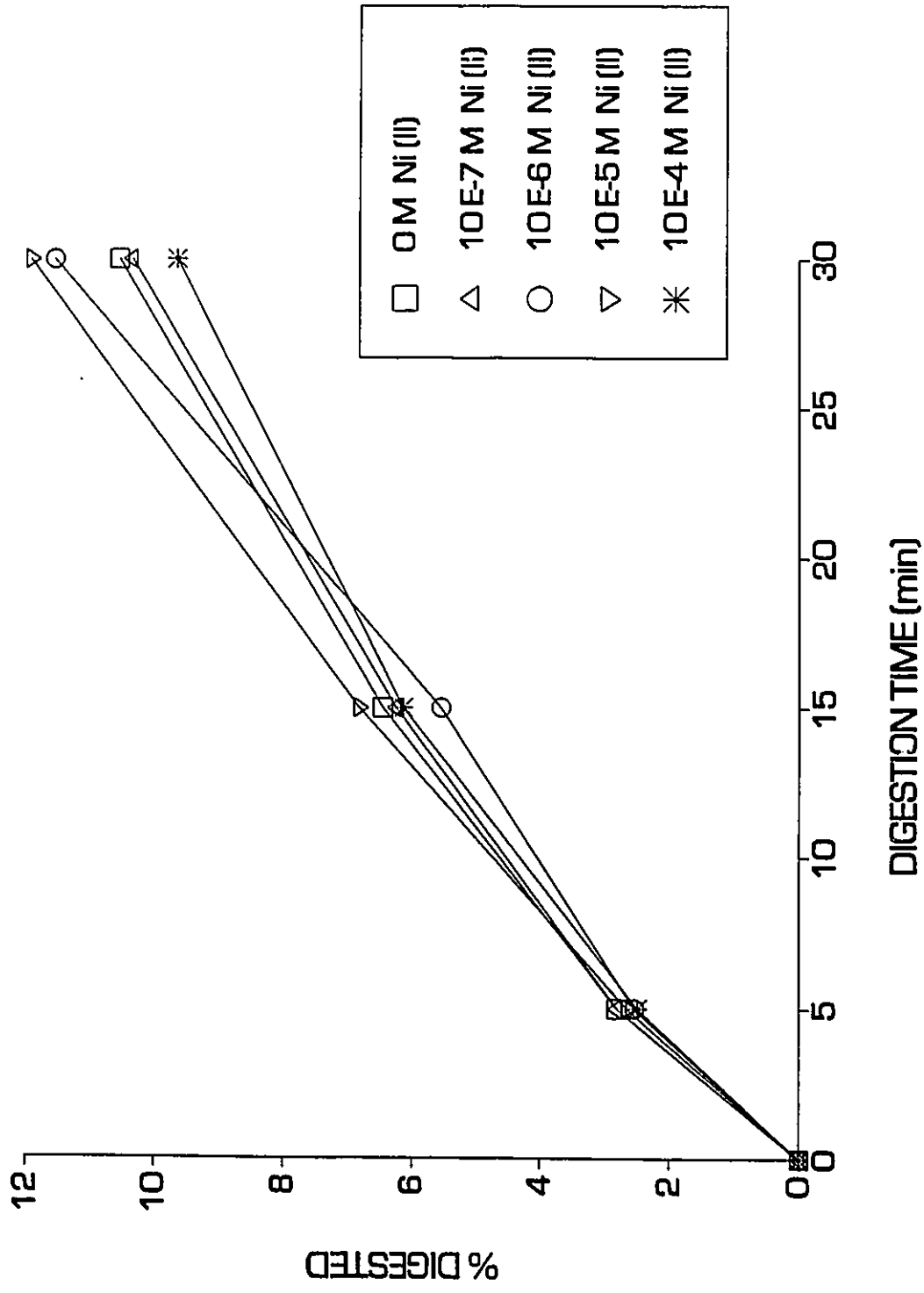
0 M Ni (II)
10E-7 M Ni (II)
10E-6 M Ni (II)
10E-5 M Ni (II)
10E-4 M Ni (II)
% DIGESTED
DIGESTION TIME (min)
0
2
4
6
8
10
12
0
5
10
15
20
25
30

Figure 39: Nuclease digestion of chromosomes following a 24 h incubation in the presence of varying amounts of Ni(II). Buffer conditions were: 10.11 mM Hepes, 0.51 mM $CaCl_2$, 60.01 mM KCl, 15.75 mM NaCl, 1.99 mM $MgCl_2$, pH 7.52 and the range of Ni(II) concentrations indicated.

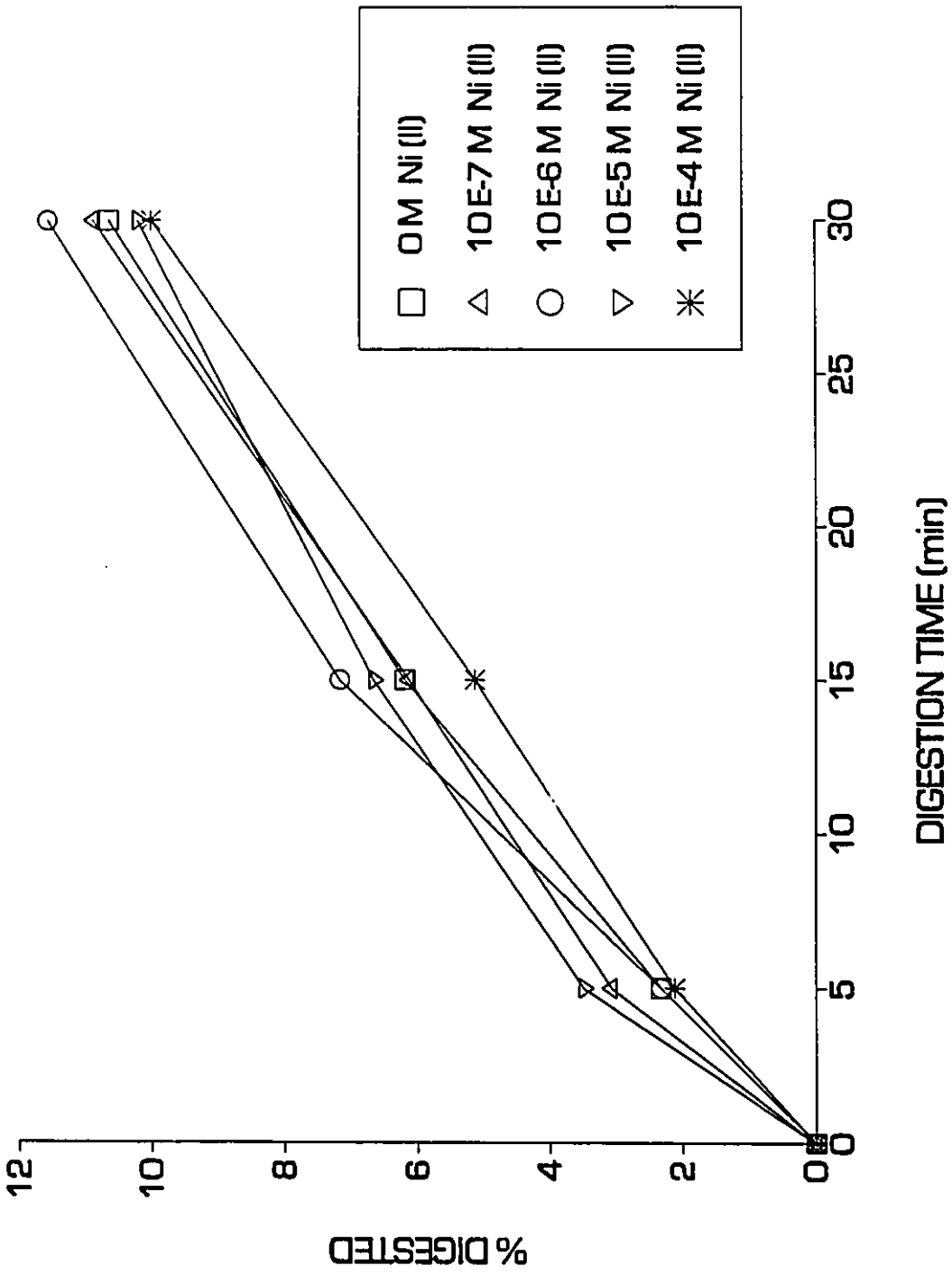
0M Ni (II)
10E-7 M Ni (II)
10E-6 M Ni (II)
10E-5 M Ni (II)
10E-4 M Ni (II)
% DIGESTED
DIGESTION TIME (min)
0
2
4
6
8
10
12
0
5
10
15
20
25
30

Figure 40: Nuclease digestion of chromosomes following a 96 h incubation in the presence of varying amounts of Ni(II). Buffer conditions were: 10.11 mM Hepes, 0.51 mM $CaCl_2$, 60.01 mM KCl, 15.75 mM NaCl, 1.99 mM $MgCl_2$, pH 7.52 and the range of Ni(II) concentrations indicated.

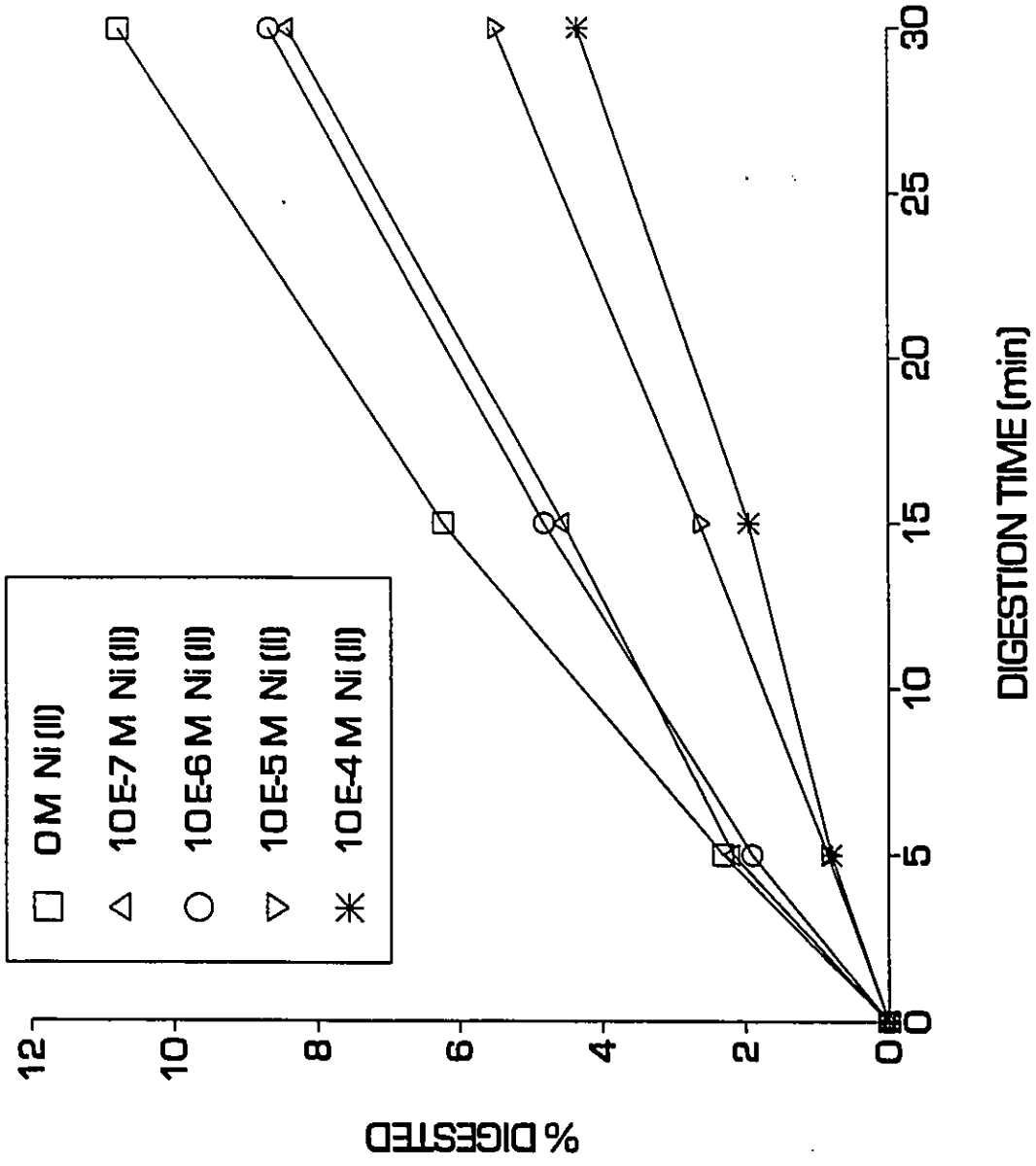
0M Ni (II)
10E-7 M Ni (II)
10E-6 M Ni (II)
10E-5 M Ni (II)
10E-4 M Ni (II)
% DIGESTED
DIGESTION TIME (min)
0
2
4
6
8
10
12
0
5
10
15
20
25
30

scenario is also evident for nuclei incubated with Ni(II) ion for 24 h (Figure 39). Exposure to Ni(II) ion for 96 h resulted in some evidence for chromosomal resistance to nuclease digestion (Figure 40). This resistance increases in a Ni(II) ion-concentration dependent fashion over the Ni(II) concentration range of 10^{-7} to 10^{-4} M.

III.3.3 Scanning Electron Micrographs of Nuclei Exposed to Ni(II)-Ion

Nuclei exposed to Ni(II) ion for 2 h do not elicit any gross structural alterations as depicted in electron micrographs (Figure 41). Nuclei are typified by one or two nucleoli and densely staining regions that are dispersed throughout the nuclei, but with some preferential localization of these densely staining regions on the inner side of the nuclear membrane. These regions become somewhat more discrete and compact at higher Ni(II) levels (i.e. 10^{-5}, 10^{-4} M). This general scenario is also consistent for nuclei exposed to Ni(II) ion for 24 h (Figure 42). At higher concentrations of Ni(II) ion (i.e. 10^{-5} or 10^{-4} M Ni(II)), changes in the densely staining nuclear regions are more pronounced and discrete (Figure 42, Panel D and E). Following an exposure to Ni(II) ion for 96 h, discrete densely staining regions are noted in nuclei exposed to as little as 10^{-6} M of Ni(II) ion by contrast to control nuclei (Figure 43, compare Panel A to Panel B and C).

Figure 41: Scanning electron micrographs (x8000) of nuclei exposed to Ni(II) for 2 h. Nickel concentrations were: A) control; B) 1.02×10^{-7} M; C) 1.02×10^{-6} M; D) 1.02×10^{-5} M; E) 1.02×10^{-4} M Ni. Buffer conditions were: 10.11 mM Hepes, 0.51 mM $CaCl_2$, 1.99 mM $MgCl_2$, 60.01 mM KCl, 15.75 mM NaCl, pH 7.52. Densely staining fibrils in nuclei are condensed chromatin or heterochromatin. Note that each nuclei contains one or two dark staining nucleoli.

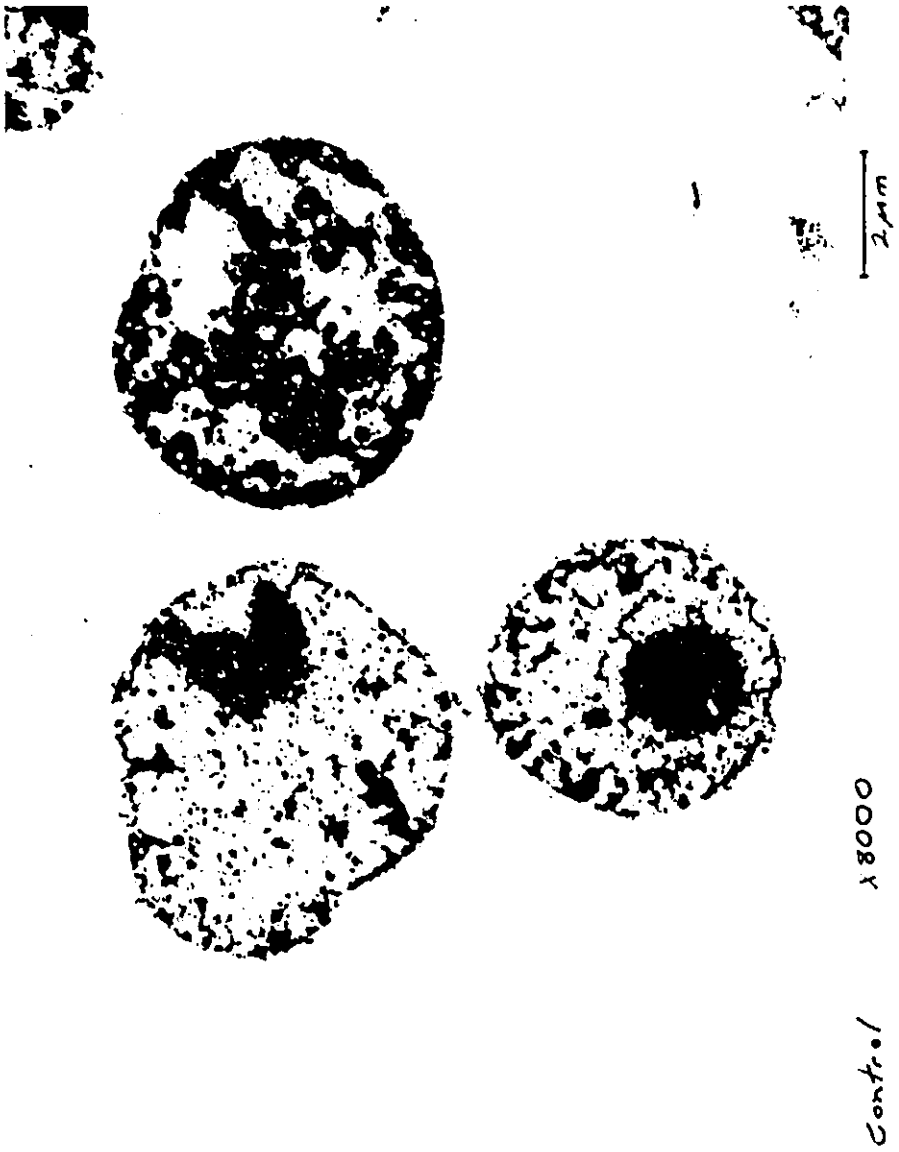

Figure 41, Panel A

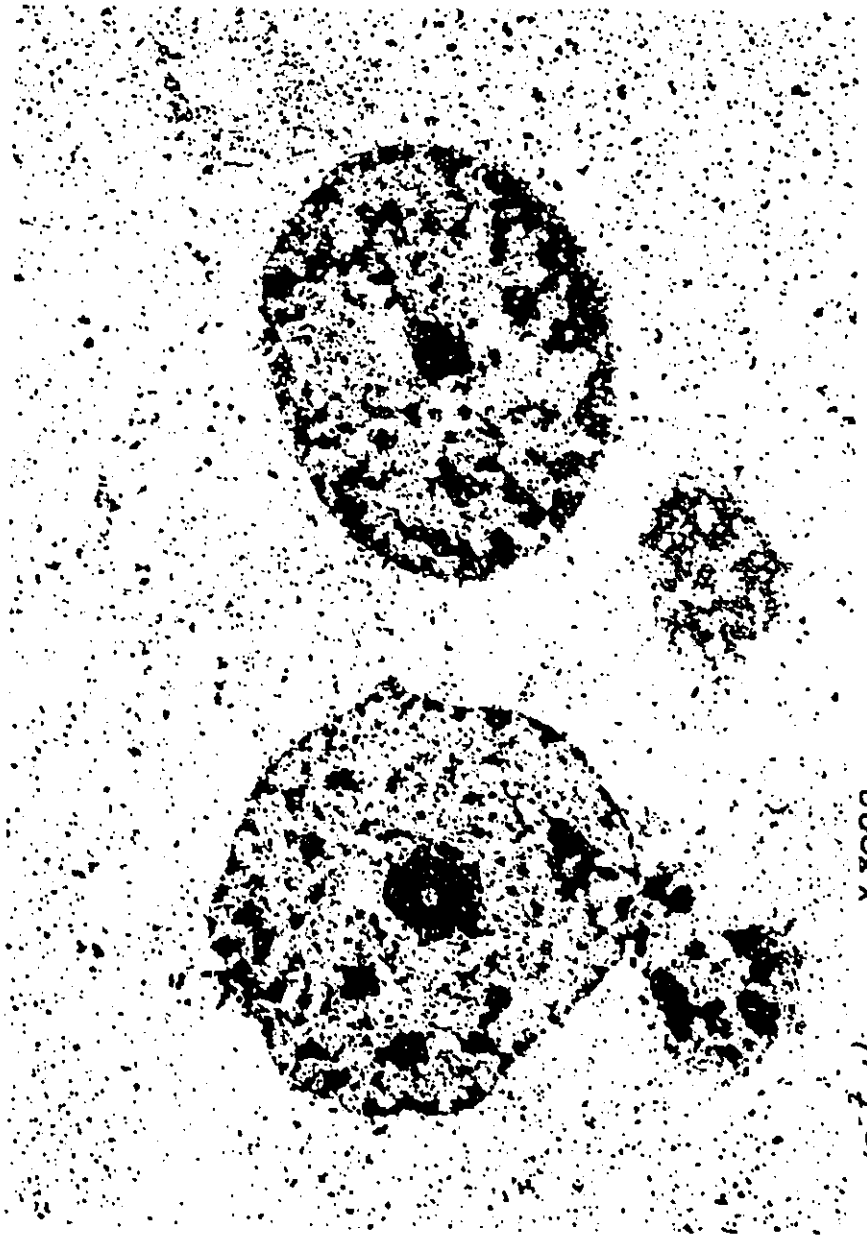

Figure 41, Panel B

Figure 41, Panel C

Figure 41, Panel D

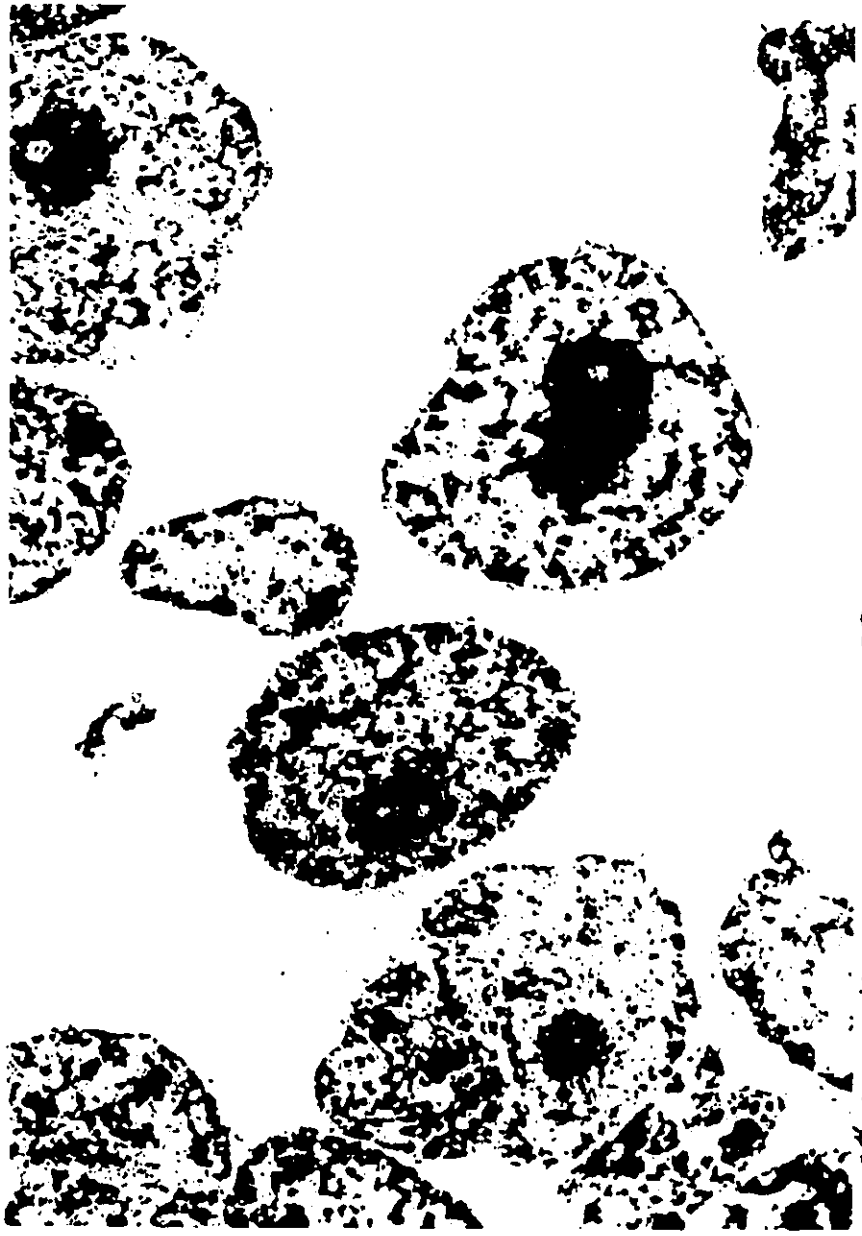

Figure 41, Panel E

Figure 42: Scanning electron micrographs (x25000) of nuclei exposed to Ni(II) for 24 h. Nickel concentrations were: A) control; B) 1.02×10^{-7} M; C) 1.02×10^{-6} M; D) 1.02×10^{-5} M; E) 1.02×10^{-4} M Ni. Buffer conditions were: 10.11 mM Hepes, 0.51 mM $CaCl_2$, 1.99 mM $MgCl_2$, 60.01 mM KCl, 15.75 mM NaCl, pH 7.52. Densely staining fibrils in nuclei are condensed chromatin or heterochromatin. Note that these structures become more distinct and darker staining in nuclei as the Ni(II) concentration increases.

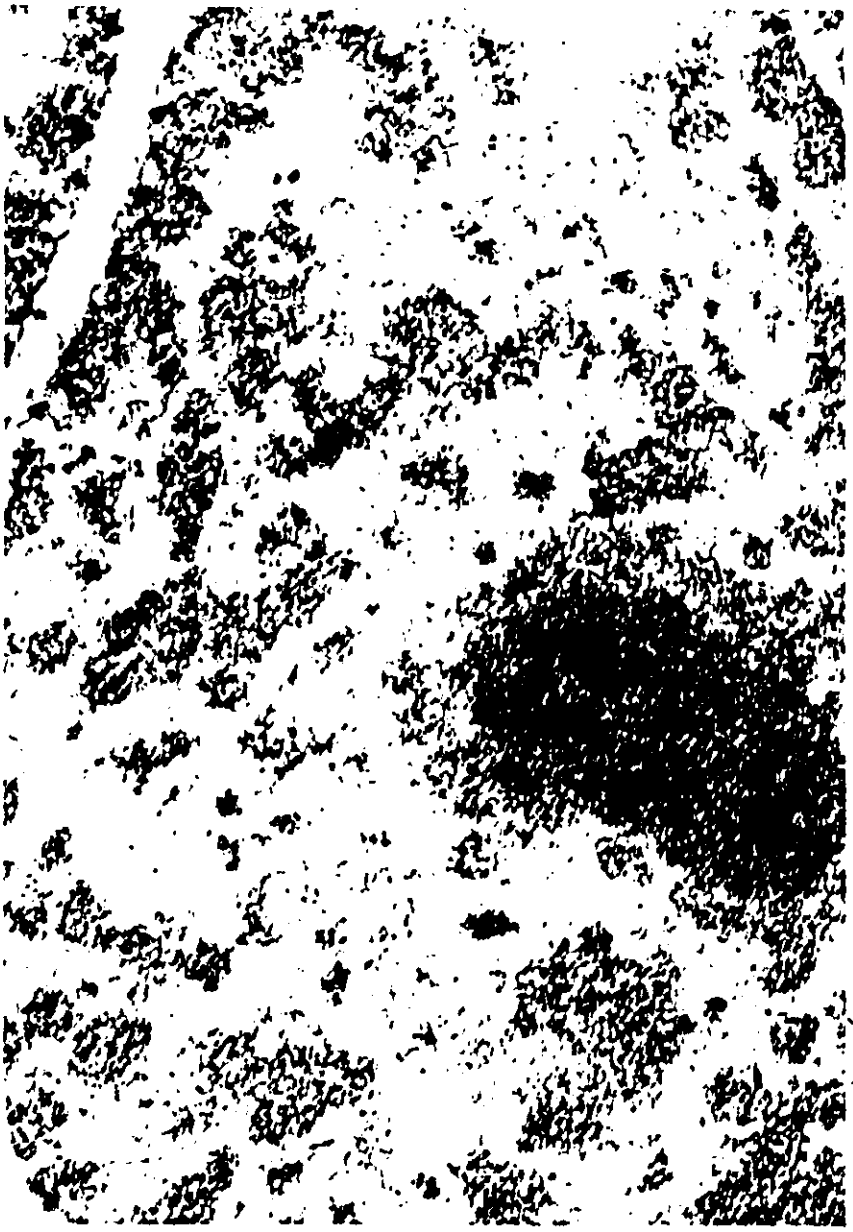

Figure 42, Panel A

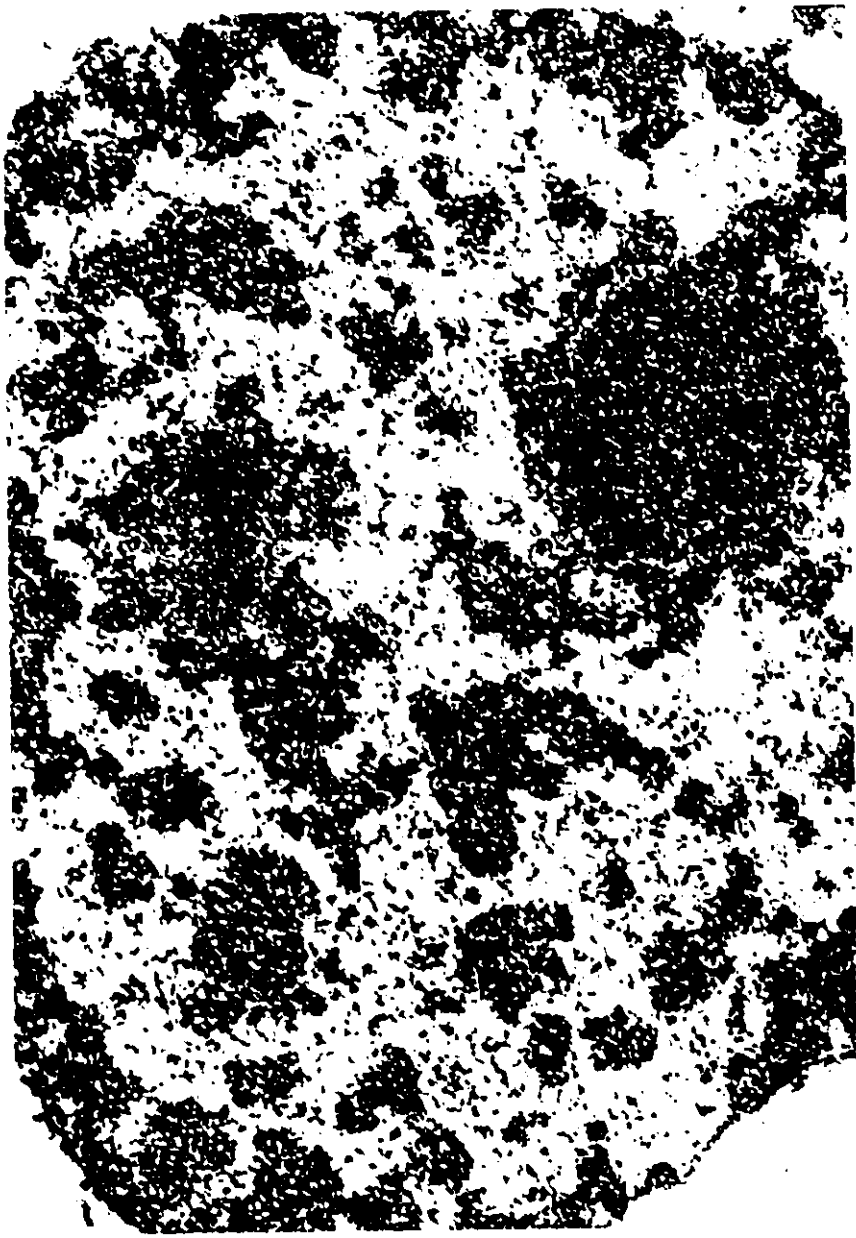

Figure 42, Panel B

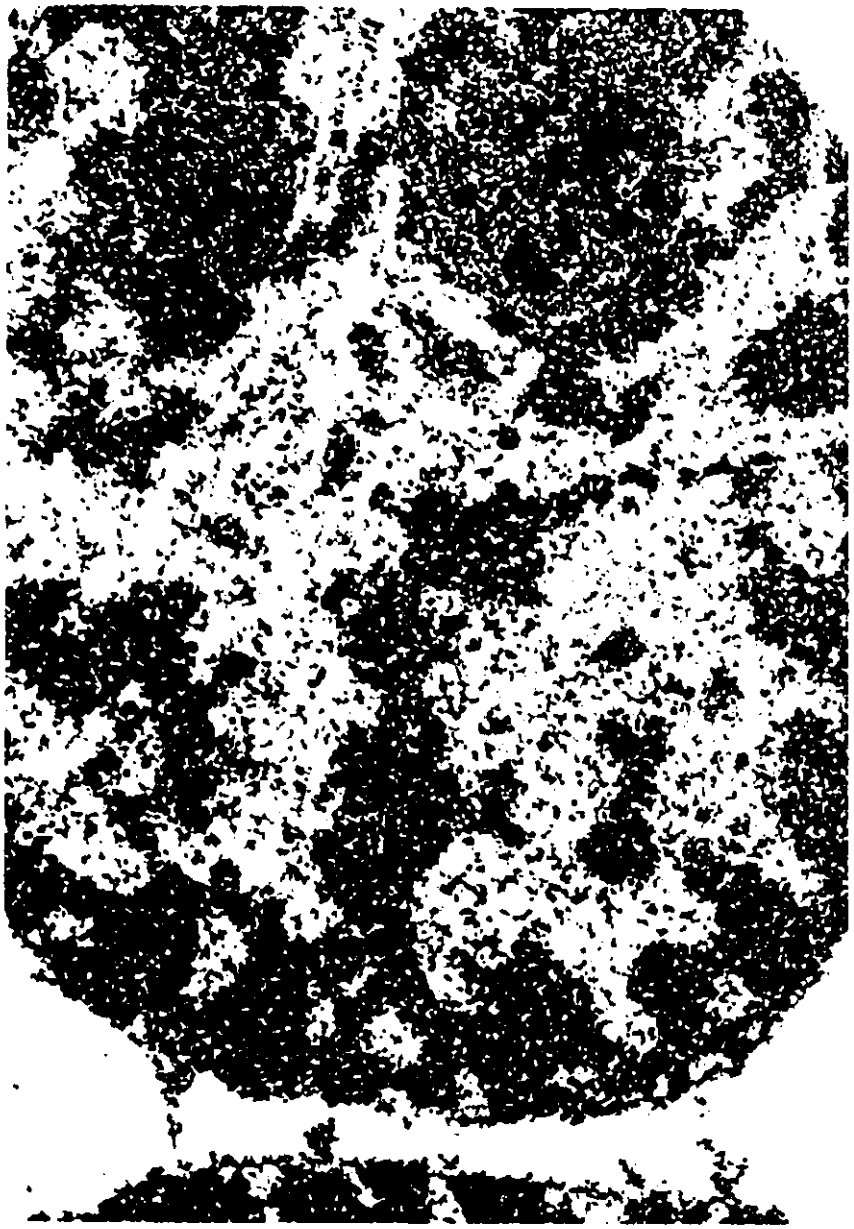

Figure 42, Panel C

Figure 42, Panel D

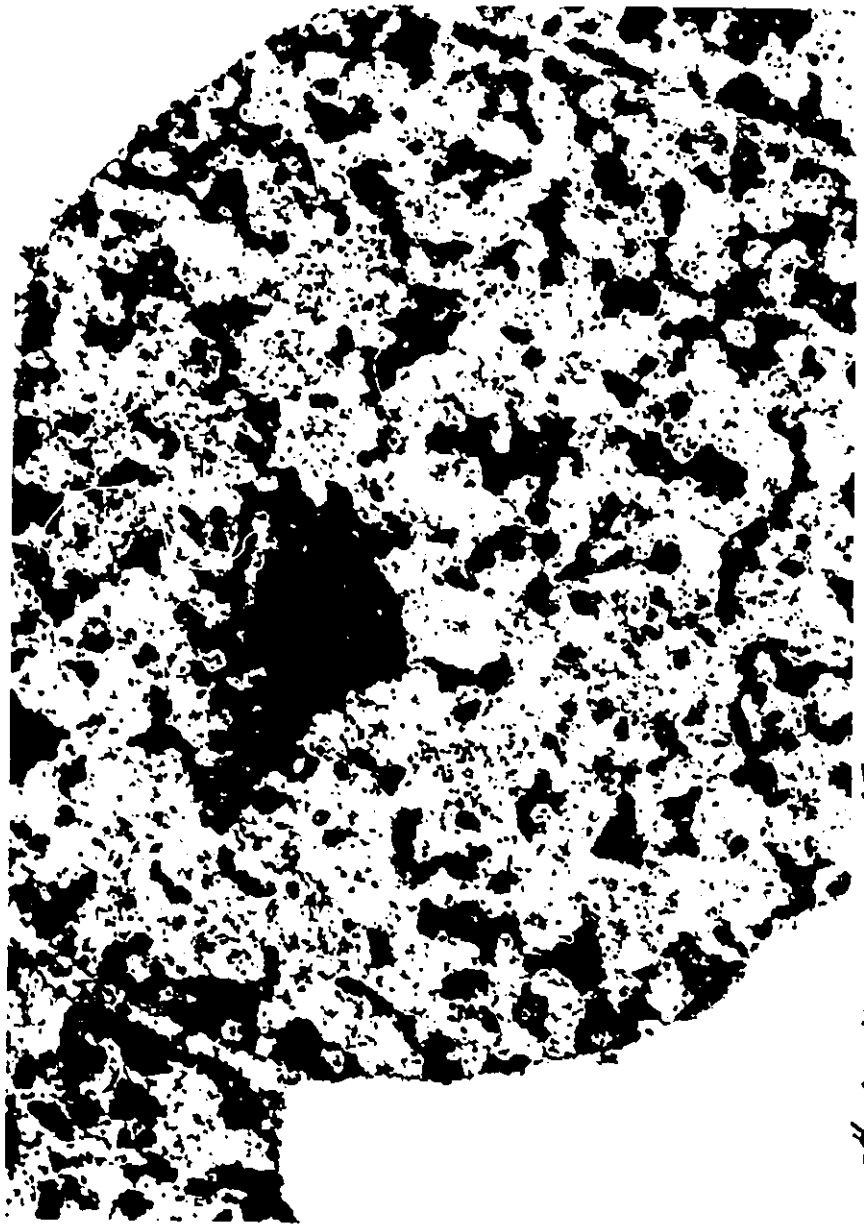

Figure 42, Panel E

Figure 43: Scanning electron micrographs (x18600) of nuclei exposed to Ni(II) for 96 h. Nickel concentrations were: A) control; B) 1.02×10^{-6} M; C) 1.02×10^{-4} M. Buffer conditions were: 10.11 mM Hepes, 0.51 mM $CaCl_2$, 1.99 mM $MgCl_2$, 60.01 mM KCl, 15.75 mM NaCl, pH 7.52. Densely staining fibrils in nuclei are condensed chromatin or heterochromatin. Note that these structures become more distinct and darker staining in nuclei as the Ni(II) concentration increases.

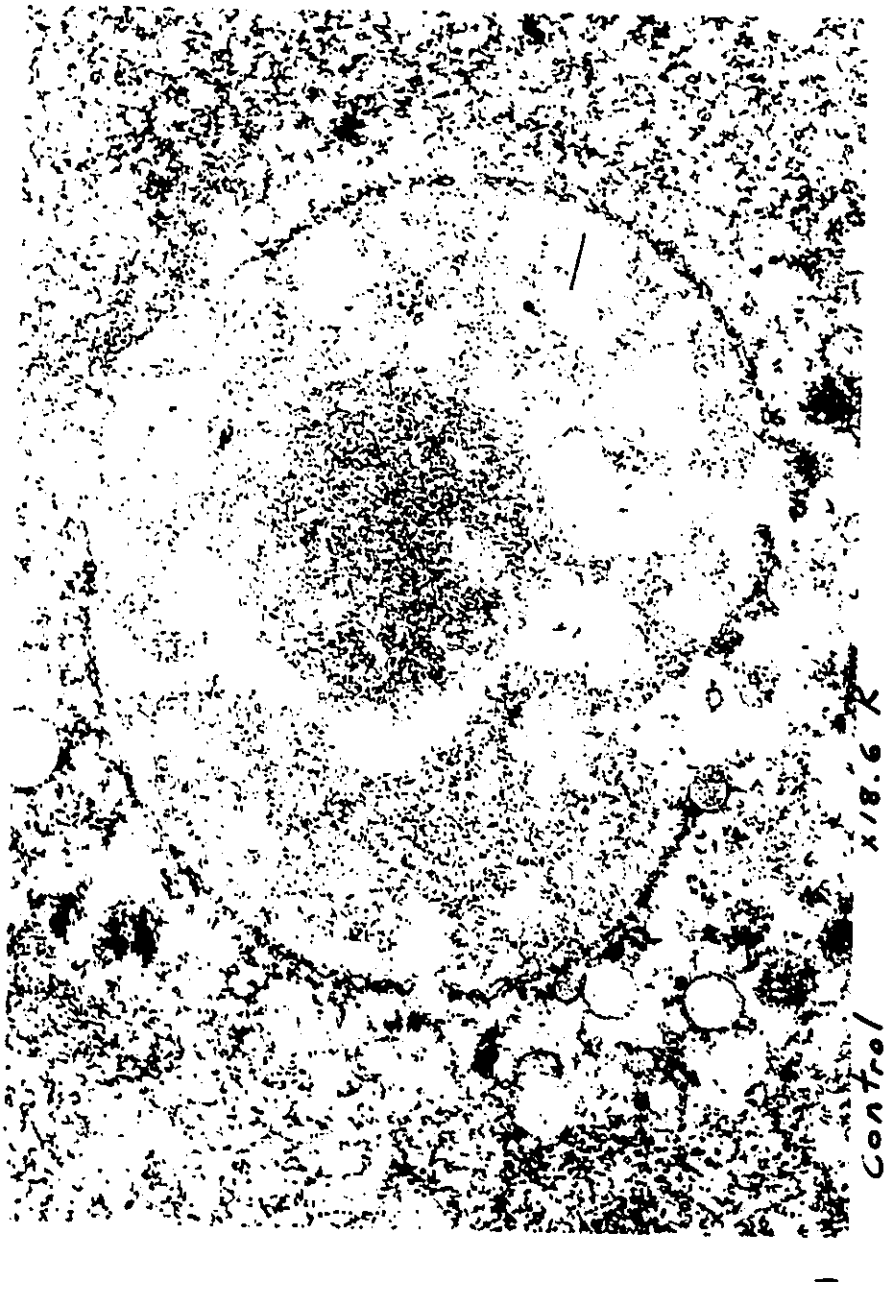

Figure 43, Panel A

Figure 43, Panel B

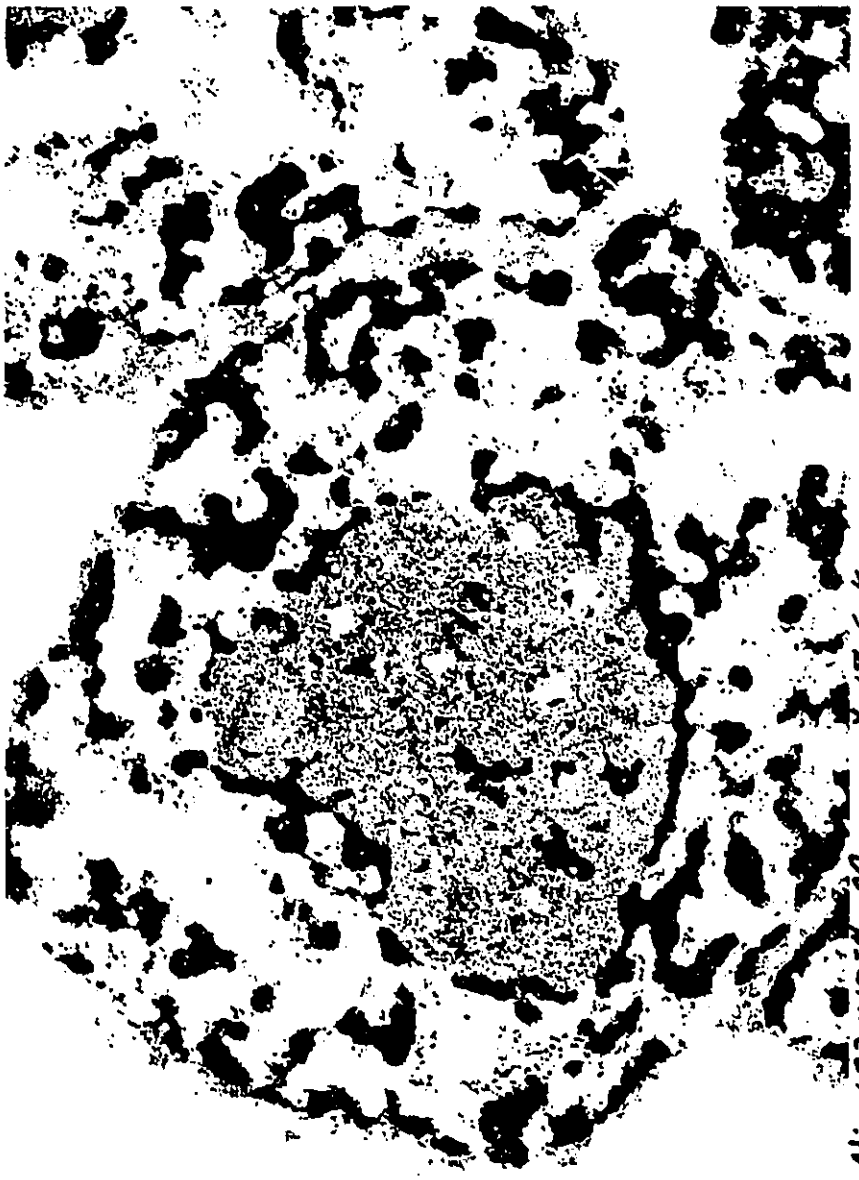

Figure 43, Panel C

III.3.4 Generation of Ni(II)-Binding Constants for Chromosomes in Nuclei

A typical Scatchard plot for the binding of Ni(II) ion to chromosomes is depicted in Figure 44. All such plots when generated with buffers containing varying amounts of Mg(II) ion were similar and typified by a biphasic curve consisting of two segments with negative slope. Dissociation constants of nickel are derived from the slopes of these negative segments. X-intercepts of these segments denote the fractional occupancy, namely moles of Ni bound per mole of DNA base pairs pertaining to a specific set of binding sites. In Table 7, a compilation is provided of binding constants for nuclei in the presence of varying amounts of Mg(II) ion. KD_1 shows no dependence on the Mg(II) level, while KD_2 increases with increasing Mg(II) concentrations. No variation in fractional occupancy of binding sites associated with KD_1 is observed. By contrast, values of fractional occupancy observed for the second binding site (i.e. KD_2) decrease with increasing Mg(II) concentrations.

III.4 DISCUSSION

The data presented in this chapter clearly demonstrate a condensational effect of Ni(II) ion on chromatin structure. This condensational state is readily affected by changes in ionic conditions, more specifically to changes in concentration of NaCl (or KCl) or more importantly, $MgCl_2$

Figure 44: Scatchard analysis of Ni(II)-binding to nuclear chromosomes. Buffer conditions were: 14.27 mM Hepes, 0.74 mM $CaCl_2$, 83.38 mM KCl, 23.04 mM NaCl, 1.57 mM $MgCl_2$, pH 7.6.

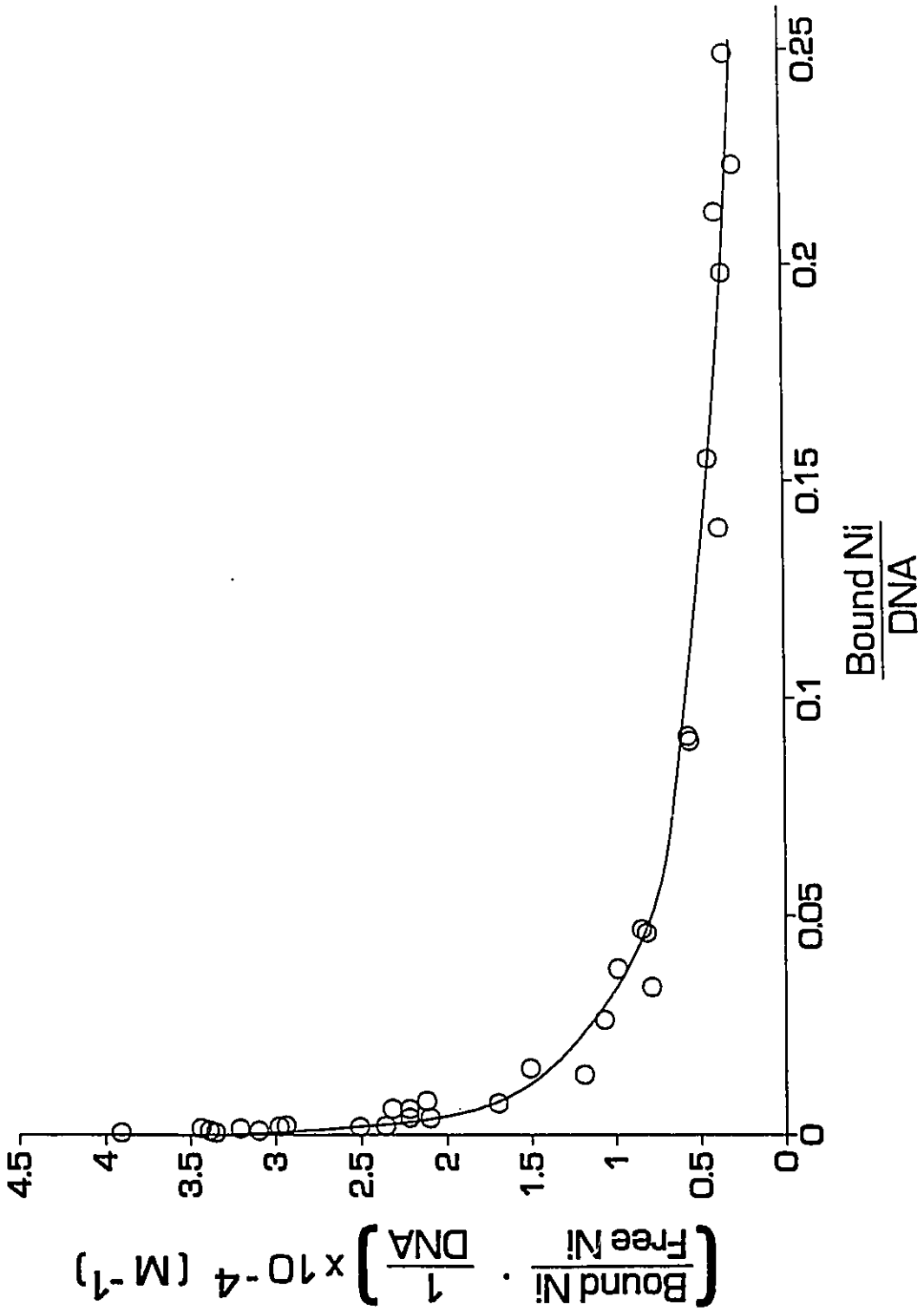
$\left(\frac{\text{Bound Ni}}{\text{Free Ni}} \cdot \frac{1}{\text{DNA}}\right) \times 10^{-4}\ (M^{-1})$
4.5
4
3.5
3
2.5
2
1.5
1
0.5
0
0
0.05
0.1
0.15
0.2
0.25
$\frac{\text{Bound Ni}}{\text{DNA}}$

Table 7: Nickel Dissociation Constants for Chromosomes of Intact Nuclei in the Presence of Mg(II)

Mg(II) Concentration[1] (mM)	KD_1 ± SD (M)[2]	Fractional Occupancy[3]	KD_2 ± SD (M)	Fractional Occupancy[3]
0.45 mM	$(2.87 \pm 0.02) \times 10^{-7}$	0.007	$(3.99 \pm 0.01) \times 10^{-5}$	0.388
1.57 mM	$(2.76 \pm 0.01) \times 10^{-7}$	0.008	$(4.40 \pm 0.01) \times 10^{-5}$	0.343
4.54 mM	$(3.02 \pm 0.01) \times 10^{-7}$	0.006	$(4.97 \pm 0.02) \times 10^{-5}$	0.293
10.08 mM	$(2.57 \pm 0.02) \times 10^{-7}$	0.005	$(5.55 \pm 0.02) \times 10^{-5}$	0.270

[1] Buffer components: 14.27 mM Hepes (pH 7.6), 0.74 mM $CaCl_2$, 84.38 mM KCl, 23.04 mM NaCl.
[2] SD, standard deviation.
[3] Defined as atoms of Ni bound per basepair of DNA in chromosomes of intact nuclei.

(i.e. Mg(II) ion; Aaronson and Woo, 1981; Weith, 1983; Ausio *et al.*, 1984; Dixon and Burkholder, 1985a,b; Greulich *et al.*, 1987; Makarov *et al.*, 1987). As previously described in the introduction to this chapter (Section I), the difference (ΔA) in absorption at 260 and 320 nm provides a convenient monitor for condensational or structural changes in chromosomes (Dixon and Burkholder, 1985b). Utilizing this difference in absorption, it is evident that Ni(II) ion has a profound effect on chromosomal structure (Figures 35 and 36). A clear transition in condensational state from a pre- to post-transition plateau is observed with a transitional midpoint at a Ni(II) ion concentration of 5×10^{-5} M. Moreover, the presence of increasing Mg(II) levels in the buffer do not abrogate this transition (Figure 36). In the absence of Ni(II) ion, increasing amounts of Mg(II) ion result in a decrease in ΔA values, which is indicative of a condensational difference (Figure 36).

We chose to quantitate the acid-soluble deoxynucleotides released by nuclease digestion by the reaction of purines with diaminobenzoic acid (DABA; Kissane and Robins, 1958). The reaction employed is a modification of the Doebner-Miller quinaldine synthesis whereby aldehydes of the type $R\text{-}CH_2\text{-}CHO$ yield strongly fluorescent products when allowed to react with DABA under conditions of prolonged heating in concentrated mineral acids. In theory, deoxynucleotides are hydrolyzed by DABA, and a fluorescent product is formed by the reaction

between DABA and the liberated deoxyribose. Under the conditions utilized in the assay, purine deoxynucleotides are readily hydrolyzed, whereas pyrimidine deoxynucleotides are resistant to acid hydrolysis. This is readily confirmed by the data presented in Table 6; pyrimidine deoxynucleotides did not demonstrate the generation of fluorescent byproducts. Accordingly, values measured for digested DNA correspond to amounts of purine deoxynucleotide released and thus are half the amount of nucleotides actually released (assuming an equal distribution of purine and pyrimidine deoxynucleotides released). Conversely, these measured amounts resulting from nuclease digestion may be interpreted to represent base pairs of DNA released. An additional conclusion derived from the data in Table 6 is that the assay is not linear over the entire concentration range examined (i.e. compare fluorescence values for 20 and 50 nmoles of dATP or dGTP). At low levels of digested material or purine deoxynucleotides (i.e. < 5 nmoles), the response is linear and suitable for the analysis of digested material (Figure 37).

Analysis of Ni(II)-ion exposed nuclei with regard to their susceptibility to nuclease digestion clearly demonstrates that exposure for 2 or 24 h does not render the chromosomes resistant to digestion (Figures 38 and 39). By contrast, 96 h exposures resulted in decreased susceptibility to nuclease digestion at all concentrations of Ni(II) ion (Figure 40). Furthermore, nuclease resistance increased in a

concentration-dependent fashion.

Electron micrographs of nuclei exposed to Ni(II) ion for 2 or 24 h suggest that changes occur in nuclear ultrastructure at higher levels of Ni(II) ion (i.e. 10^{-5}, 10^{-4} M; Figures 41 and 42). This is consistent with the condensational data presented in Figures 35 and 36. Correlation of condensational transitions monitored by ΔA and ultrastructural changes observed in electron micrographs has been documented (Dixon and Burkholder, 1985b).

Collectively the condensational, nuclease digestion and EM data for 2 and 24 h exposures suggest that condensations of chromosomes by Ni(II) ion occur but do not result in structures which are resistant to nuclease digestion. By contrast, the data for 96 h exposure suggests that Ni(II) ion induces chromosomal condensations at all nickel levels which result in nuclease digestion resistance (see Figure 40 for digestion data; Figure 43 for EMs). Clearly, this latter Ni(II)-ion induced process is time dependent and results in ultrastructural changes in nuclei which are more stable, resulting in a decreased nuclease digestion susceptibility. A recent report by Kasprzak and Bone (1989) has documented the ability of Ni(II) ion to generate protein-protein and protein-DNA crosslinks in a time-dependent (i.e. 24 to 96 h) fashion. Furthermore, these crosslinks were demonstrated to arise from the participation of nickel-catalyzed redox reactions. Protein-protein or protein-DNA crosslink formation may very

well explain the observed chromosomal condensations. Interestingly, a reduced susceptibility of condensed chromatin to nuclease digestion has been clearly documented for heterochromatin (Horvath and Horz, 1981) and brain tissue samples from Alzheimer patients (Lewis *et al.*, 1981; McLachlan *et al.*, 1984; Lukiw *et al.*, 1987; McLachlan *et al.*, 1989).

The generation of binding constants for Ni(II)-chromosomes demonstrated that two binding sites exist (Figure 44). The compilation of constants for Ni(II)-chromosome binding presented in Table 7 provides some interesting conclusions. The high affinity site (i.e. KD_1) does not depend significantly on the amount of Mg(II) present. Furthermore, this site corresponds to one binding site per 125-200 bp of DNA. This latter value for fractional occupancy must be viewed in the context that chromosomes consist of DNA, histones and non-histone proteins and that binding is not necessarily to the DNA alone but may contain complex sites involving components of DNA and protein. The second site (i.e. KD_2) demonstrates some dependence on Mg(II) ion concentrations. As Mg(II) concentrations are increased (and thus increasing condensation of chromosomes), this dissociation constant increases in magnitude. Moreover as the Mg(II) ion concentration increases, the value for fractional occupancy decreases (i.e. 1 Ni/2.6 bp to 1 Ni/3.7 bp) in a concentration dependent fashion. It is interesting to note that the values of KD_2 for Ni(II) ion roughly correspond to

the transition midpoints observed in Figure 36 and that increasing Mg(II) levels do not alter these transition midpoints, but do affect pretransition plateaus as monitored by ΔA. While these changes in KD_2 and fractional occupancies are slight, they suggest that the condensational processes elicited by Mg(II) ion are directly or indirectly associated with the Ni(II) binding sites involved in KD_2. Nieboer and Richardson (1980) have described an elegant system for the classification of metal ions with regards to their binding preferences for oxygen versus nitrogen/sulfur centres. Magnesium ion is classified as a *Class A* metal ion, possessing a preference for oxygen centres. By contrast, *Class B* metal ions possess a preference for nitrogen/sulfur centres. *Borderline* metal ions display ambivalence to oxygen, nitrogen and sulfur centres. In this classification scheme, the Ni(II) ion is designated as *Borderline*. In spite of the preference of *Class B* metal ions for nitrogen/sulfur ligands, both *Class B* and *Borderline* ions form complexes with oxygen ligands which are more stable than those of *Class A* ions of comparable size and charge. Thus, this classification scheme is supportive of the conclusion that KD_2 sites for Ni(II)-chromosome binding may share some common site components with that of Mg(II) binding, a class A ion.

A comparison of the Ni(II) binding-constant data for chromosomes in intact nuclei with that for DNA or polydeoxynucleotides (compare Table 7 with Table 4) provides

some interesting observations. Both sets of data are comparable in magnitude, although some differences are apparent. If one assumes a relatively equal distribution of A/T and G/C basepairs (i.e. 50% of each; compare with calf thymus DNA, Table 4), the results suggest that the binding sites of Ni(II) ion for chromosomes in nuclei are slightly more avid as reflected by the relative decreases in the magnitude of both KD_1 and KD_2. The differences in values for fractional occupancy also suggest that distinct differences may occur in the actual binding sites of chromosomes in comparison to naked DNA. In chromatin, proteins packaged into higher order structures likely contribute to the differences observed in binding parameters.

The data presented in this chapter clearly demonstrate that Ni(II) ion affects chromosomal condensation states in nuclei. The Ni(II)-ion induced condensational or structural changes which were both concentration and time dependent. High affinity sites for Ni(II) binding to chromosomes were identified which do not appear to bind or be influenced by Mg(II). In addition, a second family of weaker binding sites have been characterized which are influenced by or bind the Mg(II) ion.

IV. INDUCTION AND ANALYSIS OF NI(II)-MUTATIONS IN A CHO CELL LINE (AS52)

IV.1 INTRODUCTION

IV.1.1 Overview

As presented in the Section I.2.3, little evidence for the mutagenicity of nickel compounds has been documented utilizing traditional prokaryotic (e.g., *S. typhimurium, E. coli*) or mammalian (e.g. CHO/HPRT, L5178Y/$TK^{+/-}$) cell systems. By contrast, a variety of cellular and biochemical studies have clearly demonstrated that nickel compounds affect chromosomes, DNA, DNA synthesis and transcription (reviewed in Chapters I, II and III).

Recently, a novel cell line has been developed demonstrating unique properties which may be of value for the detection and characterization of nickel-induced mutations. This line, designated AS52, is a derivative of a Chinese hamster ovary (CHO-K1-BH4) cell line (Tindall *et al.*, 1984; Tindall *et al.*, 1986). Following X-ray irradiation and selection in 6-thioguanine (6-TG), a new line designated X3/5 was isolated in which the gene for hypoxanthine-guanine phosphoribosyltransferase (HPRT) is deleted. As a functional replacement the homologous gene from *E. coli*, xanthine-guanine phosphoribosyltransferase (XPRT or *gpt;* Mulligan & Berg, 1980)

has been stably integrated into the parental CHO genome. This final cell line was designated AS52.

Comparison of mutation frequencies induced in this new cell line (AS52; *gpt* selection) with that in traditional CHO line (CHO-K1-BH4; HPRT selection) suggests an equal susceptibility to most mutagens. Traditional point mutagens (e.g. EMS, UV light), frameshift mutagens (e.g., ICR 191) or antitumour agents/drugs demonstrated comparable responses in both lines (Hsie *et al.*, 1986; Stankowski, Jr. *et al.*, 1986; Tindall *et al.*, 1986; Stankowski, Jr. and Tindall, 1987; Tindall and Stankowski, Jr., 1987; Aaron and Stankowski, Jr., 1989; Ma *et al.*, 1993). By contrast X-ray irradiation, radiomimetic compounds (e.g., streptonigrin, bleomycin), oxidizing agents (e.g., hydrogen peroxide, potassium superoxide) or clastogens (e.g., formaldehyde, ethanol) reproducibly induced mutations at the *gpt* locus of AS52 cells but were equivocal or non-mutagens at the HPRT locus (Hsie *et al.*, 1986; Stankowski, Jr. and Tindall, 1987; Tindall and Stankowski, Jr., 1987; Hsie, 1987; Hsie *et al.*, 1990; Ma *et al.*, 1993). Southern blot hybridization analyses of mutations induced by these latter chemicals indicated primarily partial or gross deletions of the *gpt* (or HPRT) locus (Stankowski, Jr. and Hsie, 1986; Stankowski, Jr. *et al.*, 1986; Tindall and Stankowski, Jr., 1987; Hsie *et al.*, 1990).

Based on the accumulated Southern blot analyses and the mutant frequency diversity between AS52 and traditional

CHO lines, it has been postulated that the lower response and recovery of HPRT mutants of deletion type mutagens is due to an inability to recover mutants containing deletions affecting adjacent essential genes on the hemizygous X chromosome. By contrast, the *gpt* locus in the AS52 line would not be similarly affected due to its presumed integration into an autosomal chromosome (Stankowski, Jr. *et al.*, 1986; Hsie, 1987; Tindall and Stankowski, Jr., 1987; Hsie *et al.*, 1990).

The development of the polymerase chain reaction (PCR) has greatly facilitated the isolation, identification and characterization of DNA segments (Saiki *et al.*, 1988; Erlich *et al.*, 1991). This technique involves the *in vitro* enzymatic amplification (> million-fold) of specific DNA fragments. The reaction is based on the annealing and extension of two short DNA primers flanking a segment of target DNA. A number of PCR cycles (e.g. 20-50) of DNA denaturation, primer binding and DNA synthesis/extension results in the exponential accumulation of a discrete fragment whose termini are defined by the 5' ends of the primers. This technology has been adopted to the assessment of DNA mutations, including that of the *gpt* locus of the AS52 cell line (Tindall and Stankowski, Jr., 1989; Xu *et al.*, 1989; Hsie *et al.*, 1990; Tindall and Whitaker, 1991). Utilizing this technique, a rapid screening of isolated DNA to detect mutations can be achieved.

IV.1.2 Specific Research Objectives

Previous work in this laboratory has demonstrated that a variety of nickel compounds are weak mutagens in the AS52 cell line (Fletcher, 1990; Fletcher *et al.*, 1993). The work presented in this chapter involves the generation, isolation and molecular characterization of AS52 mutants induced by several nickel compounds. These include soluble nickel sulfate ($NiSO_4$), insoluble nickel subsulfide (Ni_3S_2) and a compound of intermediate solubility, nickel hydroxide ($Ni(OH)_2$). For comparison, spontaneous mutants and those induced by the point mutagen ethyl methanesulfonate (EMS) are also examined. In the course of these studies, PCR analysis demonstrated the presence of a second DNA segment related to the *gpt* sequence integrated into the AS52 genome. This second *gpt*-like segment is also fully identified and characterized (i.e. DNA sequence, RNA transcription status, etc.). Components of this work have previously been published and discussed in the scientific literature (Nieboer *et al.*, 1992; Fletcher *et al.*, 1993; Rossetto *et al.*, 1993).

IV.2 MATERIALS AND METHODS

IV.2.1 Chemicals and Reagents

In Table 8, a compendium is provided of the various chemicals and reagents, their sources as well as any other relevant information pertaining to the experiments described in this chapter. Doubly deionized distilled water (DDI) was

Table 8: Chemicals, Reagents and Kits

Chemical Name	Formula	Source	Grade	Lot #
General Chemicals:				
Ethylmethanesulfonate	NA	Sigma	Reagent	85F-023
Nickel Hydroxide	$Ni(OH)_2$	Lab Prep	NA	NA
Nickel Subsulfide	Ni_3S_2	Inco	NA	NA
Nickel Sulfate	$NiSO_4$	BDH Chem. Co.	Analytical	86226
Sodium Chloride	NaCl	BDH Chem. Co.	Analytical	105850/22120
Potassium Chloride	KCl	BDH Chem. Co.	Analytical	96582/7360
Potassium Dihydrogen Orthophosphate	KH_2PO_4	BDH Chem. Co.	Assured	87380
Disodium Hydrogen Orthophosphate	Na_2HPO_4	BDH Chem. Co.	Assured	89627
Tris(hydroxymethyl)-aminomethane	NA*	Boehringer Mannheim	Electrophoretic	DCA121/3-93
Magnesium Chloride	$MgCl_2$	BDH Chem. Co.	Analytical	105685/29914
Tween 20	NA	Sigma Chem. Co.	Reagent	128F0561
Nonidet P-40	NA	Sigma Chem. Co.	Reagent	38F-00271
Phenol	NA	BRL	Ultrapure	AA3201
Chloroform	$CHCl_3$	Caledon	Reagent	01374A
Sodium Acetate	$NaOOCCH_3$	BDH Chem. Co.	Assured	2139310
4-(2-hydroxyethyl)-1-piperazine ethanesulfonic Acid (HEPES)	NA	Sigma Chem. Co.	Cell Culture	110H-5613
Ethylene-diaminetetracetic Acid (EDTA)	NA	BDH Chem. Co.	Assured	96257/5589
Sodium Hydroxide	NaOH	BDH Chem. Co.	Analytical	104030/13238
Sodium Chloride	NaCl	BDH Chem. Co.	Analytical	105850/22120
Ficoll	NA	Pharmacia	Tissue Culture	LK00724
Polyvinylpyrollidone (PVP)	NA	Pierce	Reagent	08247-23
Bovine Serum Albumin (BSA)	NA	Sigma Chem. Co.	Fraction V	114F-0388
Sodium Dodecyl Sulfate (SDS)	NA	BRL	Electrophoretic	AJ3210
[γ-^{32}P]-Adenosine-5'-Triphosphate Tetra (Triethylammonium) Salt (ATP)	NA	New England Nuclear	NA	NA
Sodium Citrate	NA	BDH Chem. Co.	Analytical	96240/6368
Salmon Sperm DNA	NA	Sigma Chem. Co.	Molecular	37F-7340
Human Placental DNA	NA	Sigma Chem. Co.	Ultrapure	128F-6693-1
Dextran Sulfate		Pharmacia	Ultrapure	PK97380

continued ...

Table 8: Chemicals, Reagents and Kits (continued)

Chemical Name	Formula	Source	Grade	Lot #
Electrophoresis:				
N,N,N',N'-tetramethylethylenediamine (TEMED)	NA	BioRad	Electrophoretic	12965
Morpholinopropanesulfonic Acid (MOPS)	NA	Sigma Chem. Co.	Reagent	60H5635
Formaldehyde	NA	BDH Chem. Co.	Reagent	99030/1359
Glycerol	NA	BDH Chem. Co.	Analytical	90229
Dithiothreitol (DTT)	NA	BioRad	Electrophoretic	12209
Agarose	NA	BRL	Electrophoretic	NA
Boric Acid	H_3BO_3	BDH Chem. Co.	Assured	87645
Bromophenol Blue	NA	BDH Chem. Co.	Assured	5536120A
Sucrose	NA	BDH Chem. Co.	Analytical	101945/115
Acrylamide	NA	BioRad	Electrophoretic	30780
Bisacrylamide	NA	BioRad	Electrophoretic	31688
Urea	NA	BioRad	Electrophoretic	NA
Xylene Cyanol	NA	Sigma Chem. Co.	Reagent	NA
Ammonium Persulfate (APS)	NA	BioRad	Electrophoretic	M5201
Formamide	NA	BDH Chem. Co.	Analytical	NA
Ethidium Bromide	NA	Sigma Chem. Co.	Reagent	92F-0353
Tissue Culture:				
MCDB 302 Media	NA	Sigma Chem. Co.	Tissue Culture	40H-4603-1
Dialyzed Fetal Bovine Serum (dFBS)	NA	Gibco/BRL	Tissue Culture	NA
Mycophenolic Acid (MPA)	NA	Sigma Chem. Co.	Tissue Culture	69F-4055
Aminopterin	NA	Sigma Chem. Co.	Tissue Culture	17F-40115
Adenine	NA	Sigma Chem. Co.	Tissue Culture	115F-04505
Thymidine	NA	Sigma Chem. Co.	Tissue Culture	127F-0835-5
Xanthine	NA	Sigma Chem. Co.	Tissue Culture	98F-08205
Penicillin G	NA	Sigma Chem. Co.	Tissue Culture	NA
Streptomycin	NA	Sigma Chem. Co.	Tissue Culture	NA
Trypsin	NA	Gibco/BRL	Tissue Culture	NA
6-Thioguanine (6-TG)	NA	Sigma Chem. Co.	Tissue Culture	15F-4023

continued ...

Table 8: Chemicals, Reagents and Kits (continued)

Chemical Name	Formula	Source	Grade	Lot #
Kits:				
Oligo Labelling Kit	Cat #27-9250	Pharmacia	NA	AA9250101
Photogene™ Nucleic Acid Detection System	Cat #81925A	BRL	NA	BCE-001
GeneAmp® RNA PCR Kit	Cat #N808-0017	Perkin Elmer Cetus	NA	RK5262
RNA Extraction Kit	Cat #27-9270-01	Pharmacia	NA	2079270011
QuickPrep™ Kit mRNA Purification	Cat #27-9254-01	Pharmacia	NA	CM9254101
Polymerase Chain Reaction (PCR):				
Ultrapure dNTP Set	dATP,dGTP,dTTP,dCTP	Pharmacia	Ultrapure	NA
Ultrapure ddNTP Set	ddATP,ddGTP,ddTTP,ddCTP	Pharmacia	Ultrapure	NA
Oligonucleotide Primers	NA	Research Genetics	NA	NA
Amplitaq DNA Polymerase	Cat #N801-0060	Perkin Elmer Cetus	Recombinant	NA
Biotin-11-dUTP	NA	Sigma	Ultrapure	NA
Enzymes:				
Polynucleotide Kinase (PNK)	NA	Pharmacia	Cloned	BA0736110
Deoxyribonuclease I (DNase I)	NA	Pharmacia	Cloned	BK0512101
Proteinase K	NA	Boehringer Mannheim	Molecular	13259025-34
Kpn I	NA	Pharmacia	Molecular	AG0908101
Hind III	NA	Pharmacia	Molecular	QG8603007

NA, not available; not applicable.

used in all solution preparation. All tissue culture solutions were filter sterilized (0.22 μm) or autoclaved. Particulate nickel compounds (i.e. $Ni(OH)_2$, Ni_3S_2) used in the generation of AS52 cell line mutants were supplied by Mr. Glenn Fletcher (McMaster University). Identities and composition of both compounds have been verified by chemical analysis and X-ray diffraction analysis (Fletcher *et al.*, 1993). The isolation of particles less than 5 μm in size was performed by sieving. High purity nickel sulphate was purchased from BDH (Analar grade) and stored as a 500 mM stock solution in DDI. Specific formulations of appropriate solutions (i.e., media, buffers, etc.) are stated in the appropriate ensuing sections.

IV.2.2 AS52 Cells: Culturing and Mutagenicity Testing

IV.2.2.1 Normal Cell Culture and Maintenance

The culturing of the AS52 cell line is based on standard protocols (Tindall and Stankowski, Jr., 1989; Nestmann *et al.*, 1991; Fletcher *et al.*, 1993). Routine or maintenance cultures were propagated in "MPA" medium: MCDB 302 medium plus 2% dialyzed and heat-inactivated fetal bovine serum (dFBS) plus MPA supplements (10 μg/ml mycophenolic acid, 3.0 μm aminopterin, 25 μg/ml adenine, 50 μm thymidine and 250 μg/ml xanthine). In addition antibiotics were added for routine culturing (100 U penicillin G and 100 μg streptomycin per mL of medium). Cells were grown in a 37°C, 95-100%

humidity, 5% CO_2 (continuous flow) incubator and routinely subcultured every 3-4 days, with typical splits of 1:8. Subculturing of cells involved an initial rinsing with phosphate buffered saline (PBS; 8 g NaCl, 0.2 g KCl, 0.2 g KH_2PO_4, 2.2 g $Na_2HPO_4 \cdot 7H_2O$ in 1 L water, pH 7.2-7.4). Following removal of this PBS wash, 1 ml of trypsin (0.125% w/v) was added per dish, swirled and then immediately removed. Upon standing for 3-5 min at room temperature, cells became rounded and started to detach from plates. Medium was then added, cells dislodged by pipetting and transferred to new plates. A doubling time of approximately 16 h (14-18 h) and plating efficiencies of 50-70% were typically observed (Fletcher *et al.*, 1993). A Coulter Model Z_F particle counter was used for cell number determinations.

IV.2.2.2 Mutagenicity Testing

For mutagenicity testing, cells were initially replated in "XAT/2" medium (MCDB 302 medium plus 2% dFBS, 6 µg/ml adenine, 60 µg/ml xanthine and 8 µm thymidine) one day prior to mutagen exposure. Exposure to soluble compounds was for 5 h, that to particulate compounds was for 24 h. Cells were then rinsed and replated as previously described (Section IV.2.2.1) in XAT/2 medium. Following several days recovery (3-4 days), cells were replated in "MCDB/2" medium (MCDB 302 medium plus 2% dFBS). On day 7 or 8, mutants were selected by plating $2x10^5$ cells/100 mm dish in MCDB/2 medium containing 10

μM of 6-thioguanine (6-TG) to select for *gpt* mutants (Mulligan and Berg, 1981). Ten days later, individual clones were picked and expanded in MCDB/2 medium to approximately 6-8x10^6 cells (two 100 mm plates of near confluent cells). A maximum of three colonies were picked and expanded from any one plate.

IV.2.3 Isolation and Quantitation of Nucleic Acids (DNA, Total RNA, mRNA) From Cultured AS52 Cells

IV.2.3.1 Isolation of DNA for Molecular Analysis

Following washing with PBS, cells from one 100 mm plate were detached by scraping. Cells were lysed in 250 μl of lysis solution (17 mm Tris, 60 mM KCl, 1 mM $MgCl_2$, 0.4% Tween-20 v/v, 0.4% Nonidet P-40 v/v, 0.5 mg/ml proteinase K, pH 8.7) overnight at 45°C (Higuchi, 1989). To this cell lysate, 250 μl of HE buffer (10 mM Hepes, 1 mM EDTA, pH 7.6) was added and the ensueing aqueous lysate mixture extracted once with an equivolume of water-saturated phenol and once with an equivolume of phenol/chloroform (50:50 v/v). Pursuant to each extraction, samples were microfuged (Eppendorf Model 5415, 16000xg, 24°C, 3 min) to ensure separation of organic and aqueous phases. To the final aqueous phase, a one tenth volume (refers to the aqueous phase) of 3M sodium acetate (pH 5.2) was added and thoroughly mixed in. Two volumes of absolute ethanol was added and the mixture was stored at -20°C overnight (Zeugin and Hartley, 1985). Precipitated DNA was collected by centrifugation (16000xg, 30 min, 5°C) and the

pellet washed with 80% absolute ethanol/water (v/v). Final pellets were air dried for approximately one hour prior to solubilization in 50 µl of HE buffer. All samples were stored at -20°C until needed.

IV.2.3.2 Isolation of DNA for Polymerase Chain Reaction (PCR) Analysis

Lysis of cells was exactly as that described in the preceding section (Section IV.2.3.1). To the 250 µl cell lysate, an equivolume of sterile water was added and the mixture heated at 95°C for 15 min. This heating step ensured the inactivation of protease and complete denaturation of genomic DNA. The samples were than frozen at -20°C until further analyzed.

IV.2.3.3 Isolation of Total RNA From Cultured AS52 Cells

The isolation of total RNA from cultured cells was performed utilizing a RNA Extraction Kit obtained from Pharmacia LKB Biotechnology Inc. (Catalogue #27-9270-01). Five plates of near confluent cells (3-4x10^6 cells/100 mm plate) were used per extraction. All glassware and utensils were autoclaved (121°C, 30 min, 28 lbs/sq. in.) in order to avoid contamination with ribonucleases. Sterile, disposable plasticware was used without pretreatment and new packages opened at the onset of each experiment. Gloves were also worn at all times to further minimize ribonuclease contamination.

Following the removal of culture medium from each plate, 2 ml of "Extraction Buffer" (buffered aqueous solution containing guanidium thiocyanate, N-lauryl sarcosine and EDTA) was pipetted onto each plate. This buffer was pipetted up and down numerous times (5-10x) in order to disrupt cells. Cell homogenates were centrifuged in a Hettich Rotanta/R centrifuge for 30 min at 4000 RPM (3000xg), 15°C to remove cellular debris. The clarified homogenate was then transferred to a prechilled beaker on ice; the homogenate passed through a 18 gauge needle 10 times in order to shear the DNA present. Two and a half millilitres of this homogenate was gently layered over 2.7 ml of a cesium trifluoroacetate (CsTFA) "cushion" in a high speed centrifuge tube. Following centrifugation in a Beckman L8-70 M ultracentrifuge (SW 50.1 rotor, 31000 RPM (125000xg), 15°C, 16 h) the RNA pellet was solubilized in 100 µl of TE buffer (10 mM Tris-HCl, 1 mM EDTA, pH 7.5) by incubating for 10 min at 65°C. To the solubilized RNA, 10 µl of 2 M potassium acetate (pH 5.0) and 2.5 volumes (275 µl) of absolute ethanol was added and thoroughly mixed, stored at -20°C overnight and the RNA pellet recovered by centrifugation (Eppendorf, 5000xg, 20 min, 24°C). The pellet was allowed to briefly air dry (15 min) before resuspension in 100 µl of 10 mM Tris-HCl (pH 7.5). Solubilized RNA was generally used immediately; long-term storage was as the precipitated RNA pellet in absolute ethanol as described above.

IV.2.3.4 Isolation of mRNA From Cultured AS52 Cells

The isolation of mRNA from cultured cells was achieved utilizing a QuickPrep™ mRNA Purification Kit obtained from Pharmacia LKB Biotechnology Inc. (Catalogue #27-9254-01). Five plates of near confluent cells (3-4x10^6 cells/100 mm plate) were used per extraction. An avoidance of contamination by ribonucleases involved the sterilization of solution and utensils or the usage of disposable plasticware as described in the preceding section for the isolation of total RNA (Section 2.3.3).

The initial isolation of total cellular RNA was as previously described in Section 2.3.3 with some modifications. The centrifugal step isolating RNA via centrifugation through cesium trifluoroacetate (CsTFA) was omitted along with the subsequent ethanol precipitations. Messenger RNA was purified from total RNA by binding to oligo(dT)-cellulose columns provided in the kit. Briefly, 4 ml of the RNA solution was applied to the surface of the resin. The RNA-resin column was inverted several times manually to resuspend the resin and subsequently mixed for 10 min on a rocking table. Leaving both top and bottom closures on the column, it was centrifuged for 2 min at 350x g (in a centrifuge tube) to separate the resin from aqueous solution. This latter solution was removed by decantation. Three millilitres of a "High-Salt Buffer" (10 mM Tris-HCl, 1 mM EDTA, 0.5 M NaCl, pH 7.4) was applied to the top of the resin and the matrix resuspended by gently

inverting the column several times. Following a similar low speed centrifugation, this wash solution was removed and discarded. This washing of resin was repeated two more times with the "High-Salt Buffer" and one time with a "Low-Salt Buffer" (10 mM Tris-HCl, 1 mM EDTA, 0.1 M NaCl, pH 7.4). An additional "Low-Salt Buffer" wash was performed but with the bottom closure of the column removed, thus allowing the buffer to wash through the column into the centrifugation tube and be discarded. A 1.5 ml microcentrifugation tube (the "collection tube") was placed inside the centrifuge tube and the column replaced into the centrifuge tube with its tip inside the opening of the "collection tube". Elution of the bound poly(A)$^+$ RNA was facilitated by three successive washes with "Elution Buffer" (10 mM Tris-HCl, 1 mM EDTA, pH 7.4) prewarmed to 65°C. Each 250 µl wash was collected by centrifugation as previously described and added into the same "collection tube". Messenger RNA was subsequently precipitated following the removal of 0.25 ml for quantitation (Section 2.3.5). To the remaining 0.5 ml of mRNA solution, 50 µl of potassium acetate solution (2.5 M, pH 5.0) and 10 µl of glycogen solution (10 mg/ml in distilled water) was added and mixed in. Absolute ethanol (1.2 ml) was then added and the sample placed at -20°C overnight. The RNA precipitate was collected by centrifugation (16000xg, 4°C, 5 min), air dried for approximately 10 min and resolubilized in 50 µl of Elution buffer immediately prior to use. Long-term storage of the

mRNA was as a precipitate in ethanol at -20°C.

IV.2.3.5 Quantitation of RNA and DNA

IV.2.3.5.1 RNA

Quantitation of RNA was performed according to methodology presented in Maniatis *et al.*, 1982. The assumption utilized in this procedure is that one A_{260} unit of RNA is equivalent to a solution concentration of 40 µg/ml. RNA solution was diluted with water and the absorbance measured at 260 nm on a Perkin Elmer Lambda 3B UV/VIS Spectrophotometer utilizing 1 cm quartz cuvettes.

IV.2.3.5.2 DNA

The quantitation of DNA involved the intercalation of ethidium bromide (EtBr) and was based on previously published and developed methodology (Morgan *et al.*, 1979). The assumption implicit in this assay is that intercalation of EtBr into reference and sample DNA is similar (see Chapter II.1.5). Reference DNA utilized was ultrapure human placental DNA (50 µg/ml). Typical concentration measurements utilized 5 µl (250 ng) of this DNA as a standard per assay. Five microliters of sample DNA were also typically analyzed. Both samples were added to 2 ml of EtBr reagent (12.38 mM KH_2PO_4, 0.5 mM EDTA, pH 11.99) and fluorescence measured as previously described (Chapter I.1.5) on a Gilson Spectra/glo Fluorometer. The sample's fluorescence was compared proportionally to the

standard's fluorescence in assigning concentrations.

IV.2.4 Electrophoretic Analysis of DNA and RNA

IV.2.4.1 DNA Agarose Gels

Both mini and regular size horizontal agarose gels were made in essentially the same fashion. Protocols were based on standard procedures as presented in Maniatis *et al.*, 1982. Regular size gels were run in a MAX Submarine Agarose Gel Unit, Model HE99 (Hoeffer Scientific Instruments); minigels were run in a MINNIE Submarine Agarose Gel Unit, Model HE33 (Hoeffer Scientific Instruments). Agarose (typically 0.5 to 1.2% (w/v)) was suspended in 1 x TBE buffer (0.089 M Tris, 0.089 M boric acid, 0.002 M EDTA, pH 7.9), heated in a microwave open until the agarose dissolved, and allowed to cool to 50°C at which time ethidium bromide (10 mg/ml in water) was added to a final concentration of 0.5 µg/ml. The gel was then poured, a comb set in place and the gel allowed to solidify at room temperature. Large gels (14.5 cm x 25 cm) were typically 0.8 cm thick and involved approximately 250 ml of agarose solution. These gels normally were divided in two by gel sample combs in order to double the samples run per gel. Minigels (6.5 cm x 10 cm) were typically 0.5 cm thick and prepared with 35 mls of agarose solution. Large gels were normally run overnight at 25 volts; minigels at 150 volts for 1.5 h. Running buffer was 1xTBE. Prior to gel loading, 1 µl of gel loading buffer (0.25% bromophenol

blue, 40% (w/v) sucrose in water) was added per every 4 µl of DNA sample loaded. Visualization and photography of DNA bands (via EtBr intercalation) was facilitated by a UV source/light box and photographed by a Polaroid MP4 camera system utilizing Polaroid Type 667 film.

IV.2.4.2 DNA Sequencing Gels

Sequencing gels were prepared according to standard protocols as presented in Maniatis *et al.*, 1982. Gels were run on a Model S2 sequencing apparatus (BRL-Life Technologies Inc.). Sequencing gels (0.7 mm x 31 cm x 39 cm) were typically 85 ml in volume and consisted of: 4% polyacrylamide (20:1 (w/w) acrylamide to bisacrylamide), 8M urea, 1 x TBE buffer (see Section 2.4.1). To this solution 60 µl of TEMED (N,N,N',N'-tetramethylethylene diamine) and 500 µl of APS (10% (w/v) ammonium persulfate) was added in order to catalyze the polymerization of the acrylamide. Running buffer was 1xTBE. Prior to loading of sample, an equivolume of gel loading buffer (90% formamide, 1xTBE, 0.02% bromophenol blue and xylene cyanol (w/v)) was added to sample and the mixture heated at 90°C for 5 min. Electrophoresis was carried out at 20 V/cm until marker dyes have migrated the full length of the gel. Gels were subsequently dried (Model 583 Gel Dryer, BioRad) and the radioactively labelled DNA visualized by exposure to X-ray film (X-OMAT AR film, Eastman Kodak Co).

IV.2.4.3 RNA Formaldehyde-Agarose Gels

RNA formaldehyde-agarose gels were prepared according to standard procedures (Rosen and Villa-Komaroff, 1990). Briefly, 1.8 g of agarose was melted in 100 ml of distilled water and allowed to cool to 55°C. Fifteen millilitres of 10 x running buffer (1x: 0.2 M MOPS, 10 mM EDTA, 10 mM sodium acetate, pH 7.0) were mixed with 27 ml of deionized formaldehyde (37% w/v) and added to the cooled agarose. The gel was cast in a MAX Submarine Agarose Gel Unit Model HE99 (Hoeffer Scientific Instruments). The cast gel (14.5 cm x 20.5 cm, 150 ml) was allowed to solidify for 1 h at room temperature in a fumehood. Samples (4 µl) were prepared for gel loading by the addition of 4 µl formaldehyde, 2 µl of 10 x buffer, 2 µl EtBr (10 mg/ml), 12 µl formamide and heated at 65°C for 10 min. Following this heat step, 1 µl of a dye mixture (0.2% (w/v) xylene cyanol, 0.2% (w/v) bromophenol blue, 10 mM EDTA, 50% (v/v) glycerol) was added. The gel samples were then vortexed and centrifuged briefly before loading (15-20 µl) onto the gel. Electrophoresis was performed at 3V/cm in 1x running buffer until the dye migrated to the bottom of the gel. RNA bands could be visualized and documented as described in Section 2.4.1.

IV.2.5 Polymerase Chain Reaction (PCR) Methodology

IV.2.5.1 PCR of DNA

All PCR experiments involved a two step DNA denaturation and primer annealing/extension process (Erlich *et al.*, 1991). All reactions were performed on a Perkin Elmer Cetus DNA Thermal Cycler. Primers utilized are described in Table 9. Typical reaction mixtures consisted of 0.5-1 μg of genomic DNA (or 50-100 ng of purified PCR product, Section 2.5.3.2), 200 μM of each deoxynucleotide, 0.5 μM of each primer in 1x PCR buffer (15 mM Tris, 35 mM KCl, 1.5 mM $MgCl_2$, pH 8.79). Samples were heated at 95°C for 5 min and then cooled to 80°C at which time 2.5 units of Taq Polymerase were added. DNA amplification consisted of 30 cycles of denaturation (95°C, 1 min) followed by an annealing/extension step (58-68°C, 5 min) which was extended by 10 min in the final cycle. Products were analyzed on 1% agarose gels as previously described (Section 2.4.1).

IV.2.5.2 Reverse Transcriptase (RT) PCR of RNA

The RT-PCR of RNA was performed with a GeneAmp RNA PCR Kit obtained from Perkin Elmer Cetus (Cat #N808-0017). All reactions were performed on a Perkin Elmer Cetus DNA Thermal Cycler. Primers utilized are listed and described in Table 9. All RNA samples were initially digested with 10 units of RNase-free DNase I (Pharmacia) for 45 min at 37°C prior to use in PCR reactions. The initial step in RT-PCR involved the

Table 9: Primers

Designation	Sequence (5'→3')	Locus Specificity[1]	Position[2]	Strand[3]	Calculated[4] Melting Temperature(°C)
1	AAGCTTGGACACAAGACAG	gpt,gpt'	-197 to -178 (both)	+	56
2	CCAGAATACTTACTGGAAAC	gpt,gpt'	539-520 (gpt); 914-895 (gpt')	-	56
3	CGTAGATAAACAGGCTGGGACACTTCAC	gpt,gpt'	-28 to -1 (both)	+	84
4	CAGTGCCAGGCGTTGAAAAGATTAGCG	gpt,gpt'	480-454 (gpt); 855-829 (gpt')	-	84
5	AAACATCCTGAAACCTCGACGCTAGTC	gpt'	96-122	+	80
6	ATCGCCGCCCTGTAGGCTACTTGATTC	gpt'	767-741	-	84
7	CAATGGAAAGGCATTATTGCCGTAAGC	gpt	82-108	+	78
8	GTATCTTGCGGGATATCAACAACATAGT	gpt	398-371	-	78
9	GATCACGACAACCAGCGCGAGCTTAAA	gpt	190-216	+	82
10	ACGATGAAGCCTTCGCCATCGCCTTC	gpt	257-232	-	82
11	AACGATCAAGGCGAGTTACATGATCCC	gpt'	365-391	+	80
12	CCGAAGAGCTAACCGCTTTGTGCACAA	gpt'	421-395	-	82
P_1	AAGGAAGGCTTTGAGAAGATCAGCAAA	P1	NA[5]	+	76
P_2	CCCATTGCGCCCATTCCAGGGTC	P1	NA	-	76

[1] gpt, normal locus; gpt', gpt pseudogene; P1, chaperone protein (Picketts *et al.*, 1989).
[2] Numbering corresponds to that used in Figures #48 and #49 in a 5'→3' direction; Brackets denote locus specified, if necessary.
[3] +, coding or putative coding strand; -, noncoding or putative noncoding strand.
[4] Calculated as: Tm (°C) = 4 (#GC bp) + 2 (#AT bp).
[5] NA, not applicable.

generation of a complementary DNA (cDNA) strand from the RNA using reverse transcriptase. Reaction mixtures (20 μl) consisted of: 10 mM Tris-HCl, pH 8.3, 50 mM KCl, 5 mM $MgCl_2$, 1 mM of each dNTP, 1 U/μl RNase inhibitor, 2.5 U/μl reverse transcriptase, 0.75 μM in appropriate primer, 0.5-1 μg RNA. Reaction tubes were incubated at 42°C for 15 min, 99°C for 5 min and then kept at 5°C for 5 min. This 20 μl of solution was diluted to 100 μl and the solution adjusted with 10 x PCR buffer (100 mM Tris-HCl, 500 mM KCl, pH 8.3) and 25 mM $MgCl_2$ so that final conditions were: 10 mM Tris-HCl, pH 8.3,, 50 mM KCl, 2 mM $MgCl_2$. This 100 μl solution was also made 0.5 μM in appropriate PCR primers and polymerase added to a final concentration of 2.5 U/μl. A two step amplification process (95°C for 1 min, 62°C for 4 min, 35 cycles) was performed as described in the previous section (section 2.5.1). Products were analyzed on 1.2% agarose gels as previously described (Section 2.4.1). The kit included a positive RNA control sample (i.e. Interleukin 1α) which was incorporated in all experiments. Furthermore, all reaction mixtures were treated in duplicate with one sample undergoing a mock reverse transcriptase reaction (i.e. no reverse transcriptase added; negative control).

IV.2.5.3 DNA Sequencing Utilizing PCR Technology

IV.2.5.3.1 Primer Labelling

Primer labelling was performed using T4 polynucleotide kinase (PNK) according to standard procedures (Maniatis *et al.*, 1982). Briefly, 1 µl of [γ-^{32}P]-ATP (3000 Ci/mmol) was added to a reaction solution containing 70 mM Tris-HCl pH 7.6, 10 mM $MgCl_2$, 10 mM dithiothreitol, 10 pmoles of primer, 30 units PNK and sterile water to a final volume of 30 µl. The reaction was incubated for 30 min at 37°C followed by 5 min at 90°C.

IV.2.5.3.2 Isolation and Purification of PCR Generated DNA Product From Agarose Gels

For certain procedures (i.e. DNA sequencing), the PCR generated product was required for further analysis. The technique utilized, the "Freeze and Squeeze" method, has previously been documented (Thuring *et al.*, 1975). Briefly, this procedure involved wrapping a gel slice containing the required DNA band in Saran Wrap™ and freezing it at -20°C for approximately 60-90 min. As the slice was allowed to defrost, it was squeezed (between thumb and forefinger) and the drop of liquid exuded collected. This drop contained much of the DNA and was of suitable purity to be used directly. In some instances, the DNA was further diluted (with DDI) and precipitated as previously described throughout the preceding sections.

IV.2.5.3.3 DNA Sequencing

Sequencing using PCR methodology was based on procedures previously documented with slight modification (Mihovilovic and Lee, 1989; Vizard *et al.*, 1990). Four termination mixes were made consisting of all four dNTPs at 20 µM and one of the following in each separate mix: 60 µm ddGTP, 800 µm ddATP, 1200 µm ddTTP; 400 µm ddCTP. To 100 ng of DNA (PCR generated and purified fragment) 1 pmole of labelled primer, 7.5 µl of termination mix, 1.5 µl of 10 x sequencing buffer (150 mM Tris, 24 mM $MgCl_2$, pH 8.0), 0.1 unit of Taq polymerase and DDI was added to a final volume of 15 µl. Similar reactions were set up for all four termination mixes each containing a single ddNTP. All four sample reactions were overlayed with parafilm oil and cycled ten times (95°C, 1 min; 60°C, 1 min; 72°C, 4 min). Samples were treated as described in Section 2.4.2 prior to analysis on a DNA sequencing gel. Analysis of sequence data was performed using PC/Gene (Version 6.6). Additional sequence data was obtained from the EMBL database.

IV.2.6 Molecular Analysis of RNA and DNA

IV.2.6.1 Southern Hybridization Analysis of DNA

IV.2.6.1.1 Labelling of Hybridization Probe

Labelling of probe was performed utilizing an Oligo Labelling Kit obtained from Pharmacia LKB Biotechnology (Cat. #27-9250). HindIII digested plasmid (pSV2gpt, provided by Dr. K. Tindall) was heat denatured at 100°C for 15 min and then

transferred to a 37°C water bath. Fifty nanograms of DNA were added to 10 μl of a reagent mix (dATP, dGTP, dTTP, $p(dN)_6$) buffer), 2 μl of BSA (RNase/DNase-free), 50 μCi of [α-^{32}P]dCTP (3000 Ci/mmole), 2 μl of Klenow enzyme (Klenow fragment of DNA polymerase I) and DDI to a final volume of 50 μl. The reaction mixture was allowed to proceed overnight at room temperature and terminated with 20 μl of termination mix included in the kit. Probes were typically labelled to a specific activity of 0.5-1.0x10^9 dpm/μg of DNA.

IV.2.6.1.2 Hybridization Analysis

For Southern (DNA) hybridization analysis, routine techniques of transfer to membrane, prehybridization, hybridization and washing were performed. Transfer membranes utilized were Hybond-N membranes (Amersham Corp.). Electrophoresis of DNA was performed as previously described in this chapter (Section 2.4.1). Approximately 2.5-5 μg of HindIII cut DNA was loaded per gel lane. Prior to transfer of DNA to membrane, agarose gels were placed twice in 200 ml of denaturing solution (0.5 m NaOH, 1.5 M NaCl) for 30 min at room temperature. The gel was then rinsed in distilled water and placed in neutralization buffer (0.5 m Tris-HCl, 1.5 M NaCl, 0.001 M EDTA, pH 7.2) for 15 min at room temperature. This neutralization was repeated. DNA was transferred onto membrane utilizing a Posiblot™ Transfer Apparatus (Stratagene) according to the manufacturer's instructions.

Transferred DNA was fixed onto the membrane by UV crosslinking with a UV Stratalinker™ 1800 Apparatus (Stratagene). Membrane prehybridization was performed in a sealed bag at 42°C for 3 h with 0.25 ml/cm^2 of the following solution: 50% formamide, 5x Denhardt's reagent (0.1% each of Ficoll, polyvinylpyrolli- done and bovine serum albumin (w/v)), 0.1% SDS, 100 µg/ml denatured and sheared salmon sperm DNA, 5 x SSPE (50 mM $NaPO_4$, 5 mM EDTA 0.90 M NaCl, pH 7.7). Denatured probe (100°C for 5 min) was added to the prehybridization solution and incubated for 16 h at 42°C. The activity of the probe in solution did not exceed 5x10^6 cpm/ml of solution. Following hybridization, filters were washed twice in 2 x SSPE, 0.1% (w/v) SDS at room temperature for 10 min, once at 1 x SSPE, 0.1% (w/v) SDS at 65°C for 15 min, and once with 0.1 x SSPE, 0.1% (w/v) SDS at 65°C for 10 min. Membranes were wrapped in Saran Wrap™ and subsequently exposed to X-ray film (XAR5; Kodak) for 1-7 days at -80°C in the presence of intensifying screens (Kodak X-OMAT Fine Intensifying Screens).

IV.2.6.2 Northern Hybridization Analysis of RNA

IV.2.6.2.1 Biotin Labelling of Hybridization Probe

The labelling of probes for Northern analysis involved a modified PCR and utilized a biotinylated deoxynucleotide analogue (bio-11-dUTP). The PCR methodology is based on previously documented techniques (Lo *et al.*, 1990). All reaction mixtures were essentially identical to those

described in Section 2.5.1 with the following modification: initial reaction dTTP is present at 50 μm; bio-11-dUTP at 150 μm. Typical cycling conditions (30 cycles, 95°C/1 min, 68°C/5 min) were as previously described. Biotinylated PCR products were purified from reaction components following a standard precipitation in absolute ethanol.

IV.2.6.2.2 Hybridization Analysis

For Northern (RNA) hybridization analysis, routine techniques of transfer to membrane, prehybridization, hybridization and washing were performed. Transfer membranes utilized were Photogene™ Nylon Membranes (BRL-Life Technologies Inc.). Electrophoresis of RNA was performed as previously described in this chapter (Section 2.4.3). Approximately 10-15 μg of mRNA was added per gel lane. RNA gels were transferred to nylon membranes without any pretreatment. RNA was transferred utilizing a Posiblot™ Transfer Apparatus (Stratagene) according to the manufacturer's instructions. RNA was fixed onto the membrane by UV crosslinking utilizing a UV Stratalinker™ 1800 Apparatus (Stratagene). Membrane prehybridization was performed in a sealed bag at 42°C for 3 h with 0.25 ml/cm^2 of the following solution: 5 x SSPE (50 mM $NaPO_4$, 5 mM EDTA, 0.90 M NaCl, pH 7.7), 50% formamide, 5 x Denhardt's reagent (0.1% each of Ficoll, polyvinyl pyrollidone and bovine serum albumin (w/v)), 1.0% SDS (w/v), 100 μg/ml denatured and

sheared salmon sperm DNA. Following this prehybridization step, solution was removed and replaced with a hybridization solution (same as prehybridization solution except formamide is omitted and dextran sulfate added to 10% (w/v)) to a final volume of 0.1 ml/cm^2 of membrane. Denatured probe (100°C/5 min) was added to a final concentration of 50 ng/ml. Incubation with probe was at 42°C for 16 h. Membranes were subsequently washed twice with 2 ml/cm^2 5 x SSC, 0.5% (w/v) SDS at 65°C, for 5 min (1 x SSC: 15 mM sodium nitrate, 0.15 M NaCl, pH 7.0). A third wash was performed with 2 ml/cm^2 0.1xSSC, 1% (w/v) SDS at 50°C for 30 min. A final wash consisted of 2 ml/cm^2 2 x SSC for 5 min at room temperature.

Detection of the biotinylated probe was facilitated by the Photogene™ Nucleic Acid Detection System (BRL, Cat. #81928A). Hybridized membranes were initially washed for 1 min at room temperature with 1 ml/cm^2 TBS-Tween 20 (100 mM Tris, 150 mM NaCl, 0.05% (w/v) Tween 20, pH 7.5). Membranes were then incubated in 0.75 ml/cm^2 of blocking solution (3% (w/v) bovine serum albumin in TBS-Tween 20) for 1 hour at 65°C with constant agitation. Subsequent to the blocking step, membranes were incubated with streptavidin-alkaline phosphatase (SA-AP; 7 μl SA-AP per 100 cm^2 of membrane diluted 1:1000 in TBS-Tween 20) for 15 min at room temperature followed by a final wash in a 1 x surfactant wash solution (1 ml/cm^2; provided in kit) for 60 min at room temperature with gentle agitation. Membranes were then placed in a Photogene™

Development Folder with 0.01 ml/cm^2 of detection reagent pipetted on them. Folders were stored overnight in the dark before exposure to X-ray film (XAR5; Kodak) for 5-30 min at room temperature.

IV.3 RESULTS

IV.3.1 PCR Analysis of AS52 DNA

IV.3.1.1 Genomic DNA

Figure 45 is a diagrammatic representation of all the primers utilized in these studies and their relationship to the genetic loci examined. Sequences are provided in Table 9. Initial attempts at amplifying target sequences involved the optimization of anneal/extension temperatures for the PCR process (Figure 46 and 47). Following an amplification with primers #1 and #2, two product DNA bands are clearly observed (Figure 46, lanes 1-4). These bands are 1111 and 736 bp in size. Along with these major products, very faint DNA background bands can be observed in most amplification reactions. Increasing the temperature of the anneal/extension step of the PCR process resulted in a relatively constant production of products up to 66°C; higher temperatures (i.e. 68-72°C) did not support the production of PCR DNA fragments (Figure 46, lanes 1-7). The DNA sequence of the *gpt* gene has previously been documented (Richardson *et al.*, 1983; Pratt and Subramani, 1983). Within this sequence resides a single KpnI restriction site, which may be utilized to distinguish this

Figure 45: Diagram of bacterial inserts of the AS52 cell line. Panel A depicts the *gpt* locus, panel B the *gpt* pseudogene (*gpt´*) locus. Straight lines correspond to bacterial plasmid DNA, solid rectangles to *gpt´* regions, open rectangles to unique *gpt* regions. Numbers identify the primers used for PCR analysis (including sequencing). The figure is not drawn to scale. Primer sequences are provided in Table 9.

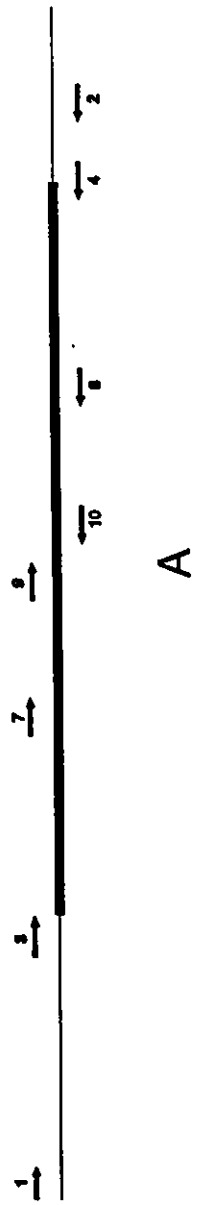

A

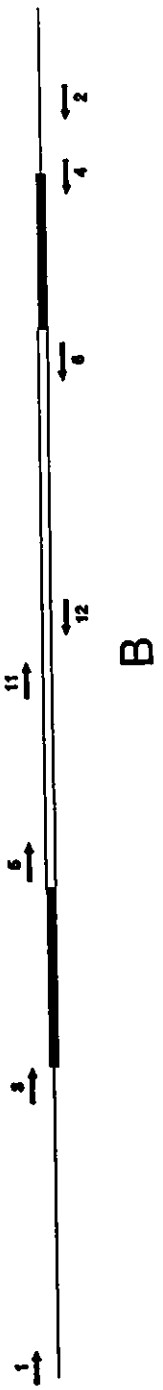

B

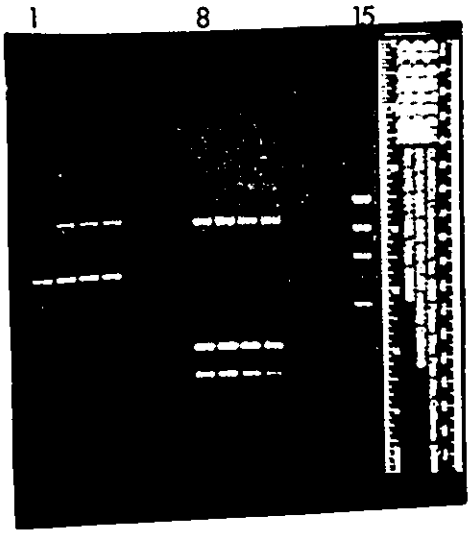

Figure 46: PCR analysis of AS52 DNA utilzing primers #1 and #2 (see Table 9). Genomic DNA was amplified as described in the text (Section 2.5.1). Annealing/extension temperatures were: lanes 1, 8, 60°C; lanes 2, 9, 62°C; lanes 3, 10, 64°C; lanes 4, 11, 66°C; lanes 5, 12, 68°C; lanes 6, 13, 70°C; lanes 7, 14, 72°C. Lanes 8 to 14 were digested with 20 units of Kpn I (Pharmacia). Lane 15 contains a DNA size standard (bp): from top - 1358, 1078, 872, 603, 310, 281/271, 234, 194, 118.

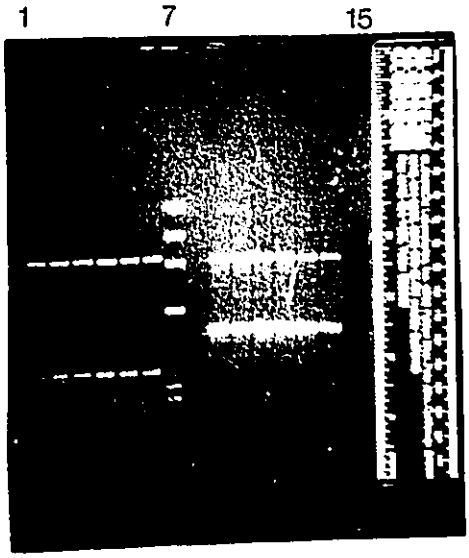

Figure 47: PCR analysis of AS52 DNA utilziing primers #3 and #4 (see Table 9). Genomic DNA was amplified as described in the text (Section 2.5.1). Annealing/extension temperatures were: lanes 1, 9, 62°C; lanes 2, 10, 64°C; lanes 3, 11, 66°C; lanes 4, 12, 68°C; lanes 5, 13, 70°C; lanes 6, 14, 72°C; lanes 8, 15, 74°C. Lanes 1 to 6 and 8 were digested with 20 units of Kpn I (Pharmacia). Lane 7 contains a DNA size standard (bp): from top 1358, 1078, 872, 603, 310, 281/271, 234, 194, 118.

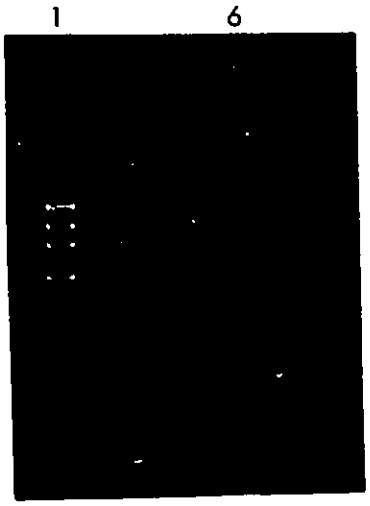

Figure 48: Nested primer PCR analysis of fragments generated by primers #1 and #2 (see Table 9). Genomic DNA was initially amplified as described in the text (Section 2.5.1) with primers #1 and #2 utilizing an annealing/extension temperature of 65°C. Individual DNA products were isolated and reamplified with primers #3 and #4 utilizing an annealing/extension temperature of 68°C. Lane 3, product from second amplification using large fragment product from primer #1/#2 amplification as DNA source; lane 4, second amplification using small fragment product from primer #1/#2 amplification as DNA source; lane 5, large fragment product from primer #1/#2 amplification; lane 6, small fragment product from primer #1/#2 amplification. Lane 1 contains a DNA size standard (bp): from top-1358, 1078, 872, 603, 310, 281/271, 234, 194, 118.

target product. Digestion of PCR products with this enzyme resulted in the digestion of the 736 bp fragment into smaller products of 429 and 317 bp as expected from the *gpt* DNA sequence; the larger fragment (i.e. 1111 bp) remained uncleaved (Figure 46, lanes 8-14). Utilizing a second primer pair (#3 and #4, Table 9, Figure 45) more proximal to the actual coding region of the *gpt* gene, resulted in a similar production of two DNA fragments following PCR amplification (Figure 47, lanes 9-14). In this case, fragment lengths were approximately 508 and 883 bp. Temperatures of up to 72°C for the anneal/extension step of the PCR process yield amplification products whereas a temperature of 74°C does not (Figure 47, compare lanes 9-14 with lane 15). A digestion with KpnI results in the cleavage of the 508 bp product into two fragments of 147 and 361 bp as expected from the published *gpt* sequence. The larger fragment of 885 bp remained uncleaved (Figure 47, lanes 1-6).

As depicted in Figure 45, primers #3 and #4 are theoretically contained in fragments delineated by primers #1 and #2 (a "nested" primer scenario). In order to verify that the two fragments produced following amplification by primers #3 and #4 were indeed shortened versions of those produced by primers #1 and #2, the experiment presented in Figure 48 was performed. Reamplification of the 1111 bp product (lane 5) with the "nested" primer pair (i.e. primers #3 and #4) resulted in the generation of the smaller 883 bp fragment

(lane 3). Similarly, reamplification of the 736 bp fragment (lane 6) with the "nested" primers resulted in the formation of the 508 bp product (lane 4).

IV.3.1.2 Sequencing of PCR Products

PCR products generated from amplification utilizing primers #3 and #4 were isolated and both DNA strands of each product were fully sequenced. No uncertainty in determining sequence information was encountered. The sequence of the smaller, 508 bp fragment is presented in Figure 49. As expected, this fragment codes for the *gpt* gene. The sequence deduced in this thesis is identical to that previously reported for the *gpt* gene in the plasmid pSV_2gpt (Richardson *et al.*, 1983; Pratt and Subramani, 1983). A protein of 152 amino acids (459 bases) is encoded by this gene.

Sequence analysis of the larger fragment (883 bp) is presented in Figure 50. A comparison of the *gpt* sequence presented in Figure 49 with that in Figure 50 highlights some interesting similarities. By comparison, a putative start codon (ATG) and stop codon (TAA) theoretically encode a protein of 277 amino acids (834 bases) assuming no internal stop codons. The initial 79 bases from this "ATG" start codon are identical to those of the *gpt* gene presented in Figure 49. In addition, the terminal 60 bases of this putative gene (to the TAA stop codon; position 774-834) are also identical to the terminal 60 coding bases of the *gpt* gene. Within these

-28 CGTAGATAAACAGGCTGGGACACTTCAC***ATG***AGCGAAAAATACATCGTCA 22
23 *CCTGGGACATGTTGCAGATCCATGCACGTAAACTCGCAAGCCGACTGATG* 72
73 *CCTTCTGAACAATGGAAAGGCATTATTGCCGTAAGCCGTGGCGGTCTGGT* 122
123 *ACCGGGTGCGTTACTGGCGCGTGAACTGGGTATTCGTCATGTCGATACCG* 172
173 *TTTGTATTTCCAGCTACGATCACGACAACCAGCGCGAGCTTAAAGTGCTG* 222
223 *AAACGCGCAGAAGGCGATGGCGAAGGCTTCATCGTTATTGATGACCTGGT* 272
273 *GGATACCGGTGGTACTGCGGTTGCGATTCGTGAAATGTATCCAAAAGCGC* 322
323 *ACTTTGTCACCATCTTCGCAAAACCGGCTGGTCGTCCGCTGGTTGATGAC* 372
373 *TATGTTGTTGATATCCCGCAAGATACCTGGATTGAACAGCCGTGGGATAT* 422
423 *GGGCGTCGTATTCGTCCCGCCAATCTCCGGTCGC**TAA***TCTTTTCAACGCC 472
473 TGGCACTG

Figure 49: Sequence of the *gpt* locus of the AS52 cell line. Translation start (ATG) and stop (TAA) codons are in bold type, with the intervening translated sequence in italics. By convention, the first base of the translation start codon (i.e. A of ATG) is designated position 1. The sequence is read 5' to 3', left to right.

-28 CGTAGATAAACAGGCTGGGACACTTCAC***ATG***AGCGAAAAATACATCGTCA 22

23 *CCTGGGACATGTTGCAGATCCATGCACGTAAACTCGCAAGCCGACTGATG* 72

73 *CCTTCTG*<u>*GTTCAAACCCCGCTTTAAACATCCTGAAACCTCGACGCTAGTC*</u> 122

123 <u>*CGCCGCTTTAATCACGGCGCACAACCGCCTGTGCAGTCGGCCCTTGATGG*</u> 172

173 <u>*TAAAACCATCCCTCACTGGTATCGCATGATTAACCGTCTGATGTGGATCT*</u> 222

223 <u>*GGCGCGGCATTGACCCACGCGAAATCCTCGACGTCCAGGCACGTATTGTG*</u> 272

273 <u>*ATGAGCGATGCCGAACGTACCGACGATGATTTATACGATACGGTGATTGG*</u> 322

323 <u>*CTACCGTGGCGGCAACTGGTGGCTTCATTCAGCTCCGGTTCCAACGATCA*</u> 372

373 <u>*AGGCGAGTTACATGATCCCATGTTGTGCACAAAGCGGTTAGCTCTTCGGT*</u> 422

423 <u>*CCTCCGATCGTTGTCAGAAGTAAGTTGGCCGCAGTGTTATCACTCATGGT*</u> 472

473 <u>*TATGGCAGCACTGCATAATTCTCTTACTGTCATGCCATCCGTAAGATGCT*</u> 522

523 <u>*TTTCTGTGACTGGTGAGTACTCAACAAGTCATTCTGAGAATAGTGTATGC*</u> 572

573 <u>*GGCGACCGAGTTGCTCTTGCCCGGCGTCAACACGGGATAATACCGCGCCT*</u> 622

623 <u>*GGTCTCTTCTCTTGAATTAGCACGTATAGCTAAAGCGTAGCGGCTTTTTT*</u> 672

673 <u>*GCTCGCAACTGACGGGAGTTACTCTGAAAATGTAGAAAAGGCTGCGTTTG*</u> 722

723 <u>*CCTTTTTCTGTTTCTATAGAATCAAGTAGCCTACAGGGCGGCGATTACCA*</u> 772

773 <u>*GG*</u>*TGGATTGAACAGCCGTGGGATATGGGCGTCGTATTCGTCCCGCCAATC* 822

823 *TCCGGTCGC****TAA***TCTTTTCAACGCCTGGCACTG

Figure 50: Sequence of the *gpt* pseudogene (*gpt'*) locus of the AS52 cell line. Theoretical translation start (ATG) and stop (TAA) codons are in bold type. The putative translated sequence is presented in italics. Sequence unique to the *gpt* pseudogene is underlined. By convention, the first base of the translation start codon (i.e. A of ATG) is designated position 1. All sequence is read 5' to 3', left to right.

Figure 51: Sequence comparison of the *gpt* pseudogene (*gpt'*) to that of β-lactamase, the ampicillin resistance gene of bacteria. Numbers correspond to base positions as denoted and described in Figure 50 (*gpt* pseudogene) or EMBL database (*E. coli* lac/β-lactamase).

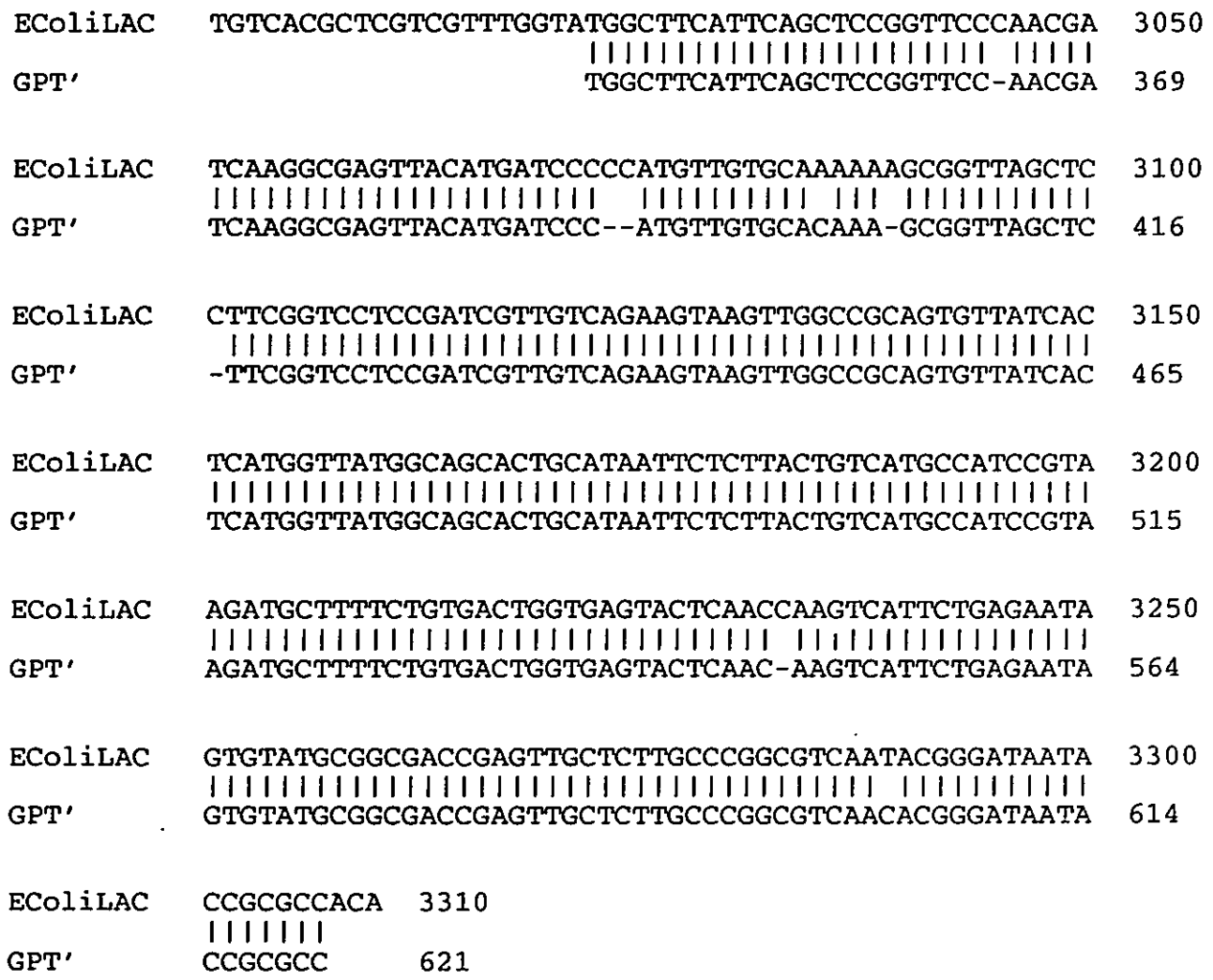
EColiLAC TGTCACGCTCGTCGTTTGGTATGGCTTCATTCAGCTCCGGTTCCCAACGA 3050
GPT' TGGCTTCATTCAGCTCCGGTTCC-AACGA 369
EColiLAC TCAAGGCGAGTTACATGATCCCCCATGTTGTGCAAAAAAGCGGTTAGCTC 3100
GPT' TCAAGGCGAGTTACATGATCCC--ATGTTGTGCACAAA-GCGGTTAGCTC 416
EColiLAC CTTCGGTCCTCCGATCGTTGTCAGAAGTAAGTTGGCCGCAGTGTTATCAC 3150
GPT' -TTCGGTCCTCCGATCGTTGTCAGAAGTAAGTTGGCCGCAGTGTTATCAC 465
EColiLAC TCATGGTTATGGCAGCACTGCATAATTCTCTTACTGTCATGCCATCCGTA 3200
GPT' TCATGGTTATGGCAGCACTGCATAATTCTCTTACTGTCATGCCATCCGTA 515
EColiLAC AGATGCTTTTCTGTGACTGGTGAGTACTCAACCAAGTCATTCTGAGAATA 3250
GPT' AGATGCTTTTCTGTGACTGGTGAGTACTCAAC-AAGTCATTCTGAGAATA 564
EColiLAC GTGTATGCGGCGACCGAGTTGCTCTTGCCCGGCGTCAATACGGGATAATA 3300
GPT' GTGTATGCGGCGACCGAGTTGCTCTTGCCCGGCGTCAACACGGGATAATA 614
EColiLAC CCGCGCCACA 3310
GPT' CCGCGCC 621

two blocks of sequence is a region of 695 bases unique to this putative gene. Analysis of the EMBL Sequence database provides a sequence match to a portion of this unique insert. As presented in Figure 51, a region of 279 bases (Figure #50, position 342 to 621) is identical to a region encoded by the B-lactamase gene (i.e. ampicillum resistance gene) of *E. coli*. Further sequence analysis of this putative gene (termed *gpt* pseudogene) utilizing PC/Gene (Version 6.6) for open translation reading frames suggests that no significance polypeptide (greater than 70 amino acids) is translated due to internal stop codons in all reading frames (data not shown).

IV.3.1.3 Analysis of RNA

Reverse transcriptase (RT)-PCR was used in the analysis of total and messenger RNA derived from cultured AS52 cells. When total RNA was examined, several conclusions are readily apparent (Figure 52, Panel A). The generation of cDNA utilizing primer #2 or #3 did not result in the formation of DNA able to support the PCR amplification of the *gpt* pseudogene (lanes 7 and 11). By contrast, cDNA formation utilizing primer #2 (but not primer #3) resulted in DNA formation which may be used to PCR amplify a 316 bp segment of the *gpt* gene (lanes 5 and 9). All negative control reactions in which cDNA cannot be generated due to the absence of reverse transcriptase in reaction mixtures consistently did not produce final amplification products (lanes 4, 6, 8, 10

and 12). A positive RNA control for interleukin 1α provided in the RT-PCR kit resulted in the amplification of an expected DNA band of 308 bp (lane 3).

Analysis of mRNA isolated from the AS52 line presents similar findings (Figure 52, Panel B). Primers #2 and #3 do not support the formation of cDNA capable of generating a *gpt* pseudogene derived product following PCR amplification (lanes 7 and 9). By contrast, cDNA generated utilizing primer #2 does support the amplification of a *gpt* specific fragment of 316 bp following PCR amplification (lane 5). Negative controls (i.e. lacking reverse transcriptase; lanes 4, 6, 8 and 10) did not yield PCR amplification products as expected; the positive control resulted in the generation of an amplified product of 308 bp again as expected (lane 3).

Figure 52, Panel C presents amplifications of control DNA (pSV2*gpt* plasmid or AS52 genomic DNA) utilizing the primer pairs previously used in RT-PCR (primers #5/#6 and #7/#8). Amplification of a 316 bp segment of the *gpt* gene is successful with both DNA sources (lanes 3 and 4). With primers #5/#6, amplification of the desired 671 bp fragment of the *gpt* pseudogene was successful only with AS52 genomic DNA as source material (lanes 5 and 6).

Northern hybridization analysis of total RNA is presented in Figure 54. Two probes utilized in this analysis contained biotin-dUTP incorporated in their sequence via PCR amplification (Figure 53). The first probe is the *gpt* gene

Figure 52: Analysis of RNA (total and messenger) from the AS52 cell line using reverse transcriptase (RT)-PCR. Panel A, total RNA from AS52 cells. Lanes 3, 4: interleukin RNA standard provided by kit (see text for details). Lanes 5-8, primer #3 used for initial cDNA generation; lanes 9-12, primer #2 used for initial cDNA generation. Samples corresponding to lanes 4,6,8,10 and 12 did not contain reverse transcriptase in the initial reaction mixtures for cDNA generation (negative controls). Lanes 5,6,9 and 10 utilized primers #7 and #8 for PCR amplification of putative cDNA; lanes 7,8,11,12 utilized primers #5 and #6 for PCR amplification of putative cDNA. Lane 1 contains DNA size (bp) standard: from top - 1358, 1078, 872, 603, 310, 281/271, 234, 194, 118, 72. Panel B, mRNA isolated from AS52 cells. Lanes 3 and 4, interleukin RNA standard; lanes 5, 7 and 8, primer #2 was used for initial cDNA generation; lanes 6, 9 and 10, primer #3 was used for initial cDNA generation. Samples corresponding to lanes 4, 6, 8 and 10 did not contain reverse transcriptase in the initial reaction mixtures for cDNA generation (negative controls). Lanes 5 and 6 utilized primers #7 and #8 for PCR amplification of putative cDNA; lanes 7-10 utilized primers #5 and #6 for PCR amplification of putative cDNA. Lane 1 contains a DNA size standard similar to the one in lane 1, panel A; panel C, control PCR of pSV2gpt plasmid and AS52 genomic DNA. Source DNA utilized for PCR amplification was pSV2gpt plasmid in lanes 3 and 5, and genomic AS52 DNA in lanes 4 and 6. Primers #7 and #8 were utilized in PCR amplification of samples in lanes 3 and 4; primers #5 and #6 were utilized in PCR amplification of samples in lanes 5 and 6. DNA size standard (lane 1) is similar to the one presented in lane 1, panel A.

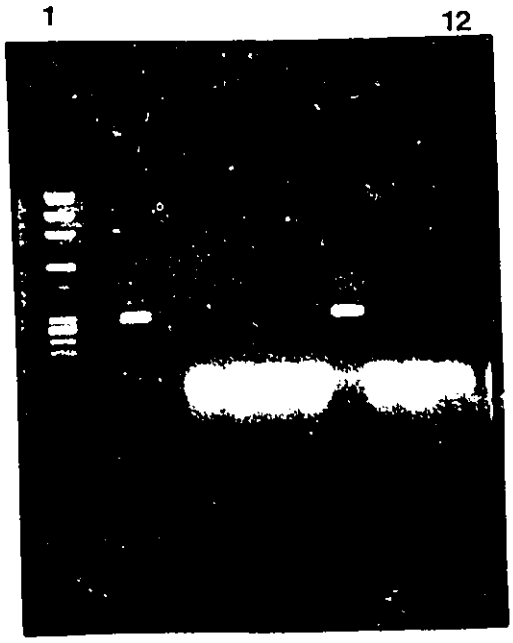

A

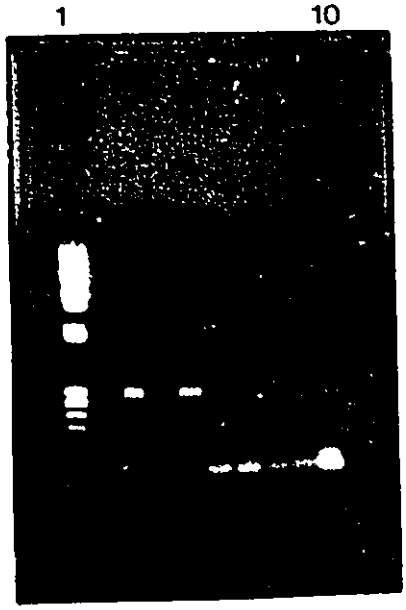

B

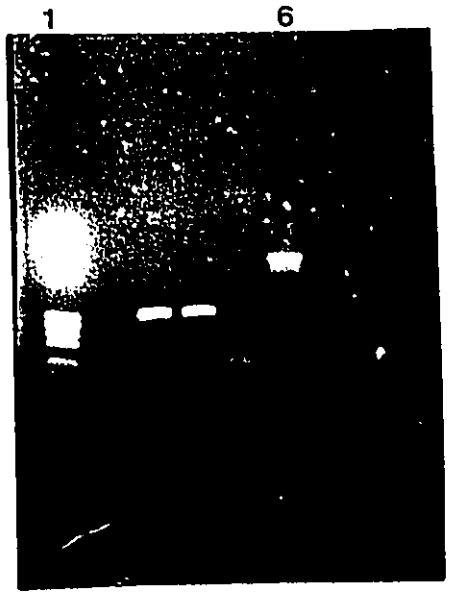

C

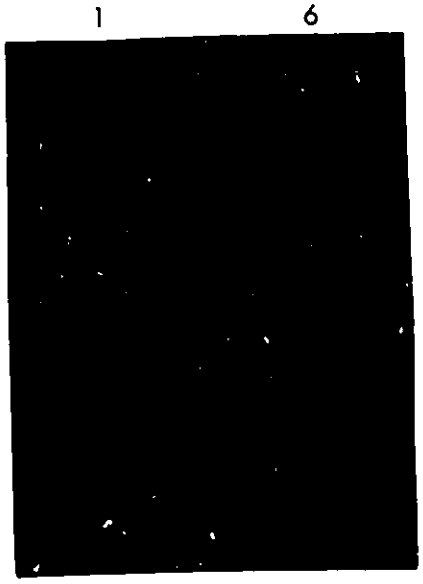

Figure 53: Generation of biotinylated PCR products to be used as probes for Northern hybridization analysis. PCR methodology was as described in the text (Section 2.6.2.1). Lane 1 contains a DNA size standard (bp): from top - 1358, 1078, 872, 603, 310, 281/271, 234, 194, 118, 72. Lane 3, isolated *gpt* gene PCR product from amplication using primers #3 and #4; lane 4, reamplification of product in lane 3 using bio-11-dUTP as deoxynucleotide substrate. Lane 5, isolated *gpt* pseudogene insert PCR product from amplification using primers #5 and #6; lane 6, reamplification of product in lane 5 using bio-11-dUTP as deoxynucleotide substrate.

Figure 54: Autoradiograms of mRNA analyzed via Northern hybridization analysis. Lanes contain from 10 to 15 µg of RNA. Panel A depicts the hybridization with a probe recognizing the complete *gpt* gene; panel B depicts the hybridization with a probe specific for the *gpt* pseudogene. Arrows denote sizes (bases) deduced from the migration of contaminating 18S and 28S ribosomal RNA: from top, 4800 and 1900 bases.

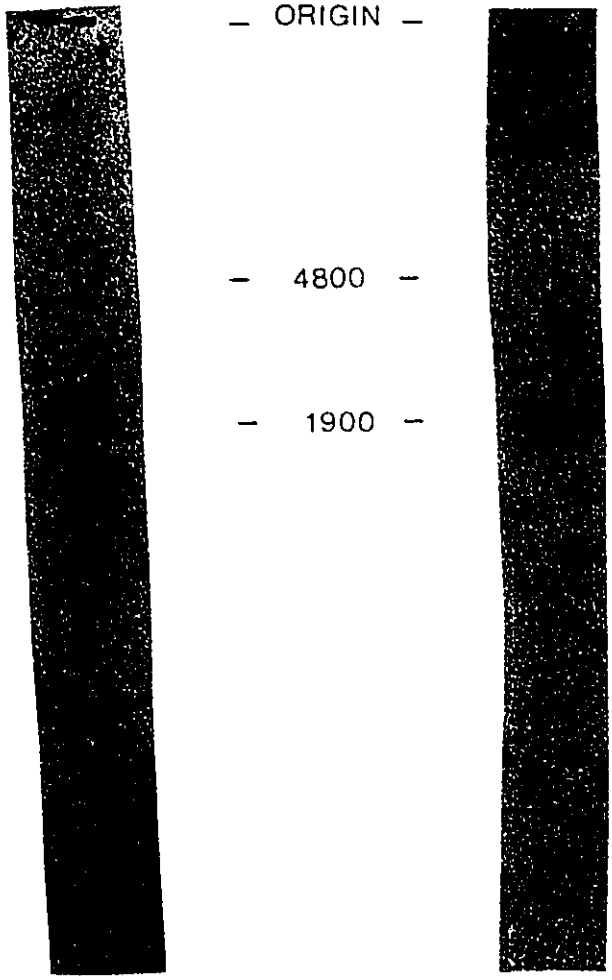
ORIGIN
4800
1900
A
B

amplified utilizing primers #3 and #4 (508 bp), the second (671 bp) is generated utilizing *gpt* pseudogene-specific primers #5 and #6 (Figure 53, lanes 3-6). Biotinylation of probes resulted in an apparent increase in DNA size as monitored by a decreased mobility in agarose gels (Figure 53, compare lanes 3 with 4, 5 with 6). The probing of Northern blots with the *gpt* probe resulted in the identification of a clear signal corresponding to a size of approximately 2200 bases (Figure 54, Panel A), whereas the *gpt* pseudogene specific probe did not recognize any RNA fragment (Panel B).

IV.3.2 AS52 Mutant Analysis

PCR analysis of AS52 mutants was performed utilizing three primer sets. The first two (primer sets #1/#2 and #3/#4) permit the amplification of both the *gpt* and *gpt* pseudogene (Figures 45-47), the third (primer set P_1/P_2) amplifies the chaperone (P1) protein of CHO cells (Picketts *et al.*, 1989). Figure 55 is a representation of mutants analyzed with primers #1 and #2; Figure 56 with primers #3 and #4; and Figure 57 with primers P_1 and P_2. An examination of the gels presented in Figures 55 and 56 provide evidence for three classes of mutants. The first involves the amplification and identification of both *gpt* and *gpt* pseudogene bands. The second involves the amplification of only the *gpt* pseudogene. A third class involves the absence of any amplification of either *gpt* or *gpt* pseudogene. Amplification of the chaperone

Figure 55: PCR analysis of AS52 mutant DNA using primers #1 and #2. Mutant DNA was amplified as described in the text (Section 2.5.1) utilizing an annealing/extension temperature of 65°C. Products are analyzed on a 1.2% agarose gel. DNA size standards (bp) are presented in lane 1 of each panel: from top - 1358, 1078, 872, 603, 310, 281/271. Panel A, lanes 2-11, correspond to Ni_3S_2 mutants, lanes 12-20, $Ni(OH)_2$ mutants; panel B, lanes 2-20 $NiSO_4$ mutants; panel C, lanes 2-10 EMS mutants, lanes 11-20, spontaneous mutants. Other than spontaneous mutants, the electrophoretic patterns depicted in Figures 55, 56, 57 correspond to the same mutant DNA samples.

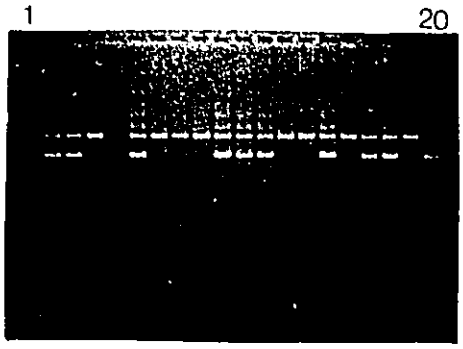

A

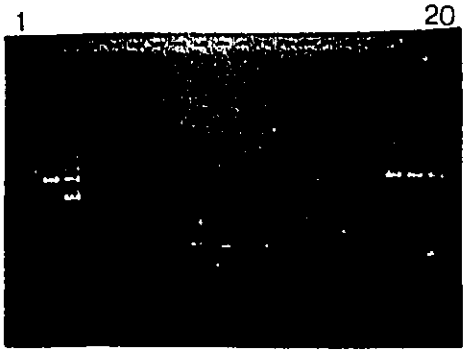

B

C

Figure 56: PCR analysis of AS52 mutant DNA using primers #3 and #4. Mutant DNA was amplified as described in the text (Section 2.5.1) utilizing an annealing/extension temperature of 68°C. Products are analyzed on a 1.2% agarose gel. DNA size standards (bp) are presented in lane 1 of each panel: from top - 1358, 1078, 872, 603, 310, 281/271. Panel A, lanes 2-11 correspond to Ni_3S_2 mutants, lanes 12-20 $Ni(OH)_2$ mutants; panel B, lanes 2-20 $NiSO_4$ mutants; panel C, lanes 2-10 EMS mutants, lanes 11-20 spontaneous mutants. Other than spontaneous mutants, the electrophoretic patterns depicted in Figures 55, 56, 57 correspond to the same mutant DNA samples.

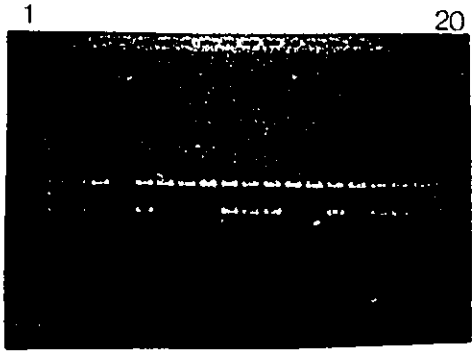

A

B

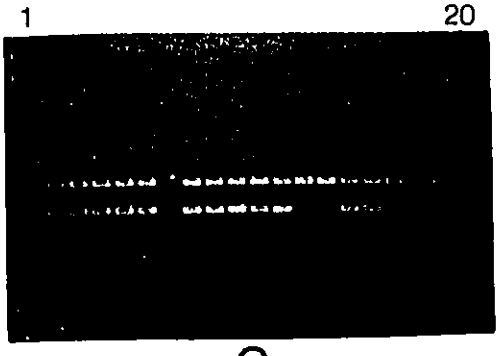

C

Figure 57: PCR analysis of AS52 mutant DNA using primers P_1 and P_2. Mutant DNA was amplified as described in the text (Section 2.5.1) utilizing an annealing/extension temperature of 68°C. Products are analyzed on a 1.2% agarose gel. DNA size standards (bp) are presented in lane 1 of each panel: from top - 1358, 1078, 872, 603, 310, 281/271. Panel A, lanes 2-11 correspond to Ni_3S_2 mutants, lanes 12-20 $Ni(OH)_2$ mutants; panel B, lanes 2-20 $NiSO_4$ mutants; panel C, lanes 2-10 EMS mutants, lanes 11-20 spontaneous mutants. Other than spontaneous mutants, the electrophoretic patterns depicted in Figures 55, 56, 57 correspond to the same mutant DNA samples.

A

B

C

TABLE 10: Summary of Mutants Analyzed

Mutagen	Concentration	Mutants/ $1x10^6$ cells	Total # Mutants Analyzed	Characterization of Observed Mutants[a]			
				Point Mutations[b] (% of total)	Deletions *gpt* band alone[c]	Deletions both bands[d]	Deletions (% of total)[e]
Control	-----	17 ± 7	24	17 (71)	5	2	(29)
EMS	200 µg/ml	68 ± 23	26	23 (88)	1	2	(12)
Ni_3S_2	7.3 µg/Ni/ml[f]	49 ± 10	28	20 (71)	7	1	(29)
$Ni(OH)_2$	1.7 µg Ni/ml[f]	128 ± 37	22	9 (41)	13	0	(59)
$NiSO_4$	58.7 µg Ni/ml[f]	67 ± 18	28	3 (11)	11	14	(89)

[a] Maximum of 3 mutant colonies cloned from any one plate of generated mutants. Both primer sets (#1/#2 and #3/#4) generated identical results. PCR amplification with primers #1/#2 was performed twice.
[b] Both PCR bands observed.
[c] Smaller PCR band not observed.
[d] Both PCR bands not observed.
[e] Both categories of deletions included.
[f] Corresponds to levels of Ni in solution.

Figure 58: Representative autoradiogram of Southern hybridization analysis of AS52 mutants. Lanes 1-11, DNA from Ni_3S_2 induced AS52 mutants; lanes 12-18, DNA from $Ni(OH)_2$ induced AS52 mutants. Numbers alongside autoradiogram correspond to DNA size standards (Kb).

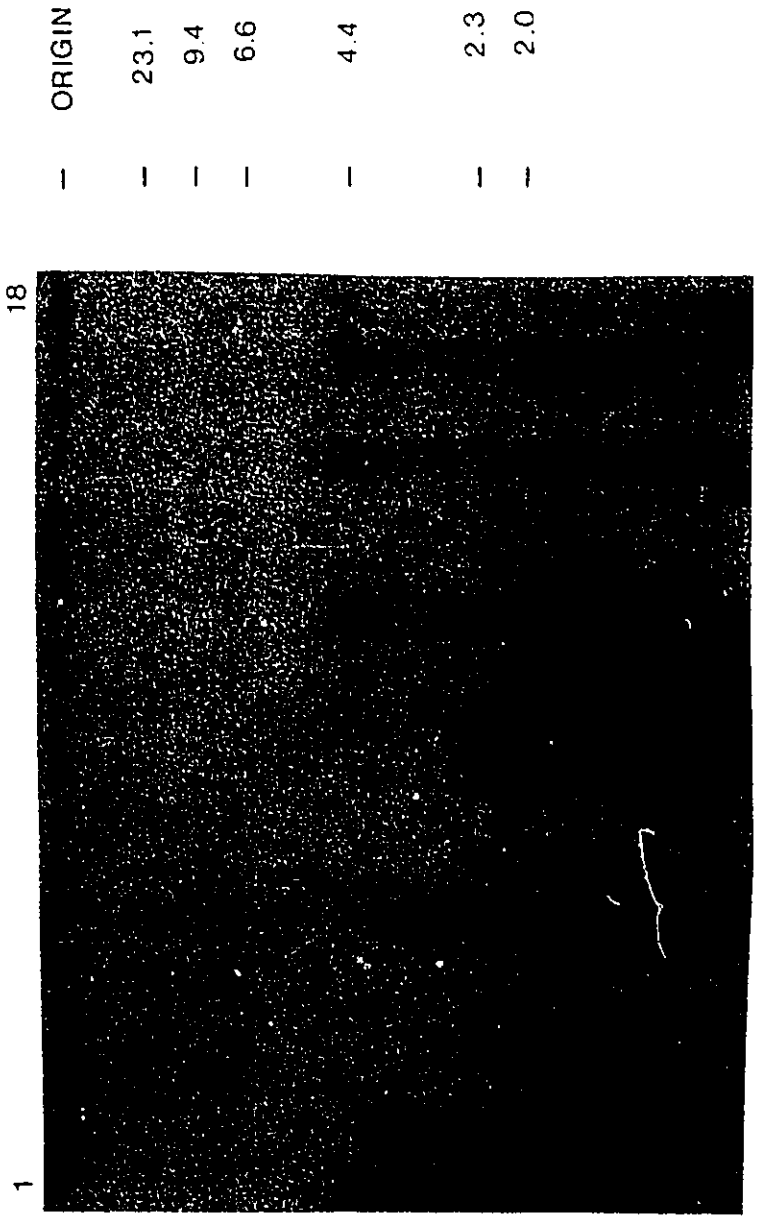
ORIGIN
23.1
9.4
6.6
4.4
2.3
2.0
18
1

(P1) protein with primers P_1 and P_2 demonstrates a consistent generation of a 1314 bp fragment as expected (Picketts *et al.*, 1989). A summary of all the mutants thus analyzed by PCR is presented in Table 10. A preliminary assessment of mutant DNA was performed utilizing Southern blot analysis and is presented in Figure 58. Results from Southern analysis corroborate those tabulated in Table 10.

IV.4 DISCUSSION

Although the AS52 cell line has become popular as a screen for mutational activity, a full characterization of the target locus has not been documented. The work presented in this chapter is the most detailed molecular analysis of the target locus to date. As a research tool, PCR has greatly facilitated the examination of genetic loci. Although theoretically simplistic, this technology is prone to much experimental variability. Perhaps the single most critical aspect of this technology is the optimization of experimental conditions, primarily the selection of primers (Saiki *et al.*, 1988; Innis and Gelfand, 1990; Erlich *et al.*, 1991). Due to the 2-step amplification adopted in this work, critical importance is given to the selection of an appropriate temperature for the anneal/extension step of the PCR process (Erlich *et al.*, 1991). As presented in Figures 46 and 47, the temperature optima of primer pairs #1/#2 and #3/#4 were evaluated. Differences in the optimal temperatures (i.e. 66°C

for #1/#2; 72°C for #3/#4) clearly reflect the difference in primer lengths (Table 9). A key aspect of the PCR process is the assumed specificity of the amplification process (Saiki *et al.*, 1988). It is clear from the work presented in Figure 46 that background DNA bands are present. It is quite likely that these result from the over amplification of target loci (i.e. too many cycles of amplification; Innis and Gelfand, 1990).

The consistent amplification of two DNA fragments utilizing primers thought to be specific for the *gpt* locus is a novel, but not altogether surprising finding. Tindall and coworkers (developers of the AS52 cell line) have reported a sporadic occurrence of a second DNA fragment amplified following a presumable *gpt*-specific PCR process (Tindall and Stankowsky, Jr., 1989; Tindall and Whitaker, 1991). Utilizing the KpnI digestion of the *gpt* fragment as a diagnostic tool, these researchers concluded that this second DNA fragment did not contain *gpt* sequences. By contrast, the sequencing data reported in this thesis presents data to the contrary (discussed below). It must be noted that the primers of Tindall and coworkers differed in both size and position from those used by ourselves.

The most efficient means of sequencing amplified DNA is to sequence the DNA product directly (Engelke *et al.*, 1988; Innis *et al.*, 1988; Mihovilovic and Lee, 1989; Vizard *et al.*, 1990). Although PCR intrinsically produces single-base

substitution errors at a rate of approximately 1 for each 10,000 nucleotides polymerized (Tindall and Kunkel, 1988; Eckert and Kunkel, 1990), this approach generates a consensus sequence thus eliminating the possibility that observed mutations are resulting from errors in the original amplification. In the present work, original primers for amplification and sequencing (i.e. primers #3 and #4) were derived from the published *gpt* sequence (Richardson *et al.*, 1983; Pratt and Subramani, 1983). Additional sequencing primers (i.e. #9 and #10 for *gpt*; #11 and #12 for *gpt* pseudogene; Figure 45, Table 9) were deduced from the sequence generated utilizing the initial primers. By contrast to the conclusions of Tindall and coworkers (see above), the sequence data for the "large" amplification product contains significant homology to the *gpt* locus (Figure 50). Although sequence information was only obtained from primers #3 and #4 at the 5′ and 3′ end of the pseudogene respectively, the ability of primers #1 and #2 to consistently coamplify this pseudogene suggests that the sequence both upstream and downstream from these sequencing primers (i.e. #3 and #4) is also shared (Figures 45-47). Sequence information presented in Figures 49 and 50 clearly illustrate that there is sequence identity between the *gpt* gene and *gpt* pseudogene at both the 5′ and 3′ ends (and probably further upstream and downstream). A fascinating aspect of the pseudogene is the replacement of *gpt* coding sequence with a block of DNA containing a region

from the β-lactamase (i.e. ampicillin resistance) gene of the parent plasmid (Mulligan and Berg, 1981) used to transform the CHO parental line (Figure 51). The most logical explanation for the presence of both an incorporated *gpt* and *gpt* pseudogene is the possibility of two distinct sites of plasmid integration into the CHO genome. The first would contain a functional *gpt* gene (with eukaryotic transcriptional control elements incorporated into plasmid, see Mulligan and Berg, 1980). The second would involve a plasmid which has undergone some recombination prior to or during genomic integration. Whether the eukaryotic transcriptional control elements are also integrated at both sites cannot be determined solely from the PCR and sequencing data. This hypothesis is supported by a recent report documenting the integration of the *gpt* gene (or *gpt* pseudogene?) to both chromosomes 3 and 6 of AS52 cells utilizing *in situ* fluorescence hybridization (Michaelis *et al.*, 1992). Since these researchers utilized a 2.0 kb fragment from the original transforming plasmid (i.e. pSV_2gpt) they would be unable to distinguish, nor differentiate, between the *gpt* and *gpt* pseudogene due to shared homology.

In order to assess the transcriptional status of the *gpt* pseudogene, reverse transcriptase (RT)-PCR was performed on total and messenger RNA isolated from AS52 cells (Figure 52). It is clear that the *gpt* gene is readily transcribed. By contrast, the *gpt* pseudogene does not support the transcription of RNA using either strand of DNA as template.

As previously mentioned in Section 3.1.2, no significant polypeptide should theoretically be coded by the *gpt* pseudogene due to internal stop codons in all reading frames. Northern hybridization analysis of messenger RNA identifies a single RNA species utilizing a *gpt* probe (Figure 54). This fragment of approximately 2100-2200 bases is theoretically expected (Mulligan and Berg, 1980; Mulligan and Berg, 1981). If a pseudogene transcript was also produced, the *gpt* probe utilized should have identified a second, longer transcript due to sequence homology. Analysis of the RNA with an *gpt* pseudogene insert specific probe does not recognize any transcript (Figure 45). Taken as a whole, the data suggest that the *gpt* pseudogene is not transcribed. Whether this is due to inactivation or loss of transcriptional control elements or due to the chromosomal location of integration cannot be ascertained from this data. The former hypothesis can be readily tested using PCR and primers amplifying regions of the integrated plasmid encompassing transcriptional control elements.

Analyses of mutated genetic loci have been greatly facilitated by the adoption of PCR technology (Xu *et al.*, 1989; Tindall and Stankowski, Jr., 1989; Hsie *et al.*, 1990; Tindall and Whitaker, 1991). Analysis of mutants generated three distinct PCR profiles (Figures 55 and 56). These are: 1) both *gpt* and pseudogene amplified; 2) *gpt* band deleted; 3) both gene and pseudogene deleted. Sequence analysis of a

number of EMS mutants has confirmed that point mutations are responsible for the first family of mutants (Franco Rossetto, unpublished data). In addition, small deletions of several base pairs or frameshift mutations would also be scored as point mutations (see Tindall and Stankowsky, 1989). Deletions of all or part of the *gpt* locus are assigned to the second family, while large multi-locus deletions/damage are assigned to the third category of mutants. It is interesting to note that the analysis and designation of mutant classification was performed with two distinct primer sets arguing against small mutations (i.e. point, frameshift, deletions) occurring solely in primer binding regions. Amplification of the distinct and unrelated chaperone/P1 protein (Picketts *et al.*, 1989) validates the overall integrity of isolated source DNA (Figure 57). Although Southern hybridization analyses performed on mutants was of a preliminary nature (Figure 58), they are nevertheless a corroboration of the results obtained from PCR analysis. It is interesting to note that Hind III cleaved AS52 DNA when probed with the parent *gpt* plasmid (pSV_2gpt) elicited two signals of approximately 4.5 and 1.9 kb (Tindall and Stankowsky, Jr., 1989). By contrast, a band at 4.5 kb is routinely observed (for normal and "point" mutated DNA) in our autoradiograms but the 1.9 kb band is absent. Perhaps the significant background smearing obscures this signal in all cases where gross or multi-locus deletions do not occur.

An overall analysis of mutant data (Table 10) reveals some interesting conclusions. Nickel compounds may be considered to be weak mutagens in the AS52 cell line. Furthermore, when compared to spontaneous or EMS induced mutants, those generated by nickel compound exposure exhibit an increase in deletions relative to point mutations; the extent of which is compound specific: $NiSO_4$ > $Ni(OH)_2$ > Ni_3S_2. Amongst these nickel mutagens no distinction is observed in their propensity to induce deletions of solely the *gpt* locus (second empirical category of mutant). By contrast, $NiSO_4$ clearly induces total deletions of both loci to a much greater extent than all other mutagens (third empirical category of mutant). As expected, EMS produces mainly point mutations; spontaneous control mutants display a more varied distribution of mutant profiles by comparison to the EMS-induced mutants.

The genotoxicological potential of nickel compounds is well established (reviewed in Chapter 1). As previously delineated, the nickel uptake pathway probably plays an important role in the delivery, compartmentalization and bioactivity of nickel intracellularly (Costa and Mollenhauer, 1980; Evans *et al.*, 1982; Cost, 1983; Sen and Costa, 1986; Sunderman, Jr., 1989; Costa, 1991). Insoluble crystalline particulates (ie. Ni_3S_2) tend to be phagocytized; lysomal interaction with the intracellular particulates results in dissolution to the Ni(II) ion with subsequent nuclear accumulation. By contrast, the uptake and intracellular

bioaccumulation and compartmentalization of soluble nickel compounds (i.e. $NiSO_4$) is not as well understood. Furthermore, these latter compounds are not as genotoxic in comparison to the more crystalline, insoluble compounds (reviewed in Chapter 1).

The mutation profile data of nickel compounds in the AS52 cell line suggest that the processes involved are compound specific. A corollary to this hypothesis is that the mutation profile is dependent on the mode of uptake and bioaccumulation. While the relatively insoluble compound (Ni_3S_2) primarily generated point mutations (or frameshift/small deletions), large deletions predominated following exposure to soluble $NiSO_4$; $Ni(OH)_2$, a compound of limited solubility, demonstrated an intermediate mutagenic profile. Christie and coworkers have recently examined the mutagenic potential of nickel compounds in the G12 cell line (Lee *et al.*, 1993). Like the AS52 line, this cell line is an $HPRT^-$ derivative of a CHO line (V79) in which the *gpt* gene has been integrated (Klein and Rossman, 1990). Although soluble $NiSO_4$ did not induce an appreciable increase in mutants from spontaneous background, crystalline NiS was a potent mutagen. One hundred percent of the NiS mutants (48 of 48) were designated as arising from point mutations in contrast to 86% of spontaneous mutants (38 of 48) utilizing PCR response as a diagnostic indicator (Lee *et al.*, 1993). While the data presented in Table 10 suggests that spontaneous mutants and

crystalline Ni_3S_2 produced similar rates of point mutations (i.e. 71%), it is still consistent with crystalline compounds preferentially inducing "point" mutations. Furthermore, since NiS was more potent a mutagen in the G12 line (40x background rate) than Ni_3S_2 in the AS52 line (4x background rate), the characterization of NiS mutants in G12 may be deemed indicative of the response of crystalline nickel compounds (see below). A puzzling feature of the G12 response is the apparent lack of $NiSO_4$ induced mutagenesis. One can postulate that the site of *gpt* integration in G12 cells does not allow for the recovery of cells with large deletions in contrast to the situation experienced in the AS52 cell line.

Before considering mechanistic possibilities, it is beneficial to summarize recent results concerning the intracellular compartmentalization of Ni(II) ions (Fletcher *et al.*, 1993). At LC_{50} values (i.e. nickel concentration at 50% cell toxicity) for 8 particulate and 3 water soluble nickel compounds, a 75-fold range in exposure levels was observed. This translated into a 10-fold range in nuclear nickel levels and a 7-fold range in cytosolic levels. Water-soluble compounds demonstrated the lowest nuclear nickel levels coupled to a preferential accumulation in the cytosol (i.e. nuclear to cytoplasmic nickel ratio of approximately 1:20). By contrast, most other compounds demonstrated significantly higher nuclear levels (i.e. nuclear to cytoplasmic nickel ratios of 1:1.5 to 1:5).

Within this context, the mutational data suggest the interesting hypothesis that mechanistically, at least two distinct mutation pathways are involved. The first, involving crystalline compounds (i.e. Ni_3S_2) likely results in the delivery of "dissolved" Ni(II) ions directly to the nucleus where they act as a primary DNA mutagen. The second pathway appears to involve the accumulation of Ni(II) ions in the cytoplasm derived from the uptake of soluble compounds (i.e. $NiSO_4$) through a distinct pathway(s). This intracellular pool of Ni(II) may subsequently interact with cellular constituents (i.e. lipids, proteins) generating secondary DNA mutagens such as active oxygen radicals. Recent advances in the elucidation of Ni(II)/Ni(III) redox chemistry within biological systems (Tom, 1987; Nieboer *et al.*, 1989; Kasprzak, 1991) corroborate such an interpretation. The generation of radical species has been shown to occur from the direct interaction of Ni(II) with DNA/chromosomes and H_2O_2 *in vitro* (Nieboer *et al.*, 1989; Kawanishi *et al.*, 1989; Nackerdien *et al.*, 1991; Datta *et al.*, 1993). Nucleoside oxidation products generated *in vivo* after the administration of nickel compounds have also been isolated (Kasprzak *et al.*, 1992b; Misra *et al.*, 1993). The possibility of Ni(II) interacting with nuclear components and H_2O_2 *in vivo* is strengthened by the demonstration that H_2O_2 is readily generated in nuclei (Peskin and Shlyahova, 1986). Peroxidation of lipids by Ni(II) is also well documented and results in the generation of reactive byproducts that are

mutagenic or damaging to DNA (Sunderman, Jr. *et al.*, 1985; Sunderman, Jr., 1986; Misra *et al.*, 1990; Rodriguez *et al.*, 1991; Misra *et al.*, 1991; Shi *et al.*, 1992).

The first half of this chapter dealt with the identification and characterization of the *gpt* gene and *gpt* pseudogene within the AS52 cell line. Molecular analysis revealed that the pseudogene shares homology with the 5′ and 3′ ends of the *gpt* gene but also contains an unique insert, part of which seems to derive from the β-lactamase gene of the parent transformation plasmid (pSV_2*gpt*). The pseudogene is not transcribed as deduced from reverse transcriptase (RT)-PCR and Northern hybridization analysis. The latter components of this chapter dealt with the mutagenicity of nickel compounds at the *gpt* locus within this cell line. The data presented clearly demonstrate that these compounds are mutagenic. Furthermore, it seems that the mutagenic profiles observed are compound specific which may derive from the mode of uptake and intracellular compartmentalization of Ni(II) ions. The apparent ability of the AS52 cell line to recover from mutations involving large deletions makes this line particularly suited to the investigation of the mechanisms of nickel mutagenesis and/or carcinogenesis.

V. CONCLUDING REMARKS

It is obvious from the work described in this thesis that the effect of the Ni(II) ion on DNA or chromosomes is diverse and complex. In addition, detrimental effects of this ion on chromosomes and DNA such as breaks, DNA and DNA-protein crosslinks, sister chromatid exchanges, chromosomal aberrations, X-chromosome fragmentation and a variety of other effects on replication and transcription pathways (reviewed in Section I.2.3.4) clearly demonstrate the broad toxicological potential at the chromosome or gene levels of the Ni(II) ion. Within this scope of damage, the question that must be addressed revolves around the relevance ascribed to the observations reported in this thesis concerning the mutagenic and carcinogenic potential of nickel compounds. As previously noted in the "Introduction" to this thesis (Chapter 1), the most common rationale furnished to explain the genotoxicity of nickel compounds is the "Nickel-Ion Hypothesis". In its simplest form, this hypothesis predicts that the Ni(II) ion in the appropriate cell compartment is the ultimate genotoxic agent, regardless of the parent nickel compound and the physicochemical and biological factors/mechanisms involved in the uptake, dissolution and compartmentalization of said compound. The intent of this thesis was to present an in-

depth analysis of the interaction of Ni(II) ion with DNA; starting from the simplest systems possible (i.e. polydeoxynucleotides), progressing to more complex systems (i.e. nuclear chromosomes), and culminating in a cellular system (i.e. AS52 cell line).

An overall examination of the data presented in Chapter II suggests that the interaction of Ni(II) ion with DNA and polydeoxynucleotides is to some extent base (or basepair) specific. A clear affinity for G/C bases is evident when structural or conformation transitions are utilized as a measure of interaction. This latter conclusion is supported by the dissociation constants generated for these polydeoxynucleotides/DNAs (presented in Table 4). The apparent nonrandom distribution of DNA sequences throughout the eukaryotic genome supports the relevance of these studies with polydeoxynucleotides. For example, the presence of polypurine•polypyrimidine tracts in promoters of many genes has induced a lot of speculation concerning the role of such sequences in transcriptional control (reviewed in Palecek, 1991; Yagil, 1991). Furthermore, the involvement of sequences capable of adopting non-canonical β-structures such as left-handed Z DNA (i.e. tracts of polyd(AT)•polyd(AT), polyd(GC)•polyd(GC), polyd(GT)•polyd(AC)) has generated tremendous activity to elucidate the role of these sequences in areas as diverse as chromosome structure, genetic recombination, and transcriptional control (reviewed in Rich

et al., 1984; Jovin *et al.*, 1987; Holliday, 1989; Juranic *et al.*, 1990; Hill, 1991).

At the chromosomal level, the structure and packing arrangements of the DNA in the nucleus involves a variety of counter ions (both mono and divalent) and proteins (reviewed in Igo-Kemenes *et al.*, 1982; Tsanev, 1983; Eissenberg *et al.*, 1985; Gross and Garrard, 1988; van Holde, 1989). Moreover, the structure and packaging of DNA is intimately involved in cellular processes such as DNA replication/repair and/or transcriptional control. It is obvious that alterations in these processes by exogenous agents (e.g., the Ni(II) ion) could theoretically lead to detrimental consequences in normal cellular functioning. The comparable values obtained for Ni(II)-ion binding constants to both naked DNA and nuclear chromosomes suggest that some common structural elements are involved in both binding scenarios.

The work presented in Chapter IV is the most detailed molecular analysis of the target loci in the AS52 cell line. This work has made a major contribution to the development and characterization of the AS52 cell line and its validation as an appropriate screen for mutagens. Furthermore, its suitability as a screen for nickel mutagenesis has provided a useful tool in delineating mechanisms of nickel genotoxicity and mutagenesis. The susceptibility of AS52 cells to mutagenesis by different species or types of nickel compounds (i.e. crystalline vs. water soluble) and the ease in which

molecular analysis can be performed should vastly accelerate our understanding of the "Nickel-Ion Hypothesis" (see Rossetto *et al.*, 1993; Fletcher *et al.*, 1993). The compound-specific mutation profile of deletions and point mutations observed in the AS52 cell line illustrates that carcinogenic compounds like those of nickel provide interesting options for studying the molecular biology of cancer. A fundamental and related question that must be addressed concerns the barriers to tumour inception and growth and how known carcinogens might be involved in this process. A variety of pathways have been postulated in which agents may effect cellular functions without damaging DNA (i.e. non-mutagenic) - the so called epigenetic mechanisms. These include an interaction or interference with signal transducing pathways (Weinstein, 1991), regulation of transcription and thus gene expression (Rahmsdorf and Herrlich, 1990; Klein *et al.*, 1990), or an involvement with active oxygen biochemistry and its possible role in gene regulation (Nieboer *et al.*, 1989; Parfett, 1992; Parfett *et al.*, 1993). Within the multistep genetic model of cancer, genetic effects may well be manifested by the turning on or off of specific genes (i.e., oncogenes or suppressor genes; Cooper, 1990) whether mutated or not. The illustrated ability of the Ni(II) ion to induce conformational changes in DNA and its demonstrated capability of generating oxygen-derived radicals clearly point to its potential involvement in such epigenetic pathways.

One cannot infer from an observed Ni(II)-ion induced effect *in vitro*, that a similar event occurs within the cellular context. DNA in nuclei are extremely concentrated (i.e. 20-40 mg/ml) and exist in conditions more akin to gel states rather than dilute aqueous solutions (Kellenberger, 1988). Nevertheless, the similarity in binding parameters observed for isolated DNA and chromosomes in intact nuclei suggest that similar factors are operative in these two divergent states. The elucidation of the basic elements of binding, especially the observation of a sequence preference, has filled a gap in knowledge. Further, the demonstration of the high affinity of chromosomes in nuclei for Ni(II) ion and its condensational effects on structure provide novel insights. The increase in mutation rate at the *gpt* and *gpt* pseudogene loci following nickel compound exposure was low but significant (Rossetto *et al.*, 1993; Fletcher *et al.*, 1993), although the results would not be sufficient to deem these compounds strongly mutagenic by traditional criteria. Characterization by PCR analysis indicated that the spontaneous and nickel-induced mutants exhibited different and compound-specific mutational spectra (thus confirming nickel compound involvement). The work reported in this thesis illustrates some of the methodological problems involved in testing "weak" mutagens and is demonstrative of alternative approaches suitable for the characterization of weakly mutagenic or nongenotoxic compounds.

IV. BIBLIOGRAPHY

Aaron CS, Stankowski LF Jr (1989). Comparison of the AS52/XPRT and the CHO/HPRT assays: evaluation of 6 drug candidates. *Mut Res* 223, 121-8.

Aaronson RP, Woo E (1981). Organization in the cell nucleus: divalent cations modulate the distribution of condensed and diffuse chromatin. *J Cell Biol* 90, 181-6.

Adam S, Bourtayre P, Liquier J, Taillandier E (1986). Interaction of transition metal ions with Z form poly d(A-C)·poly d(G-T) and poly d(A-T) studied by I.R. spectroscopy. *Nucl Acids Res* 14, 3501-13.

Adam S, Liquier J, Taboury JA, Taillandier E (1986). Right- and Left-handed helixes of poly[d(A-T)]·poly[d(A-T)] investigated by infrared spectroscopy. *Biochemistry* 25, 3220-5.

Alexeev DG, Lipanov AA, Skuratovskii IY (1987). Poly(dA)-poly(dT) is a B-type double helix with a distinctively narrow minor groove. *Nature* 325, 821-3.

Al-Rabaee RH, Sigee DC (1984). Scintillation and autoradiographic studies on ^{63}nickel uptake in Pseudomonas tabaci. *J Cell Sci* 69, 87-105.

Amacher DE, Paillet SC (1980). Induction of trifluorothymidine resistant mutants by metal ions in L5178Y/TK$^{+/-}$ cells. *Mut Res* 78, 279-88.

Andersen O (1985). Evaluation of the spindle-inhibiting effect of Ni^{++} by quantitation of chromosomal supercontraction. *Res Commun Chem Pathol Pharmacol* 50, 379-86.

Andersen I, Svenes KB (1989). Determination of nickel in lung specimens of thirty-nine autopsied nickel workers. *Int Arch Occup Environ Health* 61, 289-95.

Arlauskas A, Baker RSU, Bonin AM, Tandon RK, Crisp PT, Ellis J (1985). Mutagenicity of metal ions in bacteria. *Environ Res* 36, 379-88.

Arndt-Jovin DJ, Jovin TM (1989). Fluorescence labelling and microscopy of DNA. *Methods in Cell Biol* 30, 417-48.

Arnott S, Selsing E (1974). Structures for the polynucleotide complexes poly(dA)-poly(dT) and poly(dT)-poly(dA)-poly(dT). *J Mol Biol* 88, 509-21.

Arrouijal FZ, Hildebrand HF, Vophi H, Marzin D (1990). Genotoxic activity of nickel subsulphide alpha-Ni_3S_2. *Mutagenesis* 5, 583-9.

Arrouijal FZ, Marzin D, Hildebrand HF, Pestel J, Haguenoer JM (1992). Differences in genotoxic activity of alpha-Ni_3S_2 on human lymphocytes from nickel-hypersensitized and nickel-unsensitized donors. *Mutagenesis* 7, 183-7.

Ausio J, Borochov N, Seger D, Eisenberg H (1984). Interaction of chromatin with NaCl and $MgCl_2$. *J Mol Biol* 177, 373-98.

Aymami J, Coll M, Frederick CA, Wang AHJ, Rich A (1989). The propeller DNA conformation of poly(dA)-poly(dT). *Nucl Acids Res* 17, 3229-45.

Baase WA, Johnson WC Jr (1979). Circular dichroism and DNA secondary nature. *Nucl Acids Res* 6, 797-814.

Behe M, Felsenfeld G (1981). Effects of methylation on a synthetic polynucleotide: the B-Z transition in poly(dG-m^5dC)-poly(dG-m^5dC). *PNAS* 78, 1619-23.

Behe MJ, Felsenfeld G, Szu SC, Charney E (1985). Temperature-dependent conformational transitions in poly(dG-dC) and poly(dG-m^5dC). *Biopolymers* 24, 289-300.

Berman HM, Young PR (1981). The intercalation of intercalating drugs with nucleic acids. *Ann Rev Biophys Bioeng* 10, 87-114.

Bernues J, Beltran R, Casasnovas JM, Azorin F (1990). DNA-sequence and metal-ion specificity of the formation of *H-DNA. *Nucl Acids Res* 18, 4067-73.

Biedermann KA, Landolph JR (1987). Induction of anchorage independence in human diploid foreskin fibroblasts by carcinogenic metal salts. *Cancer Res* 47, 3815-23.

Biggart NW, Costa M (1986). Assessment of the uptake and mutagenicity of nickel chloride in Salmonella tester strains. *Mut Res* 175, 209-15.

Bokma JT, Johnson WC Jr, Blok J (1987). CD of the Li-salt of DNA in ethanol/water mixtures: evidence for the B- to C-form transition in solution. *Biopolymers* 26, 893-909.

Borochov N, Ausio J, Eisenberg H (1984). Interaction and conformational changes of chromatin with divalent ions. *Nucl Acids Res* 12, 3089-97.

Bourtayre P, Adam S, Liquier J, Taboury JA, Taillandier E (1984). Left-handed structures of alternating purine-pyrimidine polynucleotides induced by Ni^{2+} ions: An I.R. spectroscopy study. In: *Progress In Nickel Toxicology* (SS Brown, FW Sunderman Jr eds). Blackwell Scientific Publishers, Oxford, 113-6.

Bourtayre P, Liquier J, Pizzorni L, Taillandier E (1987). Z form of poly d(A-T)·poly d(A-T) in solution studied by CD and UV spectroscopies. *J Biomolec Struc Dyn* 5, 97-104.

Boysen M, Solberg LA, Andersen I, Hogetveit AC, Torjussen W (1982). Nasal histology and nickel concentration in plasma and urine after improvements in the work environment at a nickel refinery in Norway. *Scand J Work Environ Health* 8, 283-9.

Butler PJG (1984). The folding of chromatin. *CRC Crit Rev Biochem* 15, 57-91.

Campos JL, Subirana JA (1991). The influences of Mg^{++} and Zn^{++} on polypurine-polypyrimidine multistranded helices. *J Biomol Struc Dyn* 8, 793-800.

Castleman H, Erlanger BF (1982). Electron microscopy of "Z" DNA. *Cold Spring Harbour Symp Quant Biol* 47 Pt 1, 133-42.

Casto BC, Meyers J, DiPaolo JA (1979). Enhancement of viral transformation for evaluation of the carcinogenic or mutagenic potential of inorganic metal salts. *Cancer Res* 39, 193-8.

Chaires JB, Norcum MT (1988). Structure and stability of Z* DNA. *J Biomol Struc Dyn* 5, 1187-1207.

Chang J, Watson WP, Randerath E, Randerath K (1993). Bulky DNA-adduct formation induced by Ni(II) in vitro and in vivo as assayed by ^{32}P-postlabelling. *Mut Res* 291, 147-59.

Chaschin VP, Arutnina GP, Norseth T (1993). Congenital defects, abortion and other health effects in nickel refinery workers. *Sci Total Environ*, in press.

Cheng YK, Pettitt BM (1992). Stabilities of double- and triple-strand helical nucleic acids. *Prog Biophys Molec Biol* 58, 225-57.

Chiocca SM, Sterner DA, Biggart NW, Murphy EC Jr (1991). Nickel mutagenesis: Alteration of the MuSVts110 thermosensitive splicing phenotype by a nickel-induced duplication of the 3' splice site. *Mol Carcinog* 4, 61-71.

Ciccarelli RB, Wetterhahn KE (1982). Nickel distribution and DNA lesions induced in rat tissues by the carcinogen nickel carbonate. *Cancer Res* 42, 3544-9.

Ciccarelli RB, Wetterhahn KE (1982). Nickel-bound chromatin, nucleic acids, and nuclear proteins from kidney and liver of rats treated with nickel carbonate *in vivo*. *Cancer Res* 44, 3892-7.

Ciccarelli RB, Wetterhahn KE (1985). In vitro interaction of 63-nickel(II) with chromatin and DNA from rat kidney and liver nuclei. *Chem-Biol Interact* 52, 347-60.

Clarkson TW, Nordberg GF, Sager PR (1985). Reproductive and developmental toxicity of metals. *Scand J Work Environ Health* 11, 145-54.

Conway K, Sen P, Costa M (1986). Antagonistic effect of magnesium chloride on the nickel chloride-induced inhibition of DNA replication in Chinese hamster ovary cells. *J Biochem Toxicol* 1, 11-26.

Cooper GM (1990). In: *Oncogenes*. Jones & Bartlett Publishers, Boston.

Costa M (1983). Sequential events in the induction of transformation in cell culture by specific nickel compounds. *Biol Trace Element Res* 5, 285-85.

Costa M (1991). Molecular mechanisms of nickel carcinogenesis. *Ann Rev Pharmacol Toxicol* 31, 321-37.

Costa M, Cantoni O, de Mars M, Swartzendruber DE (1982). Toxic metals produce an S-phase-specific cell cycle block. *Res Commun Chem Pathol Pharmacol* 38, 405-19.

Costa M, Mollenhauer HH (1980). Carcinogenic activity of particulate nickel compounds is proportional to their cellular uptake. *Science* 209, 515-7.

Crapper McLachlan DR, Lewis PN, Lukiw WJ, Sima A, Bergeron C, De Boni U (1984). Chromatin structure in dementia. *Ann Neurol* 15, 329-34.

Crapper McLachlan DR, Lukiw WJ, Kruck TPA (1989). New evidence for an active role of aluminum in Alzheimer's disease. *Can J Neurol Sci* 16, 490-7.

Datta AK, Misra M, North SL, Kasprzak KS (1992). Enhancement by nickel(II) and L-histidine of 2'-deoxyguanosine oxidation with hydrogen peroxide. *Carcinogenesis* 13, 283-7.

Datta AK, Shi X, Kasprzak KS (1993). Effect of carnosine homocarnosine and anserine on hydroxylation of the guanine moiety in 2'-deoxyguanosine, DNA and nucleohistone with hydrogen peroxide in the presence of nickel(II). *Carcinogenesis* 14, 417-22.

de Mars M, Sterner DA, Chiocca SM, Biggart NW, Murphy EC Jr (1990). Regulation of RNA splicing in *gag*-deficient mutants of Moloney murine sarcoma virus MuSVts110. *J Virol* 64, 1421-8.

Dickerson RE (1983). The DNA helix and how it is read. Sci Am 249(6), 94-111.

Dickerson RE, Drew HR, Conner BN, Kopka ML, Pjura PE (1982). Helix geometry and hydration in A-DNA, B-DNA, and Z-DNA. *Cold Spring Harbor Symp Quant Biol* 47 Pt 1, 13-24.

Dickerson RE, Drew HR, Conner BN, Wing RM, Fratini AV, Kopka ML (1982). The anatomy of A-, B-, and Z-DNA. *Science* 216, 475-84.

DiPaolo JA, Casto BC (1979). Quantitative studies of *in vitro* morphological transformation of Syrian hamster cells by inorganic metal salts. *Cancer Res* 39, 1008-13.

Dixon DK, Burkholder GD (1985a). Fractionation of micrococcal nuclease-digested chromatin solubilized at physiologic ionic strength. *Exp Cell Res* 156, 563-9.

Dixon DK, Burkholder GD (1985b). The effects of sodium and magnesium-ion interactions on chromatin structure and solubility. *Eur J Cell Biol* 36, 315-22.

Doll R (author-in-chief) (1990). Report of the inter-national committee on nickel carcinogenesis in man. *Scand J Work Environ Health* 16, 1-82.

Drew H, Takano T, Tanaka S, Itakura K, Dickerson RE (1980). High-salt d(CpGpCpG), a left-handed Z' DNA double helix. *Nature* 286, 567-73.

Dubins JS, LaVelle JM (1986). Nickel(II) genotoxicity: potentiation of mutagenesis of simple alkylating agents. *Mut Res* 162, 187-99.

Earnshaw WC, Laemmli UK (1983). Architecture of metaphase chromosomes and chromosome scaffolds. *J Cell Biol* 96, 84-93.

Eckert KA, Kunkel TA (1990). High fidelity DNA synthesis by the *Thermus aquaticus* DNA polymerase. *Nucl Acids Res* 18, 3739-44.

Eichhorn GL, Shin YA, Butzow JJ (1982). Transitions induced by metal complexes among several forms of DNA. *Cold Spring Harbour Symp Quant Biol* 47 Pt 1, 125-7.

Eissenberg JC, Cartwright IL, Thomas GH, Elgin SCR (1985). Selected topics in chromatin structure. *Ann Rev Genet* 19, 485-536.

Engelke DR, Hoener PA, Collins FS (1988). Direct sequencing of enzymatically amplified human genomic DNA. *PNAS* 85, 544-8.

EPA (1986). In: *Health Assessment Document for Nickel and Nickel Compounds: EPA/600/8-83/012FF.* United States Environmental Protection Agency, Research Triangle Park, NC.

Erlich HA, Gelfand D, Sninsky JJ (1991). Recent advances in the polymerase chain reaction. *Science* 252, 1643-51.

Evans RM, Davies PJA, Costa M (1982). Video time-lapse microscopy of phagocytosis and intracellular fate of crystalline nickel sulfide particles in cultured mammalian cells. *Cancer Res* 42, 2729-35.

Fazakerley GV (1984). Zinc Z-DNA. *Nucl Acids Res* 12, 3643-8.

Fearon ER, Vogelstein B (1990). A genetic model for colorectal tumorigenesis. *Cell* 61, 759-67.

Fletcher GG (1990). Evaluation of the "Nickel-ion hypothesis" of cytotoxic responses in AS52 CHO cells. MSc. Thesis, McMaster University, Hamilton, Canada.

Fletcher GG, Rossetto FE, Turnbull JD, Nieboer E (1993). Toxicity, uptake, and mutagenicity of particulate and soluble nickel compounds. *Environ Hlth Perspect*, in press.

Gennart JPH, Baleux C, Verellen-Dumoulin CH, Buchet JP, De Meyer R, Lauwerys R (1993). Increased sister chromatid exchanges and tumor markers in workers exposed to elemental chromium-, cobalt- and nickel-containing dusts. *Mutat Res* 299, 55-61.

Girod JC, Johnson WC Jr, Huntington SK, Maestre MF (1973). Conformation of deoxyribonucleic acid in alcohol solutions. *Biochemistry* 12, 5092-6.

Gosule LC, Schellman JA (1978). DNA condensation with polyamines - spectroscopic studies. *J Mol Biol* 121, 311-26.

Grandjean P, Nielsen GD, Andersen O (1989). Human nickel exposure and chemobiokinetics. In: *Nickel and the Skin: Immunology and Toxicology* (HI Maibach, T Menne eds). CRC Press, FL, 9-34.

Green MHL, Muriel WJ, Bridges BA (1976). Use of a simplified fluctuation test to detect low levels of mutagens. *Mut Res* 38, 33-42.

Greulich KO, Wachtel E, Ausio J, Seger D, Eisenberg H (1987). Transition of chromatin from the "10 nm" lower order structure, to the "30 nm" higher order structure as followed by small angle X-ray scattering. *J Mol Biol* 193, 709-21.

Gross DS, Garrard WT (1988). Nuclease hypersensitive sites in chromatin. *Ann Rev Biochem* 57, 159-97.

Grunberger D, Santella RM, Hanau LH, Erlanger BF (1985). Stabilization of Z-DNA conformation by chemical carcinogens. *Carcinogenesis* 10, 465-80.

Hacques MF, Marion C (1986). DNA polymorphism: Spectroscopic and electro-optic characterization of Z-DNA and other types of left-handed helical structures induced by Ni^{2+}. *Biopolymers* 25, 2281-93.

Hanlon S, Chan A, Berman S (1978). Specific cation effects on conformational transitions of DNA in aqueous solutions, *Biochim Biophys Acta* 519, 526-36.

Hansen K, Stern RM (1983). *In vitro* toxicity and transformation potency of nickel compounds. *Environ Hlth Perspect* 51, 223-6.

Harris CC (1991). Chemical and physical carcinogenesis: advances and perspectives for the 1990s. *Cancer Res (Suppl) 51*, 5023-44s.

Hartwig A, Beyersmann D (1987). Enhancement of UV and chromate mutagenesis by nickel ions in the Chinese hamster HGPRT assay. *Toxicol Environ Chem* 14, 33-42.

Haugen AA, Ryberg D, Hansteen IL, Dalen H (1989). Transformation of human kidney epithelial cells to tumorigenicity by nickel(II) and v-Ha-ras oncogene. *Biol Trace Element Res* 21, 451-8.

Heck JD, Costa M (1982). In vitro assessment of the toxicity of metal compounds - mutagenesis. *Biol Trace Element Res* 4, 319-30.

Higgins ITT (1979). In: *Airborne Particles* (ITT Higgins editor-in-chief). University Park Press, Baltimore, 107-45.

Higinbotham KG, Rice JM, Diwan BA, Kasprzak KS, Reed CD, Perantoni AO (1992). GGT to GTT transversions in codon 12 of the K-*ras* oncogene in rat renal sarcomas induced with nickel subsulfide or nickel subsulfide/iron are consistent with oxidative damage to DNA. *Cancer Res* 52, 4747-51.

Higuchi R (1989). Rapid, efficient DNA extraction for PCR from cells or blood. *Amplifications* 2, 1-3.

Hill R (1991). Z-DNA: a prodrome for the 1990s. *J Cell Sci* 99, 675-80.

Holliday R (1989). Untwisting B-Z DNA. *Trends in Genetics* 5, 12-3.

Horvath P, Horz W (1981). The compaction of mouse heterochromatin as studied by nuclease digestion. *FEBS Lett* 134, 25-8.

Hsie AW (1987). The use of the *hgprt* versus *gpt* locus for quantitative mammalian cell mutagenesis. In: *Banbury Report 28: Mammalian Cell Mutagenesis* (MM Moore, DM Demarini, FJ de Serres, KR Tindall eds). Cold Spring Harbor Laboratory, Boston, 37-46.

Hsie AW, Recio L, Katz DS, Lee CQ, Wagner M, Schenley RL (1986). Evidence for reactive oxygen species inducing mutations in mammalian cells. *PNAS* 83, 9616-20.

Hsie AW, Xu Z, Yu Y, Sognier MA, Hrelia P (1990). Molecular analysis of reactive oxygen-species-induced mammalian gene mutation. *Teratogen Carcinogen Mutagen* 10, 115-24.

Htun H, Dahlberg JE (1989). Topology and formation of triple-stranded H-DNA. *Science* 243, 1571-6.

IARC (1990). In: *Evaluation of Carcinogenic Risks to Humans, Vol. 49, Chromium, Nickel and Welding.* International Agency for Research on Cancer, Lyon, pp.257, 447.

Igo-Kemenes T, Horz W, Zachau HG (1982). Chromatin. *Ann Rev Biochem* 51, 89-121.

Innis MA, Gelfand DH (1990). Optimization of PCR. In: *PCR Protocols: A Guide to Methods and Applications* (MA Innis, DH Gelfand, JJ Sninsky, TJ White eds). Academic Press Inc., San Diego, 3-12.

Innis MA, Myambo KB, Gelfand DH, Brow MAD (1988). DNA sequencing with *Thermus aquaticus* DNA polymerase and direct sequencing of polymerase chain reaction-amplified DNA. *PNAS* 85, 9436-40.

Ivanov VI, Minchenkova LE, Schyolkina AK, Poletayev AI (1973). Different conformations of double-stranded nucleic acid in solution as revealed by circular dichroism. *Biopolymers* 12, 89-110.

Jensen RH, Davidson N (1966). Spectrophotometric, potentiometric, and density gradient ultracentrifugation studies of the binding of silver ion by DNA. *Biopolymers* 4, 17-32.

Jia X, Marzilli LG (1991). Zinc ion-DNA polymer interactions. *Biopolymers* 31, 23-44.

Jia X, Zon G, Marzilli LG (1991). Multinuclear NMR investigation of Zn^{2+} binding to a dodecamer oligodeoxyribonucleotide: insights from ^{13}C NMR spectroscopy. *Inorg Chem* 30, 228-39.

Jordan CF, Lerman LS, Venable JH Jr (1972). Structure and circular dichroism of DNA in concentrated polymer solutions. *Nature New Biology* 236, 67-70.

Jovin TM, Soumpasis DM, McIntosh LP (1987). The transition between B-DNA and Z-DNA. *Ann Rev Phys Chem* 38, 521-60.

Juranic Z, Kidric M, Tomin R, Juranic I, Spuzic I, Petrovic J (1991). The importance of the specific Z-DNA structure and polyamines in carcinogenesis: fact or fiction. *Medical Hyp* 35, 353-7.

Kaldor J, Peto J, Easton D, Doll R, Herman C, Morgan L (1986). Models for respiratory cancer in nickel refinery workers. *JNCI* 77, 841-8.

Kanematsu N, Hara M, Kada T (1980). Rec assay and mutagenicity studies on metal compounds. *Mut Res* 77, 109-16.

Kapp LN, Brown SL, Klevecz RR (1974). Detecting small quantities of DNA on CsCl gradients. *Biochim Biophys Acta* 361, 140-3.

Kargacin B, Klein CB, Costa M (1993). Mutagenic responses of nickel oxides and nickel sulfides in Chinese hamster V79 cell lines at the xanthine-guanine phosphoribosyl transferase locus. *Mut Res* 300, 63-72.

Kasprzak KS (1991). The role of oxidative damage in metal carcinogenicity. *Toxicology* 4, 604-15.

Kasprzak KS (1992). Animal Studies: An Overview. In: *Nickel and Human Health: Current Perspectives. Advances in Environmental Sciences and Technology, Vol 25* (E Nieboer, JO Nriagu eds). Wiley, New York, 387-420.

Kasprzak KS, Bare RM (1989). *In vitro* polymerization of histones by carcinogenic nickel compounds. *Carcinogenesis* 10, 621-4.

Kasprzak KS, Diwan BA, Rice JM, Misra M, Riggs CW, Olinski R, Dizdaroglu M (1992). Nickel(II)-mediated oxidative DNA base damage in renal and hepatic chromatin of pregnant rats and their fetuses. Possible relevance to carcinogenesis. *Chem Res Toxicol* 5, 809-15.

Kasprzak KS, North SL, Hernandez L (1992). Reversal by nickel(II) of inhibitory effects of some scavengers of active oxygen species upon hydroxylation of 2'-deoxyguanosine in vitro. *Chem Biol Interact* 84, 11-9.

Kasprzak KS, Waalkes MP, Poirier LA (1986). Antagonism by essential divalent metals and amino acids of nickel(II)-DNA binding in vitro. *Toxicol Appl Pharmacol* 82, 336-43.

Kawanishi S, Inoue S, Yamamoto K (1989). Site-specific DNA damage induced by nickel(II) ion in the presence of hydrogen peroxide. *Carcinogenesis* 10, 2231-5.

Kellenberger E (1988). About the organisation of condensed and decondensed non-eukaryotic DNA and the concept of vegetative DNA (a critical review). *Biophys Chem* 29, 51-62.

Kennard O, Hunter WN (1989). Oligonucleotide structure: a decade of results from single crystal X-ray diffraction studies. *Q Rev Biophys* 22, 327-32.

Kissane JM, Robins E (1958). The fluorometric measurement of deoxyribonucleic acid in animal tissues with special reference to the central nervous system. *J Biol Chem* 233, 184-8.

Klein CB, Conway K, Wang XW, Bhamra RK, Lin X, Cohen MD, Annab L, Barrett JC, Costa M (1991). Senescence of nickel-transformed cells by an X chromosome: possible epigenetic control. *Science* 251, 796-9.

Klysik J, Zacharias W, Galazka G, Kwinkowski M,Uznanski B, Okruszek A (1988). Structural interconversion of alternating purine-pyrimidine inverted repeats cloned in supercoiled plasmids. *Nucl Acids Res* 16, 6915-32.

Kohwi Y (1989). Cationic metal-specific structures adopted by the poly(dG) region and the direct repeats in the chicken adult B^A globin gene promoter *Nucl Acids Res* 17, 4493-4502.

Kohwi Y, Kohwi-Shigematsu T (1988). Magnesium ion-dependent triple-helix structure formed by homopurine-homopyrimidine sequences in supercoiled plasmid DNA. *PNAS* 85, 3781-5.

Kohwi-Shigematsu T, Kohwi Y (1991). Detection of triple-helix related structures adopted by poly(dG)-poly(dC) sequences in supercoiled plasmid DNA. *Nucl Acids Res* 19, 4267-71.

Kuehn K, Sunderman FW Jr (1982). Dissolution half-time of nickel compounds in water, rat serum, and rat cytosol. *J Inorg Biochem* 17, 29-39 .

Kypr J, Vorlickova M (1988). Conformations of DNA duplexes containing (dA-dT) sequences of bases and their possible biological significance. In: *Structure And Expression (Vol.2): DNA and Its Drug Complexes* (MH Sarma, RH Sarma eds). Adenine Press, New York, 105-21.

Langmore JP, Paulson JR (1983). Low angle X-ray diffraction studies of chromatin structure in vivo and in isolated nuclei and metaphase chromosomes. *J Cell Biol* 96, 1120-31.

Lamos ML, Walker GT, Krugh TR, Turner DH (1986). Fluorescence-detected circular dichroism of ethidium bound to poly(dG-dC) and poly(dG-m^5dC) under B- and Z-form conditions. *Biochemistry* 25, 687-91.

Larramendy ML, Popescu NC, DiPaulo JA (1981). Induction by inorganic metal salts of sister chromatid exchanges and chromosome aberrations in human and syrian hamster cell strains. *Environ Mutagen* 3, 597-606.

Lechner JF, Tokiwa T, McClendon IA, Haugen A (1984). Effects of nickel sulfate on growth and differentiation of normal human bronchial epithelial cells. *Carcinogenesis* 5, 1697-1703.

Lee YW, Pons C, Tummolo DM, Klein CB, Rossman TG, Christie NT (1993). Mutagenicity of soluble and insoluble nickel compounds at the *gpt* locus in G12 Chinese hamster cells. *Environ Mol Mutagen* 21, 365-71.

Lee-Chen SF, Wang MC, Yu CT, Wu DR, Jan KY (1993). Nickel chloride inhibits the DNA repair of UV-treated but not methyl methanesulfonate-treated Chinese hamster ovary cells. *Biol Trace Element Res* 37, 39-50.

Lerman LS (1973). Chromosomal analogues: long-range order in psi-condensed DNA. *Cold Spring Harbour Symp Quant Biol* 38, 59-73.

Lerman LS (1974). Chromosomal analogues: long-range order in condensed DNA. *Cold Spring Harbour Symp Quant Biol* 38, 59-73.

Leslie AGW, Arnott S, Chandrasekaran R, Ratliff RL (1980). Polymorphism of DNA double helices. *J Mol Biol* 143, 49-72.

Lewis PN, Lukiw WJ, De Boni U, Crapper McLachlan DR (1981). Changes in chromatin structure associated with Alzheimer's disease. *J Neurochem* 37, 1193-202.

Lilley DMJ, McClellan JA (1987). Alternating adenine-thymine tracts in supercoiled and linear DNA molecules. In: *Structure And Expression (Vol.2): DNA and Its Drug Complexes* (MH Sarma, RH Sarma eds). Adenine Press, New York, 73-93.

Lipford GB, Feng Q, Wright GL Jr (1990). A method for separating bound versus unbound label during radioiodination. *Anal Biochem* 187, 133-5.

Liquier J, Bourtayre P, Pizzorni L, Sournies F, Labarre JF, Taillandier E (1984). *Anticancer Res* 4, 41-4.

Lo YMD, Mehal WZ, Fleming KA (1990). Incorporation of biotinylated dUTP. In: *PCR Protocols: A Guide to Methods and Applications* (MA Innis, DH Gelfand, JJ Sninsky, TJ White eds). Academic Press Inc., San Diego, 113-8.

Loeb LA, Mildvan AS (1981). The role of metal ions in the mechanism of DNA and RNA polymerase. In: *Metal Ions in Genetic Information Transfer* (GL Eichhorn, LG Marzilli eds). Elsevier, New York, 103-23.

Lukiw WJ, Kruck TPA, Crapper McLachlan DR (1987). Alterations in human linker histone-DNA binding in the presence of aluminum salts in vitro and in Alzheimer's disease. *Neurotoxicology* 8, 291-302.

Luo SQ, Plowman MC, Hopfer SM, Sunderman FW Jr (1993). Mg^{2+}-deprivation enhances and Mg^{2+}-supplementation diminishes the embryotoxic and teratogenic effects of Ni^{2+}, Co^{2+}, Zn^{2+}, and Cd^{2+} for frog embryos in the FETAX assay. *Ann Clin Lab Sci* 23, 121-9.

Lyamichev VI, Mirkin SM, Frank-Kamenetskii MD (1987). Structure of $(dG)_n$-$(dC)_n$ under superhelical stress and acid pH. *J Biomol Struc Dyn* 5, 275-82.

Lyamichev VI, Mirkin SM, Kumarev VP, Baranova LV, Vologodski AV, Frank-Kamenetskii MD (1989). Energetics of the B-H transition in supercoiled DNA carrying $d(CT)_x$-$d(AG)_x$ and $d(C)_n$-$d(G)_n$ inserts. *Nucl Acids Res* 17, 9417-23.

Ma H, An J, Hsie AW, Au WW (1993). Mutagenicity and cytotoxicity of 2-methoxyethanol and its metabolites in Chinese hamster cells (the CHO/HPRT and AS52/GPT assays). *Mut Res* 298, 219-25.

Maehle L, Metcalf RA, Ryberg D, Bennett WP, Harris CC, Haugen A (1992). Altered *p53* gene structure and expression in human epithelial cells after exposure to nickel. *Cancer Res* 52, 218-21.

Makarov VL, Smirnov I, Dimitrov SI (1987). Higher order folding of chromatin is induced in different ways by monovalent and by bivalent cations. *FEBS Lett* 212, 263-6.

Marzilli LG (1977). Metal-ion interactions with nucleic acids and nucleic acid derivatives. *Prog Inorg Chem* 23, 255-393.

Marzilli LG (1981). Metal complexes of nucleic acid derivatives and nucleotides: Binding sites and structures. In: *Metal Ions in Genetic Information Transfer* (GL Eichhorn, LG Marzilli eds). Elsevier, New York, 47-85.

Mastromatteo E (1986). Nickel. *J Am Indust Hyg Assoc* 47, 589-601.

McCall M, Brown T, Kennard O (1985). The crystal structure of d(G-G-G-G-C-C-C-C): a model for poly(dG)-poly(dC). *J Mol Biol* 183, 385-96.

Michaelis K, Helvering L, Kindig D, Garriott M, Richardson K (1992). Localization of the xanthine guanine phosphoribosyl transferase gene(*gpt*) of *E. coli* in AS52 metaphase cells by fluorescence in situ hybridization. *Environ Mol Mutagen* 19 (Suppl 20), 42.

Mihovilovic M, Lee JE (1989). An efficient method for sequencing PCR amplified DNA. *BioTechniques* 7, 14-6.

Miskovsky P, Chinsky L, Laigle A, Turpin PY (1989). The Z-conformation of poly(dA-dT)·poly(dA-dT) in solution as studied by ultraviolet resonance raman spectroscopy. *J Biomolec Struc Dyn* 7, 623-37.

Misra M, Olinski R, Dizdaroglu M, Kasprzak KS (1993). Enhancement by L-histidine of nickel(II)-induced DNA-protein cross-linking and oxidative DNA base damage in the rat kidney. *Chem Res Toxicol* 6, 33-7.

Misra M, Rodriguez RE, Kasprzak KS (1990). Nickel induced lipid peroxidation in the rat: Correlation with nickel effect on antioxidant defense systems. *Toxicology* 64, 1-17.

Misra M, Rodriguez RE, North SL, Kasprzak KS (1991). Nickel-induced renal lipid peroxidation in different strains of mice: Concurrence with nickel effect on antioxidant defense systems. *Toxicol Lett* 58, 121-33.

Miyaki M, Akamatsu N, Ono T, Koyama H (1979). Mutagenicity of metal cations in cultured cells from Chinese hamster. *Mut Res* 68, 259-63.

Morgan JG (1958). Some observations on the incidence of respiratory cancer in nickel workers. *Br J Indust Med* 15, 224-34.

Morgan LG (1979). Manufacturing processes - refining of nickel. *J Soc Occup Med* 29, 33-5.

Morgan AR, Lee JS, Pulleyblank DE, Murray NL, Evans DH (1979). Review: ethidium fluorescence assays. Part 1: physicochemical studies. *Nucl Acids Res* 7, 547-69.

Morita H, Umeda M, Ogawa HI (1991). Mutagenicity of various chemicals including nickel and cobalt compounds in cultured mouse FM3A cells. *Mut Res* 261, 131-7.

Mulligan RC, Berg P (1980). Expression of a bacterial gene in mammalian cells. *Science* 209, 1422-7.

Mulligan RC, Berg P (1981). Selection for animal cells that express the *Escherichia coli* gene coding for xanthine-guanine phosphoribosyltransferase. *PNAS* 78, 2072-6.

Nackerdien Z, Kasprzak KS, Rao G, Halliwell B, Dizdaroglu M (1991). Nickel(II)- and cobalt(II)-dependent damage by hydrogen peroxide to the DNA bases in isolated human chromatin. Cancer *Res* 51, 5837-42.

Neidle S, Abraham Z (1984). Structural and sequence-dependent aspects of drug intercalation into nucleic acids. *CRC Crit Rev Biochem* 17, 73-121.

Nejedly K, Klysik J, Palecek E (1989). Supercoil-stabilized left-handed DNA in the plasmid $(dA\text{-}dT)_{16}$ insert formed in the presence of Ni^{2+}. *FEBS Lett* 243, 313-7.

Nelson HCM, Finch JT, Luisi BF, Klug A(1987). The structure of an oligo(dA)-oligo(dT) tract and its biological implications. *Nature* 330, 221-6.

Nestmann ER, Brillinger RL, Gilman JPW, Rudd CJ, Swierenga SHH (1991). Recommended protocols based on a survey of current practice in genotoxicity testing laboratories: II. Mutation in Chinese hamster ovary, V79 Chinese hamster lung and L5178Y mouse lymphoma cells. *Mut Res* 246, 255-84.

Newman SM, Summitt RL, Nunez LJ (1982). Incidence of nickel-induced sister-chromatid exchange. *Mut Res* 101, 67-75.

Nicolini C (1988). Nuclear architecture and three-dimensional organization of chromatin: their role in the control of cell function. In: *Heterochromatin: Molecular and Structural Aspects* (RS Verma ed). University of Cambridge, Cambridge, 228-49.

Nieboer E (1992). Occupational Exposures to Nickel. In: *Nickel and Human Health: Current Perspectives. Advances in Environmental Sciences and Technology, Vol. 25* (E Nieboer, JO Nriagu eds). Wiley, New York, 37-47.

Nieboer E, Fletcher GG (1993a). Mode of Absorption of the Main Essential and Beneficial Metal Ions: Nickel. In: *Handbook on Metal-Ligand Interactions in Biological Fluids* (G Berthon ed). Marcel Dekker, New York, in press.

Nieboer E, Fletcher GG (1993b). Toxicity of Essential and Beneficial Metal Ions: Nickel. In: *Handbook on Metal-Ligand Interactions in Biological Fluids* (G Berthon ed). Marcel Dekker, New York, in press.

Nieboer E, Maxwell RI, Rossetto FE, Stafford AR, Stetsko PI (1986). Concepts in nickel carcinogenesis. In: *Frontiers in Bioinorganic Chemistry* (AV Xavier ed). VCH, Germany, 142-51.

Nieboer E, Richardson DHS (1980). The replacement of the nondescript term 'heavy metals' by a biologically and chemically significant classification of metal ions. *Environ Pollution (Series B)* 1, 3-26.

Nieboer E, Rossetto FE, Menon CR (1988). Toxicology of Nickel Compounds. In: *Nickel and its Role in Biology. Metal Ions in Biological Systems, Vol. 23* (H Sigel, A Sigel eds). Marcel Dekker, New York, 359-402.

Nieboer E, Rossetto FE, Turnbull JD (1992). Molecular biology approaches to biological monitoring of genotoxic substances. *Toxicol Lett* 64/65, 25-32.

Nieboer E, Tom RT, Rossetto FE (1989). Superoxide dismutase activity with hydrogen peroxide of histidine-containing nickel(II)-oligopeptide complexes and nickel(II)-induced structural changes in synthetic DNA. *Biol Trace Element Res* 21, 23-33.

Nieboer E, Tom RT, Sanford WE (1988). Nickel Metabolism in Man and Animals. In: *Nickel and its Role in Biology. Metal Ions in Biological Systems, Vol. 23* (H Sigel, A Sigel eds). Marcel Dekker, New York, 91-121.

Nieboer E, Yassi A, Jusys AA, Muir DCF (1984). In: *The Technical Feasibility and Usefulness of Biological Monitoring in the Nickel Producing Industry (Special Document)*. McMaster University, Hamilton.

Nielsen GD (1992). Oral Challenge of Nickel-Allergic Patients with Hand Eczema. In: *Nickel and Human Health: Current Perspectives. Advances in Environmental Science and Technology Vol. 25* (E Nieboer, JO Nriagu eds). Wiley, New York, 201-10.

Nielsen GD, Flyvholm M (1984). Risks of high nickel intake with diet. In: *Nickel in the Human Environment: IARC Sci. Publ. No. 53* (FW Sunderman Jr editor-in-chief). International Agency for Research on Cancer, Lyon, 333-8.

Nishimura Y, Torigoe C, Tsuboi M (1986). Salt induced B-A transition of poly(dG)-poly(dC) and the stabilization of A form by its methylation. *Nucl Acids Res* 14, 2737-48.

Nishimura M, Umeda M (1979). Induction of chromosomal aberrations in cultured mammalian cells by nickel compounds. *Mut Res* 68, 337-49.

Niyogi SK, Feldman RP (1981). Effect of several metal ions on misincorporation during transcription. *Nucl Acids Res* 9, 2615-27.

Niyogi SK, Feldman RP, Hoffman DJ (1981). Selective effects of metal ions on RNA synthesis rates. *Toxicology* 22, 9-21

Palecek E (1991). Local supercoil-stabilized DNA structures. *Crit Rev Biochem Mol Biol* 26, 151-226.

Panyutin IG, Kovalsky OI, Budowsky EI (1989). Magnesium-dependent supercoiling-induced transition in $(dG)_n$-$(dC)_n$ stretches and formation of a new G-structure by $(dG)_n$ strand. *Nucl Acids Res* 17, 8257-71.

Parfett CLJ (1992). Induction of proliferin gene expression by diverse chemical agents that promote morphological transformation in C3H/10T1/2 cultures. *Cancer Lett* 64, 1-9.

Parfett CLJ, MacMillan JE, Pilon R (1993). Oxidative stress mediates tumour promoter-induced proliferin gene expression in C3H10T1/2 cells. *Int J Oncol*, in press.

Patierno SR, Costa M (1985). DNA-protein cross-links induced by nickel compounds in intact cultured mammalian cells. Chem Biol *Interactions* 55, 75-91.

Patierno SR, Costa M (1987). Effects of nickel(II) on nuclear protein binding to DNA in intact mammalian cells. *Cancer Biochem Biophys* 9, 113-26.

Patierno SR, Sugiyama M, Basilion JP, Costa M (1985). Preferential DNA-protein cross-linking by $NiCl_2$ in magnesium-insoluble regions of fractionated Chinese hamster ovary cell chromatin. *Cancer Res* 45, 5787-94.

Patierno SR, Sugiyama M, Costa M (1987). Effect of nickel(II) on DNA-protein binding, thymidine incorporation, and sedimentation pattern of chromatin fractions from intact mammalian cells. *J Biochem Toxicol* 2, 13-23.

Perera FP (1991). Perspectives on the risk assessment for nongenotoxic carcinogens and tumour promoters. Environ Health *Perspect* 94, 231-5.

Peskin AV, Shlyahova L (1986). Cell nuclei generate DNA-nicking superoxide radicals. FEBS Lett 194, 317-21.

Pennington JAT, Jones JW (1987). Molybdenum, nickel, cobalt, vanadium, and strontium in total diets. *J Am Diet Assoc* 87, 1644-50.

Picketts DJ, Mayanil CSK, Gupta RS (1989). Molecular cloning of a Chinese hamster mitochondrial protein related to the "chaperonin" family of bacterial and plant proteins. *J Biol Chem* 264, 12001-8.

Pikalek P, Necasek J (1983). The mutagenic activity of nickel in Corynebacterium sp. *Folia Microbiol* 28, 17-21.

Pohl FM, Jovin TM, Baehr W, Holbrook JJ (1972). Ethidium bromide as a cooperative effector of a DNA structure. *PNAS* 69, 3805-9.

Pratt D, Subramani S (1983). Nucleotide sequence of the *Escherichia coli* xanthine-guanine phosphoribosyl transferase gene. *Nucl Acids Res* 11, 8817-23.

Preisler RS (1987). The B-DNA to Z-DNA transition in alkali and tetraalkylammonium salts correlated with cation effects on solvent structure. *Biochem Biophys Res Comm* 148, 609-16.

Rahmsdorf HJ, Herrlich P (1990). Regulation of gene expression by tumor promoters. *Pharmacol Ther* 48, 157-88.

Rasmuson A (1985). Mutagenic effects of some water-soluble metal compounds in a somatic eye-color test system in *Drosophila melanogaster*. *Mut Res* 157, 157-62.

Riazance-Lawrence JH, Johnson WC Jr (1992). Multivalent ions are necessary for poly[d(AC)-d(GT)] to assume the Z form: a CD study. *Biopolymers* 32, 271-6.

Rich A, Nordheim A, Wang AHJ (1984). The chemistry and biology of left-handed Z-DNA, *Ann Rev Biochem* 53, 791-846.

Richardson KK, Fostel J, Skopek TR (1983). Nucleotide sequence of the xanthine guanine phosphoribosyl transferase gene of *E. coli*. *Nucl Acids Res* 11, 8809-16.

Ridoux JP, Liquier J, Taillandier E (1988). Raman spectroscopy of Z-form poly[d(A-T)]·poly[d(A-T)]. *Biochemistry* 27, 3874-8.

Rivedal E, Sanner T (1981). Metal salts as promoters of *in vitro* morphological transformation of hamster embryo cells initiated by benzo(a)pyrene. *Cancer Res* 41, 2950-3.

Robison SH, Cantoni O, Costa M (1982). Strand breakage and decreased molecular weight of DNA induced by specific metal compounds. *Carcinogenesis* 3, 657-62.

Robison SH, Cantoni O, Heck JD, Costa M (1983). Soluble and insoluble nickel compounds induce DNA repair synthesis in cultured mammalian cells. *Cancer Lett* 17, 273-9.

Robison SH, Costa M (1982). The induction of DNA strand breakage by nickel compounds in cultured Chinese hamster ovary cells. *Cancer Lett* 15, 35-40.

Rodriguez RE, Misra M, North SL, Kasprzak KS (1991). Nickel-induced lipid peroxidation in the liver of different strains of mice and its relation to nickel effects on antioxidant systems. *Toxicol Lett* 57, 269-81.

Rodriguez-Arnaiz R, Ramos MP (1986). Mutagenicity of nickel sulphate in *Drosophila melanogaster*. *Mut Res* 170, 115-7.

Rosen KM, Villa-Komaroff L (1990). An alternative method for the visualization of RNA in formaldehyde agarose gels. *Focus* 12, 23-4.

Rossetto FE, Nieboer E (1993). The interaction of metal ions with synthetic DNA: induction of conformational and structural transitions. *J Inorg Biochem*, in press.

Rossetto FE, Turnbull JD, Nieboer E (1993). Characteri-zation of nickel-induced mutations. *Sci Total Environ*, in press.

Rossman TG, Molina M, Meyer LW (1984). The genetic toxicology of metal compounds: I.Induction of alpha prophage in *E. coli* $WP2_s$. *Environ Mutagen* 6, 59-69.

Roy KB, Miles HT (1983). A thermally driven interconversion of B and Z-DNA. *Biochem Biophys Res Comm* 115, 100-5.

Sager PR, Clarkson TW, Nordberg GF (1986). Reproductive and developmental toxicity of metals. In: *Handbook on the Toxicology of Metals, Vol. I* (L Friberg, GF Nordberg, VB Vouk eds). Elsevier, Amsterdam, 391-433.

Sagi J, Szemzo A, Otvos L, Vorlickova M, Kypr J (1991). Destabilization of the duplex and the high-salt Z-form of poly(dG-methyl^{5}dC) by substitution of ethyl for the 5-methyl group. *Int J Biol Macromol* 13, 329-36.

Saiki RK, Gelfand D, Stoffel S, Scharf SJ, Higuchi R, Horn GT, Mullis KB, Erlich HA (1988). Primer-directed enzymatic amplification of DNA with a thermostable DNA polymerase. *Science* 239, 487-91.

Sanford WE, Nieboer E (1992). Renal Toxicity of Nickel in Humans. In: *Nickel and Human Health: Current Perspectives. Advances in Environmental Sciences and Technology, Vol. 25* (E Nieboer, JO Nriagu eds). Wiley, New York, 123-34.

Sealey PG, Southern EM (1984). Gel electrophoresis of DNA. In: *Gel Electrophoresis of Nucleic Acids: A Practical Approach*. IRL Press Ltd., Oxford, 21-59.

Sen P, Conway K, Costa M (1987). Comparison of the localization of chromosome damage induced by calcium chromate and nickel compounds. *Cancer Res* 47, 2142-7.

Sen P, Costa M (1985). Induction of chromosomal damage in Chinese hamster ovary cells by soluble and particulate nickel compounds: preferential fragmentation of the heterochromatic long arm of the X-chromosome by carcinogenic crystalline NiS particles. *Cancer Res* 45, 2320-5.

Sen P, Costa M (1986). Pathway of nickel uptake influences its interaction with heterochromatic DNA. *Toxicol Appl Pharmacol* 84, 278-85.

Shi X, Dalal NS, Kasprzak KS (1992). Generation of free radicals from lipid hydroperoxides by Ni^{2+} in the presence of oligopeptides. *Arch Biochem Biophys* 299, 154-62.

Shin YA, Butzow JJ, Sinsel LD, Clark P, Pillai RP, Johnson WC, Eichhorn GL (1988). Metal-induced sequential transitions among DNA conformations. *Biopolymers* 27, 1415-32.

Shin YA, Eichhorn GL (1977). Reversible change in psi structure of DNA-poly(Lys) complexes induced by metal binding. *Biopolymers* 16, 225-30.

Shin YA, Feroli SL, Eichhorn GL (1986). Psi compaction of poly[d(AT)]-poly[d(AT)]. *Biopolymers* 25, 2133-48.

Singh I (1983). Induction of reverse mutation and mitotic gene conversion by some metal compounds in Saccharomyces cerevisiae. *Mut Res* 117, 149-52.

Singh I (1984). Induction of gene conversion and reverse mutation by manganese sulphate and nickel sulphate in Saccharomyces cerevisiae. *Mut Res* 137, 47-9.

Sirover MA, Loeb LA (1976). Infidelity of DNA synthesis in vitro: screening for potential metal mutagens or carcinogens. *Science* 194, 1434-6.

Smart GA, Sherlock JC (1987). Nickel in foods and the diet. *Food Addit Contam* 4, 61-71.

Stankowski LF Jr, Hsie AW (1986). Quantitative and molecular analyses of radiation-induced mutation in AS52 cells. *Radiat Res* 105, 37-48.

Stankowski LF Jr, Tindall KR (1987). Characterization of the AS52 cell line for use in mammalian cell mutagenesis studies. In: *Banbury Report 28: Mammalian Cell Mutagenesis* (MM Moore, DM Demarini, FJ de Serres, KR Tindall eds). Cold Spring Harbor Laboratory, Boston, 71-9.

Stankowski LF Jr, Tindall KR, Hsie AW (1986). Quantitative and molecular analyses of ethyl methanesulfonate- and ICR 191-induced mutation in AS52 cells. *Mut Res* 160, 133-47.

Sunderman FW Jr (1975). In: *Nickel*. National Academy Of Sciences, Washington, D.C.

Sunderman FW Jr (1986). Metals and lipid peroxidation. *Acta Pharmacol Toxicol* 59, 248-55.

Sunderman FW Jr (1989). Mechanisms of nickel carcinogenesis. *Scand J Work Environ Hlth* 15, 1-12.

Sunderman FW Jr, Aitio A, Morgan LG, Norseth T (1986). Biological monitoring of nickel. *Toxicol Indust Health* 2, 17-78.

Sunderman FW Jr, Allpass PR, Mitchell JM, Baselt RC (1979). Eye malformations in rats: induction by prenatal exposure to nickel carbonyl. *Science* 203, 550-3.

Sunderman FW Jr, Marzouk A, Hopfer SM, Zaharia O, Reid MC (1985). Increased lipid peroxidation in tissues of nickel chloride-treated rats. *Ann Clin Lab Sci* 15, 229-36.

Sunderman FW Jr, Reid MC, Shen SK, Kevorkian CB (1983). Embryotoxicity and teratogenicity of nickel compounds. In: *Reproductive and Developmental Toxicity of Metals* (TW Clarkson, GF Nordberg, PR Sager eds). Plenum Press, New York, 399-416.

Sunderman FW Jr, Shen SK, Reid MC, Allpass PR (1980). Teratogenicity and embryotoxicity of nickel carbonyl in Syrian hamsters. *Teratogen Carcinogen Mutagen* 1, 223-33.

Taboury JA, Bourtayre P, Liquier J, Taillandier E (1984) Interaction of Z form poly(dG-dC)·poly(dG-dC) with divalent metal ions: localization of the binding sites by I.R. spectroscopy. *Nucl Acids Res* 12, 4247-58.

Taboury JA, Taillandier E (1985). Right-handed and left-handed helices of poly(dA-dC)·(dG-dT). *Nucl Acids Res* 13, 4469-83.

Taillandier E, Taboury JA, Adam S, Liquier J (1984). Left-handed helical structure of poly[d(A-C)]·poly[d(G-T)] studied by infrared spectroscopy. *Biochemistry* 23, 5703-6.

Thomas TJ, Bloomfield VA (1985). Toroidal condensation of Z-DNA and identification of an intermediate in the B to Z transition of poly(dG-m^5dC)·poly(dG-m^5dC). *Biochemistry* 24, 713-9.

Thomas TJ, Thomas T (1990). Conformational transitions of polynucleotides in the presence of rhodium complexes. *J Biomolec Struc Dyn* 7, 1221-35.

Tindall KR, Kunkel TA (1988). Fidelity of DNA synthesis by the *Thermus aquaticus* DNA polymerase. *Biochemistry* 27, 6008-13.

Tindall KR, Stankowski LF Jr (1987). Deletion mutations are associated with the differential-induced mutant frequency response of the AS52 and CHO-K1-BH4 cell lines. In: *Banbury Report 28: Mammalian Cell Mutagenesis* (MM Moore, DM Demarini, FJ de Serres, KR Tindall eds). Cold Spring Harbor Laboratory, Boston, 283-92.

Tindall KR, Stankowski LF Jr (1989). Molecular analysis of spontaneous mutations at the *gpt* locus in Chinese hamster ovary (AS52) cells. *Mut Res* 220, 241-53.

Tindall KR Jr, Stankowski LF Jr, Machanoff R, Hsie AW (1984). Detection of deletion mutations in pSV2*gpt*-transformed cells. *Mol Cell Biol* 4, 1411-5.

Tindall KR, Stankowski LF Jr, Machanoff R, Hsie AW (1986). Analyses of mutation in pSV2*gpt*-transformed CHO cells. *Mut Res* 160, 121-31.

Tindall KR, Whitaker RA (1991). Rapid localization of point mutations in PCR products by chemical (HOT) modification. *Environ Mol Mutagen* 18, 231-8.

Tinoco I Jr, Bustamente C, Maestre MF (1980). The optical activity of nucleic acids and their aggregates. *Ann Rev Biophys Bioeng* 9, 107-41.

Tom RT (1987). Novel reactions of nickel(II)-oligopeptide complexes with dioxygen species. MSc. Thesis, McMaster University, Hamilton, Canada.

Torjussen W, Andersen I (1979). Nickel concentrations in nasal mucosa, plasma, and urine in active and retired nickel workers. *Ann Clin Lab Sci* 9, 289-98.

Tossavainen A, Nurminen M, Mutanen P, Tola S (1980). Application of mathematical modelling for assessing the biological half-times of chromium and nickel in field studies. *Br J Ind Med* 37, 285-91.

Tsanev R (1983). Transcriptionally active chromatin. *Molec Biol Rep* 9, 9-17.

Tsanev R, Tsaneva I (1986). Molecular organization of chromatin as revealed by electron microscopy. *Meth Achiev Exp Pathol* 12, 63-104.

Tunis-Schneider MJB, Maestre MF (1970). Circular dichroism spectra of oriented and unoriented deoxyribonucleic acid films - a preliminary study. *J Mol Biol* 52, 521-41.

Tveito G, Hansteen IL, Dalen H, Haugen A (1989). Immortalization of normal human kidney epithelial cells by nickel(II). *Cancer Res* 49, 1829-35.

Umeda M, Nishimura M (1979). Inducibility of chromosomal aberrations by metal compounds in cultured mammalian cells. *Mut Res* 67, 221-9.

van de Sande J, Jovin T (1982). Z* DNA, the left-handed helical form of poly[d(G-C)] in $MgCl_2$-ethanol, is biologically active. *EMBO J* 1, 115-20.

van de Sande J, McIntosh LP, Jovin TM (1982). Mn^{2+} and other transition metals at low concentration induce the right-to-left helical transformation of poly[d(G-C)]. *EMBO J* 1, 777-82.

van Holde KE (1985). In: *Physical Biochemistry, 2nd Edition*. Prentice-Hall Inc., New Jersey, 51-92.

van Holde KE (1988). In: *Chromatin*. Springer-Verlag, New York.

Veien NK, Andersen MR (1986). Nickel in Danish food. *Acta Derm Venereol (Stockh)* 66, 502-9.

Vizard D, Hadman M, Bianca D, Manzer D (1990). A simplified biochemistry for DNA sequencing. *BioTechniques* 8, 430-7.

Vorlickova M, Sagi J, Szabolcs A, Szemzo A, Otvos L, Kypr J (1988). Conformations of the synthetic DNA poly(amino^{2}dA-dT) duplex in high-salt and aqueous alcohol solutions. *Nucl Acids Res* 16, 279-89.

Votavova H, Kucerova D, Felsberg J, Sponar J (1986). Changes in conformation, stability and condensation of DNA by univalent and divalent cations in methanol-water mixtures. *J Biomolec Struc Dyn* 4, 477-89.

Votavova H, Pirkova J, Gut V, Sponar J, Blaha K (1991). Effect of basic oligopeptides on the B-Z transition of poly(dG-dC)-poly(dG-dC) in water-methanol solutions. *Biopolymers* 31, 275-83.

Waksvik H, Boysen M (1982). Cytogenetic analyses of lymphocytes from workers in a nickel refinery. *Mut Res* 103, 185-90.

Waksvik H, Boysen M, Hogetveit AC (1984). Increased incidence of chromosomal aberrations in peripheral lymphocytes of retired nickel workers. *Carcinogenesis* 5, 1525-7.

Walter A, Luck G (1977). Interactions of Hg(II) ions with DNA as revealed by CD measurements. *Nucl Acids Res* 4, 539-50.

Walker GT, Stone M, Krugh TR (1985). Ethidium binding to left-handed (Z) DNAs results in regions of right-handed DNA at the intercalation site. *Biochemistry* 24, 7462-71.

Walton AG, Blackwell J (1973). In: *Biopolymers*. Academic Press, London, 229-95.

Wang AHJ, Quigley GJ, Kolpak FJ, van der Marel G, van Boom JH, Rich A (1981). Left-handed double helical DNA: variations in the backbone conformation. *Science* 211, 171-6.

Warner JS (1984). Occupational exposure to airborne nickel in producing and using primary nickel products. In: *Nickel in the Human Environment: IARC Sci. Publ. 53,* (FW Sunderman Jr editor-in-chief). Oxford University Press, 419-37.

Weinberg RA (1989). Oncogenes, antioncogenes, and the molecular bases of multistep carcinogenesis. *Cancer Res* 49, 3713-21.

Weith A (1983). Mg^{2+}-dependent compactness of heterochromatic chromosome segments. *Exp Cell Res* 146, 199-203.

Wells RD, Larson JE, Grant RC, Shortle BE, Cantor CR (1970). Physicochemical studies on polydeoxyribonucleotides containing defined repeating nucleotide sequences. *J Mol Biol* 54, 465-97.

WHO (1991). In: *Environmental Health Criteria 108: Nickel.* World Health Organization, Geneva.

Widom J, Baldwin RL (1980). Cation-induced toroidal condensation of DNA studies with $Co^{3+}(NH_3)_6$. *J Mol Biol* 144, 431-53.

Woisard A, Fazakerley GV, Guschlbauer W (1985). Z-DNA is formed by poly(dC-dG) and poly(dm^5-dG) at micro or nanomolar concentrations of some zinc(II) and copper(II) complexes. *J Biomolec Struc Dyn* 2, 1205-20.

Wolf B, Berman S, Hanlon S (1977). Structural transitions of calf thymus DNA in concentrated LiCl solutions. *Biochemistry* 16, 3655-62.

Xu Z, Yu Y, Hsie AW, Caskey CT, Rossiter B, Gibbs RA (1989). Deletion screening at the hypoxanthine-guanine phosphoribosyltransferase locus in Chinese hamster cells using the polymerase chain reaction. *Teratogen Carcinogen Mutagen* 9, 177-87.

Yagil G (1991). Paranemic structures of DNA and their role in DNA unwinding. *Crit Rev Biochem Mol Biol* 26, 475-559.

Yamane T, Davidson N (1962). On the complexity of deoxyribonucleic acid by silver(I). *Biochim Biophys Acta* 55, 609-21.

Zacharias W, Larson JE, Klysik J, Stirdivant SM, Wells RD (1982). Conditions which cause the right-handed to left-handed DNA conformational transitions. *J Biol Chem* 257, 2775-82.

Zacharias W, Martin JC, Wells RD (1983). Condensed form of $(dG\text{-}dC)_n\text{-}(dG\text{-}dC)_n$ as an intermediate between the B- and Z-type conformations induced by sodium acetate. *Biochemistry* 22, 2398-2405.

Zehfus MH, Johnson WC Jr (1981). Properties of P-form DNA as revealed by circular dichroism. *Biopolymers* 20, 1589-603.

Zehfus MH, Johnson WC Jr (1984). Conformations of P-form DNA. *Biopolymers* 23, 1269-81.

Zeugin JA, Hartley JL (1985). Ethanol precipitation of DNA. *Focus* 7, 1-2.

VII. APPENDIX

VII.1 LIST OF PUBLICATIONS

Publications

1. *Rossetto FE*, Nieboer E. The interaction of metals with synthetic DNA: induction of conformational and structural transitions. *J Inorg Biochem*, in press.

2. *Rossetto FE*, Turnbull JD, Nieboer, E. Characterization of nickel-induced mutations. *The Science of the Total Environment*, in press.

3. Fletcher, GG, *Rossetto FE*, Turnbull JD, Nieboer E. Toxicity, uptake, and mutagenicity of particulate and soluble nickel compounds. *Environ Health Perspect*, in press.

4. Bryant DW, *Rossetto FE*, Li W-P, Turnbull, JD. A comparison of the sequences of the *gpt* from *Salmonella Typhimurium* and *Escherichia Coli*. *Mutation Res*, in press.

5. Nieboer E, *Rossetto FE*, Turnbull JD (1992). Molecular biology approaches to biological monitoring of genotoxic substances. *Toxicology Letters*, 64/65, 9-16.

6. Nieboer E, Tom RT, *Rossetto FE* (1989). Superoxide dismutase activity and novel reactions with hydrogen peroxide of histidine-containing nickel(II)-oligopeptide complexes and nickel(II)-induced structural changes in synthetic DNA. *Biol Trace Element Res* 21, 23-33.

7. Nieboer E, *Rossetto FE*, Menon CR (1988). Nickel toxicology. In: *Nickel and Its Role in Biology: Metal Ions in Biological Systems*, Vol. 22, H. Sigel (Ed.), Marcel Dekker, New York, pp. 359-402.

8. Nieboer E, Maxwell RI, *Rossetto FE*, Stafford AR, Stetsko PI (1986). Concepts in Nickel Carcinogenesis. In: *Frontiers in Bioinorganic Chemistry*, A.V. Xavier (Ed.), VCH Publishers, FDR Germany, pp. 142-151.

Abstracts

1. Bryant DW, *Rossetto FE*, Li W-P, Turnbull JD (1993). A comparison of the sequences of the *gpt* genes from *Salmonella* and *Escherichia Coli*. Twenty-fourth Annual Meeting of the Environmental Mutagen Society, April 17-22, Norfolk, Virginia, U.S.A.

2. Fletcher GG, *Rossetto FE*, Turnbull JD, Nieboer E (1993). Toxicity, uptake and mutagenicity of particulate and soluble nickel compounds. Second International Meeting on Molecular Mechanisms of Metal Toxicity and Carcinogenicity, Jan. 10-17, Madonna Di Campiglio, Italy.

3. *Rossetto FE*, Turnbull JD, Nieboer E (1992). Characterization of nickel-induced mutations. Fifth International Conference on Nickel Biochemistry, Toxicology and Ecologic Issues, Sudbury, Ontario, Canada, Sept. 7-11.

4. *Rossetto FE*, Fletcher GG, Tom RT, Turnbull JD, Nieboer E (1991). Metal carcinogenesis. Fifth International Conference on Bioinorganic Chemistry, University of Oxford, U.K., August 4-10.

5. Nieboer E, Fletcher GG, *Rossetto FE*, Tom RT (1990). The nickel-ion hypothesis of cytotoxic responses. International Symposium on Trace Elements in Health and Disease, Espoo, Finland, June 5-8, p. 34.

6. Tom RT, *Rossetto FE*, Nieboer E (1988). Novel reactions of nickel(II)-oligopeptide complexes with dioxygen species and nickel(II)-induced cooperative transitions of synthetic DNA. First International Meeting on Molecular Mechanisms of Metal Toxicity and Carcinogenicity, Sept. 19-22, Urbino, Italy, p. 11.

7. *Rossetto FE*, Nieboer E (1988). Ni(II)-induced structural changes in synthetic DNA. Fourth International Conference on Nickel Metabolism and Toxicology, Helsinki, Finland, Sept. 5-9, p.34.

8. *Rossetto FE*, Nieboer E (1987). Characterization of Nickel(II)-Induced DNA and Chromosomal Aberrations. International Conference on Detection Methods for DNA - Damaging Agents in Man, Helsinki, Finland, Sept. 2-4.

In Preparation

1. *Rossetto FE,* Nieboer E. The interaction of nickel(II)-ion with chromosomal DNA.

2. *Rossetto FE,* Nieboer E. Ni(II)-induced structural changes in synthetic DNA.

3. *Rossetto FE,* Turnbull JD, Li W-P, Nieboer E. Characterization of the *gpt* Pseudogene in the CHO (AS52) cell line.

VII.2 REPRINTS

Nieboer E, *Rossetto FE*, Turnbull, JD (1992). Molecular biology approaches to biological monitoring of genotoxic substances. *Toxicology Letters* 64/65, 25-32.

Rossetto FE, Nieboer, E (1993). The interaction of metal ions with synthetic DNA: induction of conformational and structural transitions. *J Inorg Biochem*, in press.

Rossetto FE, Turnbull JD, Nieboer, E. Characterization of nickel-induced mutations. *The Science of the Total Environment*, in press.

Toxicology Letters, 64/65 (1992) 25–32
© 1992 Elsevier Science Publishers B.V., All rights reserved 0378-4274/92/$ 5.00

Molecular biology approaches to biological monitoring of genotoxic substances

Evert Nieboer[a], Franco E. Rossetto[a] and John D. Turnbull[b]

[a]*Department of Biochemistry and Occupational Health Program and* [b]*Department of Medicine and Occupational Health Program, McMaster University, Hamilton, Ontario (Canada)*

Key words: Biomarkers; Genotoxicity; Genetic monitoring and screening; Susceptibility to environmental agents; Compound-specific DNA lesions

SUMMARY

Genetic testing is subdivided into *genetic monitoring* (evaluation over time of induced genetic changes) and *genetic screening* (detection of inherited traits). Genetic factors in relation to susceptibility to environmental agents are briefly examined, as well as mutation assays suitable for use in genetic monitoring, techniques for identifying specific DNA lesions, and oncogene products as biomarkers. *In vitro* studies with AS52 Chinese hamster ovary cells indicate that the distribution of lesions (e.g., point mutations or segment deletions) at the xanthine-guanine phosphoribosyl transferase (*gpt*) gene in mutants generated by exposure to nickel compounds show some substance specificity. This ability is viewed as a promising development for the molecular epidemiology of occupational and environmental cancers. It is concluded that technical limitations pertaining to specificity and sensitivity, as well as ethical and legal implications, need to be resolved before routine application of genetic monitoring and screening is feasible.

INTRODUCTION

The techniques of molecular biology have spawned rapid development in our knowledge about the localization, structure and function of human genes. Mapping of genetic disorders to specific chromosomes, gene isolation and cloning, and the identification of specific gene defects are now routine procedures. Nevertheless, our knowledge of the human genome is very incomplete. It is estimated to have about 5×10^4 to 10^5 expressed genes; of

Correspondenceto: E. Nieboer, Department of Biochemistry and Occupational Health Program, McMaster University, 1200 Main Street West, Hamilton, Ontario, Canada, L8N 3Z5.

this number, only about 2000 genes have been identified and assigned to specific chromosomes (i.e., 2–4%). The goal of the *human genome project is* to map and sequence the entire genome [1]. It is expected that the work derived from this initiative has the potential of revolutionizing biology and medicine. Repercussions for related developments and opportunities in toxicology might therefore be expected. Not surprisingly, genetic testing in relation to workplace and environmental exposures to toxic contaminants is a topic of considerable current relevance and importance. The goal of this article is to review recent developments pertinent to this subject, including results obtained in the authors' laboratory.

COMPONENTS OF GENETIC TESTING

It seems useful to divide genetic testing into two separate activities, namely *genetic monitoring* and *genetic screening*. Genetic monitoring involves periodic examination of individuals to evaluate modifications that evolve over time within their genetic material, perhaps due to occupational or environmental exposures [2]. Chromosomal damage or increases in DNA mutations might be the measured outcomes. The assertion is that such changes might constitute increased risk of future illness (e.g., cancer or reproductive deficits). By contrast, the emphasis in genetic screening is to detect inherited traits that predispose an individual to a pathologic effect if exposed to certain chemicals [2,3].

Before considering each of the two components of genetic testing in more detail, brief comments on biological markers and molecular epidemiology are warranted. Henderson et al. [4] point out that biomarkers might be identified for any of a continuum of events ranging from exposure to pathologic outcome measurements. Urinary metabolites of toxicants, chemical adducts with DNA or protein, or the direct measurement of an exogenous substance in body fluids are examples of useful indices of exposure. On the other hand, outcomes such as chromosomal aberrations, increased mutation frequencies in peripheral blood cells or reduced enzyme levels have the potential of serving both as indicators of exposure and markers of an early biological response. Recently, the concept of molecular epidemiology has emerged in which biologically determined markers of dose and early effects are employed to assess risk of disease [3,5]. "Biomonitoring generally involves cross-sectional or serial sampling to evaluate exposure-dose relationships, whereas in molecular epidemiologic studies a hypothesis is proposed regarding the relationship between markers of dose or response on the one hand and risk (e.g., cancer) on the other. Molecular epidemiologic studies may take the form of case-control, prospective, nested case-control, or inter-

TABLE I

GENETIC FACTORS AND SUSCEPTIBILITY TO ENVIRONMENTAL AGENTS

High risk group or deficiency	Estimated carrier frequency (%)	Environmental agent(s)	References
Thalassaemias	2 to 7	Lead, benzene	7,8
Cystic fibrosis	5	Respiratory irritants	8,9
Glucuronyl transferase	—	Organic xenobiotics	8
Flavin monooxygenase	1	Amines (*N*-oxygenation)	10
Xeroderma pigmentosum	0.3	Light, genotoxics	8
Alzheimer	—	Aluminum?	11,12
Multifactorial genetic diseases (hypertension; coronary heart disease)	—	Lead, carbon disulfide (and PCBs?)	13

vention studies" [3]. The ability of molecular biology techniques to detect and quantitate induced changes that are permanent at the level of DNA makes them attractive tools in this essentially preventive strategy.

GENETIC SCREENING

With screening, a one-time test for each specific trait in an individual is required, while monitoring generally involves multiple tests over time of, for example, one worker or a group of workers. Current techniques usually involve direct amplification of the genomic DNA employing the polymerase chain reaction technique (PCR), followed by inspection of restriction enzyme-cut DNA ethidium bromide-stained gels; alternatively, allele-specific oligonucleotide probes (ASOs) can be used for any disorder for which the nucleotide sequence of the mutant and normal alleles are known [6,7].

Calabrese [8] suggests that approximately 50 human genetic conditions can potentially enhance peoples susceptibility to industrial pollutants. A small sampling is provided in Table I. It should be emphasized that this listing, or the more extensive tabulation provided by Calabrese [8], largely constitutes conjecture.

Genetic factors could also be protective. Individuals appear to have different capacities for P-450 mono-oxygenases induction, and from a pharmacokinetic perspective, different clearance rates of xenobiotics (providing toxic intermediates are not formed) [14]. Our own work on metallothionein mRNA and protein induction by cadmium in peripheral-blood human leukocytes suggests that variation in both basal and induced MT mRNA levels reflects environmental or experimental (intra-individual) and possibly

genetic (inter-individual) differences [15]. Induction capability appeared to differ by as much as a factor of 10 in 39 normal, non-smoking adult donors aged 20–40 years. Consequently, if metallothionein induction is protective for renal damage, genetic factors could exert a positive influence.

GENETIC MONITORING

Mendelsohn [16] describes a number of relatively new approaches employed in monitoring radiation workers. These may be divided into two distinct approaches that involve (1) screening a large number of cells for mutants with altered surface proteins or (2) selecting and cloning mutant cells [16,17]. The former approach for identifying somatic gene mutations is typified by the glycophorin A (GPA) assay involving allele-specific monoclonal antibodies and employing cytometry of erythrocytes for enumeration [18]. The well-known hypoxanthine (guanine) phosphoribosyltransferase (HPRT) system provides the most common mutant selection assay. A relative new approach is the human leukocyte antigen A (HLA-A) mutation assay [19]. As in the GPA assay, allele-specific antibodies to cell surface proteins are employed. By contrast, mutant cells are isolated by immunoselection, cloned and counted. Normal lymphocytes are therefore eliminated as in the HPRT assay. The nature of the mutant lesions can be identified by a combination of techniques such as restriction enzyme cleavage [6,7]; chemical mismatch cleavage [20,21]; DNA amplification (PCR), hybridization and sequencing [20,21]. For example, radiation-induced mutants have been shown to exhibit a large component of deletions [16].

Our own studies with AS52 Chinese hamster ovary cells [22] illustrate that the nature of DNA lesions in mutants may show some substance specificity. Typical results are presented in Table II. The experiment involved isolating individual mutant colonies generated in a standard mutagenicity assay by exposure to the compounds indicated, and selecting for resistance to 6-thioguanine [22]. The mutant colonies were clonally expanded to approximately $1–2 \times 10^6$ cells. Following washing, cells were lysed and 0.5–1 μg of mutant DNA was further amplified by PCR for 35 cycles [23]. Products were analyzed by electrophoresis on a 1% agarose gel and then subsequently stained with ethidium bromide. Two major bands resulted from DNA isolated from normal AS52 cells as previously noted [22]. Sequencing and restriction enzyme analysis showed that the smaller band (low relative molecular mass) is the stably integrated and functional bacterial xanthine-guanine phosphoribosyl transferase (*gpt*) gene. The larger band consists of *gpt*-coding sequences with a large insert of bacterial origin in the middle of the *gpt* gene. The PCR analysis of the mutants revealed four empirically distinct alterations at the *gpt* locus: (1) both PCR DNA bands

TABLE II

PCR ANALYSIS OF AS52 *gpt* MUTANTS

Compound	Mutants of total with *gpt* band deleted[a] (%)
EMS[b]	4
$PbSO_4$	16
Spontaneous	21
Ni_3S_2	25
$Ni(OH)_2$	59

[a]PCR analysis revealed three other empirically distinct alterations at the *gpt* locus (see text for details).
[b]EMS, ethylmethanesulphonate.

remain intact (interpreted as a point or frameshift mutation); (2) the smaller DNA band is deleted (i.e., corresponding to the functional *gpt* gene; these results are summarized in Table II); (3) both bands are deleted; (4) only the larger band is deleted (observed only for lead compounds). Collectively, this mutational analysis showed that the observed distribution of mutations was compound dependent. It is to be noted that the nickel compounds were weakly mutagenic in the mutation assays, while the mutation frequencies of the lead compounds were not raised above background.

Oncogene proteins are also showing promise as biomarkers in the molecular epidemiology of occupational carcinogenesis [24]. The most successful marker has been the increased expression of the p21 *ras* gene protein in tumour tissue, cytological specimens and serum. For example [25], in pneumoconiosis patients (36 with asbestosis; 10 with silicosis) 7/18 cancer patients were p21-positive *versus* 2/28 in non-cancer patients (P=0.012). There was some indication that this marker may be useful in early detection in a significant fraction of respiratory malignancies. In the same study, determination of the platelet-derived growth factor (PDGF) in serum indicated it may serve as a marker for the development of severe and progressive pneumoconioses.

CONCLUDING REMARKS

The ability to establish distributions of deletions and point mutations in well-defined loci that show some substance dependence is an exciting development for the molecular epidemiology of occupational and environmental cancers. Identification of gene or DNA locus deletions is gaining importance in the pathogenesis of cancer as it appears to constitute a primary mechanism for inactivating suppressor genes [26]; similarly, point

mutations appear prominent in converting proto-oncogenes to oncogenes [26]. The challenge in employing such biomarkers in early detection and in devising preventive strategies is considerable. Although techniques such as the HLA-A and GPA assays have been recommended as monitoring tools and seem effective for exposure to ionizing radiation and mutagenic chemicals [16,27–29], they are restricted to specific host genotypes. Similarly, the requirement of mutant selection limits the application of the HPRT protocol [30]. A potentially more versatile approach involves the detection of single base-pair mutations utilizing the mentioned chemical mismatch-cleavage analysis [20,21,31]. However, there are indications that limitations may exist in the specificity and sensitivity of this assay since the reactivity of mismatches appears dependent on sequence context [32]. Exploitation of components of mismatch-repair systems of prokaryotic or eukaryotic systems [33] offers some hope for improved base-pair mismatch detection. Regardless, a genetic monitoring or screening test needs to be proven valid (i.e., correct identification of true positive and true negative results) and reliable (i.e., reproducible by the same and other laboratories).

It is clear that cancer is a multistep process, perhaps requiring as many as 5–10 genetic alterations for malignant tumour development [26]. The identification of one early event within this genetic cascade need not be interpreted as definitive evidence for the development of a clinical tumour. There are also ethical and legal implications that must be fully addressed and considered before widespread genetic screening or monitoring is undertaken (e.g., privacy, confidentiality, potential discrimination and subject health [2]). Routine application in monitoring environmental or occupational genotoxic exposures is therefore some years away. Environmental monitoring using non-human subjects is more feasible in the short term.

ACKNOWLEDGEMENT

Our appreciation is extended to Wang-Ping Li and Glenn G. Fletcher for technical assistance. Financial support from the International Lead Zinc Research Organization, Inc., Research Triangle Park, NC and the Ontario Workplace Health and Safety Agency, Toronto, ON, is grateful acknowledged.

REFERENCES

1 Federation of American Societies of Experimental Biology (1991) The human genome initiative. FASEB J. 5 (1), 1–78.
2 Office of Technology Assessment (1990). Summary, Genetic Monitoring and Screening in the Workplace, Report OTA-BA-456. Washington: Congress of the United States.
3 Perera, F.P. (1987) Molecular cancer epidemiology: a new tool in cancer prevention. JNCI 78, 887–898.

4 Henderson, R.F., Bechtold, W.E., Bond, J.A. and Sun, J.D. (1989) The use of biological markers in toxicology. Crit. Rev. Toxicol. 20, 65–82.
5 Cullen, M.R. (1989) The role of clinical investigations in biological markers research. Environ. Res. 50, 1–10.
6 Watson, J.D., Gilman, M., Witkowski, J. and Zoller, M. (1992) Recombinant DNA, 2nd Ed., Freeman, New York.
7 Weatherall, D.J. (1991) The New Genetics and Clinical Practice, 3rd Ed. Oxford University Press, Oxford.
8 Calabrese, E.J. (1986) Ecogenetics: historical foundation and current status. J. Occup. Med. 28, 1096–1102.
9 Rommens, J.M., Iannuzzi, M.C., Kerem, B.-S., Drumm, M.L. et al. (1989) Identification of the cystic fibrosis gene: chromosome walking and jumping. Science 245, 1059–1065.
10 Al-Waiz, M., Ayesh, R., Mitchell, S.C., Idle, J.R. and Smith, R.L. (1987) A genetic polymorphism of the *N*-oxidation of trimethylamine in humans. Clin. Pharmacol. Ther. 42, 588–594.
11 Selkoe, D.J. (1991) Amyloid protein and Alzheimer's disease. Sci. Amer. 265 (Nov), 68–78.
12 Orme, J. and Ohanian, E.V. (1990) Assessing the health risks of aluminum. Environ. Geochem. Health. 12, 55–58.
13 Wilson, J.D., Braunwald, E., Isselbacher, K.J., Petersdorf, R.G. et al. (1991) Harrison's Principles of Internal Medicine, 12th Ed., Vol. 1. McGraw-Hill, New York, pp. 21–92.
14 Nebert, D.W. (1989) The *Ah* locus: genetic differences in toxicity, cancer, mutation, and birth defects. Crit. Rev. Toxicol. 20, 153–174.
15 Harley, C.B., Menon, C.R., Rachubinski, R.A. and Nieboer, E. (1989) Metallothionein mRNA and protein induction by cadmium in peripheral-blood leucocytes. Biochem. J. 262, 873–879.
16 Mendelsohn, M.L. (1990) New approaches for biological monitoring of radiation workers. Health Physics 59, 23–28.
17 Compton, P.J.E., Hooper, K. and Smith, M.T. (1991) Human somatic mutation assays as biomarkers of carcinogenesis. Environ. Health Perspect. 94, 135–141.
18 Langlois, R.G., Nisbet, B.A., Bigbee, W.L., Ridinger, D.N. and Jensen, R.H. (1990) An improved flow cytometric assay for somatic mutations at the glycophorin A locus in humans. Cytometry 11, 513–521.
19 McCarron, M.A., Kutlaca, A. and Morley, A.A. (1989) The HLA-A mutation assay: improved technique and normal results. Mut. Res. 225, 189–193.
20 Cotton, R.G.H., Rodrigues, N.R. and Campbell, R.D. (1988) Reactivity of cytosine and thymine in single-base-pair mismatches with hydroxylamine and osmium tetroxide and its application to the study of mutations. Proc. Natl. Acad. Sci. USA 85, 4397–4401.
21 Tindall, K.R. and Whitaker, R.A. (1991) Rapid localization of point mutations in PCR products by chemical (HOT) modification. Environ. Mol. Mutagen. 18, 231–238.
22 Tindall, K.R. and Stankowski, Jr. L.F. (1989) Molecular analysis of spontaneous mutations at the *gpt* locus in Chinese hamster ovary (AS52) cells. Mut. Res. 220, 241–253.
23 Oste, C. (1988) Polymerase chain reaction. Biotechniques 6, 162–167.
24 Brandt-Rauf, P.W. (1991) Oncogene proteins as biomarkers in the molecular epidemiology of occupational carcinogenesis. The example of the *ras* oncogene-encoded p21 protein. Int. Arch. Occup. Environ. Health 63, 1–8.
25 Brandt-Rauf, P.W., Smith, S., Hemminki, K., Koskinen, H., Vainio, H., Niman, H. and Ford, J. (1992) Serum oncoproteins and growth factors in asbestosis and silicosis patients. Int. J. Cancer 50, 881–885.
26 Cooper, G.M. (1990) Oncogenes. Jones and Bartlett, Boston.
27 Langlois, R.G., Bigbee, W.L. and Jensen, R.H. (1990) The glycophorin A assay for somatic cell mutations in humans. Prog. Clin. Biol. Res. 340C, 47–56.
28 Jensen, R.H., Grant, S.G., Langlois, R.G. and Bigbee, W.L. (1991) Somatic cell genotoxicity at the glycophorin A locus in humans. Prog. Clin. Biol. Res. 372, 329–339.
29 Grist, S.A., McCarron, M., Kutlaca, A., Turner, D.R. and Morley, A.A. (1992) In vivo

human somatic mutation: frequency and spectrum with age. Mut. Res. 266, 189–196.
30 Ostrosky-Wegman, P., Montero, R., Palao, A., Cortinas de Nava, C., Hurtado, F. and Albertini, R.J. (1990) 6-Thioguanine-resistant T-lymphocyte autoradiographic assay. Determination of variation frequencies in individuals suspected of radiation exposure. Mut. Res. 232, 49–56.
31 Grompe, M., Muzny, D.M. and Caskey, C.T. (1989) Scanning detection of mutations in human ornithine transcarbamoylase by chemical mismatch cleavage. Proc. Natl. Acad. Sci. USA 86, 5888–5892.
32 Bhattacharyya, A. and Lilley, D.M.J. (1989) Single base mismatches in DNA long- and short-range structure probed by analysis of axis trajectory and local chemical reactivity. J. Mol. Biol. 209, 583–587.
33 Grilley, M., Holmes, J., Yashar, B. and Modrich, P. (1990) Mechanisms of DNA-mismatch correction. Mut. Res. 236, 253–267.

The Interaction of Metal Ions With Synthetic DNA: Induction of Conformational and Structural Transitions

Franco E. Rossetto and Evert Nieboer

Department of Biochemistry, McMaster University, Hamilton, Ontario, Canada

ABSTRACT

The propensity of a large number of metal ions to induce cooperative conformational or structural transitions in double-stranded poly d(G-C) was assessed primarily by UV and CD spectrometry. This ability was seen to be an intrinsic property of most metal ions. The observed (metal ion)/(polydeoxynucleotide) mole ratio calculated per G-C base pair and corresponding to the midpoints of the principal transition ranged from 0.3 (Ag(II)) to 100 (Al(III)). A strong correlation was seen [$y = -1.01(\log x) + 3.26$, $r = 0.95$, $n = 20$] between the (metal ion)/(poly d(G-C)) mole ratio required for the transition midpoint (x) and a covalent index to complex stability (y) of the metal ions. This relationship was independent of the types of transitions observed (monophasic or biphasic) or of specific conformations (e.g., B, Z, ψ). The y index measures the ability of metal ions to bind to nitrogen and/or sulphur donor atoms in ligands compared to oxygen centers; equilibrium analysis indicates that the mole-ratio x decreases with increasing affinity of metal ions for poly d(G-C). Thus the observed relationship suggests that base-nitrogen binding facilitates the induced transitions. In general, metal ions designated as *Class B* or nitrogen/sulphur seeking (Ag(I), Hg(II), and Ru(III)) induced monophasic transitions, whereas *Class A* or oxygen seeking ions (La(III), Ce(III), Tb(III), Dy(III)) induced biphasic transitions. Transitions generated by ions of more ambivalent ligand preference (*Borderline* ions) were either monophasic (Mn(II), Fe(III), Cu(II), Cd(II), In(III), and Pb(II)) or biphasic (Cr(III), Co(II), Ni(II) and Zn(II)). Poorly defined transition-curve profiles were observed for Pt(II), Pd(II), and Al(III). Specific conformational assignments were made for some of the observed transitions. For a limited number of metal ions (Ni(II), Cu(II), Cd(II), Ag(I), Hg(II)), interaction with calf thymus DNA was similarly examined. In these instances, the susceptibility to DNase I digestion of both the DNA and polydeoxynucleotide complexes was assessed.

ABBREVIATIONS

AA, atomic absorption spectrometry; cis-Pt(II), cis-diamminedichloroplatinum(II); CD, circular dichroism; DDW, doubly-deionized distilled water; dien, diethylenetriamine; DNase I, deoxyri-

Address reprint requests and correspondence to: Evert Nieboer, Department of Biochemistry, McMaster University, 1200 Main Street West, Hamilton, Ontario, Canada, L8N 3Z5.

© 1993 Elsevier Science Publishing Co., Inc., 655 Avenue of the Americas, NY, NY 10010 0162-0134/93/$6.00

bonuclease I; EtBr, ethidium bromide; en, ethylenediamine; HEPES, 4-(2-hydroxyethyl)-1-piperazineethanesulfonic acid; Ln(III), general symbol for trivalent lanthanide ions; NMR, nuclear magnetic resonance spectrometry; poly d(G-C), the duplex DNA polymer with repeating deoxyguanylate (G) and deoxycytidylate (C) residues in both complementary strands; poly d(G-m^{5}C), poly d(G-C) with the cytosines methylated at the C-5 position.

INTRODUCTION

DNA is now known to exist as a diverse and dynamic array of helical and higher-order structures. The most common conformations are the right-handed A, B, C types, and the left-handed Z type [1–3]. Values of helical parameters such as helical twist, rise per base pair, base inclination, propeller twist, and base roll indicate that within these helical families resides a degree of structural flexibility [2]. Transitions between helical conformations are facilitated by mono- and divalent ions [4–10], changes in helix hydration [11, 12], or a combination of both [13–15]. More specific conditions for generating left-hand Z helices include base alkylation, binding of known organic carcinogens, and insertion of appropriate nucleotide sequences into regions of supercoiling (reviewed in [3]).

In addition to simple helices, DNA can adopt a number of higher-order structures in the presence of multivalent cations (e.g., di- and trivalent metals, spermidine^{3+}), neutral or anionic polymers, and/or organic cosolvents. These structures consist of inter- or intramolecularly collapsed, condensed or aggregated DNA molecules (toroids, rods, spheres), some of which may be devoid of helical content. The most widely examined is the ψ-form of DNA [16–23], although the P, H, and H* forms have posed a special experimental challenge [24–28].

Common to both helical and tertiary or quaternary structural transitions is the ability of metal ions to participate in such processes. We have investigated the ability of metals to promote conformational transitions in poly d(G-C). As an index of structural alterations, we have employed CD and UV spectrometry. The former is a sensitive indicator of DNA structure and has been utilized extensively (for theoretical considerations, see [29]). Nucleic acids absorb light in the far UV region with an ϵ_{max} at approximately 260 nm. This absorption is due to π-π^* transitions (and to a lesser extend n-π^* transitions in the high-wavelength tail of the absorption spectrum) of the electrons of the purine and pyrimidine rings. Base stacking and hydrogen bonding within the double helix result in a pronounced decrease in absorption intensity (hypochromism) in comparison to the random-coil form [30]. Certain alterations in DNA conformation or structure are reflected as hyper- or hypochromic and/or red-bathochromic shifts in UV spectra as observed for Z-DNA (reviewed in [3, 31]) or metal induced ψ-DNA [18, 32, 33]. In order to monitor changes at the ϵ_{max} and in the far UV tail of the spectra, we have measured differences in the quotient of absorbances at 295 nm and 260 nm (A295/260; referred to as the absorbance ratio). This spectral ratio is sensitive to changes in UV spectra resulting from alterations in DNA conformation or structure. It has been employed previously in studies of the B → Z transition (reviewed in [3]) and has been found to correlate with the corresponding CD data [6, 14, 23].

We have surveyed twenty metal ions in an effort to identify and characterize their propensity to induce alternate conformational or structural states in poly

d(G-C). In addition, the ability of metals to bind to DNA has been correlated with their proclivity in facilitating altered conformations or structures.

MATERIALS AND METHODS

DNA and Related Chemicals

Poly d(G-C) as purchased from Pharmacia P-L Biochemicals and calf thymus DNA from Sigma Chemicals. Both were dissolved in phosphate buffer (10 mM, pH 7.6) or HEPES buffer (10 mM, pH 7.6). Quantification of these solutions was achieved utilizing a molar absorptivity (ϵ) at 255 nm of 8400 M^{-1} cm^{-1} for poly d(G-C) and at 260 nm of 6000 M^{-1} cm^{-1} for calf thymus DNA [34]. Deoxyribonuclease I from Sigma Chemical Co. was dissolved in 25 mM $MgSO_4$ (BDH Chemical Co., analytical grade) to a final concentration of 90 μg/ml. Ethidium bromide (0.5 μg/ml; Sigma Chemical Co.) was made up in a phosphate (20 mM)/EDTA (0.5 mM) buffer at pH 11.8.

Metal Salts

All metal salts were of analytical or reagent grade. $MnCl_2 \cdot 4H_2O$, $Co(NO_3)_2 \cdot 6H_2O$, $Pb(NO_3)_2$, $Cd(NO_3)_2 \cdot 4H_2O$, $Ni(NO_3)_2 \cdot 6H_2O$, $Cu(NO_3)_2 \cdot 3H_2O$, $HgCl_2$, $Hg(NO_3)_2 \cdot xH_2O$, $AgNO_3$, $FeCl_3 \cdot 6H_2O$, $Zn(NO_3)_2 \cdot 6H_2O$, $Ce_2(SO_4)_3 \cdot H_2O$, $Al_2(SO_4)_3 \cdot 16H_2O$ were purchased from BDH Chemical Co.; $PdCl_2$, $RuCl_3 \cdot 3H_2O$, $Cr(C_2H_3O_2)_3 \cdot H_2O$ from Fisher Chemical; $In(CH_2H_3O_2)_3$ from Research Organic/Inorganic Chemical Corp.; La_2O_3 from Sigma Chemical; $DyCl_3$, $TbCl_3$ from ICN Pharmaceuticals; $(NH_4)_2PtCl_4$ from Johnson Matthew Inc.; and $CeCl_3 \cdot xH_2O$, $Ce(NO_3)_3 \cdot 6H_2O$ from Alfa Products. The metal salts were dissolved in DDW and adjusted to pH 1–2 with the appropriate acid (HNO_3, HCl, or acetic). This was done to prevent the formation of stable metal hydroxides [35]. La_2O_3 was initially dissolved with gentle heating in 15 mM HCl. All acids were of Ultrex grade (J.T. Baker Chemical Co.) or A.C.S. grade (Fisher Chemical Co.). Prior to use, these stock solutions were diluted with DDW to appropriate working concentrations. These working solutions were of sufficiently low acidity so as not to alter the pH of the buffer employed in the poly d(G-C) studies. For those metal salts with an undetermined number of waters of hydration (i.e., x), the elemental composition provided on the product data sheet was employed to calculate the metal-ion concentration of stock solutions.

Conformational Transitions

To 500 μl of poly d(G-C) (or calf thymus DNA) appropriate volumes of metal working solutions were added. The total volumes of poly d(G-C) and metal solutions did not exceed 750 μl. The mixture was incubated at 37°C for 2.5 hr. Conformational transitions were monitored by measuring the UV absorbance at 295 nm and 260 nm. This was measured on a Perkin-Elmer Lamba 3B UV/VIS spectrometer using 1 cm quartz cuvettes. Complete spectra (230–350 nm) were recorded for all additions of Ag(I), Hg(II), and Ni(II) with both DNA samples. For the metal ions Pt(II), Pd(II), Ru(III), and Fe(III), poly d(G-C) in phosphate buffer (10 mM, pH 7.6) was employed. For all other metal ions the poly d(G-C) was dissolved in HEPES buffer (10 mM, pH 7.6). Background absorbances of the metal ions were obtained by adding the appropriate aliquots of metal working solutions to sample-matched volumes of DDW in the case of Pt(II),

Pd(II), Ru(III), Fe(III), Pb(II), or of HEPES buffer (all other metal ions). Background corrections were significant for Al(III), Ce(III), Cr(III), Cu(II), Fe(III), In(III), Pd(II), Pt(II), and Ru(III). Circular dichroism experiments were performed on an $AVIV_R$ circular dichroism spectropolarimeter in the 350 nm–230 nm spectral region at room temperature with 1-cm quartz cuvettes for the Ag(I), Al(III), Cu(II), Hg(II), Ni(II), Pt(II), and Zn(II) complexes of poly d(G-C). The CD spectral data were stored and manipulated on an IBM PC Sr. computer. Calculated mole ratios refer to the moles of metal ions added per mole of G-C base pair (or calf thymus DNA base pair).

Deoxyribonuclease I Digestions

Aliquots (250 μl) of metal-poly d(G-C) or calf thymus DNA complexes of Ni^{2+}, Cu^{2+}, Cd^{2+}, Ag^{+}, and Hg^{2+} were digested with 10 μl of DNase I at ambient temperature (c. 23°C) for 1 hr. Reactions were terminated by the addition of 10 μl of 0.5 M EDTA, resulting in the chelation of all metal ions present in solution. To 25 μl of digested or undigested sample, 2 ml of EtBr solution was added and the fluorescence was assessed with a Sequoia Turner spectrofluorometer model 450 at an excitation wavelength of 525 nm and emission at 600 nm.

RESULTS

Overview of Spectrometric Data

Two major types of metal-ion induced cooperative conformational transitions were observed. The first is monophasic in nature, whereas the second type is biphasic. Of the metal ions tested, Ni(II), Co(II), Cr(III), La(III), Dy(III), Ce(III), Tb(III), and Zn(II) gave biphasic transition curves. Simple monophasic transition curves (designated as *Type I* Monophasic) were observed for the metal ions Ag(I), Cu(II), Fe(III), Ru(III), Cd(II), and Mn(II). Although the transition curves observed for the group Hg(II), Pb(II), and In(III), as well as for the group Al(III), Pt(II), and Pd(II), appeared to be monophasic, they were interpreted to consist of overlapping phases; respectively, they are designated as *Type II* and *Type III* Monophasic. It is important to note that these designations of transition types are empirical, stemming from the inspection of spectral ratio data, analysis of CD spectra, and in some instances DNase I digestion profiles. In the case of ions which have significant background absorbances at 260 nm or 295 nm in the absence of DNA polymer, improper background compensation might contribute some uncertainty to the UV spectral measurements.

Biphasic Transition

The distinctive feature of the biphasic transitions is the pretransition plateau seen at an absorbance ratio of 0.20 ± 0.03 ($x \pm$ sd, corresponding to seven metals each assessed in duplicate; Ni(II), Co(II), Cr(III), Lu(III), Py(III), Ce(III), and Tb(III)). As previously reported for Co(II) and Ni(II), this is suggestive of the formation of a stable DNA-cation complex whose conformation serves as an intermediate in the B → Z transition of poly d(G-C) [6, 15, 36, 37]. As is evident from the transition curves (Fig. 1A), the formation of this intermediate conformation is well-defined and occurs over relatively narrow (metal ion)/(poly

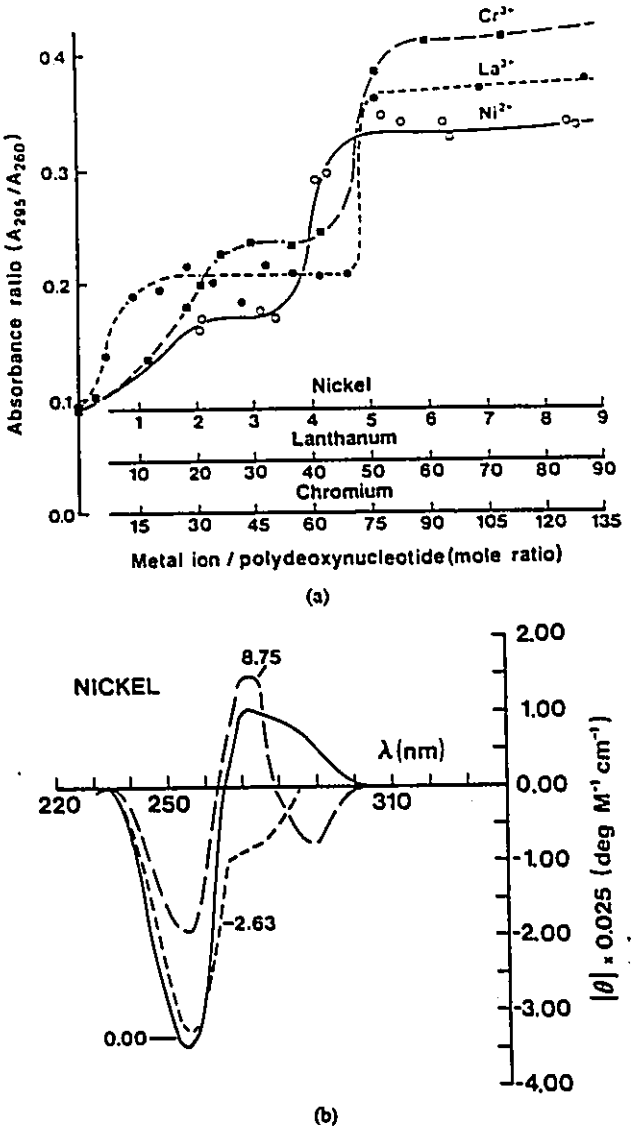

FIGURE 1. Biphasic transitions. (A) A representative selection of biphasic transition curves. Each sample contained approximately 13 nmols of poly d(G-C) in the presence of appropriate moles of metal ion. The final volume of the mixture was from 0.50 to 0.75 ml. Incubation was for 2.5 hr at 37°C. (B) CD spectra of poly d(G-C) in the presence of increasing amounts of Ni(II). Each sample contained approximately 80 nmoles of poly d(G-C) and the appropriate moles of metal ion in a total volume of 3.0 ml. Incubation was for 2.5 h at 37°C. The numbers adjacent to the spectra denote Ni(II)/poly d(G-C) mole ratios.

d(G-C)) mole ratios. Further addition of metal results in a rapid increase in absorbance ratio to a plateau of approximately 0.35 ± 0.03 indicative of a cooperative transition to a new conformation.

The CD spectra depicting the interaction of varying amounts of Ni(II) with poly d(G-C) are presented in Figure 1B. The initial addition of Ni(II) to poly d(G-C) results in the loss of the positive signal peak at 275 nm and the concomitant development of a very small negative shoulder at this wavelength. It is this conformation of poly d(G-C) which corresponds to the pretransitional plateau seen in the biphasic transition curves and is highly reminiscent of the C-conformer of DNA [1, 5]. At higher levels of Ni(II), the CD spectrum is inverted with a positive maximum at 270 nm and a negative signal at 287 nm and these characteristics are consistent with those observed for Z-conformations induced by a number of metal ions (e.g., Mg(II), Mn(II), Co(II), Ni(II)), as previously reported [6, 14, 15, 37, 38].

Additional evidence for the assignment of the Z-conformation to the final transition product is presented for Ni(II) in Figure 2. The insensitivity of Z-DNA to DNase I digestion has been documented [39]. By contrast to poly d(G-C), calf thymus DNA does not yield an absorbance ratio transition curve, nor is protection rendered to DNase I activity. For poly d(G-C), the absorbance ratio and DNase I digestion yield complementary transition curves. It is obvious that the pretransition C-form is also sensitive to DNase I digestion.

For zinc, absorbance ratio values for the major transition plateau were unusually low (0.24 ± 0.02, $N = 2$), as was that for the pretransition (0.12 ± 0.01, $N = 2$; data not shown). The magnitude of the former ratio (and its corresponding CD spectra) resembles that of the pretransition C-DNA plateau previously discussed, suggesting that Zn(II) does not induce the Z-conformation. Zinc complexes have been demonstrated to be efficient inducers of Z-conformers [7]. Somewhat surprisingly, the amount of Zn(II) ion reported to facilitate the $B \rightarrow Z$ transition was approximately fourfold less than that used in the present study.

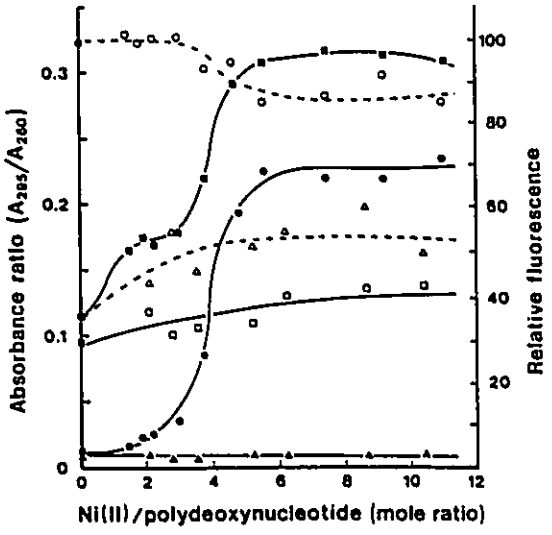

FIGURE 2. Differential effects of nickel(II) on poly d(G-C) and calf thymus DNA. A conformational transition is clearly evident for poly d(G-C) but is absent for calf thymus DNA: compare ■--■ with □--□ (absorbance ratio data), and ●-●-● with ▲-▲-▲ (EtBr fluorescence after DNase-I digestion). For comparison, the fluorescence of undigested poly d(G-C), O-O-O, and calf thymus DNA, △-△-△, are also shown. Experimental details are given in the text.

The transitions induced by the lanthanide metals are distinguished from the other biphasic transitions by their protracted pretransition plateau (e.g., La^{3+} in Fig. 1). Otherwise, no discrepancies exist except for Ce(III). For this metal, the absorbance ratio corresponding to the second plateau had a value of 0.6. The background contribution to the measured absorbance of Ce(III)-DNA complex formation may account for this enhancement. The ability of Tb(III) to induce Z-conformations has been verified by CD [40] and that of Eu(III) by differential pulse polarography [41]. From the work presented here (and discussed below) and reviewed above, we conclude that for Ni(II), Co(II), Cr(III) (and possibly Zn(II)) the absorbance ratio data depict a B → C → Z conformational transition. For the lesser characterized Ln(III) metals, a similar sequence of transitions is tentatively assigned.

Type I Monophasic Transitions. For monophasic transitions, the increase of metal-ion interaction with poly d(G-C) results in a sharp, cooperative transition devoid of any discernible intermediate (Fig. 3). As observed in the biphasic transitions, a plateau in absorbance ratio is observed at 0.35 ± 0.03 ($\bar{x} \pm$ sd, corresponding to six metals each assessed in duplicate; Ag(I), Cu(II), Fe(III), Ru(III), Cd(II), and Mn(II)). By comparison to the previously characterized Mn(II) systems [6, 15], the posttransitional plateaus for Mn(II) and Cd(II) probably correspond to a Z-type conformation. In the latter case, DNase I digestion analysis corroborates this conclusion (data not shown). Over the experimental range of mole-ratio values, Cd(II) did not alter the A(295 nm)/A(260 nm) ratio of claf thymus DNA, nor did it protect the latter against DNase I digestion. A definitive assignment of conformation to the plateau regions for Ru(III) and Fe(III) is impossible strictly from absorbance data, although recent reports suggest a similar outcome for these two metals. Trivalent complexes of other Group VIIIB metals (including rhodium and ruthenium) are capable of inducing transitions to the Z conformer [42–44].

The analysis of the UV spectral and CD data of the Ag(I)-poly d(G-C) interaction pose a more challenging interpretation. Figure 3A depicts the absorbance ratio data and Figure 3B the CD spectra. The absorbance ratio data in this figure is typical of the other *Type I* monophasic transitions observed. For the Ag(I) data points in Figure 3A, the UV-absorption spectral changes were similar to those observed and reported for Z-transitions and quite distinct from those observed for calf thymus DNA by ourselves and others [32, 33, 45]. In addition, the transition curve depicted in Figure 3A was reproduced exactly by DNase I digestion. Ag(I) did not render calf thymus DNA digestion resistant, although the Ag(I) addition did result in a small but systematic increase in the A(295 nm)/A(260 nm) ratio. By contrast, the CD spectrum of Ag(I) suggests a transition to a form that is not a simple Z-conformer. The interaction of poly d(G-C) with low amounts of Ag(I) results in a CD spectrum similar to that of the parent B-conformation, but with some notable differences. The amplitude of the negative signal at 250 nm has increased and an additional positive signal at 290 nm is evident (Fig. 3B). Further addition of Ag(I) results in a nonconservative CD spectrum with some characteristics of a condensed ψ-form [17, 18, 22, 46]. Thus a small positive peak is seen at 300 nm; the negative signal at 250 nm has also increased in magnitude, and a very large negative maximum has appeared at 275 nm. This latter negative peak is also reminiscent of ψ-DNA.

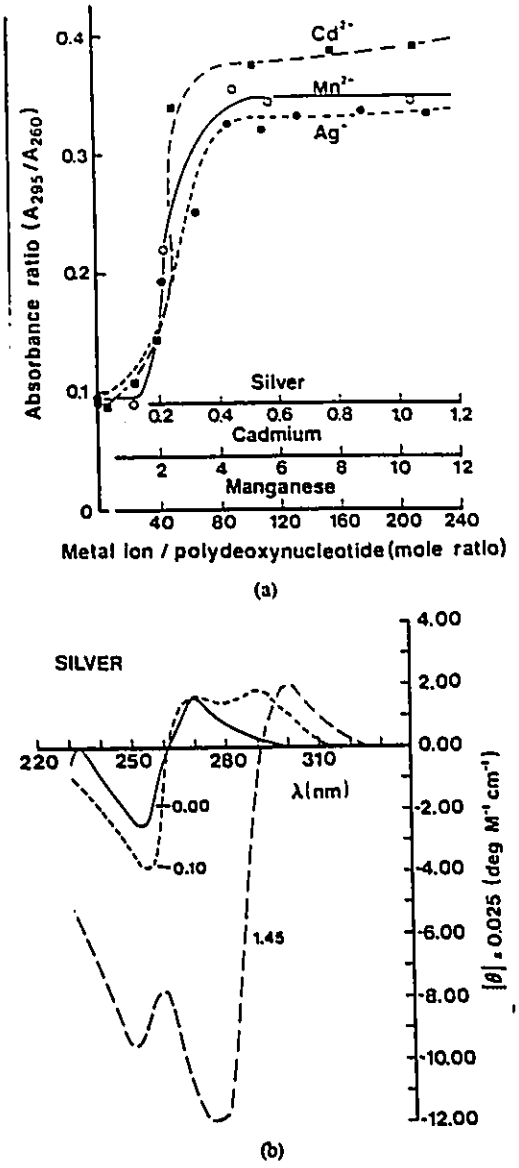

FIGURE 3. Type I monophasic transitions. (A) A representative selection of Type I monophasic transition curves. The experimental protocol is outlined in the legend to Figure 1A. (B) CD spectra of poly d(G-C) in the presence of increasing amounts of Ag(I). The experimental protocol is outlined in the legend to Figure 1B. The numbers adjacent to the spectra denote Ag(I)/poly d(G-C) mole ratios.

The interaction of Ag(I) ion with DNA (in particular calf thymus DNA) is well documented. Three distinct complexes are formed (I, II, and III) with progressively higher amounts of Ag(I) ion [32, 33, 45, 47, 48]. CD analysis of Complexes I and II of Ag(I) with calf thymus DNA is helpful in interpreting the spectra in Figure 3B [45]. Complex I occurs at low ratios of Ag(I) to DNA (≤ 0.3 mole ratio) and its CD spectrum is typified by a distinct negative peak at 250 nm, a negative shoulder at 265 nm, and a small positive peak at 290 nm [45]. The CD negative spectra depicted in Figure 3B for the interaction of poly d(G-C) with analogous levels of Ag(I) are similar, except for the negative shoulder at 265 nm which is replaced by a positive signal. At higher Ag(I) levels (Complex II for calf

thymus DNA; mole ratio 0.3 to 2.0), the CD traces again demonstrate extensive similarities with minor differences [45]. Based on a variety of experimental data, Complex I has been assigned a modified B-conformation, while Complex II reflects a novel conformation in which both base-pair tilt and roll differ substantially from that seen in the B-conformation and which is unlike DNA aggregation or the ψ-conformation [45, 47, 48]. Utilizing infrared spectroscopy, it has been demonstrated that comparable levels of Ag(I) ion interacting with poly d(G-C)·poly d(G-C) induce a B-family conformer somewhat distinct from the B-family structure of the Complex I of Ag(I) with calf thymus DNA [49].

For Cu(II), the sharp absorbance ratio transition curve could also be reproduced by the DNase I digestion susceptibility protocol. However, in this case Cu(II) also protected calf thymus DNA, although a 4-fold greater (metal ion)/(DNA) mole ratio was required to elicit the same result. CD spectra pertaining to plateau levels of Cu(II)-poly d(G-C) are reminiscent of Ag(I)-DNA at plateau mole ratios (see Fig. 3B; negative peak at 250 nm, larger negative peak at 275 nm, small positive peak at 300 nm), although peak amplitudes are not as pronounced (data not shown). This is consistent with alternate B-type conformations observed in calf thymus DNA following interaction with comparable mole ratios of Cu(II) ion [50]. Collectively, the Ag(I) and Cu(II) data suggest that distinct right-handed helical structures or variants of the B-type family occur which differ from defined DNA aggregates or ψ-DNA.

Type II and Type III Monophasic Transitions. Type II Transitions constitute a minor variation of the monophasic curve previously discussed, and is typical of In(III), Hg(II), and Pb(II) (Fig. 4A). In all cases transitions are sharp, but the posttransitional absorbance ratio plateaus were elevated from the anticipated value (0.35 ± 0.03) to values of 0.66 ± 0.07 ($x \pm$ sd, the 3 metals each assessed in duplicate). Of the metal ions for which transition curves are depicted in Figure 4A, Hg(II) was studied in considerable detail. The response of the poly d(G-C) system was identical to that of calf thymus DNA. Thus, these two DNA forms exhibit similar changes in the UV-absorption spectra, portray identical transition curves, have nonconservative CD spectra, and the transition curves can be reproduced by DNase I digestion as depicted for Ni(II) in Figure 4B.

The UV absorption spectra of both poly d(G-C) and calf thymus DNA suggest the formation of an initial conformer (characterized by ϵ_{max} at 260 nm; data not shown) for additions up to one-half base pair equivalent of Hg(II). Further additions result in the generation of a new form (ϵ_{max} at 290 nm; data not shown). CD spectra of Hg(II)-poly d(G-C) corroborate this conclusion. At low levels of Hg(II), poly d(G-C) exhibits a spectrum similar to native B-DNA but with an increased negative amplitude at 250 nm and an additional positive signal at 280 nm (Fig. 4B). Higher levels of Hg(II) (approximately one base pair equivalent of Hg(II)) induce a large negative signal at 280 nm; further increases induce a shift of this signal to 290 nm followed by a decrease in signal intensity. When viewed in context with the Ag(I) and Cu(II) results (e.g., Fig. 3), these data suggest that Hg(II) initially induces a B-variant form which subsequently undergoes additional conformational change(s). Similar results with Hg(II)-calf thymus DNA suggesting B-variant form(s) of DNA have also previously been reported [18]. (Interestingly, these latter transitions may also encompass some Z-variant conformations of Hg(II)-poly d(G-C) as previously documented utiliz-

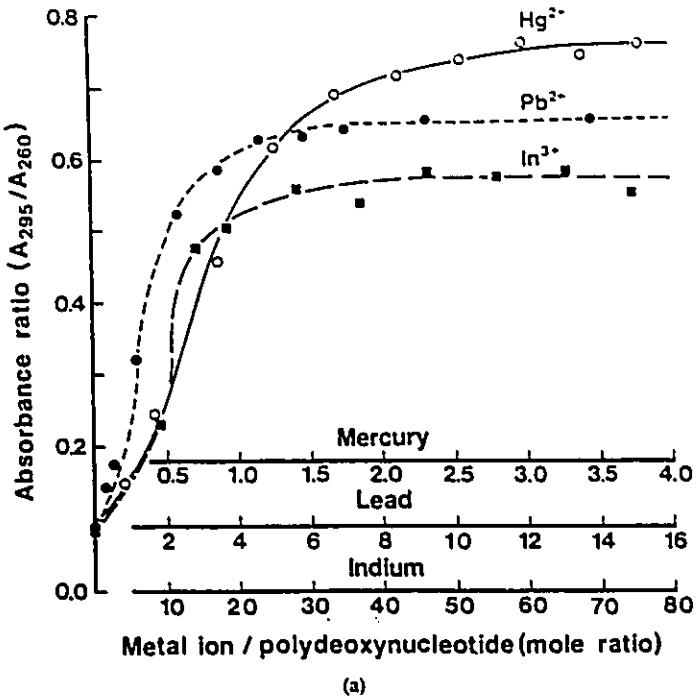

(a)

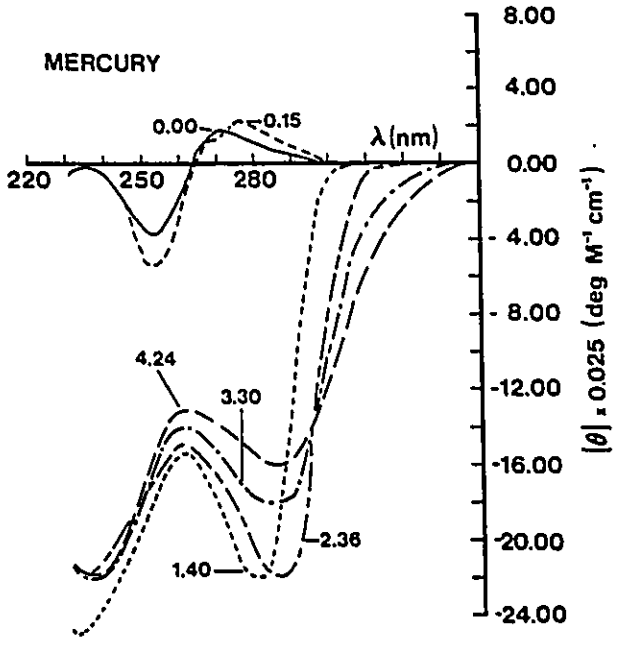

(b)

FIGURE 4. Type II monophasic transitions. (A) Type II monophasic transitions. The experimental protocol is outlined in the legend to Figure 1A. (B) CD spectra of poly d(G-C) in the presence of increasing amounts of Hg(II). The experimental protocol is outlined in the legend to Figure 1B. The numbers adjacent to the spectra denote Hg(II)/poly d(G-C) mole ratios.

ing infrared spectroscopy [51].) Although CD spectra are not available for both Pb(II)- and In(III)-poly d(G-C), extreme hyperchromism at both wavelengths (260 nm and 290 nm) in the UV spectra may reflect underlying conformational changes resulting from interaction with these metal ions.

The transition curves obtained with the three cations Al(III), Pt(II), and Pd(II) lack a sharp transition and are therefore ill-defined (Fig. 5). They are designated as *Type III* Monophasic transitions. All three are quite similar in nature, with absorbance ratio plateaus of approximately 0.50 for the Al(III) curve and 0.70 for both Pd(II) and Pt(II). These transition profiles suggest that the mechanism involved in this phase transition is different from those seen for the *Type I* and *Type II* monophasic and the biphasic transitions.

The characterization of the interaction of cis-Pt(II) with poly d(G-m^5 C) in a B- or Z-conformation seems relevant to the discussion of our data [8]. The interaction of cis-Pt(II) with poly d(G-m^5 C) in a B-conformation is different from the mode of attachment of this molecule with poly d(G-m^5 C) already in a Z-conformation. In the former case, the main adduct is bidentate in nature and seems to arise from the intrastrand cross-linkage between two guanine residues separated by a cytosine. The product of this interaction is thought to be a distorted Z-helical conformation and is characterized by a low-intensity CD spectrum with positive peaks at 230 nm and 275 nm and a small negative peak at 300 nm. Cis-Pt(II) interaction with the Pt(II)-free Z-conformer of poly d(G-m^5

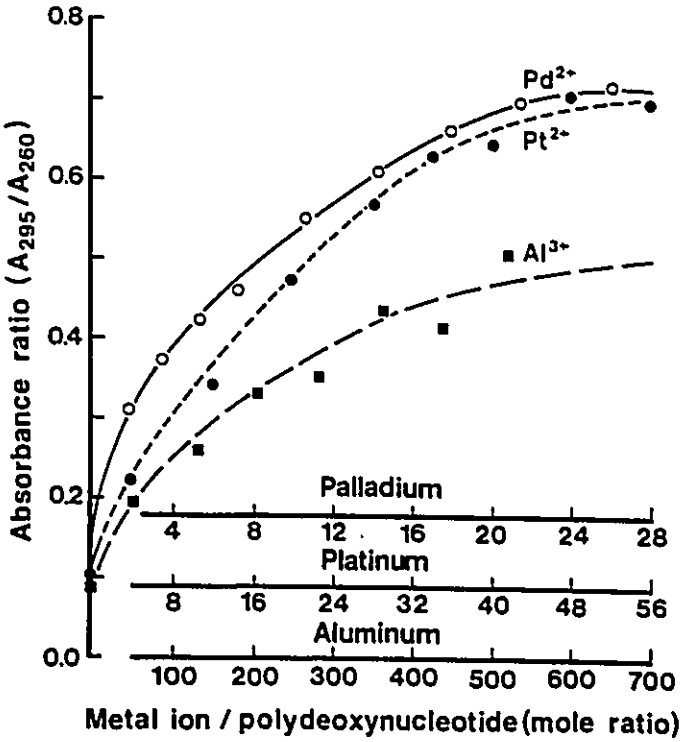

FIGURE 5. Changes in the absorbance ratio induced by Al(III), Pt(II), and Pd(II); designated as Type III monophasic transitions. The experimental protocol is described in the legend to Figure 1A.

C) resulted in the formation of monodentate Z-type adduct (characterized by a much stronger negative band at 297 nm in the CD spectrum). Heating of this adduct generated the bidentate cis-Pt(II) distorted Z-conformer. Our CD data do not support a similar interpretation for the transition induced by $PtCl_4^{2-}$. As $PtCl_4^{2-}$ interacts with poly d(G-C), distinct changes occur in the CD spectra (data not shown). For the initial additions (mole ratio < 20), the alterations were qualitatively similar to those for low Ag(I) and Hg(II): increased negative intensity occurred at 250 nm and increased positive intensity at > 260 nm (compare to Figs. 3B and 4B). Subsequent additions resulted in loss in area of the 250 nm negative band. These CD features are reminiscent of the interaction of cis-Pt(II) with DNA of various sources [52].

There is strong independent evidence that the reaction of $(NH_4)_2PtCl_4$ (or K_2PtCl_4) with polydeoxynucleotides is determined by the potential of three of its chloride ligands to be displaced [53–55]. Consequently, the observed stoichiometry of Pt bound to DNA is determined by the number of chloride leaving groups [56]. This is strong evidence that the reactivity of Pt(II) increases with the number of labile ligands in its coordination sphere. Our CD results for $(NH_4)_2PtCl_4$ when combined with the analytical data of Macquet and Theophanides [56] suggest that the Pt(II) absorbance ratio curve in Figure 5 may reflect an intra- or intermolecular condensation process as increasing amounts of Pt(II) bind to the polynucleotide. Intrastrand and interstrand cross-links may be expected [57, 58]. It should be mentioned that the $(NH_4)_2PtCl_4$ stock solutions used in our work were allowed to age at $pH \leq 2$ and ambient temperature for > 90 days. Thus, the observed reactivity may have been predetermined somewhat by the extent of chloride hydrolysis prior to the reaction with poly d(G-C) [53, 54]. Due to the chemical similarities of Pd(II) to Pt(II) [59, 60], the same cross-linkage hypothesis can be extended to the interaction of Pd(II) with poly d(G-C). It is relevant to point out that Pd(II) is kinetically labile, unlike Pt(II). Al(III) also has demonstrated ability to promote DNA cross-links [61]. The species of aluminum involved in this complex of cross-linked DNA are thought to be Al(III) and $Al(OH)^{2+}$. Reactions of Al(III), like Pt(II), are slow. Despite the possibility that cross-links of some kind may be involved in the interaction of Pt(II), Pd(II), and Al(III) with poly d(G-C), fundamental differences probably exist in the nature of the specific cross-links, mechanisms involved, and in the final structure of DNA.

Classification of Metal Ions According to Binding Preferences. Based on crystallographic evidence for proteins, metal cations can be separated into three distinct classes according to preference for donor atoms of functional groups: nitrogen/sulphur seeking or *Class B* (e.g., Ag(I), Hg(II), Pd(II), and Pt(II)); oxygen seeking or *Class A* (e.g., Ca(II), Al(III), and Ln(III)); and *Borderline* ions which display ambivalence to O-, N-, and S-type donors (e.g., Ni(II), Cd(II), Co(II), Mn(II), Pb(II), Zn(II), and Fe(III)) [62, 63]. The nondescript terminology, *Class A* and *Class B*, originates from a related classification scheme employed for many years in metal-ion solution chemistry which was established empirically from thermodynamic data [64–66].

Division of metal ions according to binding preference is supported by crystallographic and spectroscopic data describing the ligand environment of a number of metal ions in a variety of biomolecules (proteins [62, 67], nucleic

acids [57, 68–70]). A useful measure employed in classifying metals is the index $X_m^2 r$ (X_m, Pauling electronegativity; r, ionic radius corresponding to the most common coordination number). $X_m^2 r$ is a quotient that compares valence orbital energy with ionic energy [63], and is therefore considered to be a measure of the relative ability of metal ions to participate in covalent interactions compared to ionic interactions. By plotting the covalent index $X_m^2 r$ versus the ionic index Z^2/r, Nieboer and Richardson [63] demonstrated a sharp separation between *Class A* and *Borderline* metal ions, but the distinction between *Class B* and *Borderline* metal ions was less clear. For *Class A* metal ions, the index $X_m^2 r$ has values less than 1.75; for *Borderline* metal ions values are greater than 1.75 but less than 3.0 (Pb(II) being the only exception); *Class B* metal ions have an index value greater than 3.0. In spite of the preference of class B ions for nitrogen/sulphur ligands, both *Class B* and *Borderline* ions form complexes with oxygen ligands which are more stable than those of *Class A* ions of comparable size and charge. This general phenomenon is independent of the type of ligand and is the basis for the much quoted Irving-Williams order of complex stability [59, 66]. Presumably, this feature suggests that in addition to the largely ionic interaction observed for *Class A* ions, *Borderline*, and *Class B* ions have significant covalent contributions to the overall interaction energy.

An Empirical Index to Conformational Transitions. A linear correlation is observed between log (metal ion to poly d(G-C) mole ratio) assessed at the midpoint of the conformational or structural transition curve and the covalent index ($X_m^2 r$) (Fig. 6). This covalent index was calculated as described in the legend to Figure 6. The transition midpoints of the *Type I* monophasic curves were easily assessed, while for biphasic transitions the values plotted were those pertaining to the midpoints of the major transitions (e.g., second step in curves of Fig. 1A). For the *Type II* Monophasic transitions, the absorbance ratio value of 0.23 was used as an estimate of the midpoint of the postulated initial transition, by analogy to Ag(I). This approach was also employed for Pt(II), Pd(II), and Al(III). Although in these latter three cases the use of this absorbance ratio may be less appropriate, the correlation is affected inconsequentially if the transition midpoint of the total overall transition were considered for these six metal ions ($y = -1.01 \log x + 3.32$; $n = 20$, $r = 0.93$; Pt(II) and Pd(II) concentrations are corrected in the manner described below). For all metal ions, the midpoint values used were derived from a minimum of at least two independently determined transition curves. Intraexperimental variation of replicate assessments of the midpoint mole ratios was small (3–5%), whereas interexperimental variation was slightly larger (5–8%).

As illustrated in the Appendix, equilibrium analysis indicates that the midphase (metal ion)/(polydeoxynucleotide) mole ratio (i.e., C_m°/C_1) decreases with increasing affinity of metal ions for poly d(G-C). An underlying assumption in interpreting the observed midphase ratios is that all of the added metal is available for interactions with the poly d(G-C) as the free hydrated metal ion. Although this is true for most of the metals, the dissociation of some of the metal salts into their respective metal cations was not complete. Anion displacement was considered as a competing reaction (see Appendix) for Cr(III), Pt(II), Pd(II), and In(III) as judged from the available equilibrium constants [35, 71]. Appropriate correction factors were employed to calculate more accurate mid-

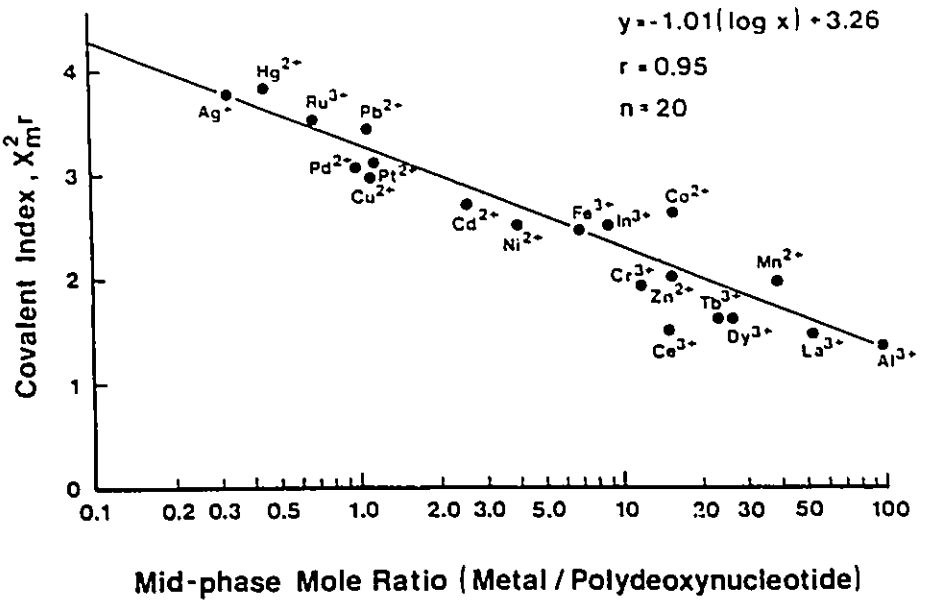

FIGURE 6. Correlation between the covalent index ($X_m^2 r$) and phase transition midpoints. For the covalent index, X_m is the Pauling electronegativity [83] and r is the effective ionic radius for the most common metal-ion coordination number (i.e., 9, lanthandies; 4, Hg(II), Pd(II), Pb(II), Pt(II) and Ag(I); and 6 for all other metal ions) [84]. A correction factor was applied to the mole ratios for Cr(III), Pt(II), Pd(II), and In(III) to compensate for competing reactions involving the anion of the metal salt (see text for detail). The use of uncorrected concentration data has little effect on the slope and intercept, but reduced the correlation coefficient somewhat ($y = -0.96$ (log x) + 3.30, $r = 0.92$, $n = 20$).

point mole ratios. The correction factors were: 0.97 (In(III), displacement of 3 acetates); 0.17 (Pt(II), displacement of the third chloride (53,56)); 0.83 (Pd(II), displacement of 2 chlorides); 0.16 (Cr(III), displacement of 3 acetates). The need for this correction is clearly illustrated by the data presented in Table 1 for the observed transition midpoints for three cerium salts. The nitrate and chloride salts yielded superimposable transition curves, while that for the sulphate was displaced toward a significantly higher metal/polydeoxynucleotide mole ratio.

TABLE 1. Transition Midpoints for Several Cerium(III) Salts

Cerium(III) Salt	Mole Ratio at Transition Midpoint	Anion Association Constant ($\log K_1$)[a]	Corrected Transition Midpoint Mole Ratio
$CeCl_3 \cdot xH_2O$	15	−0.1	15
$Ce(NO_3)_3 \cdot 6H_2O$	15	0.2	15
$Ce_2(SO_4)_3 \cdot xH_2O$	325	3.6	20

[a] From Smith and Martell [71], for 25°C and 0 or 1 M ionic strength.

$K_1 = [MX]/[M][X]$ where M = metal ion and X = anion of salt.

This is consistent with the equilibrium data which shows that the nitrate and chloride salts are virtually completely dissociated under the experimental conditions while 94% of the Ce(III) is present as the monosulphate complex $Ce(SO_4)^+$. By analogy with Pt(II) and Pd(II), a correction might have been anticipated for $HgCl_2$. However, experimentally, $HgCl_2$ and $Hg(NO_3)_2 \cdot xH_2O$ gave nearly superimposable responses suggesting that the chlorides are not displaced. (Chloride binds Hg^{2+} avidly: $\log K_1 = 7.2$ and $\log K_2 = 6.8$ [35].) As is evident from the regressional parameters provided in the legend to Figure 6, the use of concentration uncorrected (metal ion)/(poly d(G-C)) mole ratios did not affect the correlation with $X_m^2 r$ significantly.

DISCUSSION

The ability of metals to participate in an array of conformational and structural transitions in DNA is well documented (see Introduction). We have chosen to monitor such changes using UV-spectrometry and CD. Although these techniques may not be definitive with respect to assigning specific conformations (see [72–74]), they are valid indicators of structural or conformational transitions nonetheless. Additional characterization of the metal/poly d(G-C) complexes by x-ray crystallography, NMR, and physicochemical analyses are required to evaluate the interpretations rendered concerning the specific nature of the events at the molecular level.

Our data support the conclusion that structural changes in DNA elicited by metals are a function of the nature and binding affinity for target sites (i.e., base nitrogens, phosphate oxygens) on DNA. Interaction of *Class A* metals with poly d(G-C) occurs predominantly with the phosphate oxygens. By contrast, *Class B* metals also possess the ability to bind strongly to nitrogen centers on the bases. On the other hand, *Borderline* metals may be considered ambivalent with respect to their affinity for both types of donor sites; the affinity for N-centers increases with the degree of *Class B* character (i.e., value of $X_m^2 r$). The most likely site of metal-nitrogen interaction in poly d(G-C) is the N-7 site of guanine, based on spectroscopic data including NMR [57, 58, 68, 69, 75, 76]. Both the N-1 site of guanine and the N-3 site of cytosine are involved in base pairing and are fairly inaccessible to metal-ion interaction unless high mole ratios are achieved. The exocyclic oxygen atoms of both guanine and cytosine may also be involved in direct and long range interactions with the metal ions via the bridging action of water molecules [57, 70, 77]. Similar long range interactions with the phosphate oxygens may also occur [70]. Thus, both phosphates and base nitrogens (especially guanine N-7) are most likely involved in the binding of metal ions to poly d(G-C). The equilibrium considerations outlined in the Appendix suggest that the midphase mole ratio plotted in Figure 6 is inversely proportional to the association constant for the metal-ion/polydeoxynucleotide interaction. Consequently, the grouping of metal ions in Figure 6 suggest that *Class B* metal ions (Ag(I), Hg(II), Pd(II), Pt(II), and Ru(III)) form the strongest complexes with poly d(G-C), *Class A* ions the weakest (Al(III), Ce(III), Dy(III), La(III), and Tb(III)), and *Borderline* ions complexes of intermediate strength (Cd(II), Cu(II), Co(II), Mn(II), Ni(II), Pb(II), Zn(II), Cr(III), Fe(III), and In(III)) consistent with previously published work [78]. These data reinforce the fact that the distinction between *Class B* ions and *Borderline* ions of significant *Class B* character is

vague (compare positions of Cu(II) and Pb(II) with Pt(II) and Pd(II) in Fig. 6). The significant displacement of Ce(III) relative to La(III) in Figure 6 may be indicative of the anomalies in metal-complex stability often observed early in the lanthanide series [79].

Although no definitive relationship between the covalent index and the type of transition observed can be reached, several generalities are apparent. The *Class B* ions used in our study consistently gave monophasic transitions, whereas *Class A* ions gave biphasic transitions. As expected, the *Borderline* ions were ambivalent in the type of transition curves they elicited. Specific conformations (or structures) cannot be assigned to all transitions although certain metals (i.e., Co(II), Ni(II), Mn(II), and Cd(II)) have been studied in detail by ourselves and others (see Results) and designations of conformations (or structures) could thus be made with some certainty.

It has been suggested that reduction of DNA phosphate repulsion (charge screening) and the polymer hydration state are important determinants of conformational or structural transitions in DNA [80]. The major conclusion derived from this study is that nitrogen-base binding by metal ions facilitates processes and such transitions. Affinity for DNA also appears to determine the ability of metal ions to induce DNA/chromosomal physical aggregation (as assessed by sedimentation analysis) or destabilize helical structure [81, 82]. The cooperative nature of the observed transitions and the strong correlation with the binding parameter $X_m^2 r$ clearly demonstrate the dynamic nature of metal-DNA interactions.

We thank Dr. R. M. Epand of the Department of Biochemistry, McMaster University for the use of his CD spectropolarimeter and assistance in data analysis. Appreciation is also expressed for the helpful discussions with Dr. C. B. Harley of the Department of Biochemistry at McMaster University and Dr. L. G. Marzilli of Emory University. Financial support from the Natural Sciences and Engineering Research Council of Canada in the form of a Strategic Research Grant (Environmental Toxicology) is gratefully acknowledged.

APPENDIX

Definition of Terms

- M = free hydrated metal ion
- L = free uncomplexed poly d(G-C)
- ML = metal ion/polydeoxynucleotide complex
- X = anion of metal salt dissolved
- MX = metal ion/anion complex
- [ ] = concentration in mol l^{-1}; for convenience activity coefficients are set to unity
- C_M = total metal concentration (in all forms)
- C_M° = value of C_M at midphase transition
- C_L = total poly d(G-C) concentration (in all forms)
- K = [ML]/[M][L] = association or formation constant
- β_2 = $[MX_2]/[M][X]^2$ = formation constant for anion of salt

Derivations

Assume that the reaction between a metal ion and poly d(G-C) is described by the reaction in Eq. (1)

$$M + L = ML. \tag{1}$$

Replacement of $[M] = C_M - [ML]$ in the equilibrium expression for K yields Eq. (2), on rearrangement

$$([ML]/C_M) = K[L]/(1 + K[L]). \tag{2}$$

For simplicity, consider the case when $K[L] \ll 1$ and $[ML] = \alpha[L]$ at the midphase transition point (α specifies the amount of complexed and uncomplexed polydeoxynucleotide). This manipulation yields the expression in Eq. (3)

$$C_M^\circ = \alpha K^{-1} \tag{3}$$

which indicates that C_M° is proportional to the reciprocal of the association constant for the metal-ion/polydeoxynucleotide interaction, providing α is approximately constant for the metal ions considered. Since C_L was a constant in the reported experiments, the metal-ion/polydeoxynucleotide mole ratio C_M°/C_L (assessed from plots such as depicted in Fig. 1–5) has the same dependence on K.

In instances where the anion of the metal salt competes with the poly d(G-C) for the metal ion, displacement reactions of the following type must be considered

$$MX_2 + L = ML + 2X, \tag{4}$$

$$\kappa = [ML][X]^2/[MX_2][L] = K/\beta_2, \tag{5}$$

$$[ML]/[MX_2][L] = K/\beta_2[X]^2. \tag{6}$$

Assuming $[MX_2] \gg [M]$, so that $[MX_2] = C_M - [ML]$ can be substituted in Eq. (6), and again making the simplification $K[L] \ll 1$, yields Eq. (7) which is analogous to Eq. (3)

$$C_M^\circ = \alpha\gamma K^{-1}. \tag{7}$$

Here $\gamma = \beta_2[X]^2$ and it corrects for the degree of complex formation between M and the anion X. Thus, the competing reaction increases C_M° by the factor γ, indicating that higher concentrations of metal salt are required to reach the same fraction of metal-bound poly d(G-C) since $\gamma > 1$ for significant complex formation with X.

REFERENCES

1. M. J. B. Tunis-Schneider and M. F. Maestre, *J. Mol. Biol.* 52, 521 (1970).
2. R. E. Dickerson, *Sci. Am.* 249 (Dec.), 94 (1983).
3. A. Rich, A. Nordheim, and A. H.-J. Wang, *Ann. Rev. Biochem.* 53, 791 (1984).

4. F. M. Pohl and T. M. Jovin, *J. Mol. Biol.* 67, 375 (1972).
5. S. Hanlon, A. Chan, and S. Berman, *Biochim. Biophys. Acta* 519, 526 (1978).
6. J. H. van de Sande, L. P. McIntosh, and T. M. Jovin, *EMBO J.* 1, 777 (1982).
7. G. V. Fazakerley, *Nucleic Acids Res.* 12, 3643 (1984).
8. J.-M. Malinge and M. Leng, *EMBO J.* 3, 1273 (1984).
9. M.-F. Hacques and C. Marion, *Biopolymers* 25, 2281 (1986).
10. D. M. Soumpasis, M. Robert-Nicoud, and T. M. Jovin, *FEBS Lett.* 213, 341 (1987).
11. V. I. Ivanov, L. E. Minchenkova, A.K. Schyolkina, and A. I. Poletayev, *Biopolymers* 12, 89 (1973).
12. R. E. Dickerson, H. R. Drew, B. N. Conner, M. L. Kopka, and P. E. Pjura, *Cold Spring Harbour Symp. Quant. Biol.* 47 1, 13 (1982).
13. J. C. Girod, W. C. Johnson Jr., S.K. Huntington, and M. F. Maestre, *Biochemistry* 12, 5092 (1973).
14. J. H. van de Sande and T. M. Jovin, *EMBO J.* 1, 115 (1982).
15. W. Zacharias, J. E. Larson, J. Klysik, S. M. Stirdivant, and R. D. Wells, *J. Biol. Chem.* 257, 2775 (1982).
16. L. S. Lerman, *Cold Spring Harbour Symp. Quant. Biol.* 38, 59 (1974).
17. Y. A. Shin and G. L. Eichhorn, *Biopolymers* 16, 225 (1977).
18. A. Walter and G. Luck, *Nucl. Acids Res.* 4, 539 (1977).
19. L. C. Gosule and J. A. Schellman, *J. Mol. Biol.* 121, 311 (1978).
20. J. Widom and R. L. Baldwin, *J. Mol. Biol.* 144, 431 (1980).
21. H. Castleman and B. F. Erlanger, *Cold Spring Harbour Symp. Quant. Biol.* 47(1), 133 (1982).
22. G. L. Eichhorn, Y. A. Shin, and J. J. Butzow, *Cold Spring Harbour Symp. Quant. Biol.* 47(1), 125 (1982).
23. W. Zacharias, J. C. Martin, and R. D. Wells, *Biochemistry* 22, 2398 (1983).
24. M. H. Zehfus and W. C. Johnson, Jr., *Biopolymers* 20, 1589 (1981).
25. M. H. Zehfus and W. C. Johnson Jr., *Biopolymers* 23, 1269 (1984).
26. Y. Kohwi and T. Kohwi-Shigematsu, *Proc. Natl. Acad. Sci. USA* 85, 3781 (1988).
27. D. Sen and W. Gilbert, *Nature* 334, 364 (1988).
28. J. Bernués, R. Beltrán, J. M. Casasnovas, and F. Azorín, *Nucl. Acids Res.* 18, 4067 (1990).
29. I. Tinoco, Jr., C. Bustamante, and M. F. Maestre, *Ann. Rev. Biophys. Bioeng.* 9, 107 (1980).
30. A. G. Walton and J. Blackwell, in *Biopolymers*, Academic Press, New York, 1973, pp. 229–295.
31. T. M. Jovin, D. M. Soumpasis, and L. P. McIntosh, *Ann Rev. Phys. Chem.* 38, 521 (1987).
32. T. Yamane and N. Davidson, *Biochim. Biophys. Acta* 55, 609 (1962).
33. R. H. Jensen and N. Davidson, *Biopolymers* 4, 17 (1966).
34. R. D. Wells, J. E. Larson, R. C. Grant, B. E. Shortle, and C. R. Cantor, *J. Mol. Biol.* 54, 465 (1970).
35. C. F. Baes, Jr. and R. E. Mesner, in *The Hydrolysis of Cations*, John Wiley & Sons, New York, 1976.
36. P. Bourtayre, L. Pizzorni, J. Liquier, J. Taboury, E. Taillandier, and J.-F. Labarre, in *Nickel in the Human Environment*, IARC Sci. Pub. No. 53, F. W. Sunderman Jr., Ed.-in-chief, Oxford Univ. Press, Oxford, 1984, pp. 227–234.
37. J. Liquier, P. Bourtayre, L. Pizzorni, F. Sournies, J.-F. Labarre, and E. Taillandier, *Anticancer Res.* 4, 41 (1984).
38. M. Behe and G. Felsenfeld, *Proc. Natl. Acad. Sci. USA* 78, 1619 (1981).
39. A. Moller, A. Nordheim, S. A. Kozlowski, D. J. Patel and A. Rich, *Biochemistry* 23, 54 (1984).
40. T. Haertle, J. Augustyniak, and W. Guschlbauer, *Nucl. Acids Res.* 9, 6191 (1981).

41. J.-M. Sequaris, M. L. Kaba, and P. Valenta, *Bioelectrochem. Bioenerg.* **13**, 225 (1984).
42. P. S. Ho, C. A. Frederick, D. Saal, A. H.-J. Wang and A. Rich, *J. Biomol. Struct. Dyn.* **4**, 521 (1987).
43. T. J. Thomas and R. P. Messner, *Biochimie* **70**, 221 (1988).
44. T. J. Thomas and T. Thomas, *J. Biomol. Struct. Dyn.* **7**, 1221 (1990).
45. B. Nordén, Y. Matsuoka, and T. Kurucsev, *Biopolymers* **25**, 1531 (1986).
46. Y. A. Shin, S. L. Feroli and G. L. Eichhorn, *Biopolymers* **25**, 2133 (1986).
47. S. K. Zavriev, L. E. Minchenkova, M. Vorlickova, A. M. Kolchinsky, M. V. Volkenstein, and V. I. Ivanov, *Biochim. Biophys. Acta* **564**, 212 (1979).
48. D. E. DiRico Jr., P. B. Keller and K. A. Hartman, *Nucl. Acids Res.* **13**, 251 (1985).
49. P. B. Keller, D. M. Loprete, and K. A. Hartman, *J. Biolmol. Struct. Dyn.* **5**, 1221 (1988).
50. V. A. Sorokin, Y. P. Blagoi, V. A. Valeev, S. V. Kornilova, G. O. Gladchenko, I. D. Reva, and V. I. Sokhan, *J. Inorg. Biochem.* **30**, 87 (1987).
51. P. B. Keller and K. A. Hartman, *J. Biomol. Struct. Dyn.* **4**, 1013 (1987).
52. R. C. Srivastava, J. Froehlich, and G. L. Eichhorn, *Biochimie* **60**, 879 (1978).
53. L. I. Elding, *Acta Chem. Scand.* **24**, 1331 (1970).
54. L. I. Elding, *Acta Chem. Scand.* **24**, 1527 (1970).
55. M. E. Howe-Grant and S. J. Lippard, in *Metal Ions in Biological Systems*, H. Sigel, Ed., Marcel Dekker Inc., New York, 1980, Vol. 11, pp. 63–125.
56. J. P. Macquet and T. Theophanides, *Biopolymers* **14**, 781 (1975).
57. G. L. Eichhorn, in *Metal Ions in Genetic Informatison Transfer*, G. L. Eichhorn and L. G. Marzilli, Eds., Elsevier, New York, 1981, pp. 1–46.
58. S. J. Lippard, *Science* **218**, 1075 (1982).
59. F. A. Cotton and G. Wilkinson, in *Advanced Inorganic Chemistry*, John Wiley & Sons, Toronto, 1980, pp. 685–686, 950–957.
60. R. B. Martin, *Acc. Chem. Res.* **18**, 32 (1985).
61. S. J. Karlik, G. L. Eichhorn, P. N. Lewis, and D. R. Crapper, *Biochemistry* **19**, 5991 (1980).
62. T. L. Blundell and L. N. Johnson, in *Protein Crystallography*, Academic Press, London, 1976, pp. 199–231.
63. E. Nieboer and D. H. S. Richardson, *Environ. Pollution (Series B)* **1**, 3 (1980).
64. S. Ahrland, J. Chatt, and N. R. Davies, *Q. Rev. Chem. Soc.* **12**, 2654 (1958).
65. E. Nieboer and W. A. E. McBryde, *Can. J. Chem.* **51**, 2512 (1973).
66. J. J. R. Fraústo da Silva and R. J. P. Williams, in *The Biological Chemistry of the Elements: The Inorganic Chemistry of Life*, Clarendon Press, Oxford, England, 1991, pp. 33–36.
67. E. Nieboer and W. E. Sanford, in *Reviews in Biochemical Toxicology*, E. Hodgson, J. R. Bend and R. M. Philpot, Eds., Elsevier Science, New York, 1985, Vol. 7, pp. 205–245.
68. A. Jack, J. E. Ladner, D. Rhodes, R. S. Brown, and A. Klug, *J. Mol. Biol.* **111**, 315 (1977).
69. L. G. Marzilli, T. J. Kisteumacher, and G. L. Eichhorn, in *Nucleic Acid—Metal Ion Interactions*, T. G. Spiro, Ed., John Wiley & Sons, New York, 1980, pp. 179–250.
70. L. G. Marzilli, in *Metal Ions in Genetic Information Transfer*, G. L. Eichhorn and L. G. Marzilli, Eds., Elsevier, New York, 1981, pp. 47–85.
71. R. M. Smith and A. E. Martell, in *Critical Stability Constants*, Plenum Press, New York, 1976, Vol. 4.
72. W. A. Baase and W. C. Johnson Jr., *Nucl. Acids Res.* **6**, 797 (1979).
73. J. C. Sutherland and K. P. Griffin, *Biopolymers* **22**, 1445 (1983).
74. M. Tomasz, J. K. Barton, C. C. Magliozzo, D. Tucker, E. M. Lafer, and B. D. Stollar, *Biochemistry* **80**, 2874 (1983).
75. X. Jia and L. G. Marzilli, *Biopolymers* **31**, 23 (1991).

76. X. Jia, G. Zon, and L. G. Marzilli, *Inorg. Chem.* 30, 228 (1991).
77. R. V. Gessner, G. J. Quigley, A. H.-J. Wang, G. A. van der Marel, J. H. van Boom, and A. Rich, *Biochemistry* 24, 237 (1985).
78. C. H. Zimmer, G. Luck, and H. Triebel, *Biopolymers* 13, 425 (1974).
79. R. J. P. Williams, *Structure and Bonding* 50, 79 (1982).
80. D. M. Soumpasis, J. Wiechen, and T. M. Jovin, *J. Biomol Struct. Dyn.* 4, 535 (1987).
81. G. L. Eichhorn and Y. A. Shin, *J. Am. Chem. Soc.* 90, 7323 (1968).
82. D. A. Knoll, M. G. Fried, and V. A. Bloomfield, in *Structure and Expression, vol. 2: DNA and Its Drug Complexes*, M. H. Sarma and R. H. Sarma, Eds., Adenine Press, New York, 1988, pp. 123–145.
83. A. L. Allred, *J. Inorg. Nucl. Chem.* 17, 215 (1961).
84. R. D. Shannon, *Acta Cryst.* A32, 751 (1976).

Received March 30, 1993; accepted June 17, 1993

CHARACTERIZATION OF NICKEL-INDUCED MUTATIONS

Franco E. Rossetto[1], John D. Turnbull[2], Evert Nieboer[1]

Department of Biochemistry[1] and Department of Medicine[2], McMaster University, 1200 Main Street West, Hamilton, Ontario, Canada, L8N 3Z5

IN PRESS: *Science of the Total Environoment*: Special Issue, Nickel Biochemistry, Toxicology, and Ecologic Issues. A Collection of Papers Presented at the Fifth International Conference on Nickel Biochemistry, Toxicology, and Ecologic Issues, 7-11 September, 1992, held in Sudbury, Ontario, Canada

SUMMARY

A Chinese hamster ovary cell line (designated AS52) has been used to test the mutagenicity of nickel compounds. This line lacks the endogenous gene for hypoxanthine phosphoribosyl transferase (HPRT) but contains an inserted bacterial gene coding for the enzyme guanine-hypoxanthine phosphoribosyl transferase (*gpt*) which is the targeted locus for selection. Isolated mutants were clonally expanded and analysed utilizing the Polymerase Chain Reaction (PCR) following exposure to ethylmethylsulfonate (EMS), Ni_3S_2, $Ni(OH)_2$, $NiSO_4$, and control conditions. Amplification of the *gpt* locus in normal AS52 cells results in the generation of two distinct bands, both of which have been characterized by restriction enzyme analysis and nucleotide sequencing. The smaller band represents the *gpt* gene. The larger band contains a large insert of bacterial origin and is non-functional. Analysis of mutants revealed three distinct patterns: 1) both PCR bands remain intact; 2) the smaller DNA band is deleted; 3) both bands are deleted. The three patterns represent point, frameshift or small deletion mutations (pattern 1), or larger deletions (pattern 2 and 3). Mutant analysis was performed with two unique sets of DNA amplification primers with identical results. When compared to spontaneous or EMS induced mutants, those generated by exposure to nickel compounds exhibited an increase in gene deletions relative to point mutations; the extent of which was compound specific: $NiSO_4$ > $Ni(OH)_2$ > Ni_3S_2. These results clearly suggest that a variety of genotoxicological mechanisms are involved in the mutagenic activity of nickel compounds.

INTRODUCTION

The development of cancer is now thought to be a multistep process. The generation and propagation of a number of stable changes in genomic DNA (ie. mutations, translocations) seem to be of critical importance (1). Nickel compounds are well documented carcinogens in both man and rodent species (2). A variety of cellular and biochemical studies have clearly demonstrated that nickel compounds affect chromosomes, DNA, DNA synthesis, and transcription (reviewed in ref. 3). By contrast, the mutagenicity of nickel compounds is not as apparent (3). Whereas soluble salts (eg. $NiSO_4$ or $NiCl_2$) are equivocal mutagenic agents in a variety of eukaryotic systems, negative results are invariably observed in standard bacterial assay systems (ie., Ames assay).

Until recently, few eukaryotic cell lines were available which clearly demonstrated suitable susceptibility to nickel-induced mutagenesis. A novel derivative of a Chinese hamster ovary (CHO-K1-BH4) cell line has been developed in which nickel compounds have been shown to be weakly mutagenic (4). This line, designated AS52, lacks the endogenous gene hypoxanthine phosphoribosyl transferase (HPRT). As a functional replacement, the bacterial gene coding for the enzyme guanine-hypoxanthine phosphoribosyl transferase (gpt) has been inserted into the CHO genome (5). We have utilized this cell line in the analysis of mutants selected and clonally expanded following *in vitro* exposure to a variety of insoluble (Ni_3S_2, $Ni(OH)_2$) and soluble ($NiSO_4$) nickel compounds. Coupled with the polymerase chain

reaction (PCR), the molecular characterization of the isolated mutants is rapid and straightforward (6,7).

MATERIALS and METHODS

The generation and isolation of AS52 mutants was based on standard protocols (7,8). Routine cell cultures were maintained in MPA medium: MCDB 302 medium plus 2% dialyzed and heat-inactivated fetal bovine serum (dFBS) plus MPA supplements (10 μg/ml mycophenolic acid, 3.0 μM aminopterin, 25 μg/ml adenine, 50 μM thymidine and 250 μg/ml xanthine). For mutagenicity testing, cells were replated in XAT/2 medium (MCDB 302 medium plus 2% dFBS and one-quarter the amount of adenine, xanthine and thymidine) one day prior to experimental exposures to mutagens. After the exposure period (24h for particulates, 5h for soluble compounds) the cells were rinsed and replated in XAT/2 medium. Following several days recovery (3-4 days), cells were replated in MCDB/2 medium (MCDB 302 medium plus 2% dFBS). On day 7 or 8, mutants were selected by plating $2x10^5$ cells / 100 mm dish in MCDB/2 medium containing 10 μM of 6-thioguanine (6-TG) to select for *gpt* mutants. Ten days later, individual clones were picked and expanded in MCDB/2 medium for subsequent PCR analysis. A maximum of 3 colonies were picked and expanded from any one plate. All reagents were of tissue culture grade and obtained from Sigma Chemical Co. or Gibco.

All mutant colonies were clonally expanded to approximately $1-3x10^6$ cells. Following washing, cells were lysed in 250 μl of lysis solution (17 mM Tris, 60 mM KCl, 1 mM $MgCl_2$, 0.4% Tween-20, 0.4% Nonidet P-40, 0.5 mg/ml Proteinase K, ph 8.7) overnight at 45 C. Aliquots of 50 μl were diluted with an equivolume of sterile water, heated at 95 C for 15 min and frozen at -20 C

until analyzed. Approximately 0.5-1 μg of DNA was amplified for 30 cycles in the following PCR buffer: 15 mM Tris, 35 mM KCl, 15 mM $MgCl_2$, pH 8.79; 200 μM of each deoxynucleotide (dNTP) and 0.5 μM of each primer. Primer sequences are depicted in Fig. 1b. DNA melting was performed at 95 C for 1 min; primer annealing/extension at 60 C (primers 1&2) or 68 C (primers 3&4, P1&P2) for 5 min which was extended by 10 min in the final cycle. Products were analyzed by electropheresis on 1% agarose gels which were subsequently stained with ethidium bromide. All reagents were of the highest grade available.

RESULTS

The ability to successfully amplify a fragment of DNA stems from a judicial choice of primers and the optimization of reaction conditions. The sequence of primers utilized in our studies are depicted in figure 1b. As can be seen from Figure 1a/b, two primer sets were chosen; the first encompassing the *gpt* gene and sequences immediately 5' and 3' to the coding region, the second soley encompassing the gene in question. Amplification of the *gpt* locus in normal AS52 cells with both primer sets resulted in the production of two bands (Fig. 2a/b, data not shown). All of the fragments generated from normal AS52 DNA have been characterized by restriction enzyme analysis and nucleotide sequencing (data not shown). The smaller fragment generated with either primer set corresponds to the functional *gpt* gene with a sequence identical to that previously reported (8). The larger fragment consists of 5' and 3' *gpt* coding

sequences (107 and 83 base pairs respectively), with 320 coding base pairs deleted from the middle of the gene replaced by an insert of 695 base pairs of bacterial origin (Fig. 1a, data not shown).

Analysis of mutants generated three distinct alterations at the *gpt* locus (Fig. 2a/b): 1) both PCR bands remain intact; 2) the smaller DNA band is deleted; 3) both bands are deleted. Sequence analysis of a number of EMS (ethyl methanesulfonate, a known point mutagen) mutants has confirmed that point mutations are responsible for the first family of mutants (data not shown). In addition, small deletions of several basepairs or frameshift mutations would also be scored as members of this family of mutants. Deletions of all or part of the *gpt* locus are assigned to the second type, while large multi-locus deletions/damage are believed to correspond to the third category of mutants. Mutant analysis was performed with two unique sets of *gpt* specific DNA amplification primers with identical results (Fig. 2a/b, data not shown). An additional control amplification at a distinct, unrelated gene locus (chaperone/P-protein (10)) was utilized to validate the overall integrity of isolated source DNA (Fig. 2c). All mutants amplified with this latter primer set invariably generated an identical fragment of 1300 bp as predicted from sequence data (10; Fig. 2c, data not shown).

When compared to spontaneous or EMS induced mutants, those generated by exposure to nickel compounds exhibited an increase in gene deletions relative to point mutations; the extent of which was compound specific: $NiSO_4$ > $Ni(OH)_2$ > Ni_3S_2 (Table 1).

Amongst these nickel mutagens no distinction was observed in their propensity to induce deletions of solely the *gpt* locus (second empirical mutant type; data not shown). By contrast, $NiSO_4$ clearly induced total deletions of both loci to a much greater extent than all other mutagens (third empirical mutant type; data not shown). As expected, EMS produced mainly point mutagens; spontaneous control mutants displayed a more varied distribution of mutant profile types.

Discussion

The genotoxicological potential of nickel compounds is well established (3). A number of studies by Costa and coworkers have demonstrated that the nickel uptake pathway may play an important role in the delivery, compartmentalization and bioactivity of nickel intracellularly (12-15). Insoluble crystaline particulates (ie., Ni_3S_2) tend to be phagocytized; lysosomal interaction with the intracellular particulates results in dissolution to the Ni(II) ion with subsequent nuclear accumulation (3, 12-15). By contrast, the uptake and intracellular bioaccumulation and compartmentalization of soluble nickel compounds (ie., $NiSO_4$) is not as well understood (3,12). Furthermore, these latter compounds are not as carcinogenic or genotoxic in comparison to more crystaline, insoluble compounds (3, 13, 16).

The data presented suggest that the processes involved in nickel-mutant generation are compound specific and thus, may be related to the mode of uptake and bioaccumulation. Therefore,

while the relatively insoluble compound Ni_3S_2 primarily generated point mutations (or frameshift/small deletions), large deletions predominate following exposure to soluble $NiSO_4$. A compound of limited solubility ($Ni(OH)_2$) demonstrated a mutagenic profile intermediate to these two latter compounds.

An interesting hypothesis is that mechanistically, at least two distinct mutation pathways are involved. The first, involving Ni_3S_2, results in the delivery of solubilized Ni(II) directly to the nucleus as envisaged by Costa and coworkers. It is this intranuclear Ni(II) that is the primary DNA mutagen. The second involves the acummulation of Ni(II) intracellularly from soluble compounds (ie., $NiSO_4$) through a distinct pathway(s). This intracellular pool of Ni(II) may subsequently interact with other biomolecules (ie.,lipids, proteins) to produce secondary molecules which may interact with DNA inducing mutations.

Recent advances in the understanding of Ni(II)/Ni(III) redox chemistry within biological systems suggest plausible mechanisms involving reactive oxygen species as integral factors in Ni(II) mutagenic activity (17-19). The generation of these mutagenic species may occur from the direct intraction of Ni(II) with DNA/chromosome in the presence of H_2O_2 (20, 21). The possibility of this occurring *in vivo* is strengthened by the demonstration that H_2O_2 is readily generated in nuclei (22). Ni(II)-peroxidation of lipids is also well documented and results in the generation of reactive byproducts damaging or mutagenic to DNA (23, 24). It is interesting to note that early proponents of the AS52 cell line cited the ability to recover large deletions

resulting from active oxygen chromosomal damage as one of the advantages of this cell line in the study of mutagenesis (25, 26).

The work presented in this report clearly demonstrates that nickel compounds are mutagenic in the AS52 cell line. Although exact mutagenic mechanisms cannot be defined, it is clear that mutagenic profiles are compound specific. Furthermore, the data are consistent with the hypothesis that the Ni(II)/Ni(III) redox process may be involved in this mutagenicity. The ability of the AS52 cell line to recover mutations stemming from large deletions makes this line particularly suited to the further investigation of the mechanisms of nickel mutagenesis and/or carcinogenesis.

Acknowledgements

The authors would like to acknowledge the excellent technical assistance of Ms.Wang-Ping Li and the advice of Mr. Glenn Fletcher in tissue culture techniques. Financial support from the Nickel Producers Environmental Research Association (NiPERA) Durham, NC, the International Lead Zinc Research Organization, Inc., Research Triangle Park, NC and the Ontario Workplace Health and Safety Agency, Toronto, Ontario is also gratefully acknowledged.

Figure Legends

Figure 1: PCR Target Within AS52 Cells

a) PCR Strategy. Dotted segments correspond to CHO genomic DNA; straight lines to bacterial plasmid DNA; solid rectangles to *gpt* coding regions; open rectangles to insert within the gene. Diagram is not drawn to scale.

b) PCR Amplification Primers. Primers #1-4 correspond to those depicted in (a). Primers P1/P2 are specific for chaperone/P-protein (see text for details).

Figure 2: PCR analysis of AS52 Mutants

a) EMS and Control Mutants. Lane 1:DNA size standards (bp), from top - 1358, 1078, 872, 603. Lanes 2-10: EMS mutants. Lanes 11-20: spontaneous control mutants.

b) Nickel Mutants. Lane 1: DNA size standards (bp), from top - 1358, 1078, 872, 603. Lanes 2-10: Ni_3S_2 mutants. Lanes 11-20: $Ni(OH)_2$ mutants.

c) Chaperone/P-Protein Amplification. Lane 1: DNA size standards (bp), from top - 1358, 1078, 872, 603. Lanes 2-10: EMS mutants. Lanes 11-20: spontaneous control mutants.

Figure 1: PCR Target Within AS52 Cells

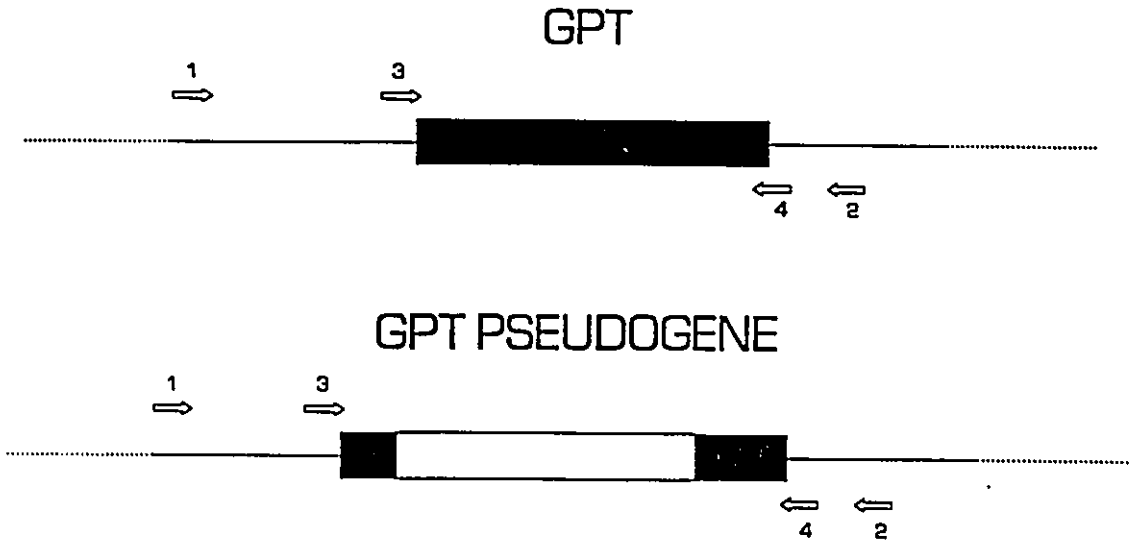

A: PCR Strategy

1: 5'-AAGCTTGGACACAAGACAG-3'
2: 5'-CCAGAATACTTACTGGAAAC-3' Set A

3: 5'-CGTAGATAAACAGGCTGGGACACTTCAC-3'
4: 5'-CAGTGCCAGGCGTTGAAAAGATTAGCG-3' Set B

P1: 5'-AAGGAAGGCTTTGAGAAGATCAGCAAA-3'
P2: 5'-CCCATTGCGCCCATTCCAGGGTC-3' Set P

B: PCR Amplification Primers

Figure 2: PCR Analysis of AS52 Mutants

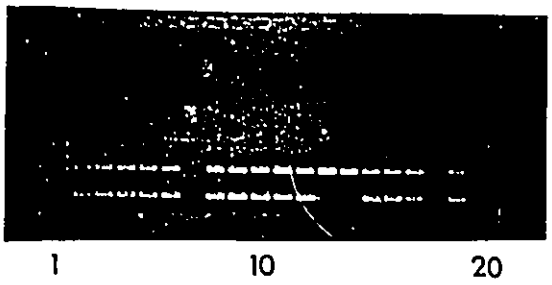

A: EMS / Control Mutants

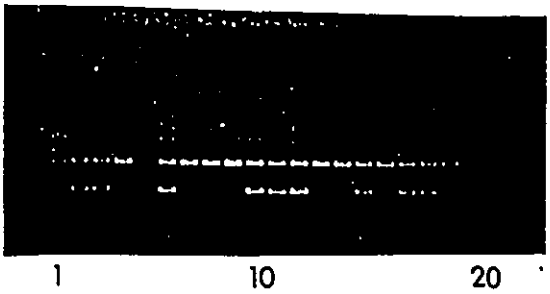

B: Nickel Mutants

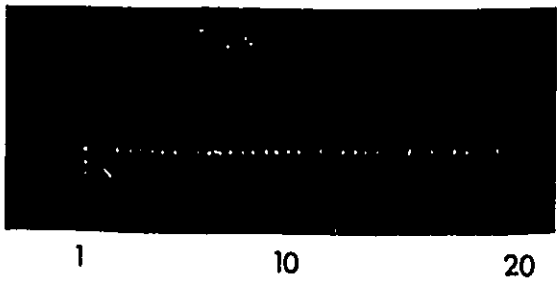

C: Chaperone/P-Protein

References

1) G.M. Cooper, Oncogenes,Jones and Bartlett, Boston, 1990, pp. 4-18.

2) F.W. Sunderman Jr., Recent advances in metal carcinogenesis. Ann. Clin. Lab. Sci., 14 (1984) 93-122.

3) E. Nieboer, F.E. Rossetto and C.R.Menon, in H. Sigel and A. Sigel (Eds.), Metal Ions In Biological Systems, Vol 23: Nickel And Its Role In Biology. Marcel Dekker Inc., New York, 1988, pp. 359-402.

4) G.G. Fletcher (1990) Evaluation of the "Nickel-ion hypothesis" of cytotoxic responses in AS52 CHO cells. MSc thesis, McMaster University, Hamilton, Canada.

5) K.R. Tindall, L.F. Stankowski Jr., R. Machanoff and A.W. Hsie, Detection of deletion mutations in pSV2*gpt*-transformed cells. Mol. Cell. Biol., 4 (1984) 1411-5.

6) C. Oste, Polymerase chain reaction. BioTechniques, 6 (1988) 162-7.

7) K.R. Tindall and L.F. Stankowski Jr., Molecular analysis of spontaneous mutations at the *gpt* locus in Chinese hamster ovary (AS52) cells. Mutat. Res., 220 (1989) 241-53.

8) E.R. Nestmann, R.L. Brillinger, J.P.W. Gilman, C.J.Rudd and S.H.H. Swierenga, Recommended protocols based on a survey of current practice in genotoxicity testing laboratories: II. Mutation in Chinese hamster ovary, V79 Chinese hamster lung and L5178Y mouse lymphoma cells. Mutat. Res., 246 (1991) 255-84.

9) K.K. Richardson, J. Fostel and T.R. Skopek, Nucleotide sequence of the xanthine guanine phosphoribosyl transferase of *E. coli*. Nucl. Acids Res., 11 (1983) 8809-16.

10) C.R. Ashman and R.L. Davidson, in M.M. Moore, D.M. Demarini, F.J. De Serres K.R. Tindall (Eds.), Banbury Report #28: Mammalian Cell Mutagenesis. Cold Spring Harbor Laboratory, U.S.A., 1987, pp. 293-300.

11) D.J. Piketts, C.S.K. Mayanil and R.S. Gupta, Molecular cloning of a Chinese hamster mitochondrial protein related to the "chaperonin" family of bacterial and plant proteins. J Biol. Chem., 264 (1989) 12001-8.

12) P. Sen and M. Costa, Pathway of nickel uptake influences its interaction with heterochromatic DNA. Toxicol. Appl. Pharmacol., 84 (1986) 278-85.

13) M. Costa and H.H. Mollenhauer, Carcinogenic activity of particulate nickel compounds is proportional to their cellular uptake. Science, 209 (1980) 515-7.

14) R.M. Evans, P.J.A. Davies and M. Costa, Video time-lapse microscopy of phagocytosis and intracellular fate of crystalline nickel sulfide particles in cultured mammalian cells. Cancer Res., 42 (1982) 2719-35.

15) M. Costa, Sequential events in the induction of transformation in cell culture by specific nickels compounds. Biol. Trace Elements. Res., 5 (1983) 285-95.

16) K.S. Kasprzak, P. Gabryel and K. Jarczewska, Carcinogenicity of nickel(II)hydroxides and nickel(II)sulfate in Wistar rats and its relation to the *in vitro* dissolution rates. Carcinogenesis, 4 (1983) 275-9.

17) K.S. Kasprzak, The role of oxidative damage in metal carcinogenicity. Toxicology, 4 (1991) 604-15.

18) R.T. Tom (1987) Novel reactions of nickel(II)-oligopeptide complexes with dioxygen species. MSc thesis, McMaster University, Hamilton, Canada.

19) E. Nieboer, R.T. Tom and F.E. Rossetto, Superoxide dismutase activity and novel reactions with hydrogen peroxide of histidine-containing nickel(II)-oligopeptide complexes and nickel(II)-induced structural changes in synthetic DNA. Biol. Trace Element Res., 21 (1989) 23-33.

20) S. Kawanishi, S. Inoue and K. Yamamoto, Site-specific DNA damage induced by nickel(II) ion in the presence of hydrgen peroxide. Carcinogenesis, 10 (1989) 2231-5.

21) Z. Nackerdien, K.S. Kasprzak, G. Rao, B. Halliwell and M. Dizdaroglu, Nickel(II)- and cobalt(II)-dependent damage by hydrogen peroxide to the DNA bases in isolated human chromatin. Cancer Res., 51 (1991) 5837-42.

22) A.V. Peskin and L. Shlyahova, Cell nuclei generate DNA-nicking superoxide radicals. FEBS Lett., 194 (1986) 317-21.

23) F.W. Sunderman Jr., A. Marzouk, S.M. Hopfer, O. Zaharia and M.C. Reid, Increased lipid peroxidation in tissues of nickel chloride-treated rats. Annals Clin. Lab. Sci., 15 (1985) 229-36.

24) F.W. Sunderman Jr., Metals and lipid peroxidation. Acta Pharmacol. Toxicol., 59 Suppl VII (1986) 248-55.

25) A.W.Hsie, in M.M. Moore, D.M. Demarini, F.J. De Serres K.R. Tindall (Eds.), Banbury Report #28: Mammalian Cell Mutagenesis. Cold Spring Harbor Laboratory, U.S.A., 1987, pp. 37-46.

26) K.R. Tindall and L.F. Stankowski Jr., in M.M. Moore, D.M. Demarini, F.J. De Serres K.R. Tindall (Eds.), Banbury Report #28: Mammalian Cell Mutagenesis. Cold Spring Harbor Laboratory, U.S.A., 1987, pp. 283-92.